

Development of a Cationic Polymer-Based siRNA Delivery System for the Regeneration of Tendon Injury



Xin Liao, B.Sc

Thesis submitted for the degree of Doctor of Philosophy

University of East Anglia

School of Pharmacy

April 2019

This copy of the thesis has been supplied on condition that anyone who consults it is understood to recognise that its copyright rests with the author and that use of any information derived therefrom must be in accordance with current UK Copyright Law.

In addition, any quotation or extract must include full attribution

Abstract

Tendon injury is one of the most common forms of musculoskeletal injuries that could occur in both human and equine patients. However, the conventional therapies have been unsuccessful when addressing the clinical need for the treatment of tendon injury. Therefore, the urgent need for more effective therapeutic strategies has set researchers along the route of exploring the causes underlying tendon injuries. In the past few decades, advances have been made in the understanding of tendon injury and its repair. Standing on the foundation of such discoveries, novel therapeutic approaches including gene therapy have been applied to the treatment of tendon injury.

It is established that tendon tissue repaired via the natural healing process after injury has a weakened mechanical property compared to the healthy tendon due to the scar tissue and adhesion formed during the repair process. Type III collagen and several cytokines including transforming growth factor-beta is reported to be closely associated with the formation of scar tissue. Consequently, it is hypothesised that through the suppression of the *COL3α1* gene, which is responsible for the production of type III collagen, the formation of scar tissue could be reduced to restore the mechanical property in the repaired tendon.

RNA interference is a reliable way to suppress the expression of a target gene using specific siRNA. However, the use of siRNA has several limitations including extracellular degradation by enzymes in tissue fluid, intracellular degradation by lysosomes and difficulties penetrating the cell membrane. Therefore, an efficient and safe siRNA delivery system is required, and the cationic polymer-based delivery system is a strong candidate. Cationic polymer poly (dimethylaminoethyl acrylate) (PDMAEA) is a biodegradable synthetic polymer that showed great potential as a delivery vector. This prompted the development of a new siRNA delivery system based on four-armed PDMAEA. It is hypothesized that the cationic four-armed PDMAEA polymer can effectively bind to negatively charged siRNA to form a nano-sized polyplex. It is also hypothesized that a four-armed PDMAEA could be more efficient than counter-part linear polymers in terms of binding to siRNA and the cytotoxicity profile. Cationic polymer PDMAEA was selected as a delivery vector for its good buffering capability, siRNA condensation efficiency and biodegradable property.

The work presented in this thesis describes the synthesis of a library of PDMAEA polymers of different molecular weights and architectures via RAFT polymerisation. The synthesized polymers were characterized by ¹H-NMR, ¹³C-NMR, GPC and potentiometric titration to confirm the desired molecular weight, architecture and pKa value. Firstly, a dsDNA with low base pair number was chosen as a model molecule to optimise the experimental conditions. Afterwards, the formation of the PDMAEA/dsDNA and PDMAEA/siRNA polyplexes were confirmed by agarose gel electrophoresis, and the solution properties, in particular the hydrodynamic diameter and zeta-potential, were confirmed using DLS. Later, the polymers and their polyplexes were tested on mouse 3T3 fibroblast cells and adult horse tenocytes to determine their cytotoxicity profiles. Finally, the optimised therapeutic siRNA-PDMAEA polyplex was applied to adult horse tenocytes stimulated with TGF- β 1 to observe the transfection and silencing effect of the *COL3 α 1* gene in induced *in vitro* conditions. The expression level of the *COL3 α 1* gene was determined by qPCR and type III collagen protein expression was monitored by immunocytochemistry. The results showed that the developed cationic PDMAEA was effective in delivering therapeutic siRNA in a clinically relevant *in vitro* condition and achieved controlled suppression of type III collagen expression. The developed delivery system could potentially be used to reduce scar tissue formation in many other tissues.

List of Publications

The work presented in this thesis has given rise to the following outputs:

Liao, X., Saeed, A., et al. A direct comparison of linear and star-shaped poly (dimethylaminoethyl acrylate) polymers for polyplexation with DNA and cytotoxicity in cultured cell lines. *European Polymer Journal*, 2017. 87: p. 458-467. (5 citations)

Walden, G., Liao, X., Saeed, A., et al. A Clinical, Biological, and Biomaterials Perspective into Tendon Injuries and Regeneration. *Tissue Engineering Part B-Reviews*, 2017. 23(1): p. 44-58. (15 citations)

Walden, G., Liao, X., Saeed, A., et al. Synthesis and Fabrication of Surface-Active Microparticles Using a Membrane Emulsion Technique and Conjugation of Model Protein via Strain-Promoted Azide-Alkyne Click Chemistry in Physiological Conditions. *Bioconjugate Chemistry*, 2019, 30 (3), pp 531–535

List of Poster Presentations

The 8th Academy of Pharmaceutical Science international PharmSci Conference, Hatfield 2017, UK

The 25th Annual Meeting of European Orthopaedic Research Society, Munich 2017, Germany.

Acknowledgement

It has been a long journey since I started my PhD at the School of Pharmacy, University of East Anglia in September 2014. In these years, I've had joy, I've had tears, I've made new friends, and I've developed my research skills. Most of all, I've had a great opportunity to study and work with some of the most brilliant scientists and this experience would benefit me in an inspiring way. I would like to take this precious opportunity to show my appreciation to those who continuously supported me through this time. First of all, I would like to express my endless gratitude to my primary supervisor, Dr Aram Saeed, for granting me this opportunity to work as a part of his group, excellent supervision, brilliant ideas, technical support, continues encouragement, shared experience, sharing his precious time for discussions and all other support and assistance throughout my PhD. Secondly, I would like to thank my secondary supervisor, Dr Graham Riley from the School of Biology, University of East Anglia for devoting his time to help me with Tendon related questions and for his advice on qPCR. Besides, I am very thankful to have received tremendous help from Dr Debbie Guest of Animal Health Trust for kindly sharing the adult equine tenocyte cell line and for her continues support with qPCR and immunocytochemistry. Many thanks to Dr Andrew Mayes from the School of Chemistry for the assistance with GPC and DLS.

Furthermore, I would like to thank Dr Ashkan Dehsorkhi, Ms Vera Silva, Ms Noelia Dominguez Falcon, Ms Lucka Bibic, Dr Mar Pugdellivol and Dr Gerard Callejo for all the joy that we shared and for all the technical (in science) and moral (in life) support provided. Many thanks to Dr Pratchaya Tipduangta and Dr Chaya Vaddhanaphuti for being considerate and supportive housemate and friend. I would like to extend my gratitude to all my friends from the University of East Anglia: Dr Susana Campos E Menezes Jorge Ramalhate, Dr Elise Wright, Mr Matthew Felgate, Ms Sofia Habib, Ms Carys Thomas, Mr Remy Narozny, Ms Valeria Gabrielli.

Last but not least, I would not have been able to achieve this endeavour without the unconditional love, continues encouragement and financial support from my beloved parents, Mr Zhirong Liao and Mrs Jinlian Liao(Li). Many thanks to all my other family members that continuously supported me.

Table of Contents

Abstract	i
List of Publications	iii
List of Poster Presentations	iii
Acknowledgement.....	iv
Table of Contents	v
List of Figures	viii
List of Tables and Schemes	x
List of Abbreviations.....	xi
1. Chapter 1 Introduction	2
1.1. Tendon and Tendon Injury.....	2
1.1.1. Tendon Function and Mechanical Properties	2
1.1.2. Tendon Anatomy and Biochemical Composition.....	3
1.1.3. Tendon Injuries and Tendon Healing.....	9
1.1.4. Current Treatment and Novel Strategy.....	15
1.2. Gene Therapy for Tendon Injury	17
1.2.1. Introduction of Gene Therapy	17
1.2.2. RNA Interference	22
1.2.3. Obstacles to Overcome in Gene therapy	25
1.3. Viral and Non-Viral Delivery Systems.....	30
1.3.1. Viral Delivery Systems.....	30
1.3.2. Non-viral Delivery Systems	39
1.4. Cationic Polymer-based Gene Delivery System	43
1.4.1. Gene Packaging.....	44
1.4.2. The Internalisation of Cationic Polyplexes	46
1.4.3. The Release of Nucleic Acids into the Cytoplasm	52
1.4.4. Examples of cationic polymers used in gene delivery	54
1.5. Controlled/living Radical Polymerisation	59
1.5.1. Different CRP Technique Applied in Polymer Synthesis	60
1.5.2. The RAFT Polymerisation Mechanism.....	62
1.5.3. RAFT Agents and its Compatibility with Monomers	64
1.6. Gene therapy for Tendon injury	68
1.7. Thesis Aims and Objectives	71
1.8. References	72
2. Chapter 2 Material and Methods	92
2.1. Introduction	92
2.2. Materials.....	92
2.3. Polymer synthesis.....	95
2.3.1. Introduction of RAFT Polymerisation.....	95
2.3.2. Experimental Conditions of PDMAEA Synthesis.....	96
2.4. Nuclear Magnetic Resonance Spectroscopy (NMR).....	96
2.4.1. Introduction of NMR.....	96
2.4.2. Experimental Conditions and Sample Preparation.....	97
2.5. Gel Permeation Chromatography (GPC).....	98
2.5.1. Introduction and the Basic Principle	98
2.5.2. Experimental Conditions and Sample Preparation.....	98
2.6. Potentiometric Titration.....	99
2.6.1. Experimental Conditions and Sample Preparation.....	99
2.7. Dynamic Light Scattering	99
2.7.1. Introduction and the Basic Principle	99
2.7.2. Experimental Conditions	101
2.8. Agarose Gel Electrophoresis.....	101
2.8.1. Introduction	101
2.8.2. Experimental Conditions and Sample Preparation.....	102

2.9.	General Cell and Tissue Culture.....	103
2.9.1.	3T3 Mouse Fibroblast and Adult Horse Achilles Tenocyte Culture	103
2.9.2.	Cell Count and Optical Microscopy	103
2.10.	CellTiter 96® AQ One Solution Cell Proliferation Assay.....	104
2.10.1.	Introduction and the Basic Principle	104
2.10.2.	Experimental Conditions and Sample Preparation.....	105
2.11.	Cell Proliferation Assay (CyQUANT® NF Kit)	105
2.11.1.	Introduction and the Basic Principle	105
2.11.2.	Experimental Conditions and Sample Preparation.....	106
2.12.	Quantitative real-time Polymerase Chain Reaction	106
2.12.1.	Introduction and the Basic Principle	106
2.12.2.	RNA Extraction	107
2.12.3.	Reverse Transcription.....	108
2.12.4.	Quantitative Polymerase Chain Reaction (qPCR).....	108
2.12.5.	Relative Quantification using $2^{-\Delta\Delta C_t}$ Method.....	109
2.13.	Fluorescent Cytochemistry.....	110
2.13.1.	Introduction and the Basic Principle	110
2.13.2.	Experimental Conditions	110
2.14.	References	111
3.	Chapter 3 The Synthesis and Characterisation of a Library of PDMAEA Polymers	114
3.1.	Introduction	114
3.2.	Material and Methods.....	116
3.2.1.	Materials.....	116
3.2.2.	Synthesis and Characterisation of 10 kDa Linear PDMAEA (PL10).....	116
3.2.3.	Synthesis and Characterisation of 20 kDa Linear PDMAEA(PL20)	117
3.2.4.	Synthesis and Characterisation of 10 kDa Star-shaped PDMAEA(PS10)	118
3.2.5.	Synthesis and Characterisation of 20 kDa Star-shaped PDMAEA (PS20) ...	119
3.2.6.	Determination of Polymer pKa Values by Potentiometric Titration.....	120
3.3.	Results	121
3.3.1.	Confirmation of Polymer Structure by $^1\text{H-NMR}$	121
3.3.2.	Confirmation of Molecular Weight by Gel Permeation Chromatography....	124
3.3.3.	Calculated pKa Values of PDMAEA Polymers.....	125
3.4.	Discussion	126
3.5.	Conclusion.....	131
3.6.	References	131
4.	Chapter 4 Characterisation of PDMAEA Polymer Solutions and PDMAEA-siRNA Polyplexes	135
4.1.	Introduction	135
4.2.	Materials and Methods.....	139
4.2.1.	Materials.....	139
4.2.2.	Characterisation of PDMAEA Polymers by DLS	139
4.2.3.	The Preparation of PDMAEA Polyplexes	140
4.2.4.	Agarose gel electrophoresis of PDMAEA (PL10, PL20, PS10, PS20)-dsDNA polyplexes	141
4.2.5.	Characterisation of PDMAEA (PL10, PL20, PS10, PS20)-dsDNA polyplex by dynamic light scattering	141
4.2.6.	Characterisation of PS10-siRNA polyplex by DLS and electrophoresis.....	141
4.3.	Results	142
4.3.1.	The Hydrodynamic Diameter of PDMAEA Polymers	142
4.3.2.	The Zeta Potential of PDMAEA Polymers	151
4.3.3.	Confirmation of PDMAEA (PL10, PL20, PS10, PS20)-dsDNA Polyplexes Formation by Electrophoresis	152
4.3.4.	Hydrodynamic Diameter and Zeta Potential of PDMAEA (PL10, PL20, PS10, PS20)-dsDNA Polyplexes	153
4.3.5.	Formation and Characterisation of PS10-siRNA Polyplexes.....	156
4.4.	Discussion	159
4.4.1.	Hydrodynamic Diameter and Zeta Potential of PDMAEA Polymers and its Polyplexes	159

4.4.2.	Formation of PDMAEA-dsDNA Polyplexes and PS10-siRNA Polyplexes..	161
4.4.3.	Selection of PS10 as a Delivery Vector for the Delivery of siRNA.	162
4.5.	Conclusion.....	162
4.6.	References	163
5.	Chapter 5 Cytotoxicity of PDMAEA Polymers and PDMAEA Polyplexes.....	166
5.1.	Introduction	166
5.2.	Materials and Methods	169
5.2.1.	Materials.....	169
5.2.2.	Cytotoxicity of PDMAEA Polymers on Mouse Fibroblast and Equine Tenocytes by MTS Assay	169
5.2.3.	Cytotoxicity of PDMAEA Polyplexes on Equine Tenocytes Determined by MTS Assay	170
5.2.4.	Cytotoxicity of PS10-siRNA Polyplexes on Equine Tenocytes Determined using Cyquant NF Cell Proliferation Assay	170
5.3.	Results	171
5.3.1.	Cytotoxicity of PDMAEA Polymers on 3T3 Mouse Fibroblast Cells Determined by MTS assay.....	171
5.3.2.	Cytotoxicity of PDMAEA Polymers on Equine Tenocytes by using MTS Assay	174
5.3.3.	Cytotoxicity of PDMAEA-dsDNA Polyplexes on Equine Tenocyte using MTS Assay	177
5.3.4.	Cytotoxicity of PS10-siRNA Polyplexes on Equine Tenocyte Cells.....	179
5.4.	Discussion	181
5.4.1.	PDMAEA Cytotoxicity on 3T3 Mouse Fibroblast and Equine Tenocyte.....	181
5.4.2.	The Influence of Molecular Weight and Structure on PDMAEA Cytotoxicity	182
5.4.3.	Cytotoxicity of PDMAEA Polyplexes in Equine Tenocytes by MTS Assay	184
5.4.4.	Cytotoxicity of PS10-siRNA polyplex in Equine Tenocytes by using MTS and Cyquant Assays	185
5.5.	Conclusion.....	187
5.6.	Reference.....	187
6.	Chapter 6 Transfection Efficiency of PDMAEA-siRNA Polyplexes Based on qPCR and Immunocytochemistry.....	192
6.1.	Introduction	192
6.2.	Material & Methods	195
6.2.1.	Materials.....	195
6.2.2.	Effect of TGF- β 1 Stimulation on <i>COL3a1</i> Gene by qPCR and Determination of Optimal Dosage.....	195
6.2.3.	Transfection of Equine Tenocyte using PS10-siRNA Polyplex	195
6.2.4.	Immunocytochemistry on Equine Tenocyte Cells.....	196
6.3.	Results	197
6.3.1.	TGF- β 1 Stimulation on <i>COL3a1</i> Gene Expression.....	197
6.3.2.	Silencing Effect of siRNA Interference using PS10 as a Delivery Vector on TGF- β 1 Stimulated Cells	199
6.3.3.	Immunocytochemistry	201
6.4.	Discussion	203
6.5.	Conclusion.....	206
6.6.	References	206
7.	Chapter 7 Conclusions and Future Work.....	209
7.1.	General Conclusions and Discussions.....	209
7.2.	Future Work.....	213
7.3.	References	215

List of Figures

Figure 1.1 Stress/strain curve of tendon tissue. In low strain, low stiffness was observed..	2
Figure 1.2 The multilayer hierarchical structure of tendon.	4
Figure 1.3 Cellular and acellular components of tendon tissue.	5
Figure 1.4 A schematic demonstration of the collagen triple helix. (A)	6
Figure 1.5 A schematic demonstration of Pro <i>cis</i> – <i>trans</i> isomerisation.	7
Figure 1.6 The tendon healing process in human and a summary of cellular and matrix changes in tendon repair.	11
Figure 1.7 A schematic illustration of normal tendon anatomy (left) compared to healed tendon after injury(right).	13
Figure 1.8 Gene therapy involves the use of a gene-expressing unit (composed of a promoter, gene, and termination signal), while small molecule (chemical) drugs target proteins, short oligonucleotides used in genetic pharmacology generally target DNA and/or RNA.	20
Figure 1.9 Mechanisms of RNA interference.	25
Figure 1.10 The barriers in siRNA/DNA delivery using cationic carriers from the administration site to the target site.	29
Figure 1.11 The 3D structure(right) and the schematic structure(left) of the adenovirus.	32
Figure 1.12 Internalisation of adenoviruses from the outside plasma membrane into the nucleus.	33
Figure 1.13 The structure of AAV determined by x-ray crystallography.	34
Figure 1.14 Retroviral internalisation and viral gene expression as shown for a simple <i>gammaretrovirus</i> example.	37
Figure 1.15 An example of a PAMAM dendrimer.	41
Figure 1.16 Examples of various polymer architectures that can be achieved.	43
Figure 1.17 Polyplexes formation via electrostatic interaction between cationic polymers and nucleic acids.	44
Figure 1.18 The clathrin-dependent endocytosis process.	47
Figure 1.19 Caveolae-dependent endocytosis.	48
Figure 1.20 The phagocytosis and micropinocytosis process.	50
Figure 1.21 Structure of Heparin, an example of glycosaminoglycan.	51
Figure 1.22 The endosome escapes of cationic polyplexes via a proton-sponge effect pathway.	54
Figure 1.23. The thermal decomposition of AIBN and the free radical polymerisation of ethylene into polyethene.	59
Figure 1.24 Nitroxide-mediated polymerization	60
Figure 1.25 Mechanism of ATRP.	61
Figure 1.26 Structures of different types of RAFT agents.	64
Figure 2.1 Structure of Dimethylaminoethyl acrylate.	92
Figure 2.2 Structure of 2-(Dodecylthiocarbonothiylthio)-2-methylpropionic acid.	93
Figure 2.3 Structure of Pentaerythritol tetrakis[2-(dodecylthiocarbonothiylthio)]	93
Figure 2.4 Structure of 2,2'-Azobis(2-methylpropionitrile).	94
Figure 2.5 NMR working principle.	97
Figure 2.6 Structure of MTS reagent.	104
Figure 2.7 The bio-reduction of MTS tetrazolium compound into a formazan product.	105
Figure 3.1 Synthesis of 10 kDa linear PDMAEA polymer (PL10).	117
Figure 3.2 Synthesis of 20 kDa linear PDMAEA polymer (PL20).	118
Figure 3.3 Synthesis of 10 kDa star-shaped PDMAEA polymer (PS10).	119
Figure 3.4 Synthesis of 20 kDa star-shaped PDMAEA polymer (PS20).	120
Figure 3.5 ¹ H NMR spectrum of 10 kDa star-shaped PDMAEA polymers.	121
Figure 3.6 ¹ H NMR spectrum of 10 kDa linear PDMAEA polymers.	122
Figure 3.7 ¹ H NMR spectrum of 20kDa star-shaped PDMAEA polymers.	123
Figure 3.8 ¹ H NMR spectrum of 20kDa linear PDMAEA polymers.	124
Figure 3.9 Gel permeation chromatography spectra of PS10, PS20, PL10 and PL20.	125
Figure 3.10 Potentiometric titration curves of PDMAEA polymers and calculated pKa values.	125
Figure 3.11 Chemical shift of methylene proton of unreacted DMAEA monomer and synthesized polymer.....	127
Figure 3.12 ¹ H NMR spectrum of DMAEA monomers.	128
Figure 3.13 A schematic demonstration of the states of protonated sites in a polymer chain during potentiometric titrations.	129
Figure 4.1 A schematic illustration of the electric double layer of a charged particle in solution.	136
Figure 4.2 The interaction energy in relationship to particles separation distance.	137
Figure 4.3 The correlation curves, intensity distribution and volume distribution of PL10 polymer in	

solutions with pHs from 6.0 to 8.5.....	144
Figure 4.4 The correlation curves, intensity size distribution and volume distribution of PS10 polymer in pH 6.0 – 8.5 solutions.....	146
Figure 4.5 The correlation curves, intensity size distribution and volume distribution of PL20 polymer in pH 6.0 – 8.5 solutions.....	148
Figure 4.6 The correlation curves, intensity size distribution and volume distribution of PS20 polymer in pH 6.0 – 8.5 solutions.....	149
Figure 4.7 Statistical analysis within the group to determine the variation between sizes at each pH.....	150
Figure 4.8 Statistical analysis between PS10, PS20, PL10 and PL20 polymers.....	151
Figure 4.9 Zeta potential of four PDMAEA polymer solutions under different pH conditions.....	152
Figure 4.10 Agarose gel (1%) electrophoresis analysis of PDMAEA-dsDNA polyplexes.....	153
Figure 4.11 The correlation curves, intensity size distribution and volume distribution of PL10, PS10, PL20, PS20 polyplexes with dsDNA pH 7.4.....	154
Figure 4.12 Mean size distribution by volume percentage and zeta potential of four PDMAEA-dsDNA polyplexes at pH 7.4.....	155
Figure 4.13 Agarose gel (1.5%) electrophoresis analysis of PS10-siRNA polyplexes.....	156
Figure 4.14 The correlation curves, intensity distribution and volume distribution of PS10-siRNA polyplexes at pH 5.4-7.4.....	157
Figure 4.15 Size and zeta potential of PS10-siRNA polyplexes at pH 5.4, 6.4 and 7.4.....	158
Figure 4.16 A schematic demonstration of a possible random coil structure of polymers in solution.....	159
Figure 4.17 A schematic demonstration of PDMAEA polymers forming large aggregates at pH 8.0 and above.....	160
Figure 4.18 Schematic figure of the formation of a possible internal hydrophilic compartment in star-shaped polymers compared to linear polymers.....	162
Figure 5.1 Mouse 3T3 fibroblast metabolic activities at 24 hours post-treatment. Samples were treated with PDMAEA polymer solutions at different concentrations.....	172
Figure 5.2 Mouse 3T3 fibroblast metabolic activities at 48 hours post-treatment. Samples were treated with PDMAEA polymer solutions at different concentrations.....	173
Figure 5.3 Mouse 3T3 fibroblast metabolic activities at 72 hours post-treatment. Samples were treated with PDMAEA polymer solutions at different concentrations.....	174
Figure 5.4 Equine tenocyte metabolic activities at 24 hours post-treatment. Samples were treated with PDMAEA polymer solutions at different concentrations.....	175
Figure 5.5 Equine tenocyte metabolic activities at 48 hours post-treatment. Samples were treated with PDMAEA polymer solutions at different concentrations.....	176
Figure 5.6 Equine tenocyte metabolic activities at 72 hours post-treatment. Samples were treated with PDMAEA polymer solutions at different concentrations.....	177
Figure 5.7 Equine tenocyte metabolic activities at 24 hours post-treatment. Samples were treated with PDMAEA-DNA polyplex solutions at different concentrations.....	178
Figure 5.8 Equine tenocyte metabolic activities at 48 hours post-treatment. Samples were treated with PDMAEA-DNA polyplex solutions at different concentrations.....	179
Figure 5.9 Equine tenocyte metabolic activity at 72 hours post-treatment. Samples were treated with PDMAEA-DNA polyplex solutions at different concentrations.....	179
Figure 5.10 Equine tenocyte metabolic activities post-treatment. Samples were treated with PS10-siRNA polyplex solutions at different concentrations.....	180
Figure 5.11 Equine tenocyte metabolic activity post-treatment. Samples were treated with PS10-siRNA polyplex solutions at different concentrations.....	181
Figure 6.1 Effect of TGF- β 1 treatment on cultured equine tenocytes treated with different concentrations of TGF- β 1 for 24 hours.....	198
Figure 6.2 TGF- β 1 stimulation effect on the expression of <i>COL3α1</i> gene in equine tenocytes over time.....	199
Figure 6.3 PS10-siRNA mediated silencing of <i>COL3α1</i> in cultured equine tenocytes.....	200
Figure 6.4 Immunocytochemistry of TGF- β 1 stimulated tenocytes treated with PS10-siRNA polyplex as well as other controls.....	202
Figure 7.1 Processes for thiocarbonylthio removal to generate thiols.....	214

List of Tables and Schemes

Table 1.1 Changes of structural molecules, Enzymes, Cytokines and signalling factors expression level in tendinopathy matrix.	14
Table 1.2 A summary of current treatment for tendinopathy.	16
Table 1.3 This table show the advantages and disadvantages of several well-studied viral gene delivery systems.	38
Table 1.4 Cationic polyplexes internalisation pathways summarised by Midoux et al.	52
Table 1.5 Commonly used cationic and neutral monomer.	55
Table 1.6 Commonly used RAFT agents and their compatibilities with monomers.	66
Table 1.7 Corresponding chemical description of RAFT agents in table 1.6.	67
Table 1.8 Use of gene transfection as an advanced delivery system for tendon healing and corresponding vectors	68
Table 1.9 Commonly targeted genes in tendon regeneration gene therapy ³⁰⁴	69
Table 3.1 Experimental conditions and molecular weight characterisation of linear and star-shaped polymers.	124
Table 4.1 Preparation of PDMAEA polyplexes.	140
Table 4.2 Size distribution of PL10 polymers in solutions with pHs from 6.0 to 8.5.	145
Table 4.3 Size distribution of PL10 polymers in solutions from pH 6.0-8.5.	147
Table 4.4 Size distribution of PL20 and PS20 polymers in solutions from pH 6.0-8.5.	147
Table 4.5 Mean size values \pm SD (N=3) by intensity and volume distribution analysis of four PDMAEA-dsDNA polyplexes at pH 7.4.	154
Table 4.6 Zeta potential of four PDMAEA-dsDNA polyplexes.	155
Table 4.7 Hydrodynamic diameter of PS10-siRNA polyplexes.	158
Table 4.8 Zeta potential of PS10-siRNA polyplexes. recorded at the corresponding pH.	158
Table 6.1 Normalised fluorescent intensity of TGF- β 1 stimulated tenocytes treated with PS10-siRNA polyplex as well as other controls. The data were presented as the mean value of three random fields with SD.	203
 Scheme 1.1 Schematic illustration of the initial stage, pre-equilibrium stage and main equilibrium stage of RAFT polymerisation process.	63

List of Abbreviations

4-arm-

DDMAT	Pentaerythritol tetrakis [2-(dodecylthiocarbonothioylthio)-2-methylpropionate]
ACL	Anterior Cruciate Ligament
Ago	Argonaute protein
AIBN	2,2'-Azobis(2-methylpropionitrile)
ANOVA	Analysis of variance
APMA	N-(3-Aminopropyl) methacrylamide hydrochloride
ATRP	Atom-transfer radical-polymerization
BMA	Butyl methacrylate
BMP	Bone morphogenetic proteins
CRP	Controlled radical polymerisation
CTA	Chain transfer agent
DDMAT	2-(Dodecylthiocarbonothioylthio)-2-methylpropanoic acid
DEAEMA	2-(Diethylamino)ethyl methacrylate
DLS	Dynamic light scattering
DMAE	Dimethylethanolamine
DMAEA	2-(Diethylamino)ethyl acrylate
DMAPMA	Dimethylamino propyl methacrylamide
DMEM	Dulbecco's Modified Eagle Medium
DP	Degree of polymerisation
ECM	Extracellular matrix
EDTA	Ethylenediaminetetraacetic acid

EE	Early endosomes
FCS	Fetal calf serum
FGF	Fibroblast growth factors
GAG	Glycosaminoglycans
GPC	Gel permeation chromatography
HEMA	Hydroxyethyl methacrylate
HPMA	N-(2-Hydroxypropyl) methacrylamide
ICC	Immunocytochemistry
IGF	Insulin-like growth factors
LBDS	Lipid-based delivery system
miRNA	Micro RNA
MMP	Matrix metalloproteinase
NMDAR	N-methyl-D-aspartate receptor
NMR	Nuclear Magnetic Resonance Spectroscopy
NSAID	Non-steroidal anti-inflammatory drug
PAMAM	Polyamidoamine
PCR	Polymerase chain reaction
PDGF	Platelet-derived growth factor
PDGFR	Platelet-derived growth factor receptor
PDMAEA	Poly[2-(Diethylamino)ethyl acrylate]
PDMAEMA	Poly[2-(Diethylamino)ethyl methacrylate]
pDNA	Plasmid DNA
PEG	Polyethylene glycol

PEI	Polyethylenimine
PGE2	Prostaglandin E2
PL10	Poly[2-(Diethylamino) ethyl acrylate] linear of 10kDa
PL20	Poly[2-(Diethylamino) ethyl acrylate] linear of 20kDa
PLGA	Poly(lactic-co-glycolic acid)
PS10	Poly[2-(Diethylamino) ethyl acrylate] star-shaped of 10kDa
PS20	Poly[2-(Diethylamino) ethyl acrylate] star-shaped of 20kDa
PTFE	Polytetrafluoroethylene
qPCR	Quantitative polymerase chain reaction
RAFT	Reversible Addition-Fragmentation chain Transfer
RISC	RNA-induced silencing complex
RNAi	RNA interference
SEC	Size exclusion chromatography
shRNA	Short hairpin RNA
siRNA	Small interfering RNA
TGF	Transforming growth factor
TGF-βR1	Transforming growth factor beta receptor I
TIMP	Tissue inhibitor of matrix metalloproteinase
VEGF	Vascular endothelial growth factor

Chapter 1

Introduction

1. Chapter 1 Introduction

1.1. Tendon and Tendon Injury

1.1.1. Tendon Function and Mechanical Properties

Tendons are strong connective tissues which connect bones and muscles. Their primary function is to transmit active forces generated by muscles^{1,2}. Besides, another important function of tendon tissue is to store elastic energy during motion³. For instance, the tendons and ligaments of the foot and leg store up to 50% of the energy required for walking and running. The energy stored can be released over a short period of time with high efficiency³. Tendon tissue contains large amounts of water, ~60% average in different types of tendon. The remaining dry weight is predominantly provided by collagen, which occupies up to 85% of the total dry weight and is in the form of fibres aligned longitudinally⁴.

Tendons display elastic behaviours similar to elastomeric materials. The stress/strain relationship in tendon tissue is nonlinear and shown in figure 1.1.

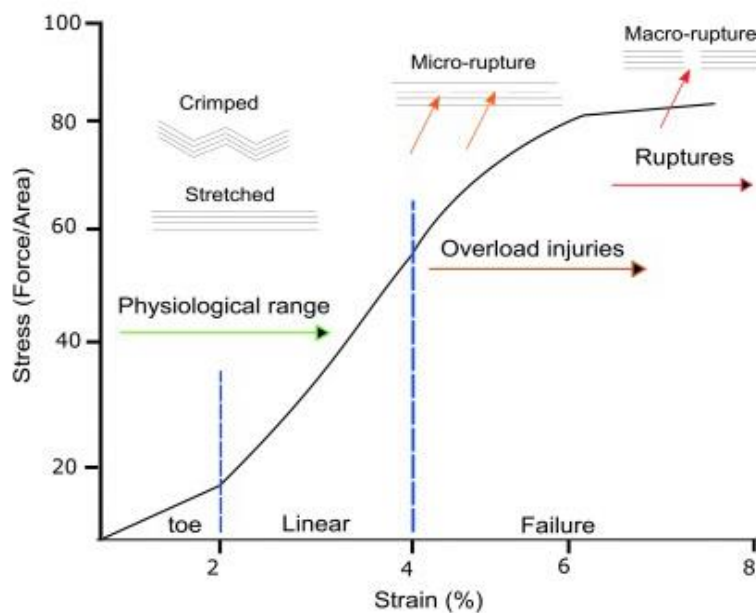


Figure 1.1 Stress/strain curve of tendon tissue. In low strain, low stiffness was observed. As the strain increases, tendon tissue showed an approximately linear elastic deformation.

Low stiffness was observed when the initial load was applied on tendon tissue, and that is because tendon collagen fibres, bearing zero loads, are not linear but rather in a crimped shape. The initial loading stretches the collagen fibres and removes the crimped

shape, turning collagen fibres into straight and stretched structures. The subsequent load applied to tendon tissue results in an approximately linear elastic deformation. If the load continues to increase to exceed the physical limits, damage to these fibres themselves or to the cross-links between fibres were observed. Excessive loads might cause injuries, including micro-, macro-, or complete rupture of tendon tissue. Pain and inflammatory response can be observed before the ultimate tensile strain limit is reached. Therefore, pain and inflammatory response are often considered as responses of severe tendon injury¹.

The function of tendon tissue is fulfilled by its multilayer, highly complex structure, as well as the protein-based extracellular matrix composition. In this chapter, the following topic will be introduced and discussed:

- 1) The anatomy and biochemical composition of tendon tissue.
- 2) What tendon injury is and the characteristics of injured tendon tissue. The healing process of tendon tissue after injury and its changes on a molecular level.
- 3) Current treatment for tendon injury and its limitation.
- 4) Potential novel therapeutic approaches for the treatment and improved healing of tendon injury.

1.1.2. Tendon Anatomy and Biochemical Composition

Tendon tissue has a highly complicated and multi-layered structure. Tendon tissue consists of tenocytes and tendon extracellular matrix (ECM), which are composed mainly of collagen, as well as other non-collagen proteins⁵. Tenocytes are considered to be the primary cellular composition of the tendon tissue, and it is an elongated specialised fibroblast⁶. Other smaller cell populations found in tendon tissue include adipose-derived stem cells and muscle cells⁷. Tenocytes are essential for tendon formation and natural repair due to their ability to produce proteins, especially in the collagen protein family. Tenocytes produce collagen as well as other proteins that are essential for the construction of the tendon extracellular matrix⁶. The produced collagen protein is a vital component of tendon ECM, occupying 60-85% of the dry weight of the tissue⁸. Figure 1.2 demonstrates the structure of tendon tissue⁹. Collagens and other proteins align in a different style to form complex linear, helical and branched

molecules that further interact with each other to form fibrils¹⁰, these fibrils merging into a collagen fibre that further consolidates into the primary fibre bundle. The outside of the primary fibre bundle is surrounded by a thin layer of connective tissue called endotenon. Endotenon contains the vascular system, nerve system and immune component that are vital for tendon tissue¹¹. The primary fibre bundles align with each other, forming the secondary fibre bundle, known as fascicle. Fascicles unite into tertiary fibre bundle and further into the tertiary fibre bundle, eventually became tendon fibre which has a layer of connective tissue called epitendon on the outside¹².

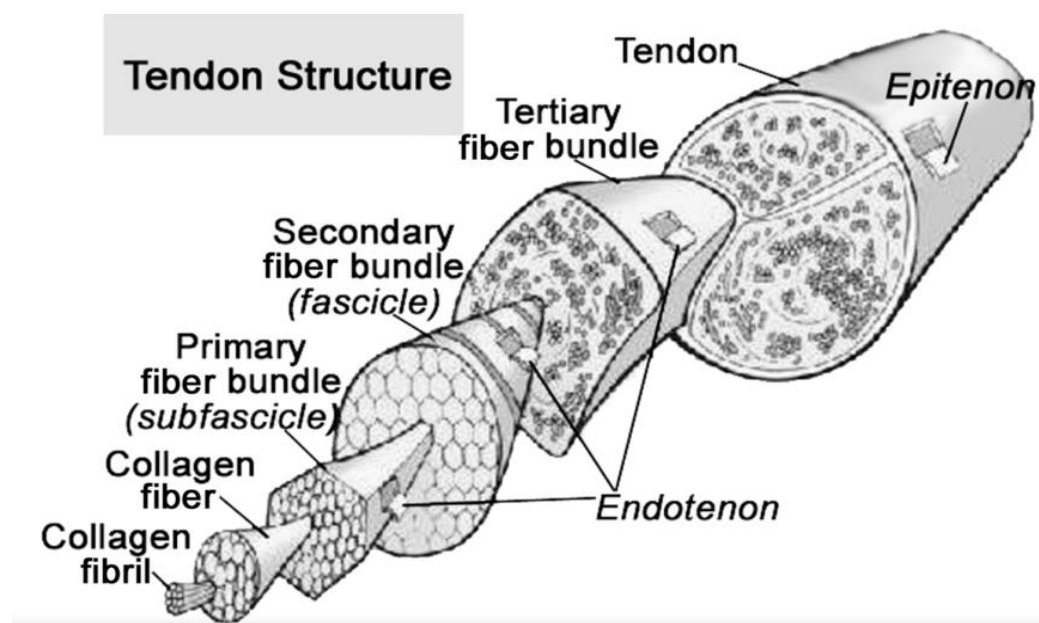


Figure 1.2 The multilayer hierarchical structure of tendon. Figure adapted from Sharma et al.⁹.

Tendon function is determined by the structure and cellular composition. Figure 1.3 shows the cellular and acellular composition of tendon tissue. The composition of tendon tissue includes collagen, elastin, glycosaminoglycan (GAG), proteoglycans and other structural proteins².

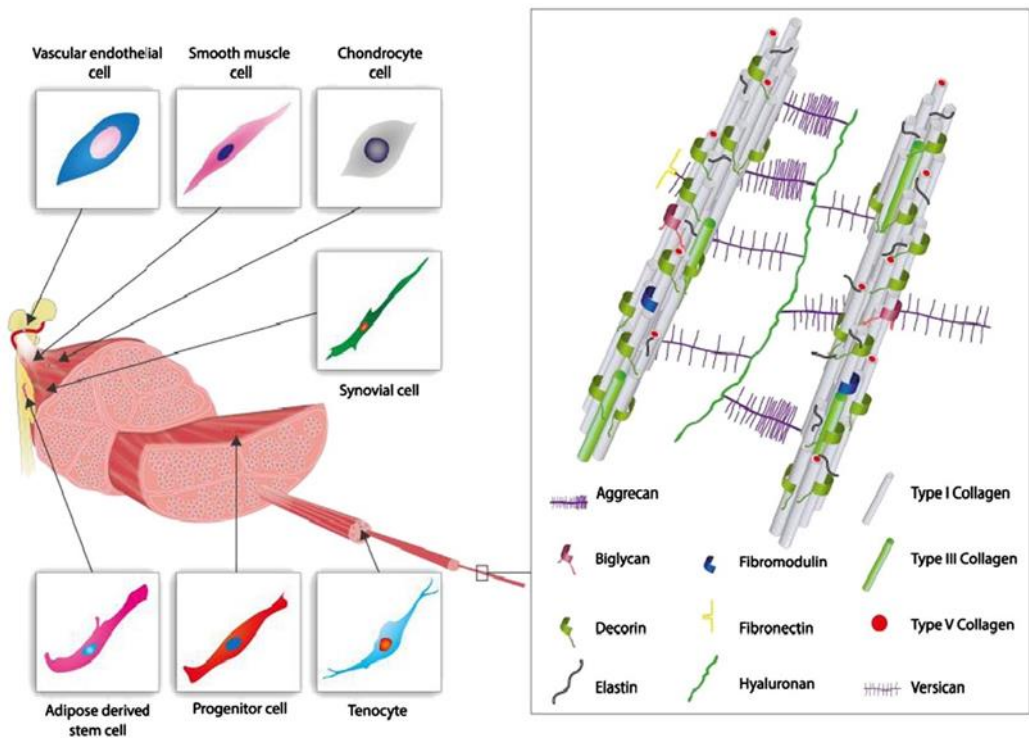


Figure 1.3 Cellular and acellular components of tendon tissue. Figure adapted from Lamos et al.¹⁰

Collagen is the primary content of tendon tissue (about 60-85% of the dry weight) and provides multiple functions including transmitting force, load bearing, maintaining the complete structure of the tendon tissue and the prevention of possible mechanical failures^{8,13,14}. All collagens are proteins whose basic units consist of either homo- or heterotrimeric assemblies formed by three sets of polypeptide chains that wind around each other, known as tropocollagen (figure 1.4). Homotrimerically assembled collagen molecules, such as type III collagen, are formed by three α chains while heterotrimerically assembled collagen molecules, such as type I collagen, is formed by two $\alpha 1$ chains and one $\alpha 2$ chain. The polypeptide chains that form into triple helix are approximately 1000 amino acids long and are comprised of triplets with a repeating sequence of Gly-Xaa-Yaa, where Xaa and Yaa frequently represent (2S)-proline (Pro, 28%) and (2S,4R)-4-hydroxyproline (Hyp, 38%), respectively¹⁵. In animals, individual tropocollagen assemble in a complex, hierarchical manner that ultimately leads to the macroscopic fibres and networks observed in tissue and basement membranes. The proline and 4(R)Hyp residue played a vital role in the correct conformation and stability of the tropocollagen as they are related to the formation of inter-strand hydrogen bonds.

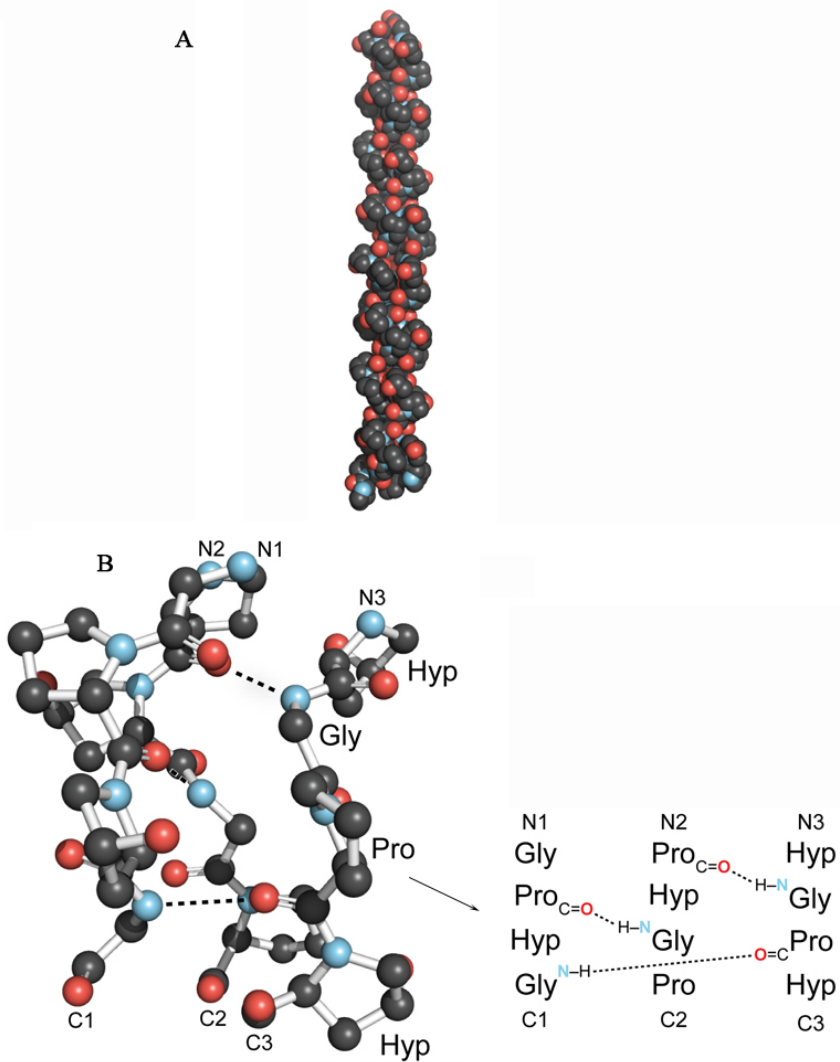


Figure 1.4 A schematic demonstration of the collagen triple helix. (A) a crystal structure of a collagen triple helix formed from (ProHypGly)₄–(ProHypAla)–(ProHypGly)₁₆. (B) Ball-and-stick image of a segment of collagen triple helix and the ladder of inter-strand hydrogen bonds. The figure is adapted from Shoulders et al.¹⁷

The importance of collagen as a scaffold for animals is determined by various of essential characteristics, including thermal stability¹⁸, mechanical strength, and the ability to engage in specific interactions with other biomolecules. These properties are derived from the fundamental structural unit of collagen, the triple helix, and it has been established that the inter-strand hydrogen bonds, Prolines isomers and the hydroxylation of Pro residues play vital roles in stabilising the tropocollagen structure¹⁷. The amide-amide hydrogen bond is the most abundant hydrogen bond within the triple helix structure (figure 1.4 B) and it's of great importance for collagen triple-helix stability. In the strands of human collagen, about 22% of all residues are either Pro or Hyp, which pre-organises the strands in a PPII conformation, thereby reducing the entropic cost for

collagen folding¹⁹. Furthermore, the Pro isomers also have certain effects on the triple-helix folding and stability. For example, Pro forms tertiary amides within a peptide or protein, which have a significant population of both the *trans* and the *cis* isomers (figure 1.5). However, all peptide bonds in collagen are *trans*, which suggests that all the *cis* peptide bonds must be isomerised to *trans* before a strand can fold into a triple helix¹⁷. Replacing a Gly-Pro amide bond with an alkene isostere that is *trans*-locked would also result in a destabilised triple helix²⁰.

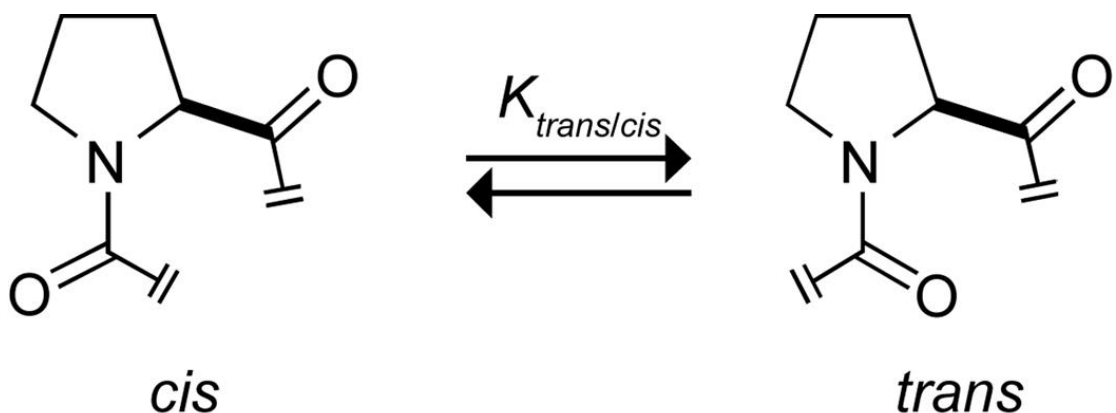


Figure 1.5 A schematic demonstration of Pro *cis*–*trans* isomerisation. The figure is adapted from Shoulders et al.¹⁷

The stabilisation effect provided by 4(R)Hyp residue in the Yaa position was explained by two different theories. The first theory suggested that the hydroxyl groups in 4(R)Hyp would form water bridges through hydrogen bond between backbone groups. Berman et al. illustrated in their study that the hydroxyl groups of Hyp were involved in the formation of water bridges with amide groups from Glycine and other carbonyl groups both inter- and intrachain²¹. The second theory explained that the hydroxyl group has an inductive effect which alters the ring puckering of the pyrrolidine ring and thus, changes the *cis*/*trans* conformation ratio in the peptide chain. A closer inspection of the collagen peptides structures by X-ray crystallography revealed a preference of γ -*endo* pucker (down puckering) of the pyrrolidine ring in the Xaa position and γ -*exo* pucker (up puckering) of the pyrrolidine ring in the Yaa position^{22,23}. Further studies verified that (2S,4R)-4-hydroxyproline residue favour the γ -*exo* pucker while its 4S isoform favour the γ -*endo* pucker²⁴. Because of the energy difference between the *cis* and *trans* conformation is greatly reduced with γ -*endo* pucker, peptides with 4S-Hydroxyproline in Yaa position would have a higher population of the *cis* conformation compared to those with 4R-Hydroxyproline²⁵. These findings may have explained the stabilising effect of 4(R)Hyp in the Yaa position. More recently, a study by Raines et al.

provided evidence to support that Hyp hydroxyl groups act primarily through stereo-electrostatic effects in the stabilisation of collagen triple helix²⁶. The combination of Van der Waals force between proline rings in adjacent peptide chains, the hydrogen bonding network that links the hydroxyl groups and the carbonyl groups and the stereo-electrostatic effects, resulted in an optimally assembled tropocollagen and enabled collagen fibrils to provide tensile strength to tissues to fulfil its function.

Type I collagen takes up to 90% of the total dry weight of all collagens and is considered the most abundant collagen in the human body^{27,28}. It is found in over 90% of the organic matrix and has a huge impact on the biomechanical properties and functional integrity of biological tissues. The fundamental unit of type I collagen is a heterotrimerically assembled molecule, typically by two $\alpha 1$ chains and one $\alpha 2$ chain, forming into a triple helical structure²⁹. The biosynthesis of type I collagen molecule is a process containing multiple post-translational modification reactions to ensure the correct conformation and interchain cross-link formation that provided the protein with necessary chemical and biological characteristics. Naturally, type I collagen is synthesised by fibroblasts and tenocytes as a soluble procollagen chain intracellularly³⁰. The synthesis of type I collagen α chains in human tissues are controlled by the *COL1A1* (for $\alpha 1$) and *COL1A2* (for $\alpha 2$), located on the long arm of chromosome 17 and chromosome 7, respectively³¹. After transcription, the polypeptides undergo post-translational modification, such as the hydroxylation of proline and lysine, under the catalytic action of different hydroxylase enzymes. This step is vital for the assembly of the collagen triple helix, the hydroxyl groups from hydroxyproline and hydroxylysine being key to the stabilisation of tropocollagen³². The healthy tendon tissues are predominantly comprised of type I collagen, and it is considered to be the major component that provides tendon tissue with tensile strength and stiffness to function properly.

Other collagen types, such as type III collagen and type V collagen, also play a vital role in tendon tissue. Type III collagen accounts for only a small amount of all collagen types in the healthy tendon. In healthy tendon, Type III collagens are mostly found in endotenon and epitendon layers³³. However, in tendon injury or in tendinopathy, type III collagens are found not only in endotenon and epitendon but all over the tendon matrix¹². Changes in gene expression also indicated that the production of type III collagen had been up-regulated in injured tendon tissue and tissue with tendinopathy³⁴. The increase

in type III collagen expression level suggested a possible increase in the production and secretion of type III collagen, which could be involved in the healing and repair process of tendon tissue. In some cases, especially injured tendon tissue, collagen types III could associate with collagen types I to form a heterotypic fibril, which has a smaller diameter than regular fibril bundles³⁵. Another vital member in the collagen family is type V collagen, which is less abundant in tendon but plays a key role in collagen fibril assembly. Typically, type V collagen is found at the centre of a collagen fibril bundle and is responsible for collagen growth and expansion³⁶. Similar to type III collagen, an increase in collagen type V has been observed in injured tendon as well. In tendon tissue suffering from tendinopathy, collagen types V can also associate with type I collagen and form heterotypic fibril, which also weakens the tendon strength by reducing the tendon fibril diameter³⁷. Other types of collagens such as XII and XIV are found essential to tendon matrix formation as well. These collagens would aid and supplement collagen I bundles' ability to glide over each other during the force transition process. When a force is applied, these molecules can decrease the interactions between fibres to avoid potential damage to tendon tissue^{38,39}.

1.1.3. Tendon Injuries and Tendon Healing

There is an unmet clinical need in the treatment of tendon injury for both human and equine patients. It is estimated that about €140 billion is spent on healthcare related to tendon injury worldwide per year and increasing⁴⁰. As it affects the population of a wide range, it is estimated that about 25% of the adult population would suffer from tendon related condition⁴¹. Though numerous therapeutic strategies have been developed, data indicated that few of them had achieved recovery that is comparable with pre-injury states⁴².

- Tendon injury and its causes

Tendon injury includes acute tendon injuries, like ruptures or tears, chronic tendon disorder or pain and acute tendon pain with inflammation, which are termed tendon rupture, tendinopathy and tendinitis respectively^{43,44}.

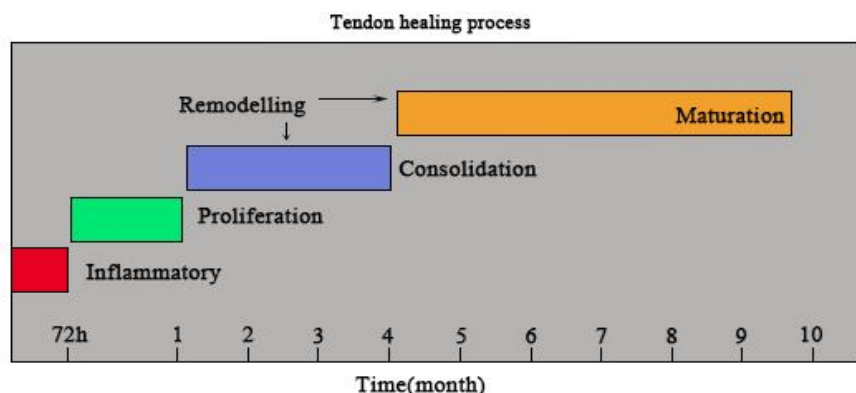
Tendinopathy is the primary tendon disorder caused by overuse or degeneration and the patient would experience chronic pain in a clinical situation⁴⁵. Tendinopathy is caused by intrinsic and extrinsic factors with interactions between each other⁴⁶. Intrinsic factors

including age, gender, anatomical variants, body weight and systemic disorder could have an effect on the tendon. It is reported that biomechanical failure and alignment faults within tendon tissue are the major reason for sport-related Achilles tendon disorder⁴⁷. It is considered that excessive loading during vigorous physical activity is responsible for degeneration pathologically⁴⁸. In some cases, the cause of tendinopathy is a result of both intrinsic and extrinsic effects. Under the influence of intrinsic factors, such as age and genetic disorder, the tendon is more prone to injury under excessive load and repetitive pressure⁴⁹. The nature repair of tendon tissue is vital, for, without enough time for the tendon to repair the damage and generated neo-tissue, the trauma would accumulate and eventually leads to more severe injury or rupture⁵⁰. Evidence showed that sedentary working/living habit, recreational sports and a propensity for obesity might be held responsible for the increasing incidence rate of tendinopathy⁵¹. Genes have recently been found related to tendinopathy, due to the lack of a specific gene related to the production of collagen V and tenascin C, some patients might have a more significant potential of being affected by tendinopathy^{52,53}.

Tendon rupture is described as an acute injury caused mainly under external load, though intrinsic factors also play an indirect role. For example, most of the tendon rupture happens in the fifth decade of a person's life. Therefore age is considered to be one of the intrinsic factors related to tendon rupture. However, Achilles and Supraspinatus rupture are mostly found in the younger population which indicates rupture is also associated with the activity level of the population. Tendon rupture tends to occur in the Achilles tendon and Anterior Cruciate Ligament (ACL). But in other tendon tissue like the Rotator cuff and Patellar tendon, cases of tendon rupture can also happen^{54,55}. In most of the ruptured tendon, degeneration is found, and as Arner et al. reported, degeneration was observed in all of their seventy-four patients with an Achilles tendon rupture⁵⁶. Tendon degeneration leads to a reduction in tensile strength, which can significantly reduce the force tendon tissue can sustain. Studies done by Tallon et al. showed that in the ruptured tendon, a higher level of degeneration was observed than that in chronic pain tendon⁵⁷. Currently, tendon rupture is generally treated with surgical options. Patients receiving surgical treatment will still suffer from long and painful recovery⁵⁸. In the past decades, a significant amount of effort has been made to better understand the molecular pathology, aetiology and the mechanism of tendon matrix remodelling, which can be used as the guideline for the research of new therapeutic treatment for tendinopathy and tendon rupture^{51,59,60}.

- The natural healing process of tendon tissue

The normal steady-state conditions of tendon tissue are maintained by a combination of cell and matrix turnover. Results from methods to measure tendon turnover indicated half-life values from two months to over a hundred years, which suggested tendons have very low turn over and thought to have limited their healing potential^{61,62,63}. Recently, a study was conducted to examine tendon turnover in human volunteers of different ages⁶⁴. Their findings suggested that collagen synthesis occurs primarily during age 0-17, and there is no significant tendon tissue turnover at later stages. Though tendons have low turnover, they are highly sensitive to mechanical stimulation and injury. Tenocytes activity increases during exercise, as well as collagen production and cell proliferation^{65,66}. This suggests that tenocytes can respond to changes in physical activity, and is an active participant in the maintenance of tendon tissue. Similar to exercise stimulation, tendon tissue can also respond to damage and injuries and initiates a natural healing process which is critical in tendon repair. The tendon healing process consists of three phases (figure 1.6).



A summary of changes in tendon healing

	Inflammatory stage	Proliferation stage	Remodelling stage
Cellular and Matrix Changes	Tenocyte proliferation ↑ Monocytes ↑ Neutrophils ↑ Platelets ↑	Type III collagen ↑ Matrix protein production ↑ Tenocyte proliferation ↑	Cellularity and matrix protein ↓ production Type III collagen ↓ Type I collagen ↑
Cytokine involved	IL-6 bFGF IGF-1 PDGF TGF- β VEGF	bFGF IGF-1 PDGF TGF- β VEGF	IGF-1 TGF- β

Figure 1.6 The tendon healing process in human and a summary of cellular and matrix changes in tendon repair.

In the initial inflammatory phase, commonly referred to as the first 24-72 hours after injury, erythrocytes and inflammatory cells such as neutrophils, monocytes and macrophages enter the site of the injury⁶⁷. Angiogenic factors are released to initiate the formation of a new vascular network, for vascular response is vital to avoid the diminution of blood supply at the site of injury⁶⁸. Other changes including increased release of cytokines, stimulation of tenocyte proliferation and involvement of more inflammatory cells, all in favour of tendon tissue repair and generation of new fibrous tissue⁶⁹. With the immigration and generation of more tenocyte, the type III collagen synthesis is also initiated⁷⁰.

The second phase is called the proliferation phase or repair phase where the tenocyte continues to proliferate, synthesis of type III collagen peaks and lasts for a few weeks. Production of other proteins proteoglycans and glycosaminoglycans is maintained at a high level as well. The synthesised type III collagen, proteoglycans and glycosaminoglycans, which are the main components of tendon ECM, are arranged in a random pattern⁷⁰.

The third phase referred to as remodelling phase, can be divided into two stages: the consolidation stage and maturation stage. During this phase, proteins and tendon ECM are resized and reshaped⁷¹. In the consolidation stage, tenocyte metabolism remains at a high level while tenocytes and collagen start to align along the direction of stress. Also, a higher level of type I collagen is synthesized and aligned with tenocytes. This stage would last from six to eight weeks and the maturation stage then follows⁷². In the maturation stage, newly synthesized fibrous tissue gradually remodels to scar tissue in a period of over a year.

A variety of cytokines play vital roles in the healing process of tendon tissue. At the start of the repair, inflammatory cytokines such as interleukin are produced by inflammatory cells. Later in the proliferation phase, a good number of cytokines including basic fibroblast growth factor (bFGF), Bone morphogenetic protein (BMP), insulin-like growth factor-1 (IGF-1), platelet-derived growth factor (PDGF), vascular endothelial growth factor (VEGF) and transforming growth factor beta (TGF- β) all contribute to the repair of tendon tissue. The changes in the tendon healing process have been summarised in figure 1.6.

It is suggested that the combination of the extrinsic and intrinsic cellular mechanisms is behind the tendon healing process^{68,73}. The intrinsic route involves the proliferation of epitenon and endotenon tenocytes typically. These intrinsic tenocytes contribute to the tendon repair by secretion of a large amount of protein, especially collagen, to reconstruct tendon ECM⁷⁴. The extrinsic route is that fibroblasts and inflammatory cells from blood vessels and circulation attach to the injury site and provide cytokines and secreted proteins⁷⁵. However, the extrinsic route does contribute to the repair of damaged tendon tissue; it also results in the formation of adhesion, and a large amount of disorganised tissue referred to as scar tissue.

In most of the patients, the post-injury tendon usually does not fully regain the mechanical properties. In figure 1.7 is demonstrated a comparison of the post-injury tendon with the healthy tendon. The left side of the figure shows the anatomy characteristics of the healthy tendon tissue. It is shown that collagen fibres are tightly bundled and aligned, supported with organised vascular systems in the connective tissue around tendon tissue. On the right side of the figure is demonstrated the tendon after injury. Thinner and disorganised collagen fibres are surrounded by an excessive number of proteoglycans (shown in yellow and blue)⁷⁶. The post-injury tendon tissue is found to have a higher level of type III collagen than type I, which is believed to be related to the formation of scar tissue. As the major component of scar tissue is type III collagen which is thinner and weaker than type I collagen, it has a reduced mechanical property and therefore, would cause the reduction of the tensile strength of tendon tissue⁷⁷.

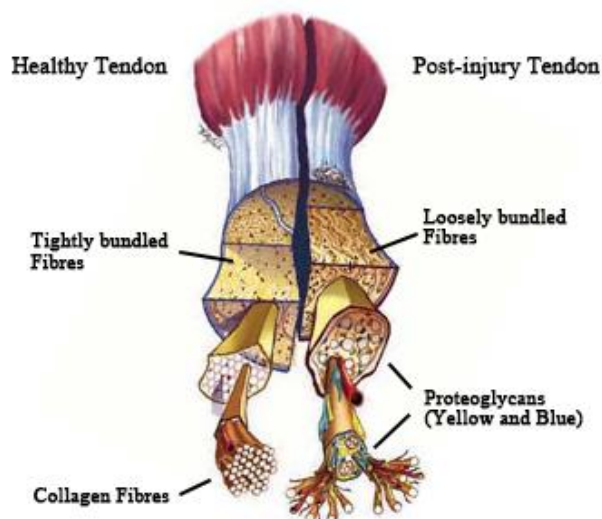


Figure 1.7 A schematic illustration of normal tendon anatomy (left) compared to healed tendon after injury (right). Figure adapted from Scott et al.⁷⁶

Due to the formation of scar tissue and disorganised collagen fibre, healed tendon tissue is found to be weaker compared with the healthy tendon⁷⁷. The weakened mechanical property may expose the repaired tendon to a higher risk of re-injury⁷⁷.

- Changes in the molecular level of tendon tissue

The molecular changes in damaged tendon tissue can serve as a guideline for researchers to better understand the mechanism of tendinopathy and tendon natural healing. Tendon matrix is a highly complicated structure and consists of multiple different components. In tendon matrix, the primary composition includes collagen proteins, proteoglycan and glycoprotein. Cytokines like a variety of growth factors and enzymes that affect the hydrolysis of the tendon matrix are also found to be regulated in damaged tendon tissue⁵⁹. The research conducted by Riley et al. showed the changes in molecular composition in injured tendon tissue⁵¹. As shown in table 1.1, there is a significant increase in collagen type I and III gene expression, especially type III collagen, in tendon matrix.

Table 1.1 Changes of structural molecules, Enzymes, Cytokines and signalling factors expression level in tendinopathy matrix. The table is adapted from Riley et al.⁵¹

In matrix		Cytokines and signalling factors	Enzymes	
Collagen type I	↑	TGF-β	↑	MMP1,2,9,19,23,25 ↑
Collagen type III	↑	IGF-I	↑	TIMP1,3 ↑
Fibronectin	↑	VEGF	↑	MMP3,7,10,12,27 ↓
Tenascin C	↑	PGE2	→	TIMP2,3,4 ↓
Aggrecan	↑	BMP	↑	
Biglycan	↑	Glutamate	↑	
Versican	→	Substance P	↑	
Decorin	→	NMDAR	↑	
Pentosidine	↓	TGF-βR1	↓	
Dematin sulphate	↓	PDGFR	↑	

Also, an increased amount of type III collagen was found in tendinopathy tendon matrix⁷⁸. Collagen is one of the most important proteins that comprise of the tendon; changes in collagen level after tendinopathy may indicate a possible therapeutic target for tendon treatment. The level of glycosaminoglycan, tenascin C, aggrecan, biglycan, chondroitin sulphate proteoglycans is increased in tendon matrix which is consistent with a healing process⁷⁸. Changes in the level of a family of enzymes called matrix metalloproteinases (MMPs) also draws attention. The matrix metalloproteinases (MMPs) are a family of enzymes responsible for the degradation of the tendon matrix in both healthy and diseased tendon. There are 23 types of MMPs in human and four

naturally occurring inhibitors known as tissue inhibitors of matrix metalloproteinase (TIMPs)⁵¹. In ruptured tendon, expression of MMP1, MMP9, MMP19, MMP25 and TIMP1 is increased, and expression of MMP3, MMP7, TIMP2, TIMP3 and TIMP4 is decreased. In chronic pain tendon, reduced the level of MMP3, MMP10 and TIMP3 was observed along with the increased expression of MMP23⁵¹.

One of the most critical kinds of molecule in tendon regeneration are growth factors. Growth factors are released from platelets, polymorph nuclear leukocytes and macrophages. They transmit a specific signal or message to cells⁷⁹. Growth factor binds to the specific receptor on the membrane of cells and then activates a series of biochemical reactions that result in collagen synthesis, fibroblast proliferation and overall tendon matrix remodelling^{9,59,80,81}.

1.1.4. Current Treatment and Novel Strategy

- Current Treatments

Currently, several conventional therapies have been applied to the healing process of tendon tissue. Different treatments are applied to different levels of injuries. For minor injuries, movement management and physical therapy can be used to control the damage and prevent further deterioration of injuries. For patients who experience pain and swelling, non-steroidal anti-inflammatory drugs (NSAIDs) are given for pain management in a clinical situation. It is reported that the overuse of NSAIDs and steroids might increase the chance of tendon injury, but this lacks sufficient supporting evidence⁸². For those who suffer from chronic or severe pain, or even a ruptured tendon, a surgical option may be applied⁸³. A summary of current treatments and new therapies in development is shown in table 1.2.

Table 1.2 A summary of current treatment for tendinopathy. Table adapted from G. Riley⁵¹. Note that this table summarises therapy for tendon chronic pain only. Now therapy for tendon rupture and tears is limited to a surgical operation.

Treatment	Putative target or mode of action
Rest or modification of activity	Removal of precipitating factors and prevention of reinjury
Orthotics	Removal of precipitating factors and prevention of reinjury
Cryotherapy	Reduction of acute inflammation and decrease in cell metabolism
Heat treatment	Stimulation of cell activity and to increase blood flow
Physiotherapy	Stimulation of cell activity and to increase blood flow
Electrical stimulation	Reduction of pain perception, stimulation of blood flow and increase in cell activity
Laser treatment (pulsed or continuous)	Possible analgesic effects and unspecified (unknown) effects on cell activity
Pulsed electromagnetic fields	Possible analgesic effects and unspecified (unknown) effects on cell activity
Ultrasound shock wave	Thermal effects on tissue, stimulation of cell activity and increased blood flow
NSAIDs	Reduction of inflammation through inhibition of prostaglandin synthesis

It's shown that most of the treatments for tendinopathy now is physical modality-based, which includes ultrasound shock wave, pulsed magnetic fields therapy and laser therapy. For minor injuries, the physical modulated therapies show a positive outcome in managing the symptoms⁷⁹. A controlled amount of exercises can be beneficial as well. Exercise is vital in both prevention and treatment of tendinopathy, but a report showed that in clinical trials there was little evidence supporting this is beneficial for the patient. Apart from physical exercise, medication has been applied as well. The use of NSAIDs in clinical treatment for tendinopathy has been employed for several years, and it was proved helpful for reducing the pain and inflammation. However, NSAIDs can only be used as a short-term pain and inflammation management approach. For some cases, when medication and movement management proved to be little help, a surgical operation is applied. However, patients treated in this way have to endure a very painful postoperative recovery and have a high chance of re-rupture rate⁵¹. In conclusion, the current conventional treatments are not sufficient for treating tendinopathy and tendon rupture (particularly to enhance the tendon regeneration). Scientists are looking for an alternative approach for curing this condition, and several new therapeutic approaches come into sight.

- Advanced Treatment Strategies for Tendon Injury

Conventional treatments for tendinopathy might not be sufficient for the proper healing of tendon tissue. Alternative approaches for the treatment of tendinopathy are urgently needed. In the past decade, significant developments have been made in the

understanding of tendon and tendinopathy, and new therapeutic strategies have been developed. Some of the strategies involve the use of growth factors and morphogenetic proteins (PDGF, TGF- β , FGF, and IGF-1). Other approaches include the use of gene therapy and gene delivery.

- Growth factors in healing tendon

Varieties of growth factors were found related to tendon healing and regenerating processes, including insulin-like growth factors (IGFs), platelet-derived growth factors and their receptors (PDGFs and PDGFRs), transforming growth factors (TGFs), Fibroblast growth factors (FGFs) and vascular endothelial growth factors (VEGFs). Different growth factors play different roles in tendon matrix healing and remodelling⁸⁴.

However, there are limitations to some of these treatments including the high cost of manufacture, lack of an efficient delivery system and difficulty in purifying the product. These problems have limited the application of growth factors and morphogenetic proteins as the treatments for tendinopathy. However, it is possible to produce endogenous growth factors and morphogenetic proteins and develop a therapeutic strategy accordingly. Gene therapy, as a potential therapeutic strategy for tendon injury, might achieve up-regulation production of these further improve the healing of tendon tissue.

1.2. Gene Therapy for Tendon Injury

1.2.1. Introduction of Gene Therapy

The term “gene therapy” was first reported by Clyde E. Keeler in 1947, where it was described as “the correction of gene-based deviations in plants and animals”⁸⁵. Subsequently, the concept has been extended to include the isolation or design, synthesis and introduction of genes into defective cells, tissue or organs^{86,87}.

The first attempt of exogenous gene delivery into human recipients was performed by Stanfield Rogers in 1970, who administrated the native Shope rabbit papillomavirus to three German siblings with a purpose of treating arginase deficiency^{88,89}. Though no satisfactory result was achieved in this trial, it is considered as the first anticipation of the potential of viral carriers.

In July 1980, another human trial led by Martin Cline attempted to treat β-thalassemia. The bone marrow cells from patients were extracted and translated with plasmids encoding the β-globin gene and the herpes simplex virus thymidine kinase (HSVtk) gene before being transplanted back into the patients. Unfortunately, this study ended with neither good nor harmful results but was criticised for ethical reasons⁹⁰.

Another decade later, in the early 1990s, Rosenberg led a trial to treat patients with advanced melanoma with lymphocytes marked with the *Escherichia coli* neomycin phosphotransferase gene using retroviral vectors. This is reported to be the first case of using a marker gene to observe the biodistribution of transgene cells⁹¹.

In the past decade, one historical event marked the beginning of a new era, for the first veterinary gene therapy vaccine, RABORAL V-RG which is a recombinant vaccinia virus in which the thymidine kinase gene has been replaced by the glycoprotein G of the rabies virus, was approved. This vaccine helped to reduce the rate of rabies in wildlife, pets and livestock and is suggested to be the predecessor of a series vaccines⁹².

Though great advances in gene therapy have been achieved, discouraging news was announced in September 1999, when Jesse Gelsinger died in the gene therapy clinical trial for liver genetic disease ornithine transcarboxylase deficiency using adenoviral vector. Other patients enrolled in the trial were also affected with minor myalgias, fever and biochemical abnormalities⁹³. It is suggested that the patients, including Jesse Gelsinger, suffered from vector toxicity. This is the first case of patient death in clinical trials and laid a shadow over the whole field of gene therapy⁹³.

The death of Jesse Gelsinger raised awareness towards the safety of gene therapy along with many other issues. It was realised that many obstacles must be overcome before gene therapy becomes practical for clinical application. Also, this incident led to the questioning of whether gene therapy could fulfil the expectation that was once promised. Undoubtedly, it was also realised that efficiency, safety and ethical issues were all important aspects of a delivery system. Although the research progress in gene therapy had been difficult and experienced several setbacks, there is no denying that the advances in the field of gene therapy and gene transfer offer an unprecedented possibility for the treatment of numerous diseases and may alleviate the suffering of a great many patients.

Nowadays, gene therapy refers to the cell delivery of a gene-expressing unit that can promote the transcription of RNA. The transgene unit normally contains a promoter, gene of interest and a polyadenylation signal. The therapeutic gene unit not only needs to cross the cell plasma membrane but also needs to penetrate the cytosol and find its way into the nucleus. Upon reaching the target cell genome, or in some cases the transgene unit is capable of replicate and express independently, the gene of interest is transcribed into RNA. The RNA either displays a therapeutic effect by itself or encodes a protein or peptide that itself is therapeutically active. In addition to gene therapy, Scherman et al. proposed the term “genetic pharmacology”, which refers to “the use of short synthetic oligonucleotides to manipulate gene expression” and principally includes the use of antisense RNA, anti-gene, or RNA-interfering strategies⁹⁴. Genetic pharmacology involves the use of short single-strand oligonucleotides as a therapeutic agent, which is distinguished from a classic small chemical base therapeutic strategy. The oligonucleotide employ as the therapeutic agent is typical with a length of around 20 base pair which is necessary to ensure the target specificity and capability of recognising the target through the Watson-Crick hydrogen bonds between base pairs. Genetic therapy involves the delivery of small oligonucleotide molecules as a therapeutic agent that target DNA or RNA strands, which differs from gene therapy and small molecule drug delivery, for later ones deliver a self-expressive DNA unit and small molecules targeting proteins, respectively. The distinction between gene therapy, genetic pharmacology and small molecule drug delivery is displayed in figure 1.8.

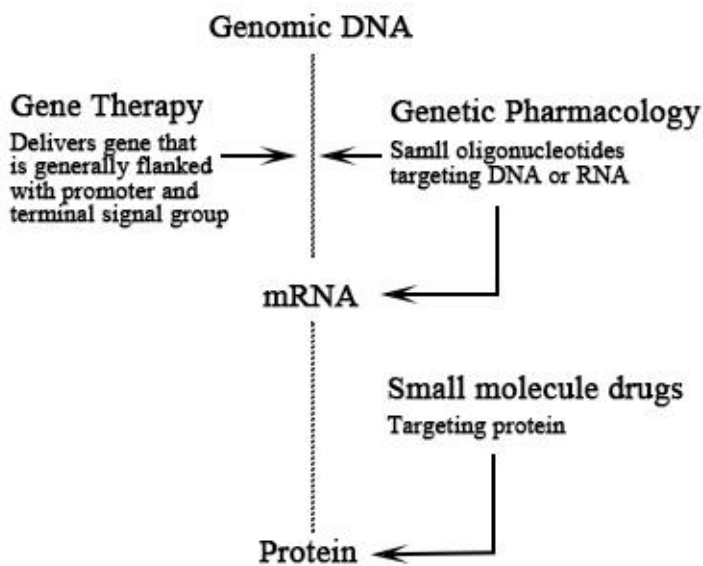


Figure 1.8 Gene therapy involves the use of a gene-expressing unit (composed of a promoter, gene, and termination signal), while small molecule (chemical) drugs target proteins, short oligonucleotides used in genetic pharmacology generally target DNA and/or RNA.

Though gene therapy and genetic pharmacology have been distinguished from each other by Scherman et al., it has been acknowledged that other authors employ the term “gene therapy” to all strategies implying the use of any oligonucleotide molecule⁹⁴.

Several advantageous properties render gene therapy indispensable for the treatment of a variety of disease. Based on the progressive understanding of genetic control over cellular activity and gene-disease activity relationship, also with the identification of the gene involved in disease development, gene therapy may provide exceptional opportunities to cure the currently untreatable conditions or considered as an exceeding alternative of the existing therapeutic strategies⁹⁵.

First of all, gene therapy is able to grant treatment to any diseases that are caused by the deficiency of gene or protein expression. For instance, this is the case for alpha-1 antitrypsin deficiency which causes patients to suffer breathing difficulties due to the lack of alpha-1 antitrypsin, which is a protein serves as a protective agent for lung tissues. Another example is Duchenne muscular dystrophy, for which the vital expression of dystrophin protein in the muscle cytosol is missing⁹⁶.

Secondly, the delivery of protein may lead to variations in concentration. This can cause uncertainty in dosage in the target tissue and can induce toxicity when protein levels reach excessive concentrations. An example of such was observed in the treatment of

haemophilia where the administered protein, recombinant clotting factors, is lower than the therapeutic threshold due to its short half-life⁹⁷. On the other hand, gene therapy, unlike recombinant protein therapy, could provide a constant expression of missing protein when the delivered gene is controlled by a permanently activated promoter. In addition, gene delivery provides the advantage of long-term protein release and availability, reducing the need for multiple injections of exogenous factors.

Another advantage of gene therapy comes from its specificity when the transgene unit is designed properly to obtain spatial control of its effect. Approaches including local delivery of therapeutic gene delivery unit or using a tissue or cell-specific vector, the expression of the desired protein could be restricted to a certain organ, tissue, even a specific cell type. Immune responses are frequently overserved in the delivery of missing protein in gene deficiency for it is considered to be exogenous by the host. By using gene therapy, one could avoid immune responses by restricting transgene expression to cell types with less antigen presence.

To conclude, gene therapy is a powerful and promising therapeutic strategy with many advantages. It might be used 1) to treat gene deficiency disease by compensating of the missing protein 2) to enhance the expression of a protein factor or cytokine 3) to trigger an apoptosis gene in the treatment of cancer 4) to inhibit or suppress the expression of a given protein. There are many studies and research that can be listed as examples as the prove of gene therapy application.

For instance, gene therapy can be applied in the treatment of Haemophilia A and B. Haemophilia A and B are congenital bleeding disorders caused by a deficiency of functional clotting factor, FVIII and FIX, respectively. Current therapy for haemophilia is largely dependent upon the delivery of protein substitution, generally recombinant or plasma-derived clotting factors FVII and FIX⁹⁷. The short half-life of the clotting factors results in the demand of a relatively higher dosage to compensate the losses, and a higher frequency of infusion is also necessary. In some cases, patients produce antibodies that neutralise the injected clotting factors which reduces the efficiency of further therapy⁹⁷. Gene therapy as a potential alternative treatment strategy might address the issues of conventional protein delivery. Studies on haemophilia animal models (mice and dogs) using adenoviral vectors that contains Factor VIII or FIX encoding gene has been reported, and the results confirm a robust clotting factor expression level with limited toxicity^{98,99}. Similar pre-clinical studies have used

lentiviral vectors to achieve long-term FVIII expression¹⁰⁰. Though proven efficient in pre-clinical studies, the administration of adenoviral vectors encoding FVIII in a phase I clinical trial stimulated an inflammatory response and was ceased to stop⁹⁷. These might have indicated the selection and use of appropriate delivery method should be considered before administration.

Another example is the use of gene therapy in the case of Duchenne muscular dystrophy (DMD) therapy. DMD is a genetic disease caused by the lack of functional dystrophin protein, controlled by genes on the X chromosome, in skeletal muscles. The symptoms of DMD include the weakness of muscle, especially upper arm muscles and the muscles of the hips and thighs¹⁰¹. Until recently, the most advanced gene therapy for this disease being developed is the use of antisense oligonucleotides to mask certain RNA sequence motifs on the pre-messenger RNA, which is called exon-skipping, so that formation of the spliceosome on the target exon is inhibited and the target exon is excluded from the mature gene transcript¹⁰¹. The exon-skipping should be able to restore the read frame of the DMD gene and in fact, as Graham et al. and Arechacala et al. reported, it did restore the expression of dystrophin in cultured DMD patient cells and in DMD disease animal models^{102,103}. On the basis of pre-clinical studies on the treatment of DMD, phase I clinical trial of the DMD exon skipping treatment has been undertaken. In phase I trial, levels of detectable dystrophin protein at 3-15% of normal levels were observed in patients four weeks after administration, and no adverse events were observed¹⁰⁴.

1.2.2. RNA Interference

The RNA interference (RNAi), as one of many gene therapy approaches, has progressed significantly in recent years. The RNA interference (RNAi) is “a process of sequence-specific posttranscriptional gene silencing induced by double-strand RNA (dsRNA)”¹⁰⁵. This biological phenomenon was initially described in insects, plants and fungi¹⁰⁶. However, only after the work of Fire and Mello in *Caenorhabditis elegans* was awarded for a Nobel-prize, it was suggested that a potential post-transcriptional gene silencing effect, referred to as RNAi, exists¹⁰⁵. Subsequent research on the use of synthetic RNA duplexes of 21 base pairs as RNAi triggers in mammalian cultured cells confirmed the possible utilisation of short double-stranded RNAs to mediate knockdown without activating cellular immune response (base pair of <30)¹⁰⁷.

Recently, the U.S. Food and Drug Administration (U.S. FDA) and the European Medicines Agency both approved Patisiran, which is an intravenously administered RNAi therapeutic targeting transthyretin (TTR) for the treatment of hereditary ATTR amyloidosis. Patisiran blocks the production of transthyretin by targeting and silencing the specific messenger RNA in the liver, reducing its accumulation in the tissues in order to stop or slow down the progression of the disease. No doubt, the approval of Patisiran is a piece of strong evidence that proves the clinical value of RNAi and this incident would inspire researchers in the field related to RNAi worldwide.

The mechanism of exogenous RNAi-mediated knockdown depends on the use of the guide strand RNA that is complementary to the target mRNA called RNAi Triggers, which includes small interfering RNA (siRNA), microRNA(miRNA) and small hairpin RNA (shRNA). A small hairpin RNA is a synthetic RNA molecule with a hairpin structure and can be used to silence target gene expression via RNA interference¹⁰⁸. The expression of shRNA in target cells normally requires the use of an expression vector, such as a plasmid, with appropriate transmembrane RNA delivery. Expressed shRNA requires the further process by the ribonuclease Dicer into smaller mature dsRNAs before mediating the RISC dependent silence.

MicroRNAs (miRNAs) are endogenous non-coding dsRNAs that regulate gene expression through a mechanism that involves the inhibition of translation and transcript degradation and are related to the regulation of many basic cellular programs¹⁰⁹. It is found that miRNA molecule could trigger RNAi-mediated gene silencing, though most of the endogenous miRNAs in mammals are not fully complementary to their mRNA target. The genome produced long dsRNAs were processed by enzymes Drosha and Pasha to generate ~70 nucleotides long loop structured molecules call pre-miRNA. The pre-miRNA molecules were then processed in the cytoplasm by enzyme Dicers to generate mature miRNAs which are around 22 nucleotides long^{110,111}. The mature miRNAs contain one guide strand, which is responsible for the recognition of mRNA templates and assist target mRNA cleavage, and one passenger strand which are degraded by enzymes in the late stage of the silencing process. MicroRNAs are responsible for the regulation of multiple biological functions and plays a vital role in differentiation and biological developments.

Small interfering RNA (siRNA) is a group of small dsRNA molecule of 20~25 base pair in length and are capable of triggering the RNAi-mediated silencing¹¹². Like miRNA,

the siRNAs contain one guide stand that is responsible for the recognition of mRNA templates and assists target mRNA cleavage and one passenger strand. In mammalian cells, most siRNAs are normally exogenous. The siRNAs are produced during the early stage of the RNAi process when larger exogenous dsRNA molecules are sliced by the Dicer into smaller fragments. Synthetic siRNAs were also used to trigger RNAi-mediated gene silencing with RNA delivery systems¹¹³.

RNAi processes start with the introduction of exogenous dsRNA such as shRNA into the target cell, followed by the encounter of dsDNA with RNase ribonuclease Dicer (demonstrated in figure 1.9). The Dicer is normally composed of one N-terminal helicase domain, one dsRNA-binding domain, one RNA binding Piwi/Argonaute/Zwille (PAZ) domain and two tandem RNase III domains¹¹⁴. The dsRNA sequence was processed into siRNAs and microRNAs(miRNA) of around 20-25 base pair. Note that exogenous siRNA sequences introduced into target cell do not require the process of Dicers^{112,115,116}. These smaller dsRNAs were involved in the formation of an RNA-induced silencing complex (RISC). RISC is a ribonucleoprotein complex composed of Argonaute proteins (Ago), dsRNA template and complementary target mRNAs. The Ago protein family plays an important role in the process of RNAi due to the presence of the PAZ domain and Piwi domain in its structure¹¹⁷. The PAZ domain of Ago protein can engage siRNA or miRNA, and the Piwi domain adopts an RNase H-like structure that is related to the cleavage of the guide strand. The siRNA or miRNA is unwound by RNA helicase to form a guide strand (antisense) and a passenger strand (sense). The guide strand directs the cleavage of target mRNA while the passenger strand is degraded during RISC activation¹¹⁸. The target mRNA is cleaved at its phosphodiester bond which is positioned between nucleotides 10 and 11, resulting in a decrease of expression of the target gene¹¹⁹.

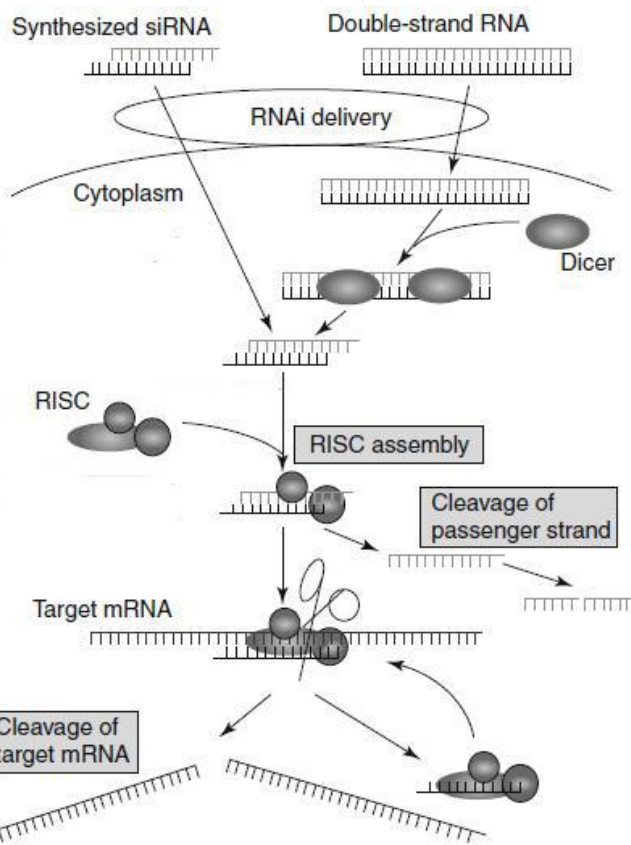


Figure 1.9 Mechanisms of RNA interference. Double-stranded RNA (dsRNA) molecule first binds to a Dicer protein, which cleaves it into small interfering RNAs (siRNAs). These siRNAs bind to the RNA-Induced Silencing Complex (RISC), which separates the siRNAs into two strands. The passenger strand is degraded while the guide strand serves as a template, which guides RISC to complementary RNA targets.

Delivery of RNA molecules showed great potential both as an experimental tool and a therapeutic application. RNAi can create repression of a specific gene and one can observe the gene-specific deficiency effect and study the role of certain genes in the development of the disease. With the advanced understanding of the role genes play in diseases development, novel treatment approaches could be developed. For example, Urban-Klein et al. reported a significant reduction of tumour growth in the animal model treated with HER-2 receptor specific siRNA- Polyethylenimine polyplexes ¹²⁰. It is clear that RNAi and delivery of RNA molecules will continue to contribute to the understanding and treating of many diseases.

1.2.3. Obstacles to Overcome in Gene therapy

Though gene therapy shows unprecedented potential in the treatment of many diseases, many scientific obstacles must be overcome before it is clinically practical for therapy.

- Vector Toxicity and Immune Response

The case of Jesse Gelsinger's tragic death is an example of an adverse effect in gene therapy that was caused by vector toxicity. The post-mortal autopsy showed that substantial amounts of the viral vector had accumulated in the spleen, lymph nodes and bone marrow and subsequently triggered a severe inflammatory response that led to intravascular coagulation, acute respiratory disorders and multiorgan dysfunction ¹²¹. Other patients administrated with similar dosages showed tolerance against the adenoviral vector, or at least showed less severe adverse effects compared to Jesse Gelsinger.

Viruses, whether wild type or specifically engineered with therapeutic genetic information, have a high chance of triggering the immune defence system of the human body. All viral vectors showed degrees of immunogenicity, while Adenovirus vectors showed the most among all, and overcoming the immunogenicity of viral vectors. The capsid of the viral vector could induce the virus-neutralizing antibody responses as well as the cytokine-mediated inflammatory responses. Also, the transgene product expressed by the transduced cells could trigger the cytotoxic T-lymphocyte response^{122,123}. Another factor that affects the toxicity is the vector dosage. Studies have shown evidence that the inflammatory response measured by immunohistochemistry have increased linearly in response to increased viral vector dose¹²⁴.

To address this issue, various strategies have been developed. Elimination of the original viral genome from the vectors can reduce the cytokine response, though capsid-mediated inflammatory response was still detected^{99,125}. Studies focused on the dose-escalation pointed out that the relationship of viral vectors and an immune response is characterised by a threshold theory: when administrated vectors exceeded a threshold limit, the cellular toxicity increases dramatically and induces severe cellular injury¹²⁶. Other approaches include the use of a less toxic vector system such as lentivirus vector or Adeno-associated virus vectors. The development of non-viral vector as an alternative for viral vectors has advanced greatly in the recent decade, and compared to viral vectors, non-viral vectors showed much lower toxicity and immunogenicity at the cost of transfection efficiency¹²⁷.

Besides vector-caused immune response and toxicity, the oligonucleotides themselves could be considered as exogenous pathogens and trigger immune response through the

activation of Toll-like receptors (TLRs). Toll-like receptors are a family of protein receptors expressed in mammalian immune cells. Members of the TLR family are involved in recognition of pathogen-associated molecules, including flagella and exogenous nucleic acids. The siRNA triggered an innate immune response are mostly by the activation of TRL7 and TRL8¹²⁸. Not all the siRNAs could trigger the activation of TLR7 and TLR8 since the recognition of RNA molecules are sequence-dependent. It is suggested that RNA sequences rich in uridine-guanosine (UG) and adenosine- uridine (AU) could be more immunostimulatory^{129,130,131}. However, RNA sequence is not the only cause of immune response, for it is reported that RNAs lack of GU and UA rich sequences are also immune active¹³¹. The structure and length of RNA molecules could also determine its immunogenicity. Though both double strands and single strands RNA could trigger immune activity, it is suggested that in some cases the single strands acts as a stronger stimulator than double strands¹³¹. It is also reported that some RNA molecules, though rich in uridine, guanosine and adenosine, are poor stimulators of immune response due to their length (<20 bp)¹²⁸. These findings may have provided a guideline for design and selection of RNA molecules and the use of siRNA that are of short, double-strand molecules lacks GU- or AU- rich regions may provide silencing activity with low immunogenicity.

- Insertional Mutagenesis

In 2000, Cavazzana-Calvo and his colleagues reported a successful establishment of a functional immune system in three children patient suffering from human severe combined immunodeficiency (SCID)-XI disease. Haematopoietic stem cells were transduced with murine leukaemia virus (MLV) with a gene that encodes the γ -c chain cytokine receptor and transplanted back into the patients¹³². The γ -c chain cytokine receptor plays a vital role in cytokine signals recognition pathways, and without it, lymphocytes cannot mature into functional T cells and natural-killer cells¹³³. Based on this study, more patients received treatment for SCID-XI and achieved satisfactory results. However, two of the patients were later found to have developed a leukaemic disorder. It is because the retrovirus genome had inserted in the LIM domain only 2 (LMO2) oncogene during the transduction of stem cells. The insertional mutation activated the expression of LMO2 gene and caused the transduced cells to derive into cancerous T cells¹³⁴.

- Vector Specificity and Off-target Effect

Wild-type viruses are limited in the ability to infect certain organs and tissues due to the route of transmission, but the engineered or recombinant viral vectors are not. For instance, adenoviruses and AAVs do not normally infect cells in the central nervous system, but once injected into the brain, both vectors showed high transfection efficiency into neurones. This could be considered as both benefit and liability: from one perspective, viral vectors showed less restriction in transfection; from another perspective, this could also lead to undesired cellular uptake by non-target cells in organs and tissues in systematic administration. Even in local administration, there is a risk of leakage and dissemination to other tissues and organs.

Another obstacle is the off-target effect in gene therapy, especially in RNAi-mediated gene silence. The first recognition of the siRNA off-target effect was observed in 2003 by Jackson et al.¹³⁵. While using several different siRNAs to target the same gene, different siRNAs treated groups showed unique results in microarray expression profiling. The off-target transcripts were analysed and strikingly, some of the transcript shares only 8 nucleotides(nt) of complementarity of the siRNA sequence. This is due to the partial sequence complementarity between the 3' untranslated region (3' UTR) of the off-target mRNA and the 5' of the small RNA molecule guide strand seed region. The seed region refers to the positions 1~8 at the 5' end of the sequence in the guide strand of small RNA interference molecules, and it plays a vital role in target recognition ¹³⁶. Since microRNA are mainly endogenous encoded non-coding RNAs that regulate hundreds of mRNA expression, the off-target effect is more commonly observed in miRNA mediated silencing. However, since siRNA and miRNA share the silencing mechanism, the off-target effect in siRNA mediated silencing should not be neglected.

- Barriers in intracellular delivery

The cellular membrane preserves human genomic information and protects it from damage and contamination¹³⁷, yet it also creates barriers for the delivery of DNA and RNA molecules. For the delivery of antisense oligonucleotides (such as siRNA and miRNA) and ribozymes intended to reach cytoplasm where the therapeutic molecular mRNA is located¹³⁸. And for the delivery of plasmid DNA, antigenic oligonucleotide and therapeutic gene sequence, it requires entry into nuclear before it could be

therapeutically active¹³⁹. Several inherent factors including charge, size and stability of nucleic acids molecules present possible barriers to its intracellular delivery. The electrostatic repulsion between the negatively charged cell membrane and the negatively charged nucleic acids (due to the phosphate backbone) is the primary cause of inefficient cellular association. The delivery of large DNA molecules such as plasmid DNA is found more difficult compared with smaller molecules such as siRNA. Besides, the nucleic acids have low stability *in vivo* and can be rapidly degraded by hydrolytic nucleases. Those molecules that do obtain intracellular access are still susceptible to degradation. Upon internalisation, DNA and RNA molecules are up-taken by endosomal vesicles where they can be degraded. The acidic environment of endosome promotes the hydrolysis and activates the lysosomal enzymes that can degrade DNA and RNA molecules. The barriers in the delivery process are demonstrated in figure 1.10.

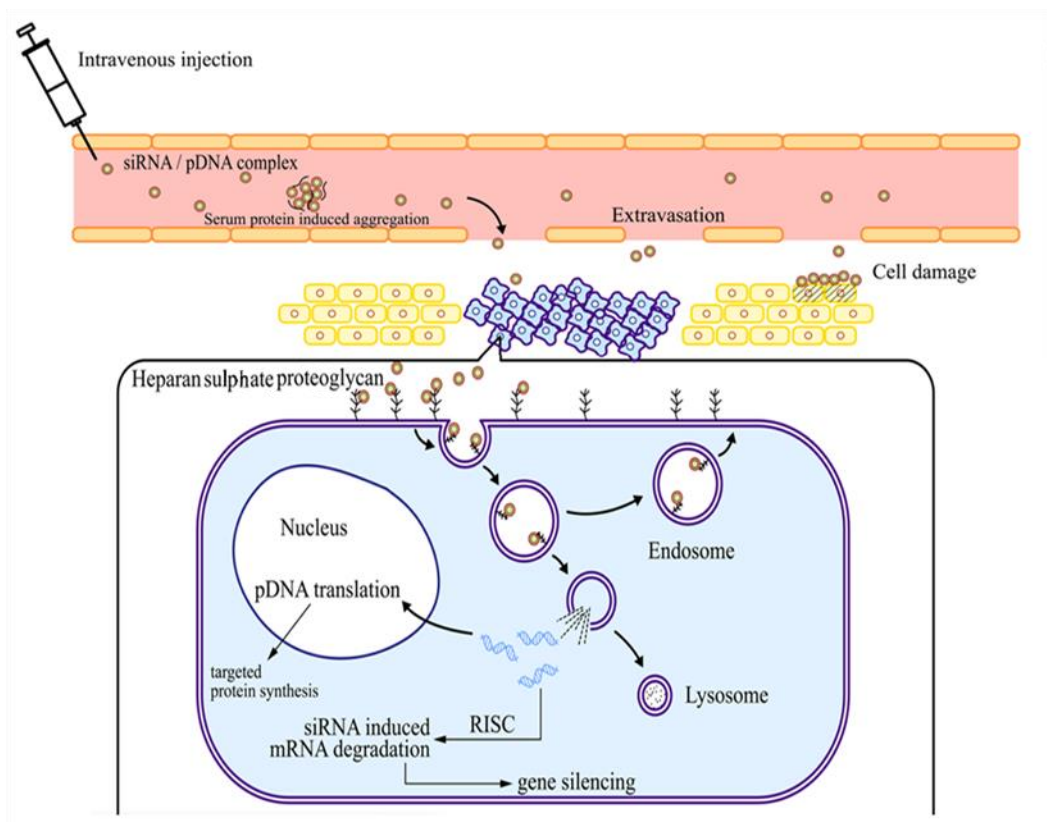


Figure 1.10 The barriers in siRNA/DNA delivery using cationic carriers from the administration site to the target site. The figure is adapted from Luo et al.¹⁴⁰

Therefore, suitable and efficient methods of DNA and RNA intracellular delivery is one of the key steps in successful gene therapy. Current nucleic acid delivery methods can be classified into three categories: Electrical methods, Mechanical methods and Vector-based methods.

Examples of mechanical methods include microinjection and particle bombardment. High transfer efficiency is achieved in microinjection at the cost of time since the gene is precisely injected into one target cell at a time¹⁴¹. Particle bombardment, or more commonly referred to as “gene gun” is to use a device powered either by pressure to shoot a payload composed of a heavy metal particle with genetic materials into the target cell or tissue. Though it is a direct and highly efficient method of delivery DNA and RNA, it is suggested to be uncontrollable, for the payload is introduced randomly into the target cells. Electroporation is an example of electrical methods used in gene delivery. It uses high voltage electrical current to increase the permeability of the target cell membrane and further facilitate the gene transfer. Though highly effective, reported to be ten times more effective than chemical-stimulated permeabilisation, it is accompanied by high cell mortality. It is well established that electrical methods and mechanical methods have achieved high transfer efficiency. However, it is also considered to be invasive and complicated for clinical situation¹⁴¹.

The use of a vector-based delivery system has received great many attention in the past few decades, and the field of vector-based delivery system has advanced dramatically. Various of vector-based delivery systems have been developed and studied to address the need for a safe, efficient and affordable intracellular delivery method in gene delivery. In the past few decades, various vectors, both viral and non-viral, were developed and studied for the transfecting ability, toxicity, biocompatibility and other characters¹⁴². However, there has been a heated debate on the use of the viral and non-viral delivery system, for both possess advantages and disadvantages that would provide the application with different challenges.

1.3. Viral and Non-Viral Delivery Systems

1.3.1. Viral Delivery Systems

It is difficult to directly use the genetic material as a therapeutic molecule without an efficient delivery system because naked DNA and RNA molecules cannot gain access into the cytoplasm. Therefore, to develop a safe and efficient delivery system that relies on the use of carriers (normally called vectors) to transport genetic material into target cells has become a primary objective for the utilisation of gene therapy. Since the early stage in the development of gene therapy technology, viruses have been widely used as

a carrier vector for gene transfer. Modification of virus vector included the removal of part of its original genome to prevent replication and added the sequence of a therapeutic gene to be expressed. Commonly used recombinant viruses include adenovirus, adeno-associated virus (AVV), retrovirus and lentivirus.

- Adenovirus Vectors

Adenoviruses are medium-sized, nonenveloped double-stranded DNA viruses with an icosahedral nucleocapsid and can infect a variety of vertebrate hosts. Adenoviruses used as delivery vectors are human adenoviruses that isolated from multiple sources including adenoids and conjunctiva of patients with upper respiratory disease or the faeces of infants with diarrhoea¹⁴³. There are more than 50 different adenovirus serotypes divided into subgroups A through E. In gene therapy, the most commonly used ones are serotypes 2 and 5 of the subgroup C, for the viral structure and biology is well studied, and the production of recombined subgroup C adenoviruses are therefore more convenient¹⁴⁴.

The structure of adenoviruses consists of an icosahedral protein capsid and one double-stranded DNA molecule that contains the viral genetic information. The icosahedral capsid is approximately 70 - 100 nm in diameter and is composed of 240 hexon capsomeres, and each capsomere is comprised of six hexon subunit which is formed by three copies of the 105kD hexon protein. The icosahedral structure has 20 faces and 12 vertices. Each vertex is formed by five units of penton base protein and three units of fibre protein and are adjacent to five hexon capsomeres. The fibre protein points outwards and interacts with a high-affinity receptor on the target cell membrane. Capsid protein IX, IIIa and VI are also found in adenoviruses structure, and their function is to interact with hexon capsomeres to stabilize the capsid structure. Inside the capsid situates the adenovirus genome which is a dsDNA molecule around 36,000 base pair¹⁴⁵. The dsDNA molecule is surrounded by capsid core protein VII, and at the 5' end of each DNA strand, a terminal protein is attached. The 3D structure and the schematic structure of the adenovirus is demonstrated in figure 1.11.

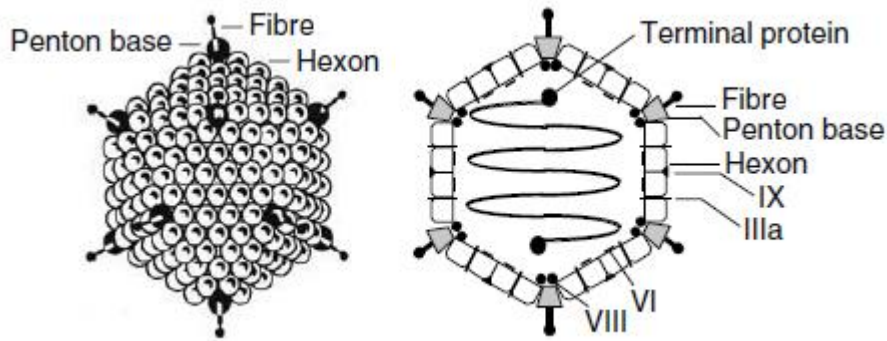


Figure 1.11 The 3D structure(right) and the schematic structure(left) of the adenovirus.

The internalisation of adenoviruses starts with the recognition of the fibre protein on the virus capsid by the coxsackievirus and adenovirus receptors (CARs) (figure 1.12)¹⁴³. The RGD sequences in the penton base protein interact with cell surface integrins $\alpha v\beta_3$ or $\alpha v\beta_5$ (for serotype 3 and 5 respectively). The adenovirus enters the cell through clathrin-mediated endocytosis and is rapidly released into cytoplasm after entering endosomes. The viruses in the cytoplasm proceeded quickly to the nucleus and were later transported onto microtubules. The virus capsid docks on the nuclear pore complex (NPC) and then the NPC dissociates the DNA from the capsid and imports the viral DNA into nucleus membrane¹⁴⁶. Though it is considered that hexon on the viral capsid plays a major role in the NPC-mediated DNA transport into the nucleus, there might be other unidentified factors involved in this process¹⁴⁷.

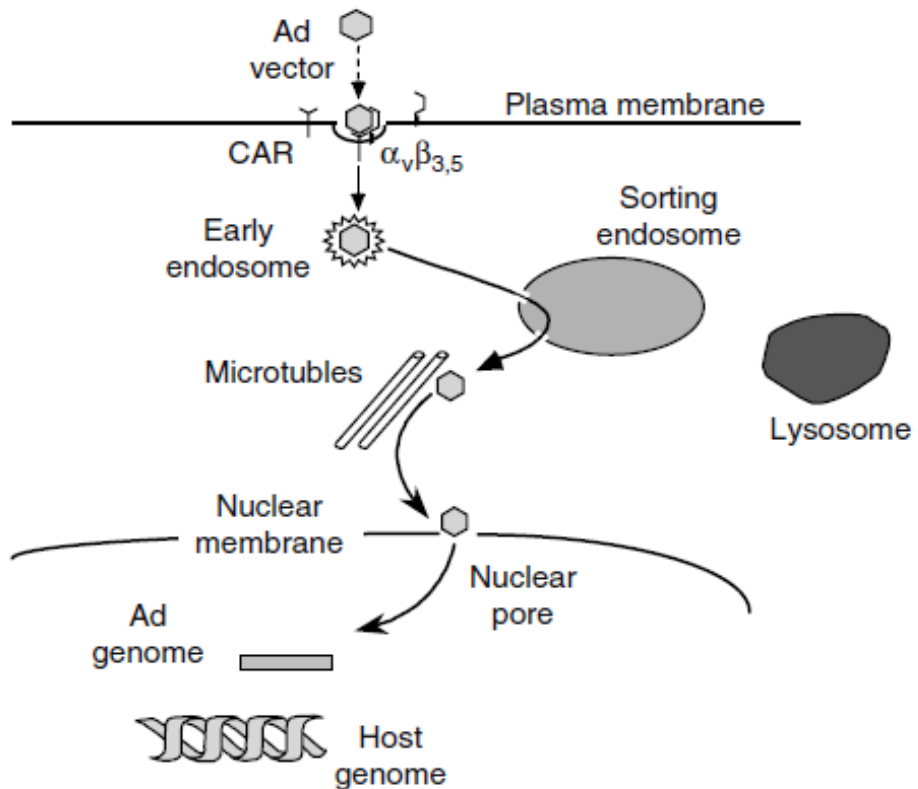


Figure 1.12 Internalisation of adenoviruses from the outside plasma membrane into the nucleus.

Adenoviruses have been widely used in gene therapy since the early stages in the gene therapy development, and nowadays adenoviruses-based vectors have been applied in the treatment of many diseases including cancer and genetic deficiency.

- Adenovirus-associated virus Vectors

Adenovirus-associated virus (AAV) is a small, DNA-containing virus that originally obtained in the laboratory preparation of adenovirus and is not related to the cause of any known diseases. It was later recognized as a different from adenovirus. The replication of AAVs are largely relying on the help of adenoviruses, but other viruses such as herpesvirus were also found to function as a helper for AAV replication, though much less efficient. AAV has a non-enveloped icosahedral symmetric structure and is about 20 nm in diameter. The capsid of AAV is composed of three types of the capsid protein, VP1, VP2 and VP3 with a ratio of 1:1:8. Inside the capsid contains a linear single-stranded DNA genome with a molecular weight of 1,500kDa. Each capsid is composed of 60 protein subunits and all the amino acid residues, except residues from VP1, could be detected on the structure. The capsid surface has a distinctive topology where three peak-like structures in each threefold icosahedral axis (figure 1.13). Each

peak is intergraded with two interacting protein subunits. The peak structure appears to be related to receptor binding interactions with heparin sulphate¹⁴⁸.

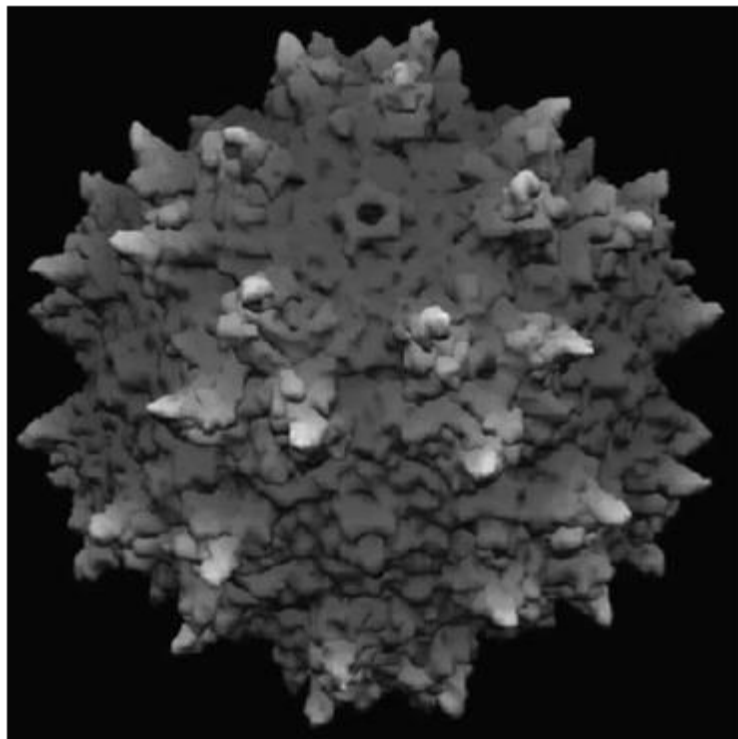


Figure 1.13 The structure of AAV determined by x-ray crystallography. Figure adapted from Xie et al.¹⁴⁸

There are 11 serotypes of AAV reported, and it is found that different serotypes of AAV are different in the ability to transfect cells and organs. Also, the route of administration and the capsid sequence of the AAV also contributed to its transfection ability.

For the majority of the AAV vectors, the internalisation of AAV into cells is mediated by endocytosis. Upon AAV surface protein binding to the heparin receptor, AAV is internalised by clathrin-mediated endocytosis^{149,150}. For different serotypes of AAV vector, clathrin-independent uptake was also found¹⁵¹.

Studies using fluorescently labelled AAV2 vector particles revealed that endocytosis could be mediated through $\alpha V\beta 5$ integrin/Rep dependent pathways¹⁵¹. After entering the cytoplasm membrane, the AAVs were delivered to endosomes. The escape of vectors from endosomes was suggested to be mediated by a latent phospholipase activity resident in the N terminus of VP1¹⁵². The escaped AAVs travel rapidly towards the nucleus and with the assistance of a helper virus, normally adenovirus or herpesvirus, they gain entry into the nucleus. Although the nuclear entry and uncoating of AAV

remain partially understood, it is suggested that it does not involve the use of the nuclear pore complex¹⁵³. It is also concluded that in the absence of helper virus, there is a reduction in the transportation of vector genome into the nucleus of the target cell¹⁵³.

AAV vectors have been developed into a delivery system for the treatment of many diseases including haemophilia B, muscular dystrophies and central nervous system diseases¹⁵⁴.

- Retroviral Vectors

Retroviruses are lipid-enveloped, single-stranded RNA viruses with approximate diameters of 100~200 nm. There are seven genera (*Alpha, Beta, Gamma, Delta, Epsilon, Lentivirus and Spumavirus*) in the *Retroviridae* family and that include many viruses widely related to a variety of diseases including cancers and acquired immune deficiency syndrome¹⁵⁵. Unlike other viruses with DNA genome, the genetic information of retroviruses is encrypted in the viral RNA genome and is reverse transcribed into a double-stranded DNA by reverse transcriptase upon uptake. The reverse transcribed DNA are subsequently delivered to the nucleus and is inserted into the host genome by the integrase protein. The virus genome inserted into the host genome, which is referred to as provirus, is expressed by the host cell protein synthesis machinery to produce viral proteins essential for the assembly of new viruses. The newly assembled immature virus particle is composed of a viral membrane, envelope protein (Env), Group antigen protein (Gag) that serves as major structural proteins, DNA polymerase (Pol) that serves as the replication enzymes, and the retroviral genome¹⁵⁶. Later in the maturation of viral particles, the Gag protein is cleaved by viral proteinase into capsid protein, matrix protein and nucleocapsid protein¹⁵⁷. The matrix protein is found to bind to the inner part of the viral membrane, while the capsid protein assembles into capsid that surrounds the nucleocapsid protein-RNA complex and enzymes critical for viral replication¹⁵⁸.

Within mature retroviruses, the capsids are found to be of different shapes and sizes. Lentiviruses and HIV-1 capsids are mainly cone-shaped, while Rous sarcoma virus (RSV) and murine leukaemia viruses (MLV) capsids are found to be polyhedral or spherical-like^{155,159,160}. Compared to icosahedral viruses, such as adenoviruses, the protein organisation of retroviruses capsids follows the principle of fullerene arrangement, which means 12 pentamers form into a hexagonal capsid¹⁶¹. In a

spherical-like retroviruses capsid, the 12 pentamers are distributed randomly, while cylindrical capsids have six pentamers at each end of the cylindrical tube. It is suggested that the immature retroviral particle contains 1000~5000 units of Gag proteins. However, during the maturation process, only a small portion was essentially converted to capsid proteins for the formation of the virus core¹⁶². Considering the various shapes and sizes of retrovirus capsid, it might be necessary to have an excess amount of Gag protein to ensure the proper maturation of the retroviruses¹⁶³.

The intracellular transportation of retroviruses starts with the receptor recognition on the cell surface, allowing fusion with the cell membrane or activates endocytosis (figure 1.14). Different retroviruses may differ in internalisation pathways. For example, the cellular entry of mouse mammary tumour virus relies on a low pH-dependent viral fusion reaction with the target cell membrane¹⁶⁴, while ecotropic murine leukaemia viruses (MLV) is internalised through macropinocytosis pathway¹⁶⁵. One unique feature of retroviruses is their ability to reverse transcribe the single-stranded RNAs into DNA and deliver the integration-competent DNA into the nucleus. After retroviruses gain entry into the cytoplasm, the viral RNA is reverse transcribed into linear double-stranded DNA by reverse transcriptase (RT). The primer binding site of the retroviral RNA is one of the most important motifs for it is critical for the initiation of reverse transcription. A cell derived tRNA serves as the primers and binds to the binding site before RT-polymerase, and the polypyrimidine tract (PPT) mediates the synthesis of the second DNA strand¹⁶⁶. The product of the reverse transcription is associated with various cellular proteins and some viral proteins (includes approximately 100 different proteins) to form a complicated structure termed the transcription preinitiation complex (PIC). Intracellular transportation of the PIC is delivered by the microtubes, and it is a host cellular protein-dependent process¹⁶⁷. However, not all retroviruses can actively cross the nuclear membranes. For instance, all viral PICs from the *Gammaretrovirus* genus cannot actively enter the nuclear membrane, possibly due to a linker molecule being missing in the nuclear transport machinery. The breakdown of the nuclear membrane during mitosis provided an opportunity for the PIC to enter the nucleus. Some other retroviruses, like lentiviruses, are able to actively enter nuclear membranes and therefore are capable of transducing resting cells. Having encountered the host genome, the viral DNA integrates into the host genome. The integration of the viral DNA into the host genome occurs without major interference of the original cellular sequences and does not form transgene concatemers. The viral DNA was transcribed

into viral mRNA and then is exported to the cytoplasm where mRNA is translated into Gag, Env and Pol, which are used as components for the assembly of new retroviruses

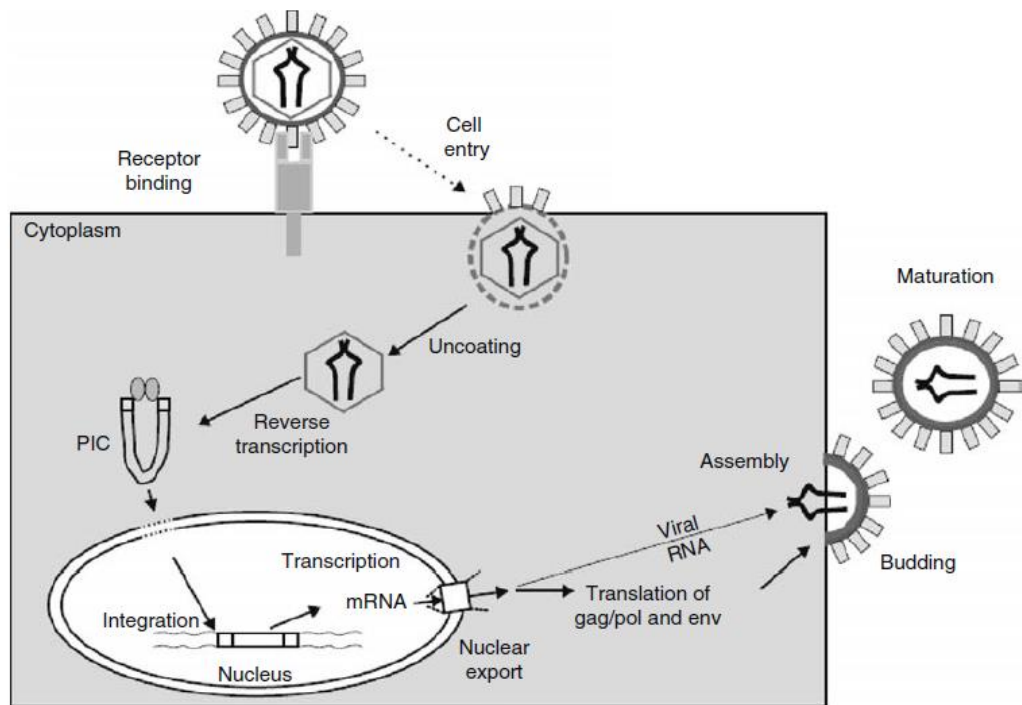


Figure 1.14 Retroviral internalisation and viral gene expression as shown for a simple gammaretrovirus example¹⁶⁴.

The therapeutic use of retroviruses as delivery agents has focused on gammaretroviral vectors. Key applications of gammaretroviral vectors include the expression of oncogenes in cancer therapy and the genetic engineering of T-lymphocytes and Hematopoietic stem cells^{168,169}.

- Advantages and Limitations of Viral Vectors

The use of viruses as gene delivery vectors exploit their natural ability to enter target cells and express the genetic information they carry. This provides viral vectors with high transfection rate and rapid transcription of the foreign gene inserted in the viral genome. Besides the high transfection efficiency, each type of viral vectors has its own characteristic advantages compared with other viral vectors. For instance, adenoviruses have a large gene capacity for foreign gene and low cell specificity, which makes it possible for adenoviral vectors to infect any cell type. Or in the case of lentivirus vectors, it can infect resting cells and with a relatively large gene capacity, unlike many other retroviral vectors that can only transfect dividing cells.

However, each type of viral vector has its own limitations as well. Adenovirus vector, though efficient with large gene capacity, has high immunogenicity and high vector toxicity, and combined with its low target cell specificity, it provides hindrance in the systematic administration of such vector. The adeno-associated virus vector is relatively safer since it is not related to the cause of any known disease, but it has a relatively smaller gene capability (can carry gene up to a length 5.8K base pair, only 15% of adenovirus vector capability) and has a rather complicated production process which indirectly increases the cost and difficulty for its application. For most of the retrovirus-based vectors, the lack of ability to transfect resting cells limits its application in targeting certain tissues. The advantages and limitations of each viral vector have been listed in table 1.3.

Table 1.3 This table show the advantages and disadvantages of several well-studied viral gene delivery systems. Table adapted from Bolt et al.¹⁷⁰

Viral Vector	Advantages	Limitations	Ref
Adenoviruses vectors	<ul style="list-style-type: none"> Large transgene capacity (up to 38 kb) low target specificity 	<ul style="list-style-type: none"> Tend to yield natural and acute immune responses Short-term gene expression 	171,172
Adeno-associated vectors	<ul style="list-style-type: none"> Comparatively higher safety 	<ul style="list-style-type: none"> Complicated production process Limited gene capacity (up to 4.8 kb) 	173,174
Retroviral vectors	<ul style="list-style-type: none"> Medium gene capacity (up to 8 kb) 	<ul style="list-style-type: none"> Low efficiency <i>in vivo</i> High immunogenicity Can only transduce dividing cells Possible random gene insertion 	175,176
Lentivirus vectors	<ul style="list-style-type: none"> Able to infect both dividing and resting cells Medium gene capacity (up to 8 kb) 	<ul style="list-style-type: none"> Difficult to design and produce High immunogenicity 	177,178

The advances in the field of viral gene therapy have led to the production of commercially available gene therapy products in the market. The first viral-based gene therapy product was Gendicine, a cancer gene therapy approved in China in 2003 that delivers the tumour suppressor gene p53 using an engineered adenovirus. More recently, the United States Food and Drug Administration (FDA) approved an adeno-associated virus (AAV) gene therapy called *Voretigene Neparvovec* from Spark Therapeutics for the treatment of a rare inherited retinal disease. Nonetheless, even the approval of viral-based gene delivery products could not eradicate the shadow once shed by the clinical trial that caused the tragic death of Jesse Gelsinger as well as immune responses observed in other patients⁹⁵. The debate over the safety of the viral vector application has lasted over several decades and continues to this day. Those who believe there could be an alternative vector that provides good gene transfection efficiency with low toxicity and immunogenicity turn their attention to search for substitutes.

1.3.2. Non-viral Delivery Systems

Non-viral Delivery vector systems provide alternative forms of delivery for gene therapy and have been studied in the past decades. The non-viral delivery approach involves the use of physical or chemical methods to achieve the delivery of nucleic materials. Physical methods are mainly based on physical stimulation such as using electrical stimulation and sonic stimulation. The chemical method is based on the use of varieties of lipids, polymers, dendrimers or other natural materials combined with DNA or RNA materials to form nanoparticles or complexes^{127,142,179,180}. Unlike viral vectors that are based on the natural ability to infect cells, non-viral vectors consistently exhibit reduced transfection efficiency due to the extra- and intracellular obstacles. However, non-viral vectors possess advantages including biocompatibility and potential for large-scale production which makes these vectors attractive for gene therapy¹⁸¹. A significant amount of studies in the past decade has focused on the development and application of non-viral delivery vectors that can overcome the barriers *in vitro* and *in vivo* for gene delivery.

- Lipid-based delivery systems

Lipid-based delivery systems (LBDS) used cationic lipid to combine with nucleic materials, forming nanosized particles called lipoplex for the delivery of genetic material. LBDS was one of the earliest gene transfer strategies used to introduce foreign genetic material into target cells. In the past decades, various studies have demonstrated the capability of delivering external genetic material into target cells using lipid-based vectors¹⁸²⁻¹⁸⁴. Early work suggested the mechanism for the lipid-based delivery system is related to the direct plasma membrane fusion of lipoplex into target cells¹⁸⁵, yet other studies revealed that the intracellular uptake of lipid-based vectors is primarily through endocytosis¹⁸⁶. After cellular entry, the lipoplexes destabilise the endosomal membrane and initiate a flip-flop reorganisation of phospholipids. These phospholipids play a major role in the release of genetic materials into cytoplasm by interaction with the cationic lipid in the lipoplexes¹⁸⁷. The cationic lipids used as delivery vectors normally contain three major structural domains: a cationic headgroup, a hydrophobic tail, and a linker domain that connects the other two. The density and nature of the cationic headgroup affect the transfection related ability and the length and type of the hydrophobic tail can affect the transfection efficiency of a given lipid as well¹⁸⁸. With

proper manipulation and modification on the headgroup and tail-group, the chemical and physical properties of the cationic lipid can be adjusted to suit the purpose of the delivery¹⁸⁹.

Cationic lipid vectors for gene delivery are widely used in gene delivery thanks to their ability to condense anionic nucleic acids. Cationic lipid-based gene delivery system has been applied to the treatment of many diseases. For example, cationic lipid-based gene delivery system has been used in the field of cancer treatment. Tabernero et al. performed an RNAi therapy targeting VEGF and kinesin spindle protein in cancer patients using cationic lipid-siRNA complexes mediated treatment¹⁹⁰. Applications in other fields such as therapy in liver diseases were also reported^{191,192}. LBDS have many advantages as a gene delivery system including high cargo capability, good biocompatibility and versatility. Another advantage of LBDS is the formulation can be modified in a variety of ways to fulfil the requirements for different patient and different diseases¹⁹³⁻¹⁹⁵.

- Dendrimers

Dendrimers are polymer compounds consisting of a central core structure with highly branched arms of symmetric pattern around it. The unique molecular structure provided dendrimers with distinctive properties (an example was shown in figure 1.15). Dendrimers are synthesised through a gradual stepwise approach which means, in general, that they have a well-defined size and structure with a relatively low polydispersity index. The high density of terminal groups provided dendrimers with multiple attachment sites and the potential for customized modification. With these critical properties, dendrimers have gained much attention and made them particularly interesting for gene delivery vectors. Dendrimers can interact with various types of nucleic acids, such as plasmid DNA or oligonucleotides, to form complexes that protect the nucleic acid from degradation¹⁹⁶. It is suggested that the interaction between dendrimer and the nucleic acid is sequence non-specific and based on electrostatic interactions¹⁹⁷.

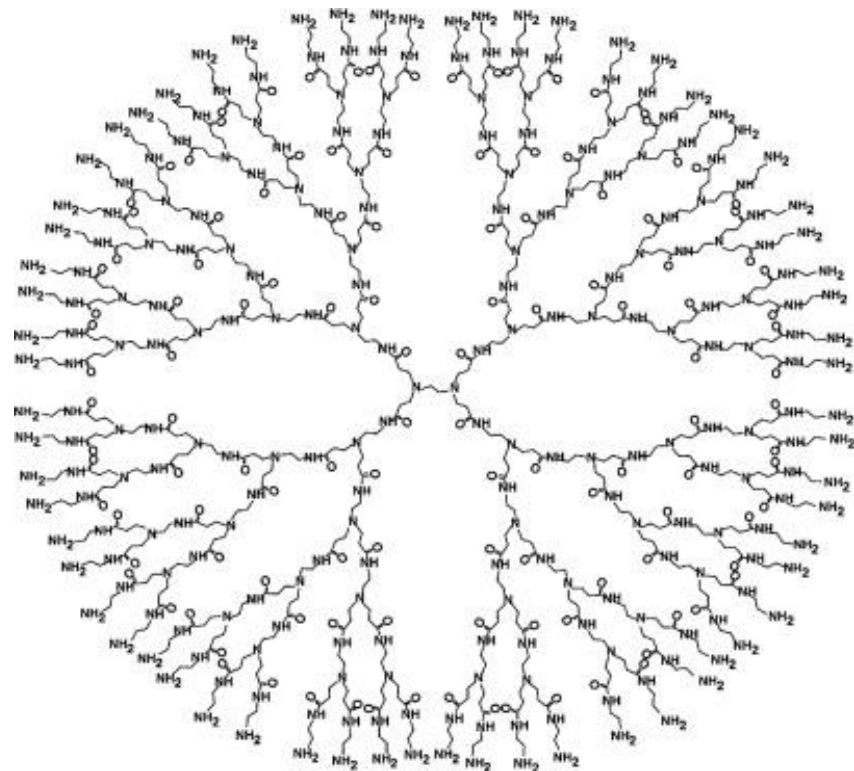


Figure 1.15 An example of a PAMAM dendrimer molecule structure ¹⁹⁸.

In 1993, Haensler et al. reported the first use of Polyamidoamine (PAMAM) dendrimers as transfection agents ¹⁹⁹. For the past decade, the use of dendrimers as a gene delivery vector has developed rapidly and has been applied to the treatment of many diseases. Maruyama-Tabata et al. intravitreally injected lipid lysine dendrimer complexes and inhibited neo-vascularisation of the choroidea by down-regulation of VEGF²⁰⁰. Sato et al. demonstrated that intratumoral injection of dendrimer-plasmid complexes that encode tissue inhibitor of the metalloproteinase-2 gene (TIMP2 gene) would inhibit the growth of tumours ²⁰¹. Undoubtedly, dendrimer-based delivery systems have demonstrated considerable potential as tools for the further development of genetic therapies.

- Polymer-based delivery systems

The polymer-based delivery system is to use nano-scale particles or micelles that are composed of a polymer and a specific loading material (genetic materials, small molecule drugs or peptides) to deliver its content to a specific tissue or organ²⁰².

Early stage studies in polymer gene delivery system focused on the use of poly-l-lysine and polyethylenimine (PEI). It is well established that polylysine is the first cationic polymer used as a gene delivery vector²⁰³. On its own, polylysine is not an efficient

gene transfer agent. Even with the aid of chloroquine, suggested to be capable of helping delivered nucleic acids escape from their vesicles and avoid lysosomal degradation²⁰⁴, polylysine-DNA complexes showed moderate transfection efficiency. The polylysine based vectors were proved to be valuable in early research studies, but its low transfection efficiency limited the application in the clinical situation. Polyethylenimine (PEI) is considered to be one of the most effective cationic polymer-based gene delivery vectors studied up to date, has been widely studied and used since 1995²⁰⁵. PEI can efficiently mediate gene delivery without any additional endosomolytic agent. Moreover, PEI has successfully mediated *in vivo* gene delivery to multiple organs including kidney and lungs²⁰⁶. However, though efficient and *in vivo* active, the further application of PEI as gene delivery vector is hindered by its relatively high toxicity.

With improved understanding of the obstacles in extra- and intracellular gene delivery and further knowledge of the key steps that affect the gene transfer efficiency, polymers were designed to address specific barriers, such as biocompatibility and endosomal escape. It is suggested that endosomal escape is a key step in gene delivery, and certain synthetic acid-responsive polymers have been produced to enhance its transgene efficiency, which is inspired by specific peptides viruses developed in their capsid to enable protonation and become fusogenic with endosomal membrane²⁰⁷. An example is provided by Tirrell et al. that synthesised polyethylacrylic acid that can cause membrane disruption at low pHs²⁰⁸. Another approach to enhance polymer delivery vector performance is to increase the biocompatibility. Cationic polymers like PEI showed significant transfection efficiency but also high toxicity. It is now known that the ability of protonation under acidic environment might be the key to efficient endosomal escape. It is suggested that a biocompatible material could be chemically modified to have a buffering capacity at physiological and lysosomal pH. In one study, a homopolymer of histidine and gluconic acid was prepared and combined with DNA and transferrin-polylysine conjugates to form polyplexes. The histidine contains imidazole groups that has the desired protonation properties (pKa ~6) and the gluconic acid increased the aqueous solubility of the homopolymers²⁰⁹. The complex showed good efficiency compared to control groups, and furthermore, the complex showed low toxicity at gene delivery concentrations²⁰⁹. Undoubtedly, polymer-based gene delivery systems showed promising potential as delivery vectors in gene therapy.

Furthermore, many novel polymers with unique architectures, including star polymers, comb polymers and many others can be generated using block copolymers (figure 1.16). These novel designs may provide the polymers with significantly different solution behaviours as well as from their ability to self-assemble. By coordinating the architecture and composition of polymers, materials with a diverse range of attributes can be generated and utilised in various applications²¹⁰.

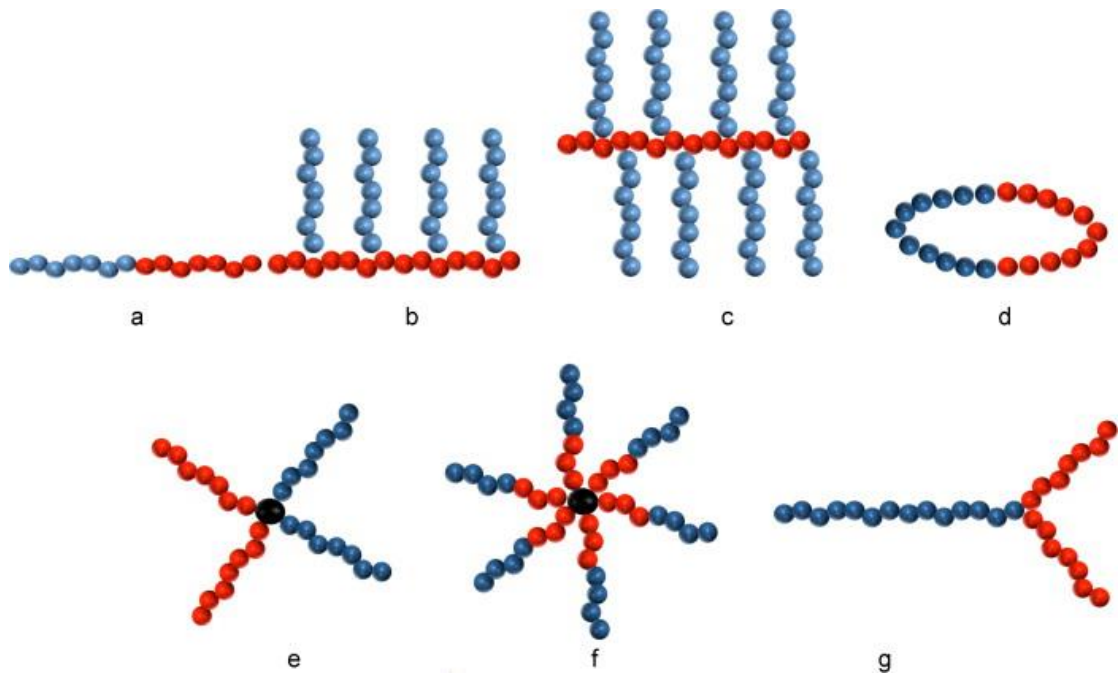


Figure 1.16 Examples of various polymer architectures that can be achieved. (a) linear; (b) graft; (c) brush or comb; (d) ring; (e) star A_nB_n ; (f) star-block $(AB)_n$; (g) AB_2 star. Figure is adapted from Gregory et al.²¹⁰.

For example, Ma et al. synthesised a novel star-shaped porphyrin-poly(L-lysine) dendrons polymer. Due to its amphiphilic property, the obtained polymer has a low critical micelle concentration in an aqueous solution and can load a moderate amount of doxorubicin. Moreover, the doxorubicin-loaded polymer shows a higher cytotoxicity under the light stimulation compared to polymer or DOX alone, which suggests that the star-shaped porphyrin-poly(L-lysine) dendrons polymer has a potential application in combined photodynamic therapy and chemotherapy²¹¹.

1.4. Cationic Polymer-based Gene Delivery System

Cationic polymers are polymers bearing positive charges or polymers synthesised with cationic moieties in their backbone and/or in their side chains. The cationic moieties include primary, secondary, tertiary and quaternary amines, as well as other positively charged groups like amidines. The cationic polymers can electrostatically condense to

genetic materials into particles termed polyplex. The size of the polyplexes ranges from tens to several hundreds nanometers in diameter²¹². Thanks to the flexibility of polymer chemistries, it might be possible to provide cationic polymers with multiple functions required for efficient gene delivery while maintaining good biocompatibility. The goal of using a cationic polymer delivery system, or any other delivery system, is to address the problems in gene delivery. This section will discuss how cationic polymer delivery vectors can be applied to address problems in gene delivery including gene packaging and protection, trans-membrane activity, and endosomal escape. Examples of well-studied cationic polymers will also be described.

1.4.1. Gene Therapy Complexation

One problem in gene delivery is the delicacy of genetic materials. Unprotected DNA or RNA is degraded by corresponding enzymes within a short period of time. An efficient delivery system can neutralise the negatively charged nucleic acid to prevent charge repulsion against the cellular membrane. Also, the condensation of polymers with nucleic acids could efficiently prevent extra- and intracellular degradation by nucleases. Three major packaging strategies have been developed to achieve polymer-gene condensation: electrostatic interaction, encapsulation, and adsorption. The majority of the cationic polymers exploited the anionic nature of DNA and RNA to achieve successful condensation via electrostatic interaction, while encapsulation (figure 1.17) and adsorption are more commonly seen in the case of neutral and biodegradable polymers such as poly(lactide-co-glycolide).

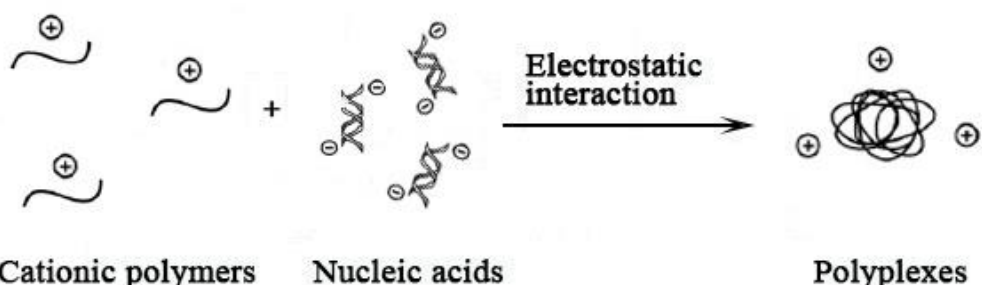


Figure 1.17 Polyplexes formation via electrostatic interaction between cationic polymers and nucleic acids.

The amine- and amino- groups in the cationic polymer can be protonated at neutral pH and below, enabling the electrostatically driven assembly of cationic polymers and

nucleic acids. Several forces are involved in the condensation of cationic polymers with nucleic acids, including bending, mixing entropy, coulombic force²¹³. Bending and mixing free energies resists the condensation process, while the coulombic force, at least under certain conditions, is in favour of the condensation. According to Bloomfield et al, the bending free energy of a DNA molecule can be described as follows²¹³:

$$\Delta G_{bending} = RTaL/2R_c^2$$

Where L is the length of the DNA with persistence length a . The radius of the bent part is R_c . The mixing free energy is described by Post et al.²¹⁴ as:

$$\Delta G_{mixing} = RTL/a$$

Nucleic acids condensed negative charges and generate powerful repulsion energy between condensed and uncondensed DNA. The free energy of the electrostatic repulsion is summarized based on Oosawa's work²¹⁵ by Bloomfield²¹³:

$$\Delta G_{repul} = \frac{n k_B T}{2 \xi z_2^2} \ln \frac{V_{uncondensed}}{V_{condensed}}$$

where n is the total number of phosphate charges, z_2 is the valence of condensing cationic. The V is the volume of the condensed and uncondensed molecules assumed to be a sphere.

One possible attraction force is the induced dipole interaction between the fluctuating ion atmosphere and its free energy is given by Marquet et al.²¹⁶:

$$\Delta G_{fluc} = \frac{3Lk_B T}{X} \frac{(\theta_2 z_2^2 \xi)^2}{(1 + \theta_2 z_2^2 \xi)^2}$$

Where X is the distance of interhelix centres in the condensed DNA.

The addition of four free energy equations, combined with experimental data collected by Bloomfield et al., provided a total free energy ΔG_{total} of -0.11 to -0.24 kJ/mole bp with cations of charge +3 or greater, suggesting by that the cation-DNA condensation process is entropically driven self-assembly²¹³. The resulting polyplexes are typically spherical, micellar, or toroidal structures with size ranging from about 20 to several hundred nanometers^{217,218}. The nitrogen to phosphate ratio (N: P ratio), also referred to as charge ratio, is used to describe the ratio between the polymer and nucleic acids used

during the polyplexes formation. The N: P ratio can significantly affect the formation of stable polyplexes, and different N: P ratios are required for different cationic polymers for stable nucleic acids condensation. High N: P ratio presents larger groups positive-charge moieties that increases the polyplexes stability due to a stronger electrostatic charge, though a strong stronger electrostatic charge that favours the polyplexes stability may lead to difficulties of nucleic acid release in the later stage of gene delivery²¹⁹. Therefore, the design and synthesis of cationic polymers should balance binding strength to ensure nucleic acid packaging and protection with the capability of the endosomal escape of nucleic acids into its target site.

1.4.2. The Internalisation of Cationic Polyplexes

Another obstacle in cationic polymer-based gene delivery is the plasma membrane. To gain cellular access, passive diffusion is typically not applicable to polyplexes due to size limitation by the membrane pores and low partition efficiency into lipid bilayers. Many intracellular delivery approaches have exploited the natural cell endocytosis process, which cells use to transport external macromolecules from the extracellular space into the cytoplasm. Many known pathways of endocytosis, including clathrin-dependent endocytosis, caveolae-mediated endocytosis, phagocytosis, macropinocytosis and clathrin- and caveolae-independent endocytosis, offered a diverse and regulated mechanism of cellular entry.

- Clathrin-dependent Endocytosis

Clathrin-mediated endocytosis, also called clathrin-dependent endocytosis, is one of the major routes and is well-characterised in most mammalian cell lines^{220,221}. The key component in this endocytosis route, clathrin protein, is composed of a heavy chain (~190 kDa) and a light chain (~25 kDa). Clathrin protein can form different lattices including hexagonal lattices and cage-like lattices composed of hexagons and/or pentagons²²². Other proteins, such as AP-2 protein, dynamin and Eps15, and over 50 other cytosolic proteins, are involved in the clathrin-mediated endocytosis process²²³.

The endocytosis process is initiated by the interaction of extracellular “cargo” molecules with the cell membrane (figure 1.18). The first step is to assemble clathrin-coated pits on the cellular membrane, which is composed of clathrin and many other proteins (figure 1.18). The clathrin-adaptor proteins, such as the heterotetrameric

adaptor protein AP2 complex, first bind to the lipids site where the external “cargo” molecule is located in the plasma membrane. Then the scaffold proteins, such as clathrin, interact with clathrin adaptors and cluster to form the coat components²²⁴. The clathrin-coated pit in contact with the external “cargo” molecules on the plasma membrane initiates the endocytosis process²²⁵. After clathrin-coated pit assembly, a group of actin molecules would polymerise at the endocytic site, forming the actin module. The actin module includes critical regulatory components such as the proteins of the Wiskott–Aldrich syndrome protein family, which play vital roles in the activation of dynamin, and the actin filaments²²⁶. The actin module is also of vital importance for the invagination and scission of the endocytosis vesicle. The actin filament polymerisation provided force for the bending of the plasma membrane and results in the formation of the endocytosis vesicle.

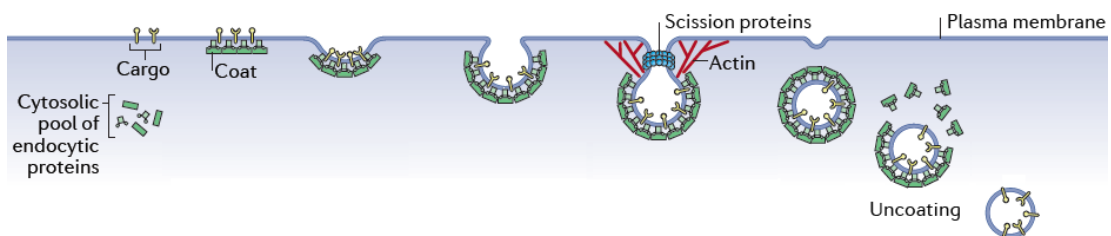


Figure 1.18 The clathrin-dependent endocytosis process. The figure is a modified reprint from Roux et al.²²⁷

Following the formation of the endocytosis vesicle, the scission of the invagination neck is mediated by a large GTPase dynamin. Dynamins assemble at the neck of the clathrin-coated pit into a helical collar. With the aid of other proteins including endophilin and amphiphysin, dynamin constricts the neck to allow fission of the endocytosis vesicle^{228,229}. The protein-coated endocytosis vesicle was released into the cytoplasm where the disassembly of the protein coat take place. Two mechanisms have been suggested in the disassembly of the coat: HSC70 (heat shock protein 70kDa) chaperone-mediated clathrin lattice degradation and phosphatidylinositol 4,5-bisphosphate (PI(4,5)P₂) dephosphorylation^{230,231}. The disassembly of the coat releases the endocytosis vesicle and enables further fusing with early endosome to initiate the intracellular transportation of its “cargo” molecules. The endocytosed “cargo” is sorted in early endosomes and further routed different destinations. The “cargo” molecule could be transported to late endosomes and lysosomes, or delivered to the secretory sorting station *trans*-Golgi

network (TGN) and was directed to different subcellular destinations, or to endosomal recycling carriers that bring the molecule back to the plasma membrane²³².

- Caveolae-Mediated Endocytosis

Caveolae are small vesicles (50–60 nm in diameter) defined as invaginations of the cell membrane that is lined by caveolin-1. Caveolae system is the hydrophobic membrane microdomains that rich in cholesterol and sphingolipids²³³⁻²³⁵. The internalisation mechanism involved varies in different cases; for instance, the internalisation of simian vacuolating virus 40 (SV40) is initiated upon virus binding to the cell surface and activates a tyrosine kinase-based signalling cascade that disrupts the local actin cytoskeleton and employs dynamin to the site of binding (figure 1.19)²³⁶. In another case, albumin triggers caveolae endocytosis through the binding to its receptor, gp60 (glycoprotein 60kDa). Most of the internalisation of caveolar ligands is a signal-mediated process that requires the presence of caveolin-1, for example, the interaction between caveolin-1 and gp60 is essential for albumin uptake²³⁷. Though some other caveolae ligand can mediate internalisation without caveolin-1, such as autocrine motility factor (AMF), a signalling factor which regulates cell motility, is internalized via a dynamin-dependent pathway in caveolin-1 deficient cells²³⁸.

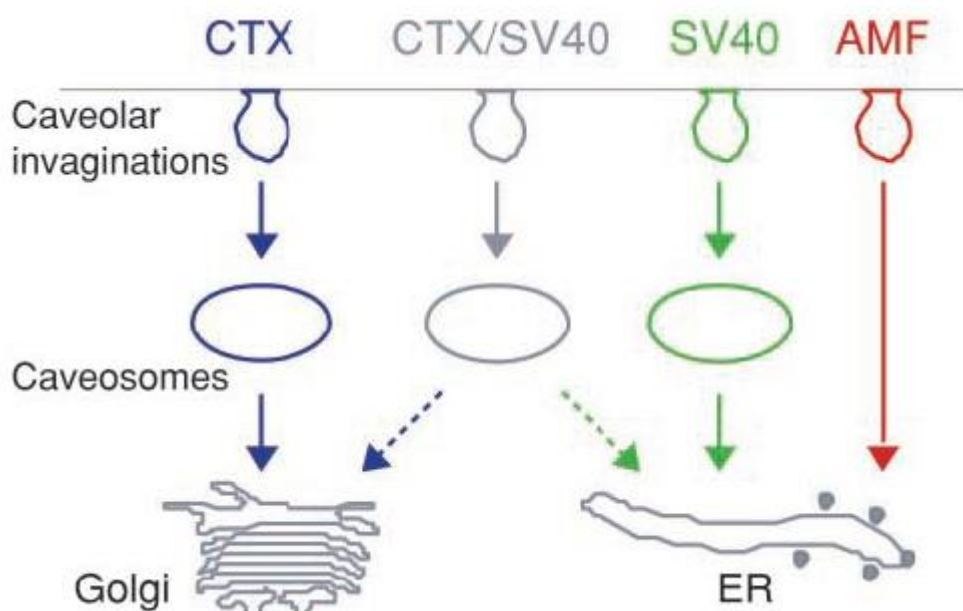


Figure 1.19 Caveolae-dependent endocytosis. The figure is adapted from Nabi et al.²³⁹

The “cargo” bound on the plasma membrane invaginates and forms caveosome that is delivered to early endosome for sorting. Depending on the content, caveosomes were

further transported to different destinations. For example, caveosomes that contain SV40 and caveolin-1 is delivered to the smooth endoplasmic reticulum (ER) without traversing the Golgi, while caveosomes that contain cholera toxin (CTX) is transported directly to Golgi²⁴⁰. CTX and SV40 could alternatively be transported to a common caveosome first before further segregated for delivery to Golgi and smooth ER, respectively. Cell treated with microtubule depolymerizing agent, nocodazole, could disrupt the delivery of SV40 and CTX delivery to Golgi and ER, but does not affect the delivery of AMF which is directly delivered to the smooth ER via a distinct pathway, suggesting the intracellular transportation of caveosomes is via microtubules²⁴¹.

- Other pathways of Endocytosis

There are other means of endocytosis pathways including macropinocytosis, and phagocytosis. Macropinocytosis is induced by tho-family GTPase triggered the actin-driven process of membrane protrusion²⁴². The large endocytic vesicles, referred to as macropinosomes, contain large amounts of extracellular medium and is an efficient route for the non-selective endocytosis of macromolecules²⁴³. Phagocytosis is conducted mainly by macrophages, monocytes and neutrophils. The endocytosis process of macropinocytosis and phagocytosis is shown in figure 1.20.

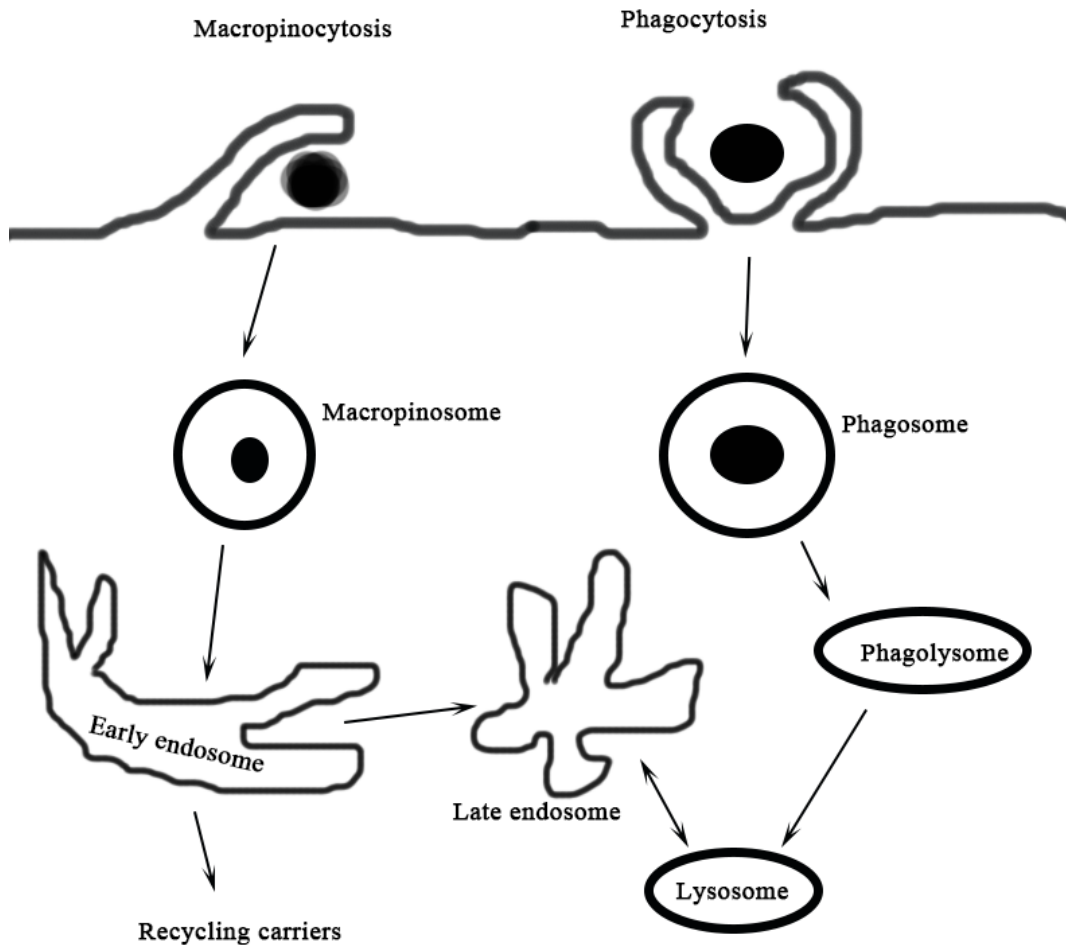


Figure 1.20 The phagocytosis and micropinocytosis process.

In mammalian cells, phagocytosis is a major way to clear large pathogens such as bacteria, dead cells, fat deposits and large debris from apoptotic bodies^{244,245}. Yet this pathway could be used for the uptake of exogenous molecules under special conditions by specific cell types. The phagocytosis requires interaction between the ligand of exogenous molecules and certain cell membrane receptors such as the fibronectin receptor and the immunoglobulin-like receptor (Fc receptors)²⁴⁵.

- Role of glycosaminoglycans (GAGs) in polyplex internalisation

Glycosaminoglycans are long unbranched biopolymers with repeating disaccharide units consisting of two hexose derivatives. These hexose derivatives are typically galactosamine or glucosamine and have either a carboxylate or sulphate group attached to one or both of the hexose derivatives which makes them negatively charged. For

example, the most common disaccharide unit in Heparin is composed of a 2-O-sulphated iduronic acid and 6-O-sulphated, N-sulphated glucosamine (figure 1.21)²⁴⁶

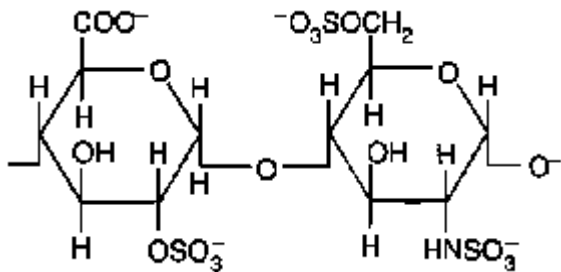


Figure 1.21 Structure of Heparin, an example of glycosaminoglycan. The disaccharide units are composed of 2-O-sulphated iduronic acid and 6-O-sulphated.

There are several types of GAGs and the amount within cells vary depending on the cell type. Since GAGs are highly negatively charged, its interaction between positively charged polyplexes has a great effect upon the uptake and transfection efficiency of polyplexes. GAGs, as typical polyanionic molecules, can compete with nucleic acids and dissociate polyplexes. Some studies did show that high concentrations of GAGs in extracellular space and on the cell membrane could reduce or even completely inhibit the transfection efficiency^{247,248}. However, in some cases, the existence of sulphate GAGs on the cell membrane would improve gene delivery efficiency. Hornof et al. reported improved uptake and transfection efficiency of PEI-polyplexes coated with low molecular weight hyaluronan²⁴⁹. Since the type and number of GAGs are cell type-dependent, this indicates that the relationship between polyplexes and GAGs can vary with different polymers on different cell lines and would have an impact on gene delivery efficiency and its therapeutic effect.

- The internalisation of cationic polymer polyplexes

A series of studies have been conducted to determine the internalisation pathways of cationic polymer based polyplexes. Midoux et al. have summarised the result of several studies in different cell lines with different cationic polymers (table 1.4)²⁵⁰.

Table 1.4 Cationic polyplexes internalisation pathways summarised by Midoux et al. (t) indicates that the transfection efficiency is reduced by inhibitors of the related pathway.

Polymers	Cells	Clathrin-dependent	Caveolae-dependent	Clathrin-independent	Other
bPEI	A549/HeLa	+	+(t)	-	-
	COS-7/HUH-7	+(t)	+	-	-
IPEI	A549/HeLa	+	+(t)	-	-
	COS-7/HUH-7	+(t)	-	-	-
	Endothelial	+(t)	-	-	-
pDMAEMA	COS-7	+	+(t)	-	-
chitosan	HEK293T /COS-7 cell	+(t)	-	-	-
	CHO	-	+	-	-

Results indicated that the internalisation of cationic polyplexes, especially for polymers rich in amine groups such as PEI and PDMAEA, is via both clathrin-dependent endocytosis and caveolae-mediated endocytosis²⁵¹. Other studies also indicated that clathrin-mediated endocytosis and caveolae-mediated endocytosis are the major routes of cellular uptake of polyplexes, with some cases where the clathrin-independent pathway is responsible for the uptake of polyplexes²⁵²⁻²⁵⁴.

1.4.3. The Release of Nucleic Acids into the Cytoplasm

After cellular entry, subsequent intracellular transportation includes several routes, such as delivery to intracellular organelles (Golgi apparatus, endoplasmic reticulum), recycled back to the cell membrane, or sorted to acidic degradative vesicles²⁴⁴. The intracellular routing depends on the internalisation pathway, though some suggested the polymer type and formulation conditions may have an impact^{252,255}. Cationic polymer based polyplexes are mainly internalised via clathrin-dependent endocytosis and caveolae-dependent endocytosis, which means they can be delivered to endosomal vesicles and shuttled through the endo-lysosomal pathway. Therapeutic nucleic acids condensed within the polyplexes, including DNA or siRNA, will need to be released into cytoplasm before they can be further processed and become active. Therefore, the release from the endosomal vesicles is critical to avoid degradation within the lysosomes by nucleases. Though most of the cationic polymers have different chemical structure, they share one feature that enables the efficient transfection, that is the ability to protonate at physiological pH. The majorities of the cationic polymers have amine- or amino functional groups in their structure which provide them with a good buffering

capability and enable protonation. The buffering capability is used to describe the ability to resist changes in pH due to the addition of an acid or base, and for cationic polymers, this is often used to describe the percentage of amine groups becoming deprotonated in an acidic environment²⁵⁶. The endosomal escape of cationic polymer-based polyplexes are tightly associated with their protonation ability and is suggested to occur via “proton sponge effect” pathways²⁵⁷.

- Mechanism of proton sponge effect

The “proton sponge effect” was first mentioned by Boussif in 1995 when describing the PEI-polyplexes internalisation behaviour²⁰⁵. The up-taken polyplexes were transported via the endo-lysosomal route and would go through a series of pH change from 7.4 to 6.0 in the endosome, then to 5.0 in the lysosome. Cationic polyplexes shuttled to endosomes would interact with protons residing inside endosomes, resulting in a high local concentration of positive charge due to protonation and consumption of H⁺ within the endosomes (figure 1.22). To maintain the pH within endosomes, the endosomal ATPase would actively “pump” protons into endosomes²⁵⁸. Besides, the influx of protons is coupled with the influx of chloride anions to keep the electrostatic balance within the endosome. As a result of the presence of cationic polymers and the continuous accumulation of protons and chloride anions, the osmotic balance changes and leads to swelling of the endosome. Meanwhile, the protonation of cationic polymers would expand its polymeric network due to electrostatic repulsion between polyplexes²⁵⁹. Under the joint force of these two phenomena, the life expectancy of the endosome is greatly reduced and eventually leads to endosomal rupture and the release of cationic polyplexes into the cytoplasm²⁰⁵.

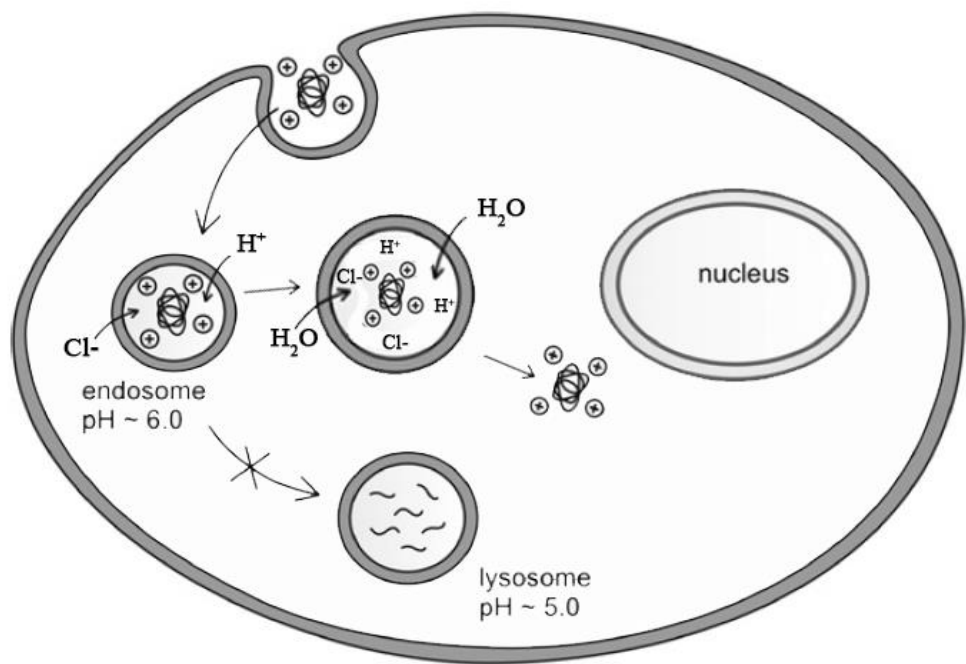


Figure 1.22 The endosome escapes of cationic polyplexes via a proton-sponge effect pathway.

1.4.4. Examples of cationic polymers used in gene delivery

In the past few decades, many polymers have been synthesized and studied. The cationic polymeric drew attention for their high transfection efficacy and varieties of modifications available. Table 1.5 below shows some of the monomers used in the synthesis of cationic polymers widely used nowadays as delivery vectors.

Table 1.5 Commonly used cationic and neutral monomer.

Structure		Name
	DMAEMA	2-dimethylaminoethyl methacrylate
	DMAPMA	N-(3-(dimethylamino) propyl) methacrylamide
	DMAEA	2-dimethylaminoethyl acrylate
	DEAEMA	2-(diethylamino)ethyl methacrylate
	APMA	3-aminopropylmethacrylamide
	AEMA	2-aminoethyl methacrylamide
	HPMA	3-hydroxypropyl methacrylamide
	HEMA	2-hydroxyethyl methacrylate
	BMA	butyl methacrylate
	PEI(linear)	polyethylenimine
	PEI(branched)	polyethylenimine

Polyethylenimine (PEI) is one of the first-generation cationic polymers and considered to be the most widely studied²⁶⁰. It contains large amounts of repeated amine groups with two alkyl group between each amine group as a spacer. Two different architectures of PEI are typically seen: Linear PEI and branched PEI. Linear PEI consists of a repeated unit of a secondary amine, and every third atom is amino nitrogen that can be protonated, while the branched PEI has a much more complicated architecture and contains all primary, secondary and tertiary amine groups²⁶¹. Linear and branched PEI

(lPEI&bPEI) both showed good transgene efficiency for gene delivery, thanks to their amine-rich structure and high buffering capability²⁶². The first successful polyethylenimine-mediated oligonucleotide transfer was conducted by Boussif et al. in 1995²⁰⁵. Subsequent studies not only focused on the use of PEI alone as gene delivery vector but also involved PEI in the design of block copolymers, which are polymers comprise two or more homopolymer subunits linked by covalent bonds. Twaites et al. reported the synthesis and application of PEI copolymers with poly- (N-isopropylacrylamide) side chains in the transfection of mouse C3H muscle myoblasts²⁶³. Besides, the relationship between molecular weight and transfection efficiency of PEI has also been studied. Godbey et al. showed that the transfecting efficacy increases as the molecular weight of lPEI changes from 600 Da to 70000 Da²⁶⁴. However, high molecular weight polymers also result in significantly higher cytotoxicity. The toxicity of PEI is explained by the combination of acute disruption of cellular membranes and damaging cellular components²⁶⁵. The free PEIs had interacted with negatively charged cell membrane proteins and had been caused by aggregation and adherence on the cell surface, which had resulted in significant necrosis²⁶⁶. The up-taken PEIs were intercellularly routed to endosomes and lysosomes, and during the endosomal escape process via the proton sponge mechanism, it would have caused endosomal and lysosomal rupture, resulting in the inhibition of normal cellular process²⁶⁷. It is also suggested that when systematically administrated, the free PEIs would interact with negatively charged serum proteins and red blood cells, resulting in the formation of precipitants and clusters²⁶⁶.

Another monomer DMAPMA, which is called N- (3-(dimethylamino)propyl) methacrylamide, is a monomer with a tertiary amine. These polymers work as a “proton-sponge” which makes them easier to condense with DNA or other genetic material. However, due to its toxicity, Armes et al. decide to synthesise a copolymer using DMAPMA and HPMA²⁶⁸. HPMA is an example of a non-ionic moiety extensively used for gene delivery applications to form a stealth layer to cationic vectors in order to avoid clearance from the macrophages¹⁴².

Another pair of cationic polymers, Poly (dimethylaminoethyl methacrylate) (PDMAEMA) and Poly (dimethylaminoethyl acrylate) (PDMAEA) have drawn attention in the past decade²⁶⁹⁻²⁷². PDMAEMA showed great potential as gene delivery vector with lower toxicity^{205,273}. PDMAEMA is also a water-soluble cationic polymer

and has groups of tertiary amines that can partially protonate in solution and create an internal cationic charge²⁰⁵. However, while *in vitro* and *ex vivo* studies showed successful gene transfer, some of the *in vivo* experiments failed to reach expectations. Storm et al. reported that when transfecting OVCAR-3 cells with these polymers, the *in vivo* transfection efficiency was significantly decreased compared to *in vitro* and *ex vivo* groups²⁷⁴. Also, there is concern about the cytotoxicity of the PDMAEMA vector when used as gene delivery system potentially due to disruption of vital organelles such as endosomes and lysosomes, even though it's much less toxic than PEI counterparts²⁷⁴. Published works suggest that the transfecting efficacy and the toxicity are directly related to the molecular weight of the PDMAEMA¹⁴², therefore, the balance between transfecting efficacy and the toxicity can be modulated by finding an optimal molecular weight of the PDMAEMA. There are other strategies to reduce the cytotoxicity of the polymer without reducing the transfecting efficacy. By designing copolymers, other more hydrophilic molecules or biodegradable molecules, such as HPMA or Polyethylene glycol (PEG), can be conjugated to the PDMAEMA which reduces the toxicity. The presence of PEG in copolymers can improve the solubility of the polyplexes due to its hydrophilic nature and further extend the circulation time in blood. Armes et al. synthesized a PDMAEMA-PEG block copolymer, and the results show that such modification can increase the hydrophilicity of the polymer-DNA of the copolymer polyplexes but reduced the cell membrane penetration ability²⁷⁵.

Poly (dimethylaminoethyl acrylate), the acrylate version of PDMAEMA, is also a cationic polymer with great potential to be used as a gene delivery system. PDMAEA has various advantages including high cargo load capability, low immunogenicity and simplicity in the process of manufacture²⁷⁶. In addition, PDMAEA polymer was found to show some unique properties in aqueous solution. It is reported that PDMAEA would slowly degrade to poly (acrylic acid) (PAA) and dimethylaminoethanol (DMAE) in aqueous solution, due to a self-hydrolysis process²⁶⁹. Like PDMAEMA, PDMAEA based copolymers were designed and synthesized to reduce its toxicity further and improve transfection efficiency. Monteiro et al. prepared a degradable diblock polymer based on PDMAEA, and it was able to be condensed with siRNA and achieve successful delivery into target cells²⁷⁷.

Novel cationic polymers such as polycation or cationic polypeptide have been applied in gene delivery. Nasanit et al. reported the use of a polypeptide as a vector for the

delivery of pDNA and which more active at transfection than current systems such as PEI²⁷⁸. Another study by Soliman et al. demonstrated the preparation of multicomponent polymer-DNA polyplex²⁷⁹. The underlying logic was to create a polymer-based polyplex that mimics the behaviour of a virus. The viral-mimetic delivery vector is composed of two parts: 1) a reducible polycation core polymer that is able to condense with nucleic acids and be capable of endosomal escape, and 2) a “shield” hydrophilic polymer attached to the core polymer that contains targeting ligands and is designed to cleave in acidic environment such as in endosomes²⁷⁹. In this study, a series of reducible polycations were synthesised and condensed with luciferase encoding pDNA to form polyplexes before being attached with PEG “shield” polymers. The transfection efficiency of viral-mimic polyplexes containing targeting ligands were determined on human colon carcinoma cell line (HCT116) and human promyelocytic leukaemia (HL60). The data indicated that the polyplexes coated with “shield” polymers showed a lower transfection efficiency compared with the non-coated ones, while the coated-polyplexes with targeting ligands showed the same level of transfection efficiency compared with the non-coated ones. Besides, the results also suggested that most of the polycation polyplexes, both uncoated and shield polymer-ligand coated ones, showed higher transfection efficiency compared to PLL polyplexes and showed the same level of efficiency compared with PEI polyplexes in both cancer relevant cell-lines²⁷⁹.

In recent years, several branched polymers have been developed via *in situ* deactivation enhanced Atom-transfer radical-polymerisation (ATRP) and have shown a higher transfection capability²⁸⁰. Based on these findings, the efficacy of the polymer is found to be related to the molecule structure of the polymer. As a matter of fact, several researchers have reported that the structure (linear or branched, length and number of arms) is closely related to the transfecting efficacy of polymeric vectors²⁸¹. In these studies, they found that with increased branching, for a fixed molecular weight polymer, there is a trend of reduced toxicity. It's shown that in order to reach a significant transfection a minimal molecular weight is necessary. Their research showed that a reasonable combination of branched structure and a suitable molecular weight would achieve low toxicity with high transfecting efficacy²⁸². Another study has suggested that the increased transfection efficiency of branched polymers compared to their linear counterparts is related to the self-assembly ability with nucleic acids. Polymers with a

higher degree of branching can condense with nucleic acids to form tighter and smaller polyplexes, which are easier to be internalised by cells²⁸³.

Cationic polymers showed great potential as gene delivery vectors and might have provided an alternative approach of gene transfer without viruses. The production of cationic polymers is largely dependent on chemical polymerisation synthesis.

1.5. Controlled/living Radical Polymerisation

Most of the cationic polymers were obtained via chemical synthesis. The classic synthesis approach is represented by free radical polymerisation, which is a chain addition reaction in which monomers are added to free radicals and propagated into polymer chains. The free radicals can be created by various methods, such as the thermal decomposition or by the photolysis. The generated free radicals, which have unpaired electrons, are highly active and tend to “attack” the monomer molecules and initiate a polymerisation reaction. In carbon-carbon double bonds, one pair of electron forms a sigma bond and the other pair is held by pi bond which are less stable than a sigma bond. The free radical “attacks” one electron from a pi bond, resulting in the formation of a stable sigma bond with the carbon atom and one free electron, turning the whole molecule into a free radical. The newly generated free radical molecule continues to add to monomer molecules and propagate into polymer chains (figure 1.23)²⁸⁴.

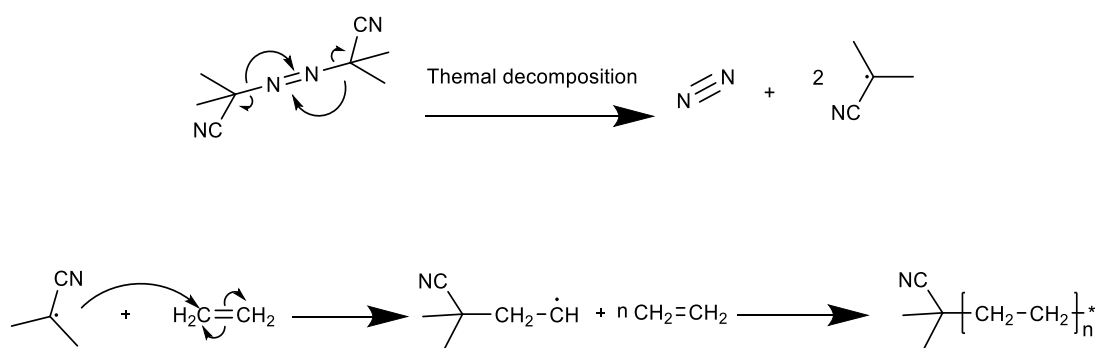


Figure 1.23. The thermal decomposition of AIBN and the free radical polymerisation of ethylene into polyethylene.

A free radical polymerisation is an approach of high value in the synthesis of polymers, both in the research and commercial scale. It provides an affordable and simple technique in the synthesis of polymers in large quantities²⁸⁵. Besides, the free radical polymerisation technique can be applied to a wide range of monomers, including methacrylates, styrenes, and acrylamides, under different conditions²⁸⁶. Nonetheless, the free radical polymerisation has little control over the polymer structure and polymer

molecular weight distribution. This is explained by irreversible termination reactions throughout the reaction process²⁸⁷.

In the past four decades, there has been a tremendous advance in the field of polymer synthesis due to the discovery and development of controlled free radical polymerisation techniques (CRP techniques)²⁸⁸. The advancement in the area of controlled polymerisation enabled the synthesis of desired macromolecules in a more convenient and efficient way. Moreover, CRP provides control over the molecular weights, molecular weight distribution (polydispersity, Φ) and well-defined functional end groups. In recent years, CRP techniques have been widely applied to the synthesis of a variety of polymers and copolymers^{289,290}. Several unique CRP techniques have been discovered and applied in the field of research and manufacture.

1.5.1. Different CRP Technique Applied in Polymer Synthesis

- Nitroxide-mediated polymerisation

One of the earliest CRP technique reported is stable free radical polymerisation (SFRP), published by Georges and his co-workers^{291,292} and the nitroxide-mediated polymerisation (NMP) is the most widely examined SFRP. The control in NMP is achieved with dynamic equilibration between dormant alkoxyamines and actively propagating radicals (figure 1.24)²⁹³.

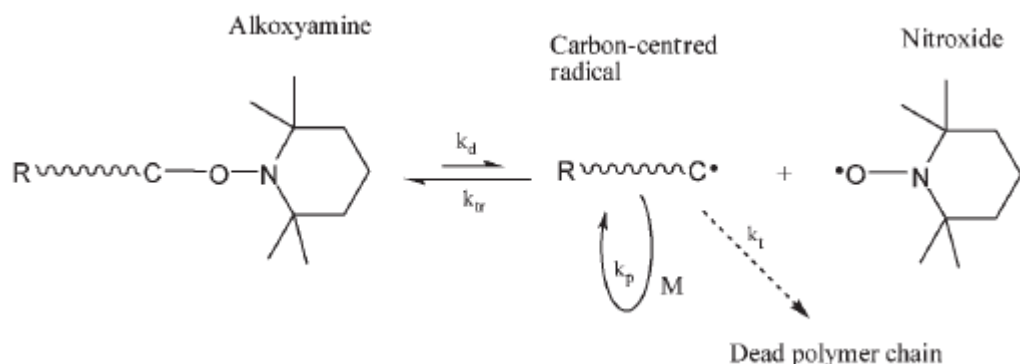


Figure 1.24 Nitroxide-mediated polymerization: k_d is the dissociation rate coefficient, k_{tr} is the trapping rate coefficient, k_p is the propagation rate coefficient and k_t is the termination rate coefficient. Figure adapted from Etmimi et al.²⁹⁴

At high temperatures, the carbon-oxygen bond of the dormant alkoxyamines is cleaved into a nitroxide and a free radical. The free radical reacts with monomers and propagates into polymer chains. The propagated polymer chain with a free electron can

be terminated by a nitroxide into a dormant alkoxyamine, before it is cleaved again into a nitroxide and a new free radical. The NMP provided control over the molecular weight of the polymer, but there are limitations such as the requirement of a relatively high reaction temperature ($\sim 120^\circ\text{C}$) and only a narrow range of monomers can be polymerised via such a technique²⁹³.

- Atom-transfer radical-polymerisation

Atom transfer radical polymerisation (ATRP) is another CRP technique that relies on the use of an alkyl halide initiator. A transition metal complex, typically Cu species, is the key to an oxidation-reduction mechanism. The alkyl halide is transferred to the transition metal complex, generating a higher oxidation state of the metal and a free radical. The free radical interacts with monomers and propagates into polymer chains. The transition metal complex with the higher oxidation state can reversibly transfer the halogen to the polymer chain with the free electron, resulting in a dormant polymer chain and a lower oxidation state complex (figure 1.25)²⁹⁵.

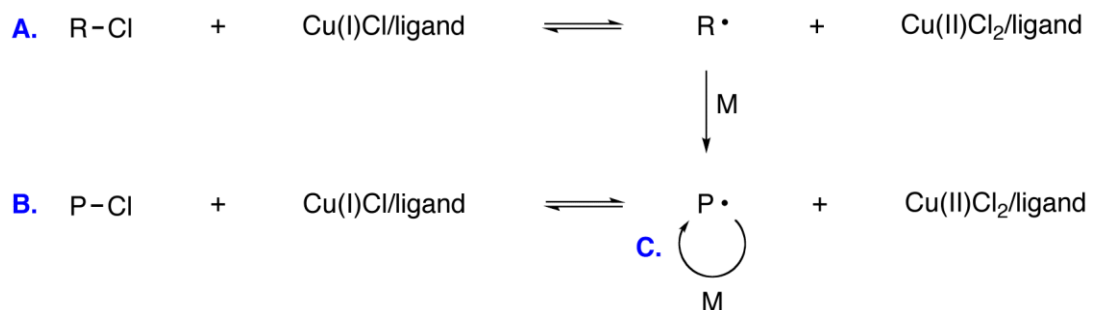


Figure 1.25 Mechanism of ATRP. An alkyl halide compound is transferred to the transition complex generating a higher oxidation state of the metal and a free radical (R^\cdot). The free radical is added to monomers to propagate into polymer chains (P).

ATRP is reported to be the most widely studied CRP technique and has been utilized in many applications. However, one disadvantage of this method is the metal catalyst can be considered as contamination, the removal of the toxic metal transition from the polymers may be critical for further application.

- Reversible addition-fragmentation chain transfer polymerisation

Reversible addition-fragmentation chain transfer (RAFT) polymerisation, another CRP technique that based on the use of thiocarbonylthio compounds as a chain transfer agent (CTA) received considerable attention in the past few years. Reversible addition-fragmentation chain transfer (RAFT) polymerisation is, by IUPAC definition, one of

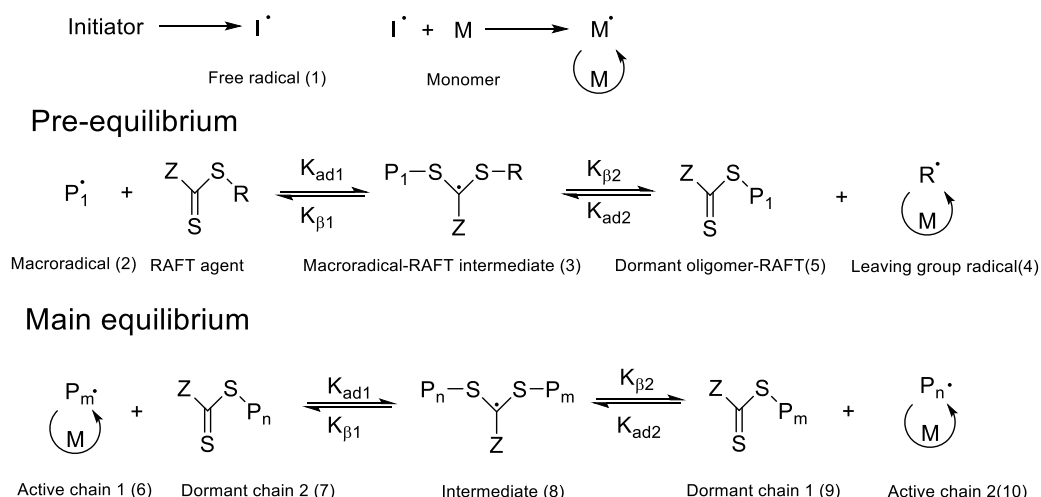
many controlled radical polymerisations in which “chain activation and chain deactivation involve a degenerative chain-transfer process which occurs by a two-step addition-fragmentation mechanism”. The control in RAFT polymerisation is achieved via the use of a degenerative chain transfer agent, which is the key to maintain a balance between addition, intermedia cleavage and propagation. First discovered by the Commonwealth Scientific and Industrial Research Organisation (CSIRO) of Australia in 1998, RAFT polymerisation developed rapidly and now is one of the most crucial CRP techniques^{287,296}. RAFT polymerisation has been used to synthesise a wide range of polymers with low polydispersity. Also, it has been applied in the synthesis of block copolymers as well as polymers with different architectures such as star-shaped, brush and comb^{297,298}. With the development of polymer-based drug delivery systems, the need for novel polymers that meet certain criteria as delivery vectors has increased dramatically. Since RAFT polymerisation technique is a versatile and convenient tool to produce well-defined polymers of various shapes and molecular weights, it has been used in the production of novel polymers that serve as drug and gene delivery vectors.

1.5.2. The RAFT Polymerisation Mechanism

With the recent development of CRP science, the RAFT polymerisation mechanism has been revealed by several studies^{299,300}. As a brief description, RAFT polymerisation process can be divided into 4 phases, being initiation, pre-equilibrium, main equilibrium and termination, as demonstrated in Scheme 1.1 using dithioesters RAFT agent as an example. Firstly, to initiate the polymerisation, free radicals must be generated. Since RAFT polymerisation shares a similarity in some essential steps with a conventional free radical polymerisation, methods employed to generated free radicals in conventional free radical polymerisation can be applied. This is of great importance, for this means that the most commonly used initiators, such as 2,2-azobis(2-methylpropionitrile) (AIBN) which can be applied in a wide range of temperature, is also applicable in RAFT polymerisations. The generated free radicals (1) would attack monomers and propagate to form macroradicals (2) which are mainly in the form of oligomeric molecules. The second phase is the pre-equilibrium phase, in which the generated macroradicals (2) add to the sulphur-carbon double bond of the RAFT agent, producing macroradicals-RAFT intermediate molecule (3). The produced macroradicals-RAFT intermediate molecule (3) undergoes β -scission, either going back to form the macroradicals (2) and the original RAFT agent or going forward to release a

leaving group radical (4) and a new dormant oligomer-RAFT (5) compound that serves as RAFT agent. When all the leaving groups from the initial RAFT agent have been released, the reaction enters the main equilibrium phase. In the main equilibrium, a propagated macroradicals living chain (6) would attack a RAFT agent-dormant chain (7) molecule, forming an intermediate molecule (8). The intermediate could go back to the living chain (6) and dormant-RAFT molecule (7), or it could move forward and replace the current dormant chain with a living chain to form a new dormant chain (10) and release the original dormant chain as a new radical chain (9). The recurring process established the equilibrium between dormant and living chains by which living/controlled characteristics are induced in the polymerisation. Towards the end of the polymerisation, as the monomers were consumed, radicals would be terminated through a bi-radical termination process and become dead species.

Initial initialtion



Scheme 1.1 Schematic illustration of the initial stage, pre-equilibrium stage and main equilibrium stage of RFAT polymerisation process. P_1' , P_m' and P_n' generally refers to free radical polymer chains generated during the reaction. K_{ad} represents the addition rate coefficients, K_β represents fragmentation rate coefficients.

Kinetic parameters have been given to describe the individual reactions in both pre-equilibrium and main equilibrium. The addition rate coefficients were referred to as K_{ad} and fragmentation rate coefficients as K_β . It is worth noticing that the K_{ad} and K_β values of the pre-equilibrium and main equilibrium are decided by different factors. In the asymmetric pre-equilibrium process, the coefficients are related to the chemical properties of the chain transfer agent and radicals employed while in the symmetric main equilibrium, it is related to the living and dormant chains.

1.5.3. RAFT Agents and its Compatibility with Monomers

RAFT agents are the chain transfer reagents employed in the process of the reversible addition-fragmentation chain transfer polymerisation, and they play a vital role. The catalogue of RAFT agents covers a wide range of compounds including dithioesters, dithiocarbamates, trithiocarbonates and xanthates as shown in figure 1.26. All these compounds share the same C=S structure which plays a vital role in the process of RAFT polymerisation.

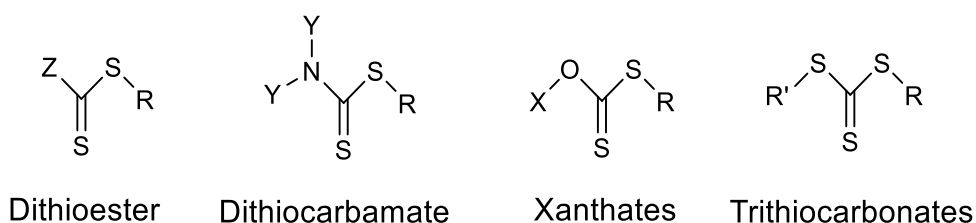


Figure 1.26 Structures of different types of RAFT agents.

Apart from the C=S structure, there are other structures that could affect the RAFT polymerisation process greatly. The important structures in these RAFT-agents are referred to as Z groups and R groups^{301,302}. The Z groups control the reactivity of the RAFT agent as it determines the reactivity of the C=S bond with radicals. Also, the Z groups have a critical effect on the lifetime of the macroradicals-RAFT intermediate molecules formed during the RAFT polymerisation.

As the Z groups govern the reactivity of the RAFT agents, the structure of R groups controls the ability to mediate the polymerisation in a controlled way. There are two key features for the R group. Firstly, the R group should be a good free radical leaving group. Secondly, the leaving group radical then generated must be able to serve as an initiator and propagate. Also, the R group will have a profound effect on the kinetics in the pre-equilibrium step and overall control of the main equilibrium.

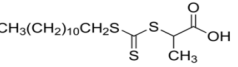
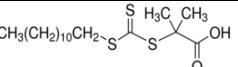
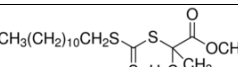
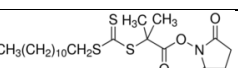
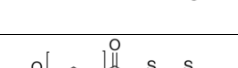
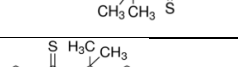
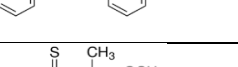
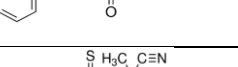
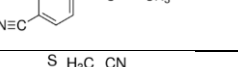
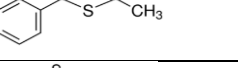
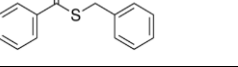
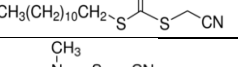
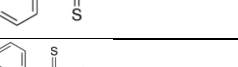
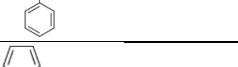
With the proper combination of Z groups and R groups, some very effective RAFT agents can be produced. However, the efficiency is closely related to the monomer employed in the polymerisation reaction. An effective RAFT agent for one type of monomer may be found to be inefficient for another. As there are a huge amount of RAFT agents available and the mechanism of how each kind of Z group and R group affect the overall property of a RAFT agent is highly complicated, and is not discussed here in this chapter. However, based on the CSIRO's RAFT agent monomer matching guide,

Grajales et al. have summarized an abundant number of the commonly used RAFT agents and their compatibilities with some most commonly used monomer types as is demonstrated in table 1.6 and 1.7³⁰³.

Table 1.6 Commonly used RAFT agents and their compatibilities with monomers.³⁰³ Where the number of + indicated the level of good compatibility with according monomers and – represent insufficient compatibility with such monomer.

Structure	Styrene	Acrylate	Acrylamide	Meth-acrylate	Meth-acrylamide	Vinyl Ester	Vinyl Amides
<chem>CH3(CH2)10CH2S-C(=S)CH2-C(=O)CH3</chem>	++	+	+	+++	+++	-	-
<chem>CH3(CH2)10CH2-S-C(=S)CH2-CH(C(=O)O)CH3</chem>	+++	+++	+++	+	+	-	-
<chem>CH3(CH2)10CH2S-C(=S)CH2-C(=O)OC(CH3)2</chem>	+++	+++	+++	+	+	-	-
<chem>CH3(CH2)10CH2S-C(=S)CH2-CH(C(=O)O)C1=CC=CC=C1</chem>	+++	+++	+++	+	+	-	-
<chem>CH3CO[CH2]nO[CH2]C(=S)CH2-CH(C(=O)SC12H25)CH3</chem>	+++	+++	+++	+	+	-	-
<chem>Ph-C(=S)S-CH2-CH(C(=O)O)CH3</chem>	++	++	++	+++	+++	-	-
<chem>Ph-C(=S)S-CH2-CH(C(=O)OCH3)CH3</chem>	++	++	++	+++	+++	-	-
<chem>Ph-C(=S)S-CH2-CH(C#N)CH3</chem>	+++	+	-	+++	+++	-	-
<chem>Ph-C(=S)S-CH2-CH(C#N)CH2CH(C(=O)O)CH3</chem>	++	+	+	+++	+++	-	-
<chem>Ph-C(=S)S-CH2-CH(C#N)CH3</chem>	++	+	-	+++	+++	-	-
<chem>Ph-C(=S)S-CH2-CHPh</chem>	++	+	+	+++	+++	-	-
<chem>CH3(CH2)10CH2S-C(=S)S-CH2CN</chem>	+++	+++	+++	-	-	-	-
<chem>Ph-N(C)C(=S)S-CH2CN</chem>	-	-	-	-	-	+++	+++
<chem>Ph-N(C)C(=S)S-CH2-CH2-CN</chem>	-	-	-	-	-	+++	+++
<chem>Ph-C(=S)S-CH2-CHPh</chem>	-	-	-	-	-	+++	+++

Table 1.7 Corresponding chemical description of RAFT agents in table 1.6.

Structure	Chemical Name
	2-(Dodecylthiocarbonothioylthio)propionic acid
	2-(Dodecylthiocarbonothioylthio)-2-methylpropionic acid
	Methyl 2-(dodecylthiocarbonothioylthio)-2-methylpropionate
	2-(Dodecylthiocarbonothioylthio)-2-methylpropionic acid N-hydroxysuccinimide ester
	Poly(ethylene glycol) methyl ether 2-(dodecylthiocarbonothioylthio)-2-methylpropionate
	2-Phenyl-2-propyl benzodithioate
	1-(Methoxycarbonyl)ethyl benzodithioate
	2-Cyano-2-propyl 4-cyanobenzodithioate
	4-Cyano-4-(phenylcarbonothioylthio)pentanoic acid
	2-Cyano-2-propyl benzodithioate
	Benzyl benzodithioate
	Cyanomethyl dodecyl trithiocarbonate
	Cyanomethyl methyl(phenyl)carbamodithioate
	Cyanomethyl diphenylcarbamodithioate
	Benzyl 1H-pyrrole-1-carbodithioate

RAFT polymerisation is one of the living/controlled polymerisations that enables control over polymer architecture and molecular weight through the selection of appropriate chain transfer agents, also called RAFT agents. To synthesise polymers with desired molecular weight, architecture and low polydispersity, the RAFT polymerisation technique was employed in this study.

1.6. Gene therapy for Tendon injury

In past decades, studies have focused on establishing gene delivery systems, both viral and non-viral, for healing and regeneration of tendon tissue. Some of their findings have been highlighted and summarised in table 1.8.

Table 1.8 Use of gene transfection as an advanced delivery system for tendon healing and corresponding vectors³⁰⁴

<u>Gene</u>	<u>Vector</u>	<u>Delivery system</u>	<u>Animal/Human model</u>	<u>Ref</u>
<i>BMP-2, Smad8</i>	Liposome	<i>in vitro</i>	Rat, Achilles tendon	³⁰⁵
<i>BMP-14</i>	Adenovirus	<i>In vivo/ in vitro</i>	Rat, Achilles tendon	¹⁷⁰
<i>TGF-β1</i>	PEI-modified PLGA Nanospheres	<i>In vivo & in vitro</i>	Chicken, flexor tendon	³⁰⁶
<i>Gal</i>	HVJ*-liposomes	<i>In vivo/in vitro</i>	Rat, patellar tendon	³⁰⁷
<i>DCN, IL-10 &TGF-β</i>	TransIT® -LT1 (polymersome)	<i>In vitro</i>	Primary human tenocytes	³⁰⁸
<i>Fmod</i>	Histidylated liposomes & linear polyethyleneimine	<i>In vitro/in vivo</i>	Rat, Achilles tendon	^{309,}
<i>FAK & BMP-12</i>	Adenovirus	<i>In vitro</i>	Chicken Achilles tendon	^{310,311}
<i>BMP-12,13</i>	Adenovirus	<i>In vivo</i>	Rabbit semitendinosus, flexor, and patellar tendons	^{9,312, 313}
<i>bFGF</i>	Adeno-associated viral vectors	<i>In vitro</i>	Rat intra-synovial tendon tenocyte	³¹⁴
<i>TGF</i>	Adenovirus	<i>In vivo</i>	Patellar tendon	³¹⁵
<i>DCN</i>	Lentiviral vectors	<i>In vivo</i>	Rat patellar tendon	³¹⁶

For example, Delalande et al. reported the used of plasmid DNA (pDNA) encoding fibromodulin encapsulated in histidylated liposomes and histidylated liner polyethyleneimine polycomplexes on a rat Achilles tendon laceration model³⁰⁹. The results showed that, based on stiffness and histological analysis, treated tendons demonstrated an enhanced healing response that resulted in a tissue that was more phenotypically similar to healthy tendon than control groups³⁰⁹. Adenovirus vectors have been used for the delivery of exogenous *FAK* gene and *BMP-12* gene into chicken tendon cells, resulting in a significant increase in expression of these genes when compared with controls, and in an enhanced healing of tendon tissue^{310,311}. In another study, adenovirus promoting the expression of *BMP-14* was transfected into the rat Achilles tendon laceration model. Histological and biomechanical effects were examined, and results showed that tendon treated with transfection exhibited 70% greater tensile strength and increased cellular proliferation of tenocytes when compared

with control groups at 2 weeks post-repair. No inflammatory response or production of undesired bone or cartilage was observed in this study¹⁷⁰. Another example provided by Lu et al. is the transfection of rat patellar tendon cells with lentiviral-encoded shRNA to silence the expression of decorin specifically. Histological and biomechanical studies showed that downregulation of decorin to an appropriate level could promote the repair and regeneration of patellar tendon, and can result in a reduction in scar formation³¹⁶.

Moreover, downregulation of the intra-synthesis of TGF- β 1 can be beneficial for the regeneration of tendon tissue. A PEI-modified poly (lactic-glycolic) acid (PLGA) nanosphere delivery system that can incorporate plasmids was shown to inhibit the expression of TGF- β 1 specifically. The biodegradable PLGA nanospheres were first blended with polyethylenimine (PEI) solution to allow PEI adsorption to the surface of these nanospheres. Plasmid DNA can electrostatically bind to the cationic moieties of PEI on the surface of the PLGA nanoparticles. Results indicated the plasmid delivered into tenocytes can inhibit the expression of TGF- β 1 with an lasting effect of more than 6 weeks³⁰⁶. In addition, Abbah et al. used plasmid DNAs encoding decorin and interleukin-10 to co-transfect human tenocytes with a commercially available cationic polymer transfection kit TransIT®-LT1 to suppress the expression of TGF- β and demonstrated positive results *in vitro*³⁰⁸.

By identifying the target gene or target receptor, the specific delivery system can be designed. Studies have focused on exploring the potential gene targets for gene therapy in the treatment of tendon injury. Some of the commonly targeted genes have been summarised in table 1.9.

Table 1.9 Commonly targeted genes in tendon regeneration gene therapy³⁰⁴.

Gene Symbol	Corresponding molecule	Primary function	Ref
<i>COL1α1</i>	Collagen type I	Extracellular Matrix structural constituent synthesis; identical protein binding;	34,82
<i>COL3α1</i>	Collagen Type III	Extracellular Matrix structural constituent synthesis; identical protein binding;	51,82
<i>COL5α1</i>	Collagen Type V	Extracellular Matrix structural constituent synthesis; identical protein binding;	37,53
<i>TNC</i>	Tenascin-C	Encodes an Extracellular Matrix protein;	10,59
<i>ACAN</i>	Aggrecan	Encodes an Extracellular Matrix protein; mutations in this gene may be involved in skeletal degeneration.	10,51
<i>MMP</i>	Matrix Metallo-Proteinase	Proteins of MMP family are involved in the hydrolysis of extracellular matrix in healthy tissue	59
<i>TGFβ1</i>	Transforming Growth Factor β1	Encodes a member of the TGFβ family of cytokines.	317,318
<i>IGF-1/IGF-2</i>	Insulin-like Growth Factor	Encodes IGF-1/IGF-2, which is processed from a precursor, bound to a receptor, and then secreted.	319
<i>PDGFA/PDGFB</i>	platelet-derived growth factor alpha/beta	Encodes PDGFA/PDGFB	320
<i>ELN</i>	Elastin	Encodes elastin, an extracellular matrix structural constituent	321
<i>FBN2</i>	fibrillin 2	Encodes fibrillin 2 an extracellular matrix structural constituent	321
<i>Sex</i>	Scleraxis	This gene encodes a protein is expressed during embryonic development of tendons and ligaments.	322,323
<i>Tnmd</i>	Tenomodulin	This gene is also a candidate gene for age-related macular degeneration, though a direct link has yet to be demonstrated	323,324
<i>Fmod</i>	fibromodulin	The encoded protein may play a role in the formation of extracellular matrix and also regulate TGF-beta level.	325

With an advanced understanding of the composition tendon tissue and knowledge of the functions tendon components during the healing process of tendon tissue, type III collagen has been identified as a critical molecule in scar tissue formation during the healing process of the tendon. The *COL3α1* gene, which produces collagen III protein, is a potential target in gene therapy for tendon injury. By using specific small interference RNA, the expression of *COL3α1* gene can be suppressed to reduce the production of type III collagen, further reducing the formation of scar tissue during tendon healing.

However, an efficient gene delivery system is required. The cationic polymer-based delivery system is a preferred tool for the delivery of nucleic materials for its good biocompatibility, potential for chemical modification, easy manufacturing process and ability to condense with the nucleic acid.

Poly (N,N'-dimethylaminoethyl acrylate) (PDMAEA), a biodegradable cationic polymer, is a strong candidate to be developed into a gene delivery system. PDMAEA is

consists of repeated units of DMAEA monomer that has a tertiary amine, which enables the quick protonation of PDMAEA under acidic environment. Protonated PDMAEA is condensed with nucleic materials to form polyplexes that serve as a gene delivery vector. Moreover, it is a biodegradable material that is perfectly suited for the *in vivo* delivery of small molecules.

1.7. Thesis Aims and Objectives

The overall **aim of this thesis** is to develop a PDMAEA based siRNA delivery system that can be locally injected into the site of injury to suppress the *COL3α1* gene expression to achieve the improvement of tendon healing.

The thesis was realised by following these four steps: **The first objective** was to synthesise a library of PDMAEA polymers of different molecular weights and architectures. The RAFT polymerisation technique was utilized to achieve controlled polymerisation with desired molecular weight and low polydispersity. It is reported that polymer molecular weight and architecture would affect its vital parameter as a delivery vector such as toxicity and transfection efficiency^{326,327,328}. The synthesized polymers were purified and characterised. These works are described and discussed in chapter three.

The second objective was to formulate the PDMAEA polymer with dsDNA and siRNA to form polyplexes. The formulated polyplexes were characterised by agarose gel electrophoresis to confirm the successful formation. The polyplexes were also characterised by dynamic light scattering to obtain their hydrodynamic diameter and zeta-potential. These works are described and discussed in chapter four.

The third objective was to determine the cytotoxicity of the synthesized PDMAEA polymers and according to polyplexes. The cytotoxicity of PDMAEA polymers and polyplexes were determined using cell proliferation assay and cell metabolic activity assay. Mouse 3T3 fibroblast cells and adult equine Achilles tenocytes were cultured as a model. These works were presented in chapter five.

The fourth objective was to transfet equine tenocytes with siRNA-PDMAEA polyplexes and observe its silencing effect by qPCR. The type III collagen protein expression was determined by immunocytochemistry. This part of the thesis is described and discussed in chapter six.

All the general materials and methods involved were documented and presented in chapter two.

The thesis is ended by a summary of the overall performance of PDMAEA polymer as a gene delivery vector based on the data presented, as well as a suggestion for further improvements of the system and possible future work.

1.8. References

- 1 Nunley, J. A. *The Achilles tendon : treatment and rehabilitation.* (Springer, 2009).
- 2 Liu, C. F. *et al.* What We Should Know Before Using Tissue Engineering Techniques to Repair Injured Tendons: A Developmental Biology Perspective. *Tissue Eng Part B-Re* **17**, 165-176, doi:10.1089/ten.teb.2010.0662 (2011).
- 3 Ker, R. F., Alexander, R. M. & Bennett, M. B. Why Are Mammalian Tendons So Thick. *J Zool* **216**, 309-324, doi:DOI 10.1111/j.1469-7998.1988.tb02432.x (1988).
- 4 Kannus, P. Structure of the tendon connective tissue. *Scand J Med Sci Sports* **10**, 312-320 (2000).
- 5 Screen, H. R., Berk, D. E., Kadler, K. E., Ramirez, F. & Young, M. F. Tendon functional extracellular matrix. *J Orthop Res* **33**, 793-799, doi:10.1002/jor.22818 (2015).
- 6 Chuen, F. S. *et al.* Immunohistochemical characterization of cells in adult human patellar tendons. *J Histochem Cytochem* **52**, 1151-1157, doi:10.1369/jhc.3A6232.2004 (2004).
- 7 Bi, Y. *et al.* Identification of tendon stem/progenitor cells and the role of the extracellular matrix in their niche. *Nat Med* **13**, 1219-1227, doi:10.1038/nm1630 (2007).
- 8 Kastelic, J., Galeski, A. & Baer, E. The multicomposite structure of tendon. *Connect Tissue Res* **6**, 11-23 (1978).
- 9 Sharma, P. & Maffulli, N. Current concepts review tendon injury and tendinopathy: Healing and repair. *J Bone Joint Surg Am* **87a**, 187-202, doi:10.2106/Jbjs.D.01850 (2005).
- 10 Lomas, A. J. *et al.* The past, present and future in scaffold-based tendon treatments. *Adv Drug Deliv Rev* **84**, 257-277, doi:10.1016/j.addr.2014.11.022 (2015).
- 11 Sabari, J. S. Joint structure and function: A comprehensive analysis, 3rd edition. *Am J Occup Ther* **55**, 358-358, doi:DOI 10.5014/ajot.55.3.358a (2001).
- 12 Riley, G. The pathogenesis of tendinopathy. A molecular perspective. *Rheumatology* **43**, 131-142, doi:10.1093/rheumatology/keg448 (2004).
- 13 Pins, G. D., Christiansen, D. L., Patel, R. & Silver, F. H. Self-assembly of collagen fibers. Influence of fibrillar alignment and decorin on mechanical properties. *Biophys J* **73**, 2164-2172, doi:10.1016/S0006-3495(97)78247-X (1997).
- 14 Silver, F. H., Christiansen, D., Snowhill, P. B., Chen, Y. & Landis, W. J. The role of mineral in the storage of elastic energy in turkey tendons. *Biomacromolecules* **1**, 180-185 (2000).
- 15 Ramshaw, J. A., Shah, N. K. & Brodsky, B. Gly-X-Y tripeptide frequencies in collagen: a context for host-guest triple-helical peptides. *J Struct Biol* **122**, 86-

91, doi:10.1006/jbsi.1998.3977 (1998).

16 Kramer, R. Z., Bella, J., Brodsky, B. & Berman, H. M. The crystal and molecular structure of a collagen-like peptide with a biologically relevant sequence. *J Mol Biol* **311**, 131-147, doi:10.1006/jmbi.2001.4849 (2001).

17 Shoulders, M. D. & Raines, R. T. Collagen structure and stability. *Annu Rev Biochem* **78**, 929-958, doi:10.1146/annurev.biochem.77.032207.120833 (2009).

18 Berg, R. A. & Prockop, D. J. Thermal Transition of a Non-Hydroxylated Form of Collagen - Evidence for a Role for Hydroxyproline in Stabilizing Triple-Helix of Collagen. *Biochem Biophys Res Co* **52**, 115-120, doi:10.1016/0006-291x(73)90961-3 (1973).

19 Cram, D. J. The Design of Molecular Hosts, Guests and Their Complexes. *Chem Scripta* **28**, 263-274 (1988).

20 Dai, N., Wang, X. J. & Etzkorn, F. A. The effect of a trans-locked Gly-Pro alkene isostere on collagen triple helix stability. *Journal of the American Chemical Society* **130**, 5396-+, doi:10.1021/ja711021m (2008).

21 Bella, J., Brodsky, B. & Berman, H. M. Hydration Structure of a Collagen Peptide. *Structure* **3**, 893-906, doi:10.1016/S0969-2126(01)00224-6 (1995).

22 Bella, J., Eaton, M., Brodsky, B. & Berman, H. M. Crystal-Structure and Molecular-Structure of a Collagen-Like Peptide at 1.9-Angstrom Resolution. *Science* **266**, 75-81, doi:10.1126/science.7695699 (1994).

23 Berisio, R., Vitagliano, L., Mazzarella, L. & Zagari, A. Crystal structure of the collagen triple helix model [(Pro-Pro-Gly)(10)](3). *Protein Sci* **11**, 262-270, doi:10.1110/ps.32602 (2002).

24 Gerig, J. T. & Mcleod, R. S. Conformations of Cis-4-Fluoro-L-Proline and Trans-4-Fluoro-L-Proline in Aqueous-Solution. *Journal of the American Chemical Society* **95**, 5725-5729, doi:10.1021/ja00798a046 (1973).

25 Torchia, D. A. Evidence for Cis Peptide Bonds in Copolypeptides of Glycine and Proline. *Biochemistry-US* **11**, 1462-&, doi:10.1021/bi00758a021 (1972).

26 Shoulders, M. D., Hodges, J. A. & Raines, R. T. Reciprocity of steric and stereoelectronic effects in the collagen triple helix. *Journal of the American Chemical Society* **128**, 8112-8113, doi:10.1021/ja061793d (2006).

27 Evans, J. H. & Barbenel, J. C. Structural and mechanical properties of tendon related to function. *Equine Vet J* **7**, 1-8 (1975).

28 Towler, D. A. & Gelberman, R. H. The alchemy of tendon repair: a primer for the (S)mad scientist. *J Clin Invest* **116**, 863-866, doi:10.1172/JCI28320 (2006).

29 Beck, K. & Brodsky, B. Supercoiled protein motifs: the collagen triple-helix and the alpha-helical coiled coil. *J Struct Biol* **122**, 17-29, doi:10.1006/jbsi.1998.3965 (1998).

30 Silver, F. H., Langley, K. H. & Trelstad, R. L. Type-I Collagen Fibrillogenesis - Initiation Via Reversible Linear and Lateral Growth Steps. *Biopolymers* **18**, 2523-2535, doi:10.1002/bip.1979.360181011 (1979).

31 Prockop, D. J. & Kivirikko, K. I. Heritable Diseases of Collagen. *New Engl J Med* **311**, 376-386, doi:10.1056/Nejm198408093110606 (1984).

32 Bienkowski, R. S., Cowan, M. J., McDonald, J. A. & Crystal, R. G. Degradation of Newly Synthesized Collagen. *Journal of Biological Chemistry* **253**, 4356-4363 (1978).

33 Tsuzaki, M., Yamauchi, M. & Banes, A. J. Tendon collagens: extracellular matrix composition in shear stress and tensile components of flexor tendons. *Connect Tissue Res* **29**, 141-152 (1993).

34 Riley, G. P. Gene expression and matrix turnover in overused and damaged

tendons. *Scand J Med Sci Spor* **15**, 241-251, doi:10.1111/j.1600-0838.2005.00456.x (2005).

35 Riley, G. P. *et al.* Tendon Degeneration and Chronic Shoulder Pain - Changes in the Collagen Composition of the Human Rotator Cuff Tendons in Rotator Cuff Tendinitis. *Ann Rheum Dis* **53**, 359-366, doi:DOI 10.1136/ard.53.6.359 (1994).

36 Wenstrup, R. J. *et al.* Type V collagen controls the initiation of collagen fibril assembly. *J Biol Chem* **279**, 53331-53337, doi:10.1074/jbc.M409622200 (2004).

37 Lu, P. *et al.* Col V siRNA engineered tenocytes for tendon tissue engineering. *PLoS One* **6**, e21154, doi:10.1371/journal.pone.0021154 (2011).

38 September, A. V. *et al.* The COL12A1 and COL14A1 genes and Achilles tendon injuries. *Int J Sports Med* **29**, 257-263, doi:10.1055/s-2007-965127 (2008).

39 Arai, K., Kasashima, Y., Kobayashi, A., Kuwano, A. & Yoshihara, T. TGF-beta alters collagen XII and XIV mRNA levels in cultured equine tenocytes. *Matrix Biol* **21**, 243-250, doi:Pii S0945-053x(02)00005-7 Doi 10.1016/S0945-053x(02)00005-7 (2002).

40 Abbah, S. A., Spanoudes, K., O'Brien, T., Pandit, A. & Zeugolis, D. I. Assessment of stem cell carriers for tendon tissue engineering in pre-clinical models. *Stem Cell Res Ther* **5**, 38, doi:10.1186/scrt426 (2014).

41 Longo, U. G., Lamberti, A., Maffulli, N. & Denaro, V. Tendon augmentation grafts: a systematic review. *Br Med Bull* **94**, 165-188, doi:10.1093/bmb/ldp051 (2010).

42 Tang, J. B. Tendon injuries across the world: treatment. *Injury* **37**, 1036-1042, doi:10.1016/j.injury.2006.07.027 (2006).

43 Sharma, P. & Maffulli, N. Biology of tendon injury: healing, modeling and remodeling. *J Musculoskelet Neuronat Interact* **6**, 181-190 (2006).

44 Khan, K. M., Cook, J. L., Kannus, P., Maffulli, N. & Bonar, S. F. Time to abandon the "tendinitis" myth. *BMJ* **324**, 626-627 (2002).

45 Rees, J. D., Maffulli, N. & Cook, J. Management of tendinopathy. *Am J Sports Med* **37**, 1855-1867, doi:10.1177/0363546508324283 (2009).

46 Williams, J. G. Achilles tendon lesions in sport. *Sports Med* **3**, 114-135 (1986).

47 Johansson, K., Lempainen, L., Sarimo, J., Laitala-Leinonen, T. & Orava, S. Different distributions of operative diagnoses for Achilles tendon overuse injuries in Italian and Finnish athletes. *Muscles Ligaments Tendons J* **6**, 111-115, doi:10.11138/mltj/2016.6.1.111 (2016).

48 Selvanetti, A., Cipolla, M. & Puddu, G. Overuse tendon injuries: Basic science and classification. *Oper Techn Sport Med* **5**, 110-117, doi:Doi 10.1016/S1060-1872(97)80031-7 (1997).

49 Benazzo, F., Zanon, G. & Maffulli, N. An operative approach to Achilles tendinopathy. *Sports Med Arthrosc* **8**, 96-101, doi:Doi 10.1097/00132585-200008010-00009 (2000).

50 Arndt, A. N., Komi, P. V., Bruggemann, G. P. & Lukkariniemi, J. Individual muscle contributions to the in vivo Achilles tendon force. *Clin Biomech* **13**, 532-541, doi:Doi 10.1016/S0268-0033(98)00032-1 (1998).

51 Riley, G. Tendinopathy--from basic science to treatment. *Nat Clin Pract Rheumatol* **4**, 82-89, doi:10.1038/ncprheum0700 (2008).

52 Mokone, G. G. *et al.* The guanine-thymine dinucleotide repeat polymorphism within the tenascin-C gene is associated with achilles tendon injuries. *Am J Sport Med* **33**, 1016-1021, doi:10.1177/0363546504271986 (2005).

53 Mokone, G. G., Schwellnus, M. P., Noakes, T. D. & Collins, M. The COL5A1 gene and Achilles tendon pathology. *Scand J Med Sci Spor* **16**, 19-26, doi:10.1111/j.1600-0838.2005.00439.x (2006).

54 Chalmers, J. Review article: Treatment of Achilles tendon ruptures. *J Orthop Surg (Hong Kong)* **8**, 97-99, doi:10.1177/230949900000800118 (2000).

55 Myklebust, G. & Bahr, R. Return to play guidelines after anterior cruciate ligament surgery. *Br J Sports Med* **39**, 127-131, doi:10.1136/bjsm.2004.010900 (2005).

56 Arner, O., Lindholm, A. & Orell, S. R. Histologic changes in subcutaneous rupture of the Achilles tendon; a study of 74 cases. *Acta Chir Scand* **116**, 484-490 (1959).

57 Tallon, C., Maffulli, N. & Ewen, S. W. B. Ruptured Achilles tendons are significantly more degenerated than tendinopathic tendons. *Med Sci Sport Exer* **33**, 1983-1990, doi:10.1097/00005768-200112000-00002 (2001).

58 Austin, J. C., Phornphutkul, C. & Wojtys, E. M. Loss of knee extension after anterior cruciate ligament reconstruction: Effects of knee position and graft tensioning. *J Bone Joint Surg Am* **89a**, 1565-1574, doi:10.2106/Jbjs.F.00370 (2007).

59 Docheva, D., Muller, S. A., Majewski, M. & Evans, C. H. Biologics for tendon repair. *Adv Drug Deliver Rev* **84**, 222-239, doi:10.1016/j.addr.2014.11.015 (2015).

60 Abbah, S. A., Spanoudes, K., O'Brien, T., Pandit, A. & Zeugolis, D. I. Assessment of stem cell carriers for tendon tissue engineering in pre-clinical models. *Stem Cell Research & Therapy* **5**, doi:ARTN 38 10.1186/scrt426 (2014).

61 Babraj, J. A. *et al.* Collagen synthesis in human musculoskeletal tissues and skin. *Am J Physiol-Endoc M* **289**, E864-E869, doi:10.1152/ajpendo.00243.2005 (2005).

62 Miller, B. F. *et al.* Coordinated collagen and muscle protein synthesis in human patella tendon and quadriceps muscle after exercise. *J Physiol-London* **567**, 1021-1033, doi:10.1113/jphysiol.2005.093690 (2005).

63 Thorpe, C. T. *et al.* Aspartic Acid Racemization and Collagen Degradation Markers Reveal an Accumulation of Damage in Tendon Collagen That Is Enhanced with Aging. *Journal of Biological Chemistry* **285**, 15674-15681, doi:10.1074/jbc.M109.077503 (2010).

64 Heinemeier, K. M., Schjerling, P., Heinemeier, J., Magnusson, S. P. & Kjaer, M. Lack of tissue renewal in human adult Achilles tendon is revealed by nuclear bomb C-14. *Faseb J* **27**, 2074-2079, doi:10.1096/fj.12-225599 (2013).

65 Mendias, C. L., Gumucio, J. P., Bakhurin, K. I., Lynch, E. B. & Brooks, S. V. Physiological loading of tendons induces scleraxis expression in epitenon fibroblasts. *J Orthopaed Res* **30**, 606-612, doi:10.1002/jor.21550 (2012).

66 Magnusson, S. P. & Kjaer, M. Region-specific differences in Achilles tendon cross-sectional area in runners and non-runners. *Eur J Appl Physiol* **90**, 549-553, doi:10.1007/s00421-003-0865-8 (2003).

67 Lin, T. W., Cardenas, L. & Soslowsky, L. J. Biomechanics of tendon injury and repair. *J Biomech* **37**, 865-877, doi:10.1016/j.jbiomech.2003.11.005 (2004).

68 Fenwick, S. A., Hazleman, B. L. & Riley, G. P. The vasculature and its role in the damaged and healing tendon. *Arthritis Res* **4**, 252-260, doi:DOI 10.1186/ar416 (2002).

69 Murphy, P. G., Loitz, B. J., Frank, C. B. & Hart, D. A. Influence of Exogenous Growth-Factors on the Synthesis and Secretion of Collagen Type-I and Type-III by Explants of Normal and Healing Rabbit Ligaments. *Biochem Cell Biol* **72**, 403-409, doi:DOI 10.1139/o94-054 (1994).

70 Frontera, W. R., IOC Medical Commission. & International Federation of Sports Medicine. *Rehabilitation of sports injuries : scientific basis.* (Blackwell

Science, 2003).

71 Hertling, D. & Kessler, R. M. *Management of common musculoskeletal disorders : physical therapy principles and methods*. 4th edn, (Lippincott Williams & Wilkins, 2006).

72 Abrahamsson, S. O. Matrix metabolism and healing in the flexor tendon. Experimental studies on rabbit tendon. *Scand J Plast Reconstr Surg Hand Surg Suppl* **23**, 1-51 (1991).

73 Kajikawa, Y. *et al*. GFP chimeric models exhibited a biphasic pattern of mesenchymal cell invasion in tendon healing. *J Cell Physiol* **210**, 684-691, doi:10.1002/jcp.20876 (2007).

74 Fujita, M., Hukuda, S. & Doida, Y. [Experimental study of intrinsic healing of the flexor tendon: collagen synthesis of the cultured flexor tendon cells of the canine]. *Nihon Seikeigeka Gakkai Zasshi* **66**, 326-333 (1992).

75 James, R., Kesturu, G., Balian, G. & Chhabra, A. B. Tendon: biology, biomechanics, repair, growth factors, and evolving treatment options. *J Hand Surg Am* **33**, 102-112, doi:10.1016/j.jhsa.2007.09.007 (2008).

76 Scott, A., Backman, L. J. & Speed, C. Tendinopathy: Update on Pathophysiology. *J Orthop Sports Phys Ther* **45**, 833-841, doi:10.2519/jospt.2015.5884 (2015).

77 Platt, M. A. Tendon repair and healing. *Clin Podiatr Med Surg* **22**, 553-560, vi, doi:10.1016/j.cpm.2005.08.001 (2005).

78 Maffulli, N., Waterston, S. W., Squair, J., Reaper, J. & Douglas, A. S. Changing incidence of Achilles tendon rupture in Scotland, a 15-year study. *Clin J Sport Med* **9**, 157-160, doi:Doi 10.1097/00042752-199907000-00007 (1999).

79 Sharma, P. & Maffulli, N. Tendinopathy and tendon injury: The future. *Disabil Rehabil* **30**, 1733-1745, doi:Pii 793021085 10.1080/09638280701788274 (2008).

80 King, W. J. & Krebsbach, P. H. Growth factor delivery: How surface interactions modulate release in vitro and in vivo. *Adv Drug Deliver Rev* **64**, 1239-1256, doi:10.1016/j.addr.2012.03.004 (2012).

81 Longo, U. G., Lamberti, A., Maffulli, N. & Denaro, V. Tissue engineered biological augmentation for tendon healing: a systematic review. *Brit Med Bull* **98**, 31-59, doi:10.1093/bmb/ldq030 (2011).

82 Magra, M. & Maffulli, N. Genetic aspects of tendinopathy. *J Sci Med Sport* **11**, 243-247, doi:10.1016/j.jsams.2007.04.007 (2008).

83 Thevendran, G., Sarraf, K. M., Patel, N. K., Sadri, A. & Rosenfeld, P. The ruptured Achilles tendon: a current overview from biology of rupture to treatment. *Musculoskelet Surg* **97**, 9-20, doi:10.1007/s12306-013-0251-6 (2013).

84 Gulotta, L. V. *et al*. Application of bone marrow-derived mesenchymal stem cells in a rotator cuff repair model. *Am J Sports Med* **37**, 2126-2133, doi:10.1177/0363546509339582 (2009).

85 Keeler, C. E. Gene Therapy. *J Hered* **38**, 294-298 (1947).

86 Osterman, J. V., Waddell, A. & Aposhian, H. V. DNA and Gene Therapy - Uncoating of Polyoma Pseudovirus in Mouse Embryo Cells. *P Natl Acad Sci USA* **67**, 37-&, doi:DOI 10.1073/pnas.67.1.37 (1970).

87 Aposhian, H. V. Use of DNA for Gene Therapy - Need, Experimental Approach, and Implications. *Perspectives in Biology and Medicine* **14**, 98-+ (1970).

88 Terheggen, H. G., Lowenthal, A., Lavinha, F., Colombo, J. P. & Rogers, S. Unsuccessful Trial of Gene Replacement in Arginase Deficiency. *Z Kinderheilkd* **119**, 1-3, doi:Doi 10.1007/Bf00464689 (1975).

89 Friedmann, T. Stanfield Rogers: Insights into virus vectors and failure of an

early gene therapy model. *Mol Ther* **4**, 285-288, doi:DOI 10.1006/mthe.2001.0454 (2001).

90 Beatler, E. The cline affair. *Mol Ther* **4**, 396-397 (2001).

91 Rosenberg, S. A. *et al.* Gene-Transfer into Humans - Immunotherapy of Patients with Advanced Melanoma, Using Tumor-Infiltrating Lymphocytes Modified by Retroviral Gene Transduction. *New Engl J Med* **323**, 570-578, doi:DOI 10.1056/Nejm199008303230904 (1990).

92 Fehlner-Gardiner, C. *et al.* Comparing Onrab (R) and Raboral V-Rg (R) Oral Rabies Vaccine Field Performance in Raccoons and Striped Skunks, New Brunswick, Canada, and Maine, USA. *J Wildlife Dis* **48**, 157-167, doi:DOI 10.7589/0090-3558-48.1.157 (2012).

93 Sibbald, B. Death but one unintended consequence of gene-therapy trial. *Can Med Assoc J* **164**, 1612-1612 (2001).

94 Scherman, D., Rousseau, A., Bigey, P. & Escriou, V. Genetic pharmacology: progresses in siRNA delivery and therapeutic applications. *Gene Ther* **24**, 151-156, doi:10.1038/gt.2017.6 (2017).

95 Scherman, D. *Advanced textbook on gene transfer, gene therapy, and genetic pharmacology : principles, delivery, and pharmacological and biomedical applications of nucleotide-based therapies.* (Imperial College Press, 2013).

96 Harper, S. Q. *et al.* Modular flexibility of dystrophin: Implications for gene therapy of Duchenne muscular dystrophy. *Nature Medicine* **8**, 253-261 (2002).

97 Matri, J., Chuah, M. K. L. & VandenDriessche, T. Preclinical and clinical progress in hemophilia gene therapy. *Curr Opin Hematol* **17**, 387-392 (2010).

98 Ehrhardt, A. & Kay, M. A. A new adenoviral helper-dependent vector results in long-term therapeutic levels of human coagulation factor IX at low doses in vivo. *Blood* **99**, 3923-3930 (2002).

99 Chuah, M. K. L. *et al.* Therapeutic factor VIII levels and negligible toxicity in mouse and dog models of hemophilia A following gene therapy with high-capacity adenoviral vectors. *Blood* **101**, 1734-1743 (2003).

100 Spencer, H. T. *et al.* Lentiviral Vector Platform for Production of Bioengineered Recombinant Coagulation Factor VIII. *Mol Ther* **19**, 302-309 (2011).

101 Emery, A. E. H., Muntoni, F. & Quinlivan, R. *Duchenne muscular dystrophy*. 4th edn, (Oxford University Press, 2015).

102 Graham, I. R., Hill, V. J., Manoharan, M., Inamati, G. B. & Dickson, G. Towards a therapeutic inhibition of dystrophin exon 23 splicing in mdx mouse muscle induced by antisense oligoribonucleotides (splicomers): target sequence optimisation using oligonucleotide arrays. *Journal of Gene Medicine* **6**, 1149-1158, doi:DOI 10.1002/jgm.603 (2004).

103 Arechavala-Gomeza, V. *et al.* Comparative analysis of antisense oligonucleotide sequences for targeted skipping of Exon 51 during dystrophin Pre-mRNA splicing in human muscle. *Hum Gene Ther* **18**, 798-810, doi:10.1089/hum.2006.061 (2007).

104 van Deutkom, J. C. *et al.* Local dystrophin restoration with antisense oligonucleotide PRO051. *New Engl J Med* **357**, 2677-2686, doi:DOI 10.1056/NEJMoa073108 (2007).

105 Fire, A. *et al.* Potent and specific genetic interference by double-stranded RNA in *Caenorhabditis elegans*. *Nature* **391**, 806-811, doi:DOI 10.1038/35888 (1998).

106 Lee, R. C., Feinbaum, R. L. & Ambros, V. The C-Elegans Heterochronic Gene Lin-4 Encodes Small RNAs with Antisense Complementarity to Lin-14. *Cell* **75**, 843-854, doi:DOI 10.1016/0092-8674(93)90529-Y (1993).

107 Sohail, M. *Gene silencing by RNA interference : technology and application.*

(CRC Press, 2005).

108 Brummelkamp, T. R., Bernards, R. & Agami, R. A system for stable expression of short interfering RNAs in mammalian cells. *Science* **296**, 550-553, doi:DOI 10.1126/science.1068999 (2002).

109 Deiters, A. Small Molecule Modifiers of the microRNA and RNA Interference Pathway. *Aaps J* **12**, 51-60, doi:10.1208/s12248-009-9159-3 (2010).

110 Lee, Y. *et al.* The nuclear RNase III Drosha initiates microRNA processing. *Nature* **425**, 415-419, doi:10.1038/nature01957 (2003).

111 Zeng, Y., Yi, R. & Cullen, B. R. MicroRNAs and small interfering RNAs can inhibit mRNA expression by similar mechanisms. *P Natl Acad Sci USA* **100**, 9779-9784, doi:10.1073/pnas.1630797100 (2003).

112 Grishok, A. *et al.* Genes and mechanisms related to RNA interference regulate expression of the small temporal RNAs that control C-elegans developmental timing. *Cell* **106**, 23-34, doi:Doi 10.1016/S0092-8674(01)00431-7 (2001).

113 Danquah, M. K. & Mahato, R. I. *Emerging trends in cell and gene therapy*. (Springer, 2013).

114 Bernstein, E., Caudy, A. A., Hammond, S. M. & Hannon, G. J. Role for a bidentate ribonuclease in the initiation step of RNA interference. *Nature* **409**, 363-366, doi:Doi 10.1038/35053110 (2001).

115 Hammond, S. M., Bernstein, E., Beach, D. & Hannon, G. J. An RNA-directed nuclease mediates post-transcriptional gene silencing in Drosophila cells. *Nature* **404**, 293-296 (2000).

116 Siomi, H. & Siomi, M. C. On the road to reading the RNA-interference code. *Nature* **457**, 396-404, doi:10.1038/nature07754 (2009).

117 Parker, J. S. & Barford, D. Argonaute: a scaffold for the function of short regulatory RNAs. *Trends Biochem Sci* **31**, 622-630, doi:10.1016/j.tibs.2006.09.010 (2006).

118 Gregory, R. I., Chendrimada, T. P., Cooch, N. & Shiekhattar, R. Human RISC couples microRNA biogenesis and posttranscriptional gene silencing. *Cell* **123**, 631-640, doi:10.1016/j.cell.2005.10.022 (2005).

119 Ahlquist, P. RNA-dependent RNA polymerases, viruses, and RNA silencing. *Science* **296**, 1270-1273, doi:DOI 10.1126/science.1069132 (2002).

120 Urban-Klein, B., Werth, S., Abuharbeid, S., Czubayko, F. & Aigner, A. RNAi-mediated gene-targeting through systemic application of polyethylenimine (PEI)-complexed siRNA in vivo. *Gene Ther* **12**, 461-466, doi:10.1038/sj.gt.3302425 (2005).

121 Marshall, E. Clinical trials - Gene therapy death prompts review of adenovirus vector. *Science* **286**, 2244-2245, doi:DOI 10.1126/science.286.5448.2244 (1999).

122 Thomas, C. E., Ehrhardt, A. & Kay, M. A. Progress and problems with the use of viral vectors for gene therapy. *Nature Reviews Genetics* **4**, 346-358, doi:10.1038/nrg1066 (2003).

123 Kafri, T. *et al.* Cellular immune response to adenoviral vector infected cells does not require de novo viral gene expression: Implications for gene therapy. *P Natl Acad Sci USA* **95**, 11377-11382, doi:DOI 10.1073/pnas.95.19.11377 (1998).

124 Thomas, C. E., Birkett, D., Anozie, I., Castro, M. G. & Lowenstein, P. R. Acute direct adenoviral vector cytotoxicity and chronic, but not acute, inflammatory responses correlate with decreased vector-mediated transgene expression in the brain. *Mol Ther* **3**, 36-46, doi:10.1006/mthe.2000.0224 (2001).

125 Reid, A. H., Fanning, T. G., Janczewski, T. A. & Taubenberger, J. K. Characterization of the 1918 "Spanish" influenza virus neuraminidase gene. *P*

126 *Natl Acad Sci USA* **97**, 6785-6790, doi:DOI 10.1073/pnas.100140097 (2000).

127 Morral, N. *et al.* Lethal toxicity, severe endothelial injury, and a threshold effect with high doses of an adenoviral vector in baboons. *Hum Gene Ther* **13**, 143-154, doi:Doi 10.1089/10430340152712692 (2002).

128 Yin, H. *et al.* Non-viral vectors for gene-based therapy. *Nature Reviews Genetics* **15**, 541-555, doi:10.1038/nrg3763 (2014).

129 Hornung, V. *et al.* Sequence-specific potent induction of IFN-alpha by short interfering RNA in plasmacytoid dendritic cells through TLR7. *Nature Medicine* **11**, 263-270, doi:10.1038/nm1191 (2005).

130 Diebold, S. S., Kaisho, T., Hemmi, H., Akira, S. & Sousa, C. R. E. Innate antiviral responses by means of TLR7-mediated recognition of single-stranded RNA. *Science* **303**, 1529-1531, doi:10.1126/science.1093616 (2004).

131 Heil, F. *et al.* Species-specific recognition of single-stranded RNA via toll-like receptor 7 and 8. *Science* **303**, 1526-1529, doi:10.1126/science.1093620 (2004).

132 Sioud, M. Induction of inflammatory cytokines and interferon responses by double-stranded and single-stranded siRNAs is sequence-dependent and requires endosomal localization. *J Mol Biol* **348**, 1079-1090, doi:10.1016/j.jmb.2005.03.013 (2005).

133 Cavazzana-Calvo, M. *et al.* Gene therapy of human severe combined immunodeficiency (SCID)-X1 disease. *Blood* **96**, 590a-+ (2000).

134 Cao, X. Q. *et al.* Defective Lymphoid Development in Mice Lacking Expression of the Common Cytokine Receptor-Gamma Chain. *Immunity* **2**, 223-238, doi:Doi 10.1016/1074-7613(95)90047-0 (1995).

135 Kaiser, J. Gene therapy - Seeking the cause of induced leukemias in X-SCID trial. *Science* **299**, 495-495, doi:DOI 10.1126/science.299.5606.495 (2003).

136 Jackson, A. L. *et al.* Expression profiling reveals off-target gene regulation by RNAi. *Nat Biotechnol* **21**, 635-637, doi:10.1038/nbt831 (2003).

137 Lai, C. Y., Jaruga, E., Borghouts, C. & Jazwinski, S. M. A mutation in the ATP2 gene abrogates the age asymmetry between mother and daughter cells of the yeast *Saccharomyces cerevisiae*. *Genetics* **162**, 73-87 (2002).

138 Patil, G. V. Biopolymer albumin for diagnosis and in drug delivery. *Drug Develop Res* **58**, 219-247, doi:10.1002/ddr.10157 (2003).

139 Hughes, G. A. Nanostructure-mediated drug delivery. *Nanomed-Nanotechnol* **1**, 22-30, doi:10.1016/j.nano.2004.11.009 (2005).

140 Kamiya, H., Tsuchiya, H., Yamazaki, J. & Harashima, H. Intracellular trafficking and transgene expression of viral and non-viral gene vectors. *Adv Drug Deliver Rev* **52**, 153-164, doi:Doi 10.1016/S0169-409x(01)00216-2 (2001).

141 Navarro, G., Pan, J. Y. & Torchilin, V. P. Micelle-like Nanoparticles as Carriers for DNA and siRNA. *Mol Pharmaceut* **12**, 301-313, doi:10.1021/mp5007213 (2015).

142 Luo, D. & Saltzman, W. M. Synthetic DNA delivery systems. *Nat Biotechnol* **18**, 33-37 (2000).

143 Mintzer, M. A. & Simanek, E. E. Nonviral Vectors for Gene Delivery. *Chem Rev* **109**, 259-302, doi:10.1021/cr800409e (2009).

144 Bergelson, J. M. *et al.* Isolation of a common receptor for coxsackie B viruses and adenoviruses 2 and 5. *Science* **275**, 1320-1323, doi:DOI 10.1126/science.275.5304.1320 (1997).

145 Bailey, A. & Mautner, V. Phylogenetic-Relationships among Adenovirus Serotypes. *Virology* **205**, 438-452 (1994).

146 Fields, B. N., Knipe, D. M. & Howley, P. M. *Fields virology*. 3rd edn, (Lippincott-Raven Publishers, 1996).

146 Greber, U. F. *et al.* The role of the nuclear pore complex in adenovirus DNA entry. *Embo J* **16**, 5998-6007, doi:DOI 10.1093/emboj/16.19.5998 (1997).

147 Saphire, A. C., Guan, T., Schirmer, E. C., Nemerow, G. R. & Gerace, L. Nuclear import of adenovirus DNA in vitro involves the nuclear protein import pathway and hsc70. *J Biol Chem* **275**, 4298-4304 (2000).

148 Xie, Q. *et al.* The atomic structure of adeno-associated virus (AAV-2), a vector for human gene therapy. *Proc Natl Acad Sci U S A* **99**, 10405-10410, doi:10.1073/pnas.162250899 (2002).

149 Duan, D. S. *et al.* Formation of adeno-associated virus circular genomes is differentially regulated by adenovirus E4 ORF6 and E2a gene expression. *J Virol* **73**, 161-169 (1999).

150 Bartlett, J. S., Wilcher, R. & Samulski, R. J. Infectious entry pathway of adeno-associated virus and adeno-associated virus vectors. *J Virol* **74**, 2777-2785, doi:Doi 10.1128/Jvi.74.6.2777-2785.2000 (2000).

151 Douar, A. M., Poulard, K., Stockholm, D. & Danos, O. Intracellular trafficking of adeno-associated virus vectors: Routing to the late endosomal compartment and proteasome degradation. *J Virol* **75**, 1824-1833, doi:Doi 10.1128/Jvi.75.4.1824-1833.2001 (2001).

152 Sonntag, F., Bleker, S., Leuchs, B., Fischer, R. & Kleinschmidt, J. A. Adeno-associated virus type 2 capsids with externalized VP1/VP2 trafficking domains are generated prior to passage through the cytoplasm and are maintained until uncoating occurs in the nucleus. *J Virol* **80**, 11040-11054, doi:10.1128/Jvi.01056-06 (2006).

153 Hansen, J., Qing, K. & Srivastava, A. Infection of purified nuclei by adeno-associated virus 2. *Mol Ther* **4**, 289-296, doi:DOI 10.1006/mthe.2001.0457 (2001).

154 Gregorevic, P. *et al.* Systemic delivery of genes to striated muscles using adeno-associated viral vectors. *Nature Medicine* **10**, 828-834, doi:10.1038/nm1085 (2004).

155 Ganser-Pornillos, B. K., Yeager, M. & Pornillos, O. Assembly and Architecture of HIV. *Adv Exp Med Biol* **726**, 441-465, doi:10.1007/978-1-4614-0980-9_20 (2012).

156 Coffin, J. M., Hughes, S. H. & Varmus, H. *Retroviruses*. (Cold Spring Harbor Laboratory Press, 1997).

157 Bharat, T. A. M. *et al.* Structure of the immature retroviral capsid at 8 angstrom resolution by cryo-electron microscopy. *Nature* **487**, 385-389, doi:10.1038/nature11169 (2012).

158 Levin, J. G., Mitra, M., Mascarenhas, A. & Musier-Forsyth, K. Role of HIV-1 nucleocapsid protein in HIV-1 reverse transcription. *Rna Biol* **7**, 754-774, doi:10.4161/rna.7.6.14115 (2010).

159 Butan, C., Winkler, D. C., Heymann, J. B., Craven, R. C. & Steven, A. C. RSV capsid polymorphism correlates with polymerization efficiency and envelope glycoprotein content: Implications that nucleation controls morphogenesis. *J Mol Biol* **376**, 1168-1181, doi:10.1016/j.jmb.2007.12.003 (2008).

160 Yeager, M., Wilson-Kubalek, E. M., Weiner, S. G., Brown, P. O. & Rein, A. Supramolecular organization of immature and mature murine leukemia virus revealed by electron cryo-microscopy: Implications for retroviral assembly mechanisms. *P Natl Acad Sci USA* **95**, 7299-7304, doi:DOI 10.1073/pnas.95.13.7299 (1998).

161 Zhang, W., Cao, S., Martin, J. L., Mueller, J. D. & Mansky, L. M. Morphology and ultrastructure of retrovirus particles. *Aims Biophys* **2**, 343-369,

doi:10.3934/biophy.2015.3.343 (2015).

162 Briggs, J. A. G. *et al.* The stoichiometry of Gag protein in HIV-1. *Nat Struct Mol Biol* **11**, 672-675, doi:10.1038/nsmb785 (2004).

163 Bush, D. L. & Vogt, V. M. In Vitro Assembly of Retroviruses. *Annu Rev Virol* **1**, 561-580, doi:10.1146/annurev-virology-031413-085427 (2014).

164 Callahan, R. & Smith, G. H. Common integration sites for MMTV in viral induced mouse mammary tumors. *J Mammary Gland Biol* **13**, 309-321, doi:10.1007/s10911-008-9092-6 (2008).

165 Rasmussen, I. & Vilhardt, F. Macropinocytosis Is the Entry Mechanism of Amphotropic Murine Leukemia Virus. *J Virol* **89**, 1851-1866, doi:10.1128/Jvi.02343-14 (2015).

166 Goff, S. P. Retrovirus restriction factors. *Mol Cell* **16**, 849-859, doi:DOI 10.1016/j.molcel.2004.12.001 (2004).

167 Panov, K. I., Friedrich, J. K. & Zomerdijk, J. C. B. M. A step subsequent to preinitiation complex assembly at the ribosomal RNA gene promoter is rate limiting for human RNA polymerase I-dependent transcription. *Mol Cell Biol* **21**, 2641-2649, doi:Doi 10.1128/Mcb.21.8.2641-2649.2001 (2001).

168 Ott, M. G. *et al.* Correction of X-linked chronic granulomatous disease by gene therapy, augmented by insertional activation of MDS1-EVI1, PRDM16 or SETBP1. *Nature Medicine* **12**, 401-409, doi:10.1038/nm1393 (2006).

169 Li, Z. X. *et al.* Insertional mutagenesis by replication-deficient retroviral vectors encoding the large T oncogene. *Ann Ny Acad Sci* **1106**, 95-113, doi:10.1196/annals.1392.003 (2007).

170 Bolt, P. *et al.* BMP-14 gene therapy increases tendon tensile strength in a rat model of Achilles tendon injury. *J Bone Joint Surg Am* **89a**, 1315-1320, doi:Doi 10.2106/Jbjs.F.00257 (2007).

171 Thrasher, A. J. *et al.* Gene therapy: X-SCID transgene leukaemogenicity. *Nature* **443**, E5-6; discussion E6-7, doi:10.1038/nature05219 (2006).

172 Zhang, Y. *et al.* Adenoviral and adeno-associated viral vectors-mediated neuronal gene transfer to cardiovascular control regions of the rat brain. *Int J Med Sci* **10**, 607-616, doi:10.7150/ijms.5700 (2013).

173 Teramoto, S., Ishii, T. & Matsuse, T. Crisis of adenoviruses in human gene therapy. *Lancet* **355**, 1911-1912, doi:10.1016/S0140-6736(05)73358-4 (2000).

174 Okada, H. *et al.* Gene Transfer Targeting Mouse Vestibule Using Adenovirus and Adeno-Associated Virus Vectors. *Otol Neurotol* **33**, 655-659, doi:10.1097/MAO.0b013e31825368d1 (2012).

175 Anson, D. S. The use of retroviral vectors for gene therapy-what are the risks? A review of retroviral pathogenesis and its relevance to retroviral vector-mediated gene delivery. *Genet Vaccines Ther* **2**, 9, doi:10.1186/1479-0556-2-9 (2004).

176 Bushman, F. D. Retroviral integration and human gene therapy. *Journal of Clinical Investigation* **117**, 2083-2086, doi:10.1172/Jci32949 (2007).

177 Goss, J. R. *et al.* Antinociceptive effect of a genomic herpes simplex virus-based vector expressing human proenkephalin in rat dorsal root ganglion. *Gene Ther* **8**, 551-556, doi:10.1038/sj.gt.3301430 (2001).

178 Real, G., Monteiro, F., Burger, C. & Alves, P. M. Improvement of lentiviral transfer vectors using cis-acting regulatory elements for increased gene expression. *Appl Microbiol Biot* **91**, 1581-1591, doi:10.1007/s00253-011-3392-2 (2011).

179 Segura, T. & Shea, L. D. Materials for non-viral gene delivery. *Annu Rev Mater Res* **31**, 25-46, doi:DOI 10.1146/annurev.matsci.31.1.25 (2001).

180 Gao, Y., Liu, X. L. & Li, X. R. Research progress on siRNA delivery with

nonviral carriers. *Int J Nanomedicine* **6**, 1017-1025, doi:10.2147/IJN.S17040 (2011).

181 Behr, J. P. Synthetic Gene-Transfer Vectors. *Accounts Chem Res* **26**, 274-278, doi:DOI 10.1021/ar00029a008 (1993).

182 Poste, G. & Papahadjopoulos, D. Fusion of mammalian cells by lipid vesicles. *Methods Cell Biol* **14**, 23-32 (1976).

183 Gregoriadis, G. Targeting of Drugs. *Nature* **265**, 407-411, doi:DOI 10.1038/265407a0 (1977).

184 Dimitriadi, G. J. Translation of rabbit globin mRNA introduced by liposomes into mouse lymphocytes. *Nature* **274**, 923-924 (1978).

185 Bennett, C. F., Chiang, M. Y., Chan, H., Shoemaker, J. E. & Mirabelli, C. K. Cationic lipids enhance cellular uptake and activity of phosphorothioate antisense oligonucleotides. *Mol Pharmacol* **41**, 1023-1033 (1992).

186 Wang, B. Y. & Jorns, M. S. Reconstitution of Escherichia-Coli DNA Photolyase with Various Folate Derivatives. *Biochemistry-US* **28**, 1148-1152, doi:DOI 10.1021/bi00429a032 (1989).

187 Zelphati, O. & Szoka, F. C. Mechanism of oligonucleotide release from cationic liposomes. *P Natl Acad Sci USA* **93**, 11493-11498, doi:DOI 10.1073/pnas.93.21.11493 (1996).

188 Felgner, J. H. *et al.* Enhanced Gene Delivery and Mechanism Studies with a Novel Series of Cationic Lipid Formulations. *Journal of Biological Chemistry* **269**, 2550-2561 (1994).

189 Remy, J. S., Sirlin, C., Vierling, P. & Behr, J. P. Gene-Transfer with a Series of Lipophilic DNA-Binding Molecules. *Bioconjugate Chem* **5**, 647-654, doi:DOI 10.1021/bc00030a021 (1994).

190 Tabernero, J. *et al.* First-in-Humans Trial of an RNA Interference Therapeutic Targeting VEGF and KSP in Cancer Patients with Liver Involvement. *Cancer Discov* **3**, 406-417, doi:10.1158/2159-8290.Cd-12-0429 (2013).

191 Du, S. L. *et al.* Cyclic Arg-Gly-Asp peptide-labeled liposomes for targeting drug therapy of hepatic fibrosis in rats. *J Pharmacol Exp Ther* **322**, 560-568, doi:10.1124/jpet.107.12481 (2007).

192 Adrian, J. E. *et al.* Effects of a new bioactive lipid-based drug carrier on cultured hepatic stellate cells and liver fibrosis in bile duct-ligated rats. *J Pharmacol Exp Ther* **321**, 536-543, doi:10.1124/jpet.106.117945 (2007).

193 Pouton, C. W. & Porter, C. J. H. Formulation of lipid-based delivery systems for oral administration: Materials, methods and strategies. *Adv Drug Deliver Rev* **60**, 625-637, doi:10.1016/j.addr.2007.10.010 (2008).

194 Porter, C. J. H., Pouton, C. W., Cuine, J. F. & Charman, W. N. Enhancing intestinal drug solubilisation using lipid-based delivery systems. *Adv Drug Deliver Rev* **60**, 673-691, doi:10.1016/j.addr.2007.10.014 (2008).

195 Mahato, R. I., Rolland, A. & Tomlinson, E. Cationic lipid-based gene delivery systems: Pharmaceutical perspectives. *Pharmaceut Res* **14**, 853-859, doi:DOI 10.1023/A:1012187414126 (1997).

196 Bielinska, A., KukowskaLatallo, J. F., Johnson, J., Tomalia, D. A. & Baker, J. R. Regulation of in vitro gene expression using antisense oligonucleotides or antisense expression plasmids transfected using starburst PAMAM dendrimers. *Nucleic Acids Res* **24**, 2176-2182, doi:DOI 10.1093/nar/24.11.2176 (1996).

197 Tang, M. X. & Szoka, F. C. The influence of polymer structure on the interactions of cationic polymers with DNA and morphology of the resulting complexes. *Gene Ther* **4**, 823-832, doi:DOI 10.1038/sj.gt.3300454 (1997).

198 Kesharwani, P. *et al.* PAMAM dendrimers as promising nanocarriers for RNAi

therapeutics. *Mater Today* **18**, 565-572, doi:10.1016/j.mattod.2015.06.003 (2015).

199 Haensler, J. & Szoka, F. C., Jr. Polyamidoamine cascade polymers mediate efficient transfection of cells in culture. *Bioconjug Chem* **4**, 372-379 (1993).

200 Maruyama-Tabata, H. *et al.* Effective suicide gene therapy in vivo by EBV-based plasmid vector coupled with polyamidoamine dendrimer. *Gene Ther* **7**, 53-60, doi:10.1038/sj.gt.3301044 (2000).

201 Sato, N. *et al.* Tumor targeting and imaging of intraperitoneal tumors by use of antisense oligo-DNA complexed with dendrimers and/or avidin in mice. *Clin Cancer Res* **7**, 3606-3612 (2001).

202 Jaimes-Aguirre, L. *et al.* Polymer-Based Drug Delivery Systems, Development and Pre-Clinical Status. *Curr Pharm Des* **22**, 2886-2903 (2016).

203 Zauner, W., Ogris, M. & Wagner, E. Polylysine-based transfection systems utilizing receptor-mediated delivery. *Adv Drug Deliver Rev* **30**, 97-113, doi:10.1016/S0169-409x(97)00110-5 (1998).

204 Cheng, J. J. *et al.* Structure - Function correlation of chloroquine and analogues as transgene expression enhancers in nonviral gene delivery. *J Med Chem* **49**, 6522-6531, doi:10.1021/jm060736s (2006).

205 Boussif, O. *et al.* A Versatile Vector for Gene and Oligonucleotide Transfer into Cells in Culture and in-Vivo - Polyethylenimine. *P Natl Acad Sci USA* **92**, 7297-7301, doi:DOI 10.1073/pnas.92.16.7297 (1995).

206 Goula, D. *et al.* Size, diffusibility and transfection performance of linear PEI/DNA complexes in the mouse central nervous system. *Gene Ther* **5**, 712-717, doi:DOI 10.1038/sj.gt.3300635 (1998).

207 Dillow, A. K. & Lowman, A. M. *Biomimetic materials and design : biointerfacial strategies, tissue engineering, and targeted drug delivery.* (Marcel Dekker, 2002).

208 Thomas, J. L. & Tirrell, D. A. Polyelectrolyte-Sensitized Phospholipid-Vesicles. *Accounts Chem Res* **25**, 336-342, doi:DOI 10.1021/ar00020a003 (1992).

209 Pack, D. W., Putnam, D. & Langer, R. Design of imidazole-containing endosomolytic biopolymers for gene delivery. *Biotechnol Bioeng* **67**, 217-223, doi:10.1002/(Sici)1097-0290(20000120)67:2<217::Aid-Bit11>3.0.Co;2-Q (2000).

210 Gregory, A. & Stenzel, M. H. Complex polymer architectures via RAFT polymerization: From fundamental process to extending the scope using click chemistry and nature's building blocks. *Prog Polym Sci* **37**, 38-105, doi:10.1016/j.progpolymsci.2011.08.004 (2012).

211 Ma, D. *et al.* Star-shaped polymer consisting of a porphyrin core and poly(L-lysine) dendron arms: synthesis, drug delivery, and in vitro chemo/photodynamic therapy. *Macromol Rapid Commun* **34**, 548-552, doi:10.1002/marc.201200742 (2013).

212 Pack, D. W., Hoffman, A. S., Pun, S. & Stayton, P. S. Design and development of polymers for gene delivery. *Nat Rev Drug Discov* **4**, 581-593, doi:10.1038/nrd1775 (2005).

213 Bloomfield, V. A. DNA condensation by multivalent cations. *Biopolymers* **44**, 269-282, doi:10.1002/(Sici)1097-0282(1997)44:3<269::Aid-Bip6>3.0.Co;2-T (1997).

214 Riemer, S. C. & Bloomfield, V. A. Packaging of DNA in Bacteriophage Heads - Some Considerations on Energetics. *Biopolymers* **17**, 785-794, doi:10.1002/bip.1978.360170317 (1978).

215 Oosawa, F. A Theory on Effect of Low Molecular Salts on Conformation of

Linear Polyions. *Biopolymers* **6**, 145-&, doi:DOI 10.1002/bip.1968.360060113 (1968).

216 Marquet, R. & Houssier, C. Thermodynamics of Cation-Induced DNA Condensation. *J Biomol Struct Dyn* **9**, 159-167, doi:DOI 10.1080/07391102.1991.10507900 (1991).

217 Koping-Hoggard, M. *et al.* Improved chitosan-mediated gene delivery based on easily dissociated chitosan polyplexes of highly defined chitosan oligomers. *Gene Ther* **11**, 1441-1452, doi:10.1038/sj.gt.3302312 (2004).

218 Wagner, E., Cotten, M., Foisner, R. & Birnstiel, M. L. Transferrin-polycation-DNA complexes: the effect of polycations on the structure of the complex and DNA delivery to cells. *Proc Natl Acad Sci U S A* **88**, 4255-4259 (1991).

219 Wong, S. Y., Pelet, J. M. & Putnam, D. Polymer systems for gene delivery-past, present, and future. *Prog Polym Sci* **32**, 799-837, doi:10.1016/j.progpolymsci.2007.05.007 (2007).

220 Robinson, M. S. The Role of Clathrin, Adapters and Dynamin in Endocytosis. *Curr Opin Cell Biol* **6**, 538-544, doi:DOI 10.1016/0955-0674(94)90074-4 (1994).

221 Takei, K. & Haucke, V. Clathrin-mediated endocytosis: membrane factors pull the trigger. *Trends Cell Biol* **11**, 385-391, doi:DOI 10.1016/S0962-8924(01)02082-7 (2001).

222 Weissman, A. M. Themes and variations on ubiquitylation. *Nat Rev Mol Cell Bio* **2**, 169-178, doi:DOI 10.1038/35056563 (2001).

223 Mousavi, S. A., Malerod, L., Berg, T. & Kjeken, R. Clathrin-dependent endocytosis. *Biochem J* **377**, 1-16, doi:10.1042/BJ20031000 (2004).

224 Henne, W. M. *et al.* FCHo Proteins Are Nucleators of Clathrin-Mediated Endocytosis. *Science* **328**, 1281-1284, doi:10.1126/science.1188462 (2010).

225 Umasankar, P. K. *et al.* Distinct and separable activities of the endocytic clathrin-coat components Fcho1/2 and AP-2 in developmental patterning. *Nat Cell Biol* **14**, 488-U108, doi:10.1038/ncb2473 (2012).

226 Sun, Y. D., Martin, A. C. & Drubin, D. G. Endocytic internalization in budding yeast requires coordinated actin nucleation and myosin motor activity. *Dev Cell* **11**, 33-46, doi:10.1016/j.devcel.2006.05.008 (2006).

227 Kaksonen, M. & Roux, A. Mechanisms of clathrin-mediated endocytosis. *Nat Rev Mol Cell Bio* **19**, 313-326, doi:10.1038/nrm.2017.132 (2018).

228 Antonny, B. *et al.* Membrane fission by dynamin: what we know and what we need to know. *Embo J* **35**, 2270-2284, doi:10.15252/embj.201694613 (2016).

229 Daumke, O., Roux, A. & Haucke, V. BAR Domain Scaffolds in Dynamin-Mediated Membrane Fission. *Cell* **156**, 882-892, doi:10.1016/j.cell.2014.02.017 (2014).

230 Ungewickell, E. The 70-Kd Mammalian Heat-Shock Proteins Are Structurally and Functionally Related to the Uncoating Protein That Releases Clathrin Triskelia from Coated Vesicles. *Embo J* **4**, 3385-3391, doi:DOI 10.1002/j.1460-2075.1985.tb04094.x (1985).

231 Posor, Y., Eichhorn-Gunig, M. & Haucke, V. Phosphoinositides in endocytosis. *Bba-Mol Cell Biol L* **1851**, 794-804, doi:10.1016/j.bbalip.2014.09.014 (2015).

232 Grant, B. D. & Donaldson, J. G. Pathways and mechanisms of endocytic recycling. *Nat Rev Mol Cell Bio* **10**, 597-608, doi:10.1038/nrm2755 (2009).

233 Matveev, S., Li, X. G., Everson, W. & Smart, E. J. The role of caveolae and caveolin in vesicle-dependent and vesicle-independent trafficking. *Adv Drug Deliver Rev* **49**, 237-250, doi:DOI 10.1016/S0169-409x(01)00138-7 (2001).

234 Harris, J., Werling, D., Hope, J. C., Taylor, G. & Howard, C. J. Caveolae and

caveolin in immune cells: distribution and functions. *Trends Immunol* **23**, 158-164, doi:Doi 10.1016/S1471-4906(01)02161-5 (2002).

235 Soldati, T. & Schliwa, M. Powering membrane traffic in endocytosis and recycling. *Nat Rev Mol Cell Bio* **7**, 897-908, doi:10.1038/nrm1960 (2006).

236 Pelkmans, L. & Helenius, A. Endocytosis via caveolae. *Traffic* **3**, 311-320, doi:DOI 10.1034/j.1600-0854.2002.30501.x (2002).

237 Razani, B. *et al.* Caveolin-1 null mice are viable but show evidence of hyperproliferative and vascular abnormalities. *Journal of Biological Chemistry* **276**, 38121-38138 (2001).

238 Benlimame, N., Le, P. U. & Nabi, I. R. Localization of autocrine motility factor receptor to caveolae and clathrin-independent internalization of its ligand to smooth endoplasmic reticulum. *Mol Biol Cell* **9**, 1773-1786, doi:DOI 10.1091/mbc.9.7.1773 (1998).

239 Nabi, I. R. & Le, P. U. Caveolae/raft-dependent endocytosis. *J Cell Biol* **161**, 673-677, doi:10.1083/jcb.200302028 (2003).

240 Basak, S., Turner, H. & Compans, R. W. Expression of SV40 Receptors on Apical Surfaces of Polarized Epithelial-Cells. *Virology* **190**, 393-402, doi:Doi 10.1016/0042-6822(92)91225-J (1992).

241 Pelkmans, L. *et al.* Genome-wide analysis of human kinases in clathrin- and caveolae/raft-mediated endocytosis. *Nature* **436**, 78-86, doi:10.1038/nature03571 (2005).

242 Ridley, A. J. Rho proteins: Linking signaling with membrane trafficking. *Traffic* **2**, 303-310, doi:DOI 10.1034/j.1600-0854.2001.002005303.x (2001).

243 Conner, S. D. & Schmid, S. L. Regulated portals of entry into the cell. *Nature* **422**, 37-44, doi:10.1038/nature01451 (2003).

244 Khalil, I. A., Kogure, K., Futaki, S. & Harashima, H. High density of octaarginine stimulates macropinocytosis leading to efficient intracellular trafficking for gene expression. *Journal of Biological Chemistry* **281**, 3544-3551, doi:10.1074/jbc.M503202200 (2006).

245 Allen, L. A. H. & Aderem, A. Mechanisms of phagocytosis. *Curr Opin Immunol* **8**, 36-40, doi:Doi 10.1016/S0952-7915(96)80102-6 (1996).

246 Berg, J. M., Tymoczko, J. L., Stryer, L. & Stryer, L. *Biochemistry*. 5th edn, (W.H. Freeman, 2002).

247 Eguchi, A. *et al.* Protein transduction domain of HIV-1 Tat protein promotes efficient delivery of DNA into mammalian cells. *Journal of Biological Chemistry* **276**, 26204-26210, doi:DOI 10.1074/jbc.M010625200 (2001).

248 Kawamura, K. S., Sung, M., Bolewska-Pedyczak, E. & Gariepy, J. Probing the impact of valency on the routing of arginine-rich peptides into eukaryotic cells. *Biochemistry-US* **45**, 1116-1127, doi:10.1021/bi051338e (2006).

249 Hornof, M., de la Fuente, M., Hallikainen, M., Tammi, R. H. & Urtti, A. Low molecular weight hyaluronan shielding of DNA/PEI polyplexes facilitates CD44 receptor mediated uptake in human corneal epithelial cells. *Journal of Gene Medicine* **10**, 70-80, doi:10.1002/jgm.1125 (2008).

250 Midoux, P., Breuzard, G., Gomez, J. P. & Pichon, C. Polymer-Based Gene Delivery: A Current Review on the Uptake and Intracellular Trafficking of Polyplexes. *Curr Gene Ther* **8**, 335-352, doi:Doi 10.2174/156652308786071014 (2008).

251 van der Aa, M. A. E. M. *et al.* Cellular uptake of cationic polymer-DNA complexes via caveolae plays a pivotal role in gene transfection in COS-7 cells. *Pharmaceut Res* **24**, 1590-1598, doi:10.1007/s11095-007-9287-3 (2007).

252 Rejman, J., Bragonzi, A. & Conese, M. Role of clathrin- and caveolae-mediated

endocytosis in gene transfer mediated by lipo- and polyplexes. *Mol Ther* **12**, 468-474, doi:10.1016/j.ymthe.2005.03.038 (2005).

253 Manunta, M., Tan, P. H., Sagoo, P., Kashefi, K. & George, A. J. T. Gene delivery by dendrimers operates via a cholesterol dependent pathway. *Nucleic Acids Res* **32**, 2730-2739, doi:10.1093/nar/gkh595 (2004).

254 Seib, F. P., Jones, A. T. & Duncan, R. Comparison of the endocytic properties of linear and branched PEIs, and cationic PAMAM dendrimers in B16f10 melanoma cells. *J Control Release* **117**, 291-300, doi:10.1016/j.jconrel.2006.10.020 (2007).

255 von Gersdorff, K. *et al.* The internalization route resulting in successful gene expression depends on polyethylenimine both cell line and polyplex type. *Mol Ther* **14**, 745-753, doi:10.1016/j.ymthe.2006.07.006 (2006).

256 Zhang, Q. F. *et al.* Linear TACN-based cationic polymers as non-viral gene vectors. *Rsc Adv* **4**, 59164-59174, doi:10.1039/c4ra11094c (2014).

257 El-Sayed, A., Futaki, S. & Harashima, H. Delivery of Macromolecules Using Arginine-Rich Cell-Penetrating Peptides: Ways to Overcome Endosomal Entrapment. *Aaps J* **11**, 13-22 (2009).

258 Vonkugelgen, I. & Starke, K. Noradrenaline-Atp Cotransmission in the Sympathetic Nervous-System. *Trends Pharmacol Sci* **12**, 319-324, doi:Doi 10.1016/0165-6147(91)90587-I (1991).

259 Kokufuta, E., Hirata, M. & Iwai, S. Effect of Ionic-Strength and Ph on Electrophoretic Mobility and Viscosity of Poly(Ethyleneimine). *Kobunshi Ronbunshu* **31**, 234-238 (1974).

260 Peer, D. *Nanotechnology for the Delivery of Therapeutic Nucleic Acids*. (Pan Stanford, 2013).

261 Lungu, C. N., Diudea, M. V., Putz, M. V. & Grudzinski, I. P. Linear and Branched PEIs (Polyethylenimines) and Their Property Space. *Int J Mol Sci* **17**, 555, doi:10.3390/ijms17040555 (2016).

262 Lu, H. D., Dai, Y. H., Lv, L. L. & Zhao, H. Q. Chitosan-Graft-Polyethylenimine/DNA Nanoparticles as Novel Non-Viral Gene Delivery Vectors Targeting Osteoarthritis. *Plos One* **9**, doi:ARTN e84703 10.1371/journal.pone.0084703 (2014).

263 Twain, B. R. *et al.* Thermoresponsive polymers as gene delivery vectors: Cell viability, DNA transport and transfection studies. *J Control Release* **108**, 472-483, doi:10.1016/j.jconrel.2005.08.009 (2005).

264 Godbey, W. T., Wu, K. K. & Mikos, A. G. Size matters: Molecular weight affects the efficiency of poly(ethylenimine) as a gene delivery vehicle. *J Biomed Mater Res* **45**, 268-275, doi:Doi 10.1002/(Sici)1097-4636(19990605)45:3<268::Aid-Jbm15>3.0.Co;2-Q (1999).

265 Godbey, W. T., Ku, K. K., Hirasaki, G. J. & Mikos, A. G. Improved packing of poly(ethylenimine)/DNA complexes increases transfection efficiency. *Gene Ther* **6**, 1380-1388, doi:DOI 10.1038/sj.gt.3300976 (1999).

266 Fischer, D., Bieber, T., Li, Y. X., Elsasser, H. P. & Kissel, T. A novel non-viral vector for DNA delivery based on low molecular weight, branched polyethylenimine: Effect of molecular weight on transfection efficiency and cytotoxicity. *Pharmaceut Res* **16**, 1273-1279, doi:Doi 10.1023/A:1014861900478 (1999).

267 Godbey, W. T., Wu, K. K. & Mikos, A. G. Poly(ethylenimine)-mediated gene delivery affects endothelial cell function and viability. *Biomaterials* **22**, 471-480, doi:Doi 10.1016/S0142-9612(00)00203-9 (2001).

268 He, L. H., Read, E. S., Armes, S. P. & Adams, D. J. Direct synthesis of

controlled-structure primary amine-based methacrylic polymers by living radical polymerization. *Macromolecules* **40**, 4429-4438, doi:10.1021/ma070670q (2007).

269 Truong, N. P., Jia, Z. F., Burges, M., McMillan, N. A. J. & Monteiro, M. J. Self-Catalyzed Degradation of Linear Cationic Poly(2-dimethylaminoethyl acrylate) in Water. *Biomacromolecules* **12**, 1876-1882, doi:10.1021/bm200219e (2011).

270 Agarwal, S., Zhang, Y., Maji, S. & Greiner, A. PDMAEMA based gene delivery materials. *Mater Today* **15**, 388-393, doi:Doi 10.1016/S1369-7021(12)70165-7 (2012).

271 Whitfield, R. *et al.* Well-defined PDMAEA stars via Cu(0)-mediated reversible deactivation radical polymerisation. *Abstr Pap Am Chem S* **253** (2017).

272 Dinari, A., Moghadam, T. T., Abdollahi, M. & Sadeghizadeh, M. Synthesis and Characterization of a Nano-Polyplex system of GNRs-PDMAEA-pDNA: An Inert Self-Catalyzed Degradable Carrier for Facile Gene Delivery. *Sci Rep-Uk* **8**, doi:ARTN 8112 10.1038/s41598-018-26260-4 (2018).

273 Neu, M., Fischer, D. & Kissel, T. Recent advances in rational gene transfer vector design based on poly(ethylene imine) and its derivatives. *Journal of Gene Medicine* **7**, 992-1009, doi:10.1002/jgm.773 (2005).

274 van de Wetering, P., Schuurmans-Nieuwenbroek, N. M. E., Hennink, W. E. & Storm, G. Comparative transfection studies of human ovarian carcinoma cells in vitro, ex vivo and in vivo with poly(2-(dimethylamino)ethyl methacrylate)-based polyplexes. *Journal of Gene Medicine* **1**, 156-165, doi:Doi 10.1002/(Sici)1521-2254(199905/06)1:3<156::Aid-Jgm29>3.0.Co;2-O (1999).

275 Rungsardthong, U. *et al.* Copolymers of amine methacrylate with poly(ethylene glycol) as vectors for gene therapy. *J Control Release* **73**, 359-380, doi:Doi 10.1016/S0168-3659(01)00295-4 (2001).

276 Dincer, S., Turk, M. & Piskin, E. Intelligent polymers as nonviral vectors. *Gene Ther* **12**, S139-S145, doi:10.1038/sj.gt.3302628 (2005).

277 Gu, W. *et al.* Polymer nanocarrier system for endosome escape and timed release of siRNA with complete gene silencing and cell death in cancer cells. *Biomacromolecules* **14**, 3386-3389, doi:10.1021/bm401139e (2013).

278 Nasanit, R. *et al.* Combination dual responsive polypeptide vectors for enhanced gene delivery. *Mol Biosyst* **4**, 741-745, doi:10.1039/b803262a (2008).

279 Soliman, M. *et al.* Multicomponent Synthetic Polymers with Viral-Mimetic Chemistry for Nucleic Acid Delivery. *Mol Pharmaceut* **9**, 1-13, doi:10.1021/mp200108q (2012).

280 Newland, B. *et al.* Single Cyclized Molecule Versus Single Branched Molecule: A Simple and Efficient 3D "Knot" Polymer Structure for Nonviral Gene Delivery. *Journal of the American Chemical Society* **134**, 4782-4789, doi:10.1021/ja2105575 (2012).

281 Cho, H. Y. *et al.* Synthesis of biocompatible PEG-Based star polymers with cationic and degradable core for siRNA delivery. *Biomacromolecules* **12**, 3478-3486, doi:10.1021/bm2006455 (2011).

282 Synatschke, C. V., Schallon, A., Jerome, V., Freitag, R. & Muller, A. H. E. Influence of Polymer Architecture and Molecular Weight of Poly(2-(dimethylamino)ethyl methacrylate) Polycations on Transfection Efficiency and Cell Viability in Gene Delivery. *Biomacromolecules* **12**, 4247-4255, doi:10.1021/bm201111d (2011).

283 Yu, S. R. *et al.* Enhanced gene transfection efficiency of PDMAEMA by incorporating hydrophobic hyperbranched polymer cores: effect of degree of branching. *Polym Chem-Uk* **3**, 3324-3329, doi:10.1039/c2py20487h (2012).

284 Sandler, S. R. & Karo, W. *Polymer syntheses*. 2nd edn, (Academic Press, 1992).

285 Moad, G., Solomon, D. H. & Moad, G. *The chemistry of radical polymerization*. 2nd fully rev. edn, (Elsevier, 2006).

286 Matyjaszewski, K. & Davis, T. P. *Handbook of radical polymerization*. (Wiley-Interscience, 2002).

287 Moad, G., Rizzardo, E. & Thang, S. H. Living radical polymerization by the RAFT process. *Aust J Chem* **58**, 379-410, doi:10.1071/Ch05072 (2005).

288 Matyjaszewski, K. *Controlled/living radical polymerization : progress in ATRP*. (American Chemical Society : Distributed by Oxford University Press, 2009).

289 Cerdá-Cristerna, B. I. *et al.* Increment in molecular weight of poly (dimethylamino-ethylmethacrylate) based polymers cause strong red blood cell aggregation but not hemolytic response. *J Control Release* **148**, E30-E31, doi:10.1016/j.jconrel.2010.07.040 (2010).

290 Matyjaszewski, K. Macromolecular engineering: From rational design through precise macromolecular synthesis and processing to targeted macroscopic material properties. *Prog Polym Sci* **30**, 858-875, doi:10.1016/j.progpolymsci.2005.06.004 (2005).

291 Harth, E., Hawker, C. J., Fan, W. & Waymouth, R. M. Chain end functionalization in nitroxide-mediated "Living" free radical polymerizations. *Macromolecules* **34**, 3856-3862, doi:10.1021/ma0019297 (2001).

292 Georges, M. K., Veregin, R. P. N., Kazmaier, P. M. & Hamer, G. K. Narrow Molecular-Weight Resins by a Free-Radical Polymerization Process. *Macromolecules* **26**, 2987-2988, doi:DOI 10.1021/ma00063a054 (1993).

293 Nicolas, J. & Guillaneuf, Y. in *Encyclopedia of Polymeric Nanomaterials* (eds Shiro Kobayashi & Klaus Müllen) 1-16 (Springer Berlin Heidelberg, 2014).

294 Mittal, V. *Polymer-graphene nanocomposites*. (RSC Pub., 2012).

295 Wang, J. S. & Matyjaszewski, K. Controlled Living Radical Polymerization - Atom-Transfer Radical Polymerization in the Presence of Transition-Metal Complexes. *Journal of the American Chemical Society* **117**, 5614-5615, doi:DOI 10.1021/ja00125a035 (1995).

296 Moad, G. *et al.* Living free radical polymerization with reversible addition-fragmentation chain transfer (the life of RAFT). *Polym Int* **49**, 993-1001, doi:Doi 10.1002/1097-0126(200009)49:9<993::Aid-Pi506>3.0.Co;2-6 (2000).

297 Wang, D. M., Wang, W. J., Li, B. G. & Zhu, S. P. Semibatch RAFT Polymerization for Branched Polyacrylamide Production: Effect of Divinyl Monomer Feeding Policies. *Aiche J* **59**, 1322-1333, doi:10.1002/aic.13890 (2013).

298 Vo, C. D., Rosselgong, J., Armes, S. P. & Billingham, N. C. RAFT synthesis of branched acrylic copolymers. *Macromolecules* **40**, 7119-7125, doi:10.1021/ma0713299 (2007).

299 Braunecker, W. A. & Matyjaszewski, K. Controlled/living radical polymerization: Features, developments and perspectives (vol 32, pg 93, 2007). *Prog Polym Sci* **33**, 165-165, doi:10.1016/j.progpolymsci.2007.10.001 (2008).

300 Moad, G., Rizzardo, E. & Thang, S. H. Radical addition-fragmentation chemistry in polymer synthesis. *Polymer* **49**, 1079-1131, doi:10.1016/j.polymer.2007.11.020 (2008).

301 Chong, Y. K. *et al.* Thiocarbonylthio compounds [S=C(Ph)S-R] in free radical polymerization with reversible addition-fragmentation chain transfer (RAFT polymerization). Role of the free-radical leaving group (R). *Macromolecules* **36**, 2256-2272, doi:10.1021/ma020882h (2003).

302 Chieffari, J. *et al.* Thiocarbonylthio compounds (S=C(Z)S-R) in free radical

polymerization with reversible addition-fragmentation chain transfer (RAFT polymerization). Effect of the activating group Z. *Macromolecules* **36**, 2273-2283, doi:10.1021/ma020883+ (2003).

303 Grajales, S. Controlled Radical Polymerization Guide.

304 Walden, G. *et al.* A Clinical, Biological, and Biomaterials Perspective into Tendon Injuries and Regeneration. *Tissue Eng Part B-Re* **23**, 44-58, doi:10.1089/ten.teb.2016.0181 (2017).

305 Hoffmann, A. *et al.* Neotendon formation induced by manipulation of the Smad8 signalling pathway in mesenchymal stem cells. *Journal of Clinical Investigation* **116**, 940-952, doi:10.1172/Jci22689 (2006).

306 Zhou, Y., Zhu, C., Wu, Y. F., Zhang, L. & Tang, J. B. Effective modulation of transforming growth factor-beta1 expression through engineered microRNA-based plasmid-loaded nanospheres. *Cyotherapy* **17**, 320-329, doi:10.1016/j.jcyt.2014.09.004 (2015).

307 Ozkan, I. *et al.* Direct in vivo gene transfer to healing rat patellar ligament by intra-arterial delivery of haemagglutinating virus of Japan liposomes. *Eur J Clin Invest* **29**, 63-67 (1999).

308 Abbah, S. A. *et al.* Co-transfection of decorin and interleukin-10 modulates profibrotic extracellular matrix gene expression in human tenocyte culture. *Sci Rep* **6**, 20922, doi:10.1038/srep20922 (2016).

309 Delalande, A. *et al.* Enhanced Achilles tendon healing by fibromodulin gene transfer. *Nanomed-Nanotechnol* **11**, 1735-1744, doi:10.1016/j.nano.2015.05.004 (2015).

310 Dai, Q., Manfield, L., Wang, Y. & Murrell, G. A. C. Adenovirus-mediated gene transfer to healing tendon - enhanced efficiency using a gelatin sponge. *J Orthopaed Res* **21**, 604-609, doi:10.1016/S0736-0266(02)00239-5 (2003).

311 Mehta, V. *et al.* Characterization of adenovirus-mediated gene transfer in rabbit flexor tendons. *J Hand Surg-Am* **30a**, 136-141, doi:10.1016/j.jhsa.2004.08.010 (2005).

312 Majewski, M. *et al.* Ex vivo adenoviral transfer of bone morphogenetic protein 12 (BMP-12) cDNA improves Achilles tendon healing in a rat model. *Gene Ther* **15**, 1139-1146, doi:10.1038/gt.2008.48 (2008).

313 Mehta, V. *et al.* Characterization of adenovirus-mediated gene transfer in rabbit flexor tendons. *J Hand Surg Am* **30**, 136-141, doi:10.1016/j.jhsa.2004.08.010 (2005).

314 Wang, X. T., Liu, P. Y., Xin, K. Q. & Tang, J. B. Tendon healing in vitro: bFGF gene transfer to tenocytes by adeno-associated viral vectors promotes expression of collagen genes. *J Hand Surg Am* **30**, 1255-1261, doi:10.1016/j.jhsa.2005.06.001 (2005).

315 Mi, Z. *et al.* Adenovirus-mediated gene transfer of insulin-like growth factor 1 stimulates proteoglycan synthesis in rabbit joints. *Arthritis Rheum* **43**, 2563-2570, doi:10.1002/1529-0131(200011)43:11<2563::AID-ANR25>3.0.CO;2-8 (2000).

316 Lu, P. *et al.* Lentiviral-encoded shRNA silencing of proteoglycan decorin enhances tendon repair and regeneration within a rat model. *Cell Transplant* **22**, 1507-1517, doi:10.3727/096368912X661292 (2013).

317 Hou, Y. *et al.* The roles of TGF-beta1 gene transfer on collagen formation during Achilles tendon healing. *Biochem Biophys Res Commun* **383**, 235-239, doi:10.1016/j.bbrc.2009.03.159 (2009).

318 Zhou, Y. *et al.* Nanoparticle-mediated delivery of TGF-beta1 miRNA plasmid for preventing flexor tendon adhesion formation. *Biomaterials* **34**, 8269-8278,

319 doi:10.1016/j.biomaterials.2013.07.072 (2013).

319 Kjaer, M. *et al.* From mechanical loading to collagen synthesis, structural changes and function in human tendon. *Scand J Med Sci Sports* **19**, 500-510, doi:10.1111/j.1600-0838.2009.00986.x (2009).

320 Suwalski, A. *et al.* Accelerated Achilles tendon healing by PDGF gene delivery with mesoporous silica nanoparticles. *Biomaterials* **31**, 5237-5245, doi:10.1016/j.biomaterials.2010.02.077 (2010).

321 El Khoury, L. *et al.* ELN and FBN2 Gene Variants as Risk Factors for Two Sports-related Musculoskeletal Injuries. *International Journal of Sports Medicine* **36**, 333-337, doi:10.1055/s-0034-1390492 (2015).

322 Subramanian, A. & Schilling, T. F. Tendon development and musculoskeletal assembly: emerging roles for the extracellular matrix. *Development* **142**, 4191-4204, doi:10.1242/dev.114777 (2015).

323 Kohler, J. *et al.* Uncovering the cellular and molecular changes in tendon stem/progenitor cells attributed to tendon aging and degeneration. *Aging Cell* **12**, 988-999, doi:10.1111/acel.12124 (2013).

324 Kwan, K. H. L. *et al.* Silver nanoparticles alter proteoglycan expression in the promotion of tendon repair. *Nanomed-Nanotechnol* **10**, 1375-1383, doi:10.1016/j.nano.2013.11.015 (2014).

325 Delalande, A. *et al.* Enhanced Achilles tendon healing by fibromodulin gene transfer. *Nanomedicine* **11**, 1735-1744, doi:10.1016/j.nano.2015.05.004 (2015).

326 Monnery, B. D. *et al.* Cytotoxicity of polycations: Relationship of molecular weight and the hydrolytic theory of the mechanism of toxicity. *Int J Pharmaceut* **521**, 249-258, doi:10.1016/j.ijpharm.2017.02.048 (2017).

327 Fischer, D., Li, Y. X., Ahlemeyer, B., Kriegstein, J. & Kissel, T. In vitro cytotoxicity testing of polycations: influence of polymer structure on cell viability and hemolysis. *Biomaterials* **24**, 1121-1131, doi:Pii S0142-9612(02)00445-3 Doi 10.1016/S0142-9612(02)00445-3 (2003).

328 Kafil, V. & Omidi, Y. Cytotoxic impacts of linear and branched polyethylenimine nanostructures in a431 cells. *Bioimpacts* **1**, 23-30, doi:10.5681/bi.2011.004 (2011).

Chapter 2

Materials and Methods

2. Chapter 2 Material and Methods

2.1. Introduction

This chapter discusses the basic information regarding the materials and methods used in the study, including characterisation techniques and experimental conditions. The basic principles of techniques will also be introduced.

2.2. Materials

- General chemical reagents

All general chemical reagents and solvents were purchased from Sigma-Aldrich UK and used as received. HPLC grade solvents used in chromatography were purchased from Fisher Scientific and degassed before use.

- Dimethylaminoethyl acrylate

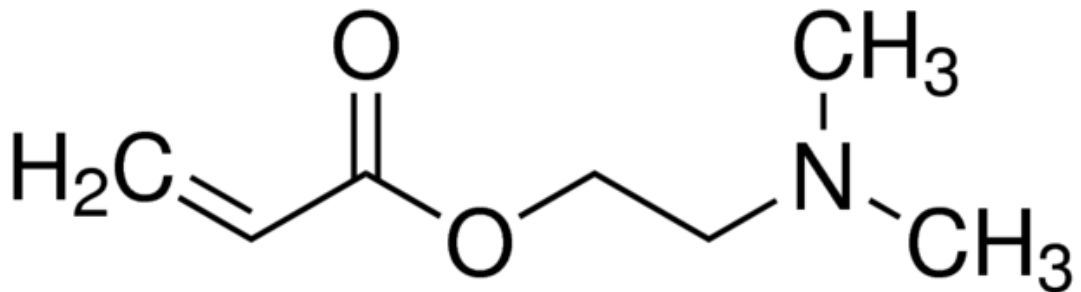


Figure 2.1 Structure of Dimethylaminoethyl acrylate.

Dimethylaminoethyl acrylate (DMAEA) is a carboxylic acid ester with a tertiary amino group towards the far end of the structure. DMAEA monomers are flammable, toxic and corrosive, and should be manipulated in a fume hood only. The DMAEA monomer used in this study is purchased from Sigma-Aldrich UK (98%), containing monomethyl ether hydroquinone as an inhibitor. Before use, the inhibitor was removed by passing DMAEA monomers through an aluminium oxide column.

- 2-(Dodecylthiocarbonothioylthio)-2-methylpropionic acid

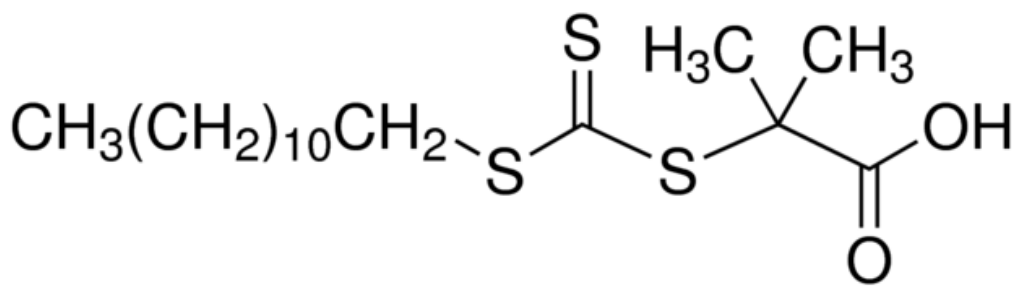


Figure 2.2 Structure of 2-(Dodecylthiocarbonothioylthio)-2-methylpropionic acid.

2-(Dodecylthiocarbonothioylthio)-2-methylpropionic acid (DDMAT) is a chain transfer agent used in reversible addition-fragmentation chain transfer polymerisation (RAFT polymerisation). It is a yellow powder. The DDMAT used in this study is purchased from Sigma-Aldrich UK (98% HPLC) and used as received.

- Pentaerythritol tetrakis[2-(dodecylthiocarbonothioylthio)-2-methylpropionate]

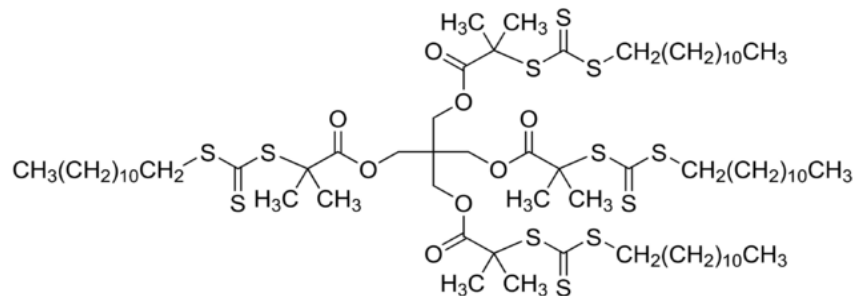


Figure 2.3 Structure of Pentaerythritol tetrakis[2-(dodecylthiocarbonothioylthio)-2-methylpropionate].

Pentaerythritol tetrakis[2-(dodecylthiocarbonothioylthio)-2-methylpropionate] (4-arm-DDMAT) is a chain transfer agent used in reversible addition-fragmentation chain transfer polymerisation. It is a yellow crystal. The 4-arm-DDMAT used in this study is purchased from Sigma-Aldrich UK (97% HPLC) and used as received.

- 2,2'-Azobis(2-methylpropionitrile)

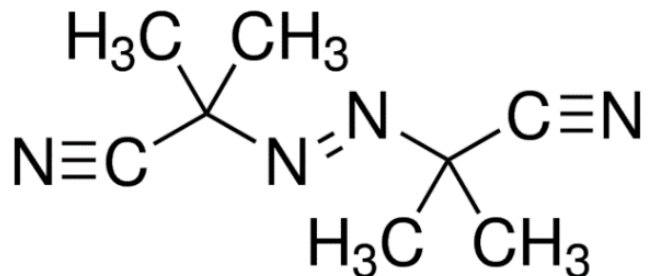


Figure 2.4 Structure of 2,2'-Azobis(2-methylpropionitrile).

2,2'-Azobis(2-methylpropionitrile) (AIBN) is one of the most commonly used radical initiators in the polymerisation reaction. It is a colourless crystal. The AIBN used in this study is purchased from Sigma-Aldrich UK (98%). AIBN was recrystallised in methanol and stored at -20°C before use.

- **Primers for qPCR**

Primers for the equine *COL3α1* gene were purchased from Sigma-Aldrich UK with the following sequences:

Forward 5'-3': GGCCATCTGGTGACAAAGGA

Reverse 5'-3': CCAGGCAAGCCCTACAAAGA

Primers for the equine *18s* gene were purchased from Thermo Fisher Scientific with the following sequences:

Forward 5'-3': CCCAGTGAGAATGCCCTCTA

Reverse 5'-3': TGGCTGAGCAAGGTGTTATG

- *COL3α1* gene-specific siRNA

The *COL3α1* specific siRNA was designed by and purchased from Sigma-Aldrich UK with the following sequences:

Sense 5'-3': CAUCACAUUAUCACUGCAAA [dT][dT]

Antisense 5'-3': UUUGCAGUGAU AUGUGAUG[dT][dT]

- **General cell culture reagents**

Dulbecco's modified Eagle medium (DMEM), L-glutamine, penicillin-streptomycin, foetal calf serum, trypsin with EDTA, trypan blue and PBS tablets were purchased from Fisher Scientific. Human recombinant transforming growth factor-beta 1 (TGF- β 1) was acquired from PEPROTECH and prepared as the manufacturer instructed. Rabbit anti-collagen III antibodies were obtained from Abcam UK, goat anti-rabbit antibodies were obtained from Sigma Aldrich UK and both diluted in PBS with 0.1% BSA to appropriate concentration before use.

- **General cell culture consumables and equipment**

Cell culture flasks, plates and culture dishes were purchased from Fisher Scientific. Tips, filtered tips, serological pipettes and pipette controllers were purchased from Starlab UK. Mechanical pipettes were obtained from Eppendorf Germany, and multichannel pipettes were purchased from Triple Red UK. Corning® 96-well black polystyrene clear bottom microplate was purchased from Fisher Scientific.

2.3. Polymer synthesis

2.3.1. Introduction of RAFT Polymerisation

RAFT polymerisation has control over the molecular weight and polydispersity of generated polymers. The control is achieved using a chain transfer agent, mostly thiocarbonylthio compounds, to mediate the polymerisation via a reversible chain-transfer process under certain conditions. Different RAFT agents have different compatibility with different monomers. The compatibility between the RAFT agent and the monomer would have a significant effect on the ultimate polymerisation result. When the RAFT agent is selected for incompatible monomers, the RAFT agent would show reduced activity in mediating the reversible chain transfer process and would result in an uncontrolled free radical polymerisation.

2-(Dodecylthiocarbonothioylthio)-2-methylpropionic acid has good compatibility with monomers such as styrene, acrylate and acrylamide but showed no compatibility with vinyl esters and vinyl amides. Therefore, it is selected to mediate the RAFT polymerisation of PDMAEA monomers.

2.3.2. Experimental Conditions of PDMAEA Synthesis

All manipulations of toxic and flammable chemical reagents were performed in a chemical fume hood with appropriate body protection equipment. The syntheses of PDMAEA polymers were performed in round bottom flasks with proper volume on a MR Hei-Standard Magnetic Stirrer (Heidolph Instruments) equipped with an appropriate heating block. The polymers were purified by precipitation into hexane in large beakers with stirring on a magnetic stirrer (Fisher Scientific). Polymer precipitants were re-dissolved in acetone and the acetone was then removed by using a Buchi rotavapor at 40°C. The collected polymers were kept in a desiccator for 24 hours and then stored at 4°C.

2.4. Nuclear Magnetic Resonance Spectroscopy (NMR)

2.4.1. Introduction of NMR

Nuclear magnetic resonance (NMR) spectroscopy is an analytical spectroscopic technique based on the magnetic properties of the atomic nucleus. Certain nuclei resonate at a specific frequency when placed in a strong magnetic field. Variations in the resonant frequency can be captured and analysed, which further provide critical structural information about molecule in which the atom resides. In many atoms (¹H, ¹³C, ¹⁵N), the spinning of the positively charged nucleus creates a micro-magnetic field. The classic model considers the spinning nucleus to have an angular momentum and which would attempt to align with the external magnetic field when placed into one. The external magnetic field would exert a torque on the spinning nucleus and result in a circular motion referred to as precession. The rate of precession is proportional to the external magnetic field strength and can be described as follows:

$$v_0 = \gamma B_0 / 2\pi$$

Where v_0 is the Larmor frequency in Hertz which represents the precession rate, γ is the magnetogyric ratio, being the ratio of magnetic moment to the angular momentum of a nucleus, and B_0 is the strength of the external magnetic field. The resonant frequency can be measured by applying a signal scan to the sample, and varying the frequency until an absorbance of energy is detected¹.

However, the classic model cannot answer all aspects of the NMR phenomenon, and therefore the quantum model has been suggested. For certain nuclei, such as ^1H or ^{13}C , there are two independent spin states which are referred to as α and β spin states. In the absence of an external magnetic field, the two spin states have the same energy level, hence at thermal equilibrium, the number of nuclei in these two states would be equal.

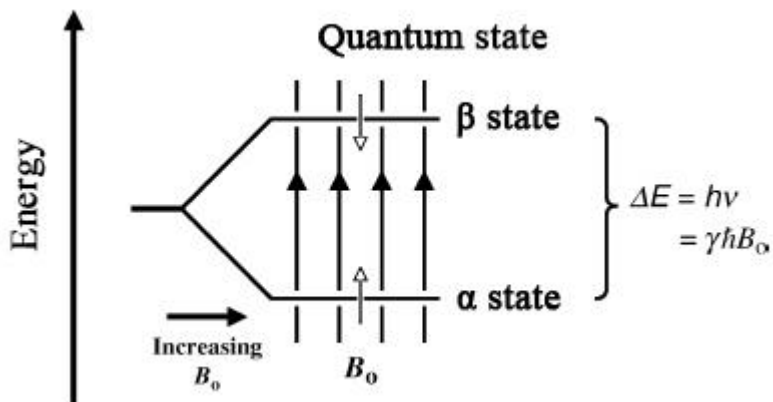


Figure 2.5 When placed in an external magnetic field, two states with different energy level can be detected, namely α state with low energy level and β state with high energy level, respectively. The figure is adapted from Jacobsen et al.¹

However, when placed in a strong external magnetic field, the α state, which is in alignment with the magnetic field, has a lower energy level than the β state, which is opposed to the external magnetic field. This would lead to a change in the thermal equilibrium, resulting in a slightly larger number of nuclei being in the α state (low energy state) and fewer being in the β state (high energy state). It is possible for a nucleus to absorb electromagnetic energy that exactly matches the energy difference (ΔE) between the α and β states and “jump” from the lower energy state to the higher energy state. The energy difference (ΔE) corresponds to the frequency of the electromagnetic radiation:

$$\Delta E = h\nu_0 = \gamma B_0 / 2\pi$$

where h is Planck’s constant, ν_0 is the resonant frequency is in the radio frequency range¹.

2.4.2. Experimental Conditions and Sample Preparation

All ^1H NMR and ^{13}C NMR spectra were recorded on a Burker Advance III 400MHz solution state spectrometer at 400MHz in CDCl_3 . All chemical shifts are recorded in

ppm relative to tetramethylsilane (TMS). Bruker Topspin 3.2 software was used to analyse the data.

For ^1H NMR spectra, samples were dissolved in CDCl_3 to a final concentration of 5 mg/mL and 400 μL of sample solution was loaded into an NMR tube. For ^{13}C NMR spectra, samples were dissolved in CDCl_3 to a final concentration of 25 mg/mL and 400 μL of sample solution was loaded into an NMR tube.

2.5. Gel Permeation Chromatography (GPC)

2.5.1. Introduction and the Basic Principle

Gel permeation chromatography (GPC), also referred to as size exclusion chromatography (SEC), is an analytical technique used to separate samples based on their molecular size. Different from other separation techniques that are based on the physical or chemical interactions between column packing and analytes, the separation of GPC is based on the molecule size or hydrodynamic diameter of analytes. When analyte dissolved in eluent flows through the porous column packing, chromatographic separation will take place. Analytes with smaller hydrodynamic diameters would be able to diffuse into the porous matrix while analytes with larger hydrodynamic diameter would move around the packing matrix. As a result, analytes with a smaller molar mass or hydrodynamic diameter would elute more slowly, while the larger one would elute faster.

GPC is commonly used in the characterisation of polymers and other macromolecules such as proteins. Abundant studies have involved the use of GPC as a characterisation technique ²⁻⁴. It is well established that GPC is an efficient and reliable method to characterise polymer molecular weight and polydispersity.

2.5.2. Experimental Conditions and Sample Preparation

Gel permeation chromatography was performed on a G7810A Agilent PL-GPC50 system connected with a refractive index detector. A PLgel 5 μm MiniMIX-C (50*4.6 mm) guard column was connected to two PLgel 5 μm Mixed-D (300*7.5 mm) columns in series and elevated at a temperature of 30°C. A mixture of HPLC grade chloroform triethylamine (95/5, v/v) was degassed and used as the eluent. The machine was calibrated using Agilent EasiVial GPC calibration polystyrene standards with a

molecular weight ranging from 180 Da to 300 kDa. The flow rate was set at 1 mL/min. Data were collected and analysed with CIRRUS™ data stream software. Samples were dissolved in eluent to a final concentration of 5 mg/mL and filtered with a 0.45 μ M PTFE membrane before injected into the machine through the injection valve manually. The number average molar mass (M_n), weight average molar mass (M_w) and the dispersity (D) were obtained.

2.6. Potentiometric Titration

2.6.1. Experimental Conditions and Sample Preparation

Volumetric burettes (50 mL, A, SLG UK) were used in the titration of PDMAEA solutions and the pH was monitored by a Mettler Toledo SevenEasy® pH meter. The pH meter was calibrated with pH buffer solution (pH 4.01, pH 7.00, pH 10.01, Thermo Fisher).

The polymer solution was prepared by dissolving 50 mg of each polymer from the stock library was dissolved in 150 mM sodium chloride (NaCl) solution and diluted to a final volume of 10 mL (final concentration 5 mg/mL). HCl solution (0.1 M) was prepared by dilution of 8.4 mL of 37% concentrated HCl in deionised water to 1 L. NaOH solution (0.1M) was prepared by dissolving 4.0 g of NaOH in 1 L of deionised water.

2.7. Dynamic Light Scattering

2.7.1. Introduction and the Basic Principle

Dynamic light scattering (DLS) is a technique commonly used to determine the size distribution of analytes such as small particles in suspension or polymers in solution⁵. In DLS experiments, the suspended particles diffuse in a random fashion by a process known as Brownian motion. This results in the fluctuation in the scattered light signals collected at the detector, owing to random fluctuations in the relative positions of the particles. Since the intensity measured by the detector is a combination of all the scattered signals from the total volume, the intensity would fluctuate randomly over time and this forms the basis of DLS experiments⁶.

The fluctuation depends on the size of the diffusing particles. Smaller particles in solution diffuse faster compared to the larger ones, resulting in a more rapidly

fluctuating intensity signal. By using a mathematical method known as autocorrelation, the fluctuation intensity data could be used to acquire critical information about the particle solution. The autocorrelation function $C(\tau)$ represents the correlation between the light scattering intensity at two different times, t and $(t+\tau)$. At an arbitrary time, the intensity is represented by $I(t)$, and $I(t+\tau)$ and the correlation function is:

$$C(\tau) = \{I(t) \cdot I(t + \tau)\}$$

When the sampling interval time becomes very large, it is considered that there is no correlation between $I(t)$ and $I(t+\tau)$, and therefore the function could be derived into:

$$C(\tau) = \{I(t) \cdot I(t)\} = \{I(t)\}^2$$

In a DLS instrument, the digital signals are collected by a detector and further processed by an autocorrelator using a second-order correlation function normalised with the long-term correlation data $\{I(t)\}^2$. The acquired normalised time correlation of the intensity is $g^{(2)}(\tau)$ can be expressed as:

$$g^{(2)}(\tau) = \frac{\{I(t) \cdot I(t + \tau)\}}{\{I(t)\}^2}$$

The relationship of $g^{(2)}(\tau)$ and the first-order correlation function can be expressed as follows, by the Siefert relationship:

$$g^{(2)}(\tau) = \beta + A|g^{(1)}(\tau)|^2$$

Where β is the baseline acquired by the instrument and A is a parameter based on the geometry of the scattering. For particles with Brownian motion diffusion, the correlation function is described as:

$$g^{(1)}(\tau) = e^{(-Dq^2\tau)}$$

Where D is the translational diffusion coefficient, and q is the magnitude of the scattering wave. For particles that are spherical and non-interacting, the hydrodynamic radius (R_h) can be deducted by using the Stokes-Einstein equation with translational diffusion coefficient D :

$$R_h = K_b T / 6\pi\eta D$$

Where K_b is the Boltzmann constant, T is the temperature and η is the viscosity. This equation demonstrates that the particle size is inversely proportional to the translational diffusion coefficient⁷.

2.7.2. Experimental Conditions

A Malvern Zetasizer Nano ZS (Malvern Instruments, UK) was used to obtain the size and zeta-potential of all polymer and polyplex solutions. The measurement of the hydrodynamic diameter of all samples was performed at 25°C using 633 nm (4 mW) He-Ne laser and the measurement angle was set at 173° backscattered. The size distribution by intensity, number and volume were recorded and analysed using Malvern Zetasizer software (Ver 7.11).

Zeta-potential of all sample solutions were determined using a Zetasizer Nano ZS based on the electrophoretic light scattering principle. The measurement of all samples was performed at 25°C in Folded Capillary Cells DTS1060 (Malvern instruments). Data were recorded using the Malvern Zetasizer software (Ver 7.11). Buffering system used was 10 mM HEPES buffer solution.

2.8. Agarose Gel Electrophoresis

2.8.1. Introduction

Agarose gel electrophoresis is one of many gel electrophoresis methods that allow for the separation of mixed analytes of macromolecules, such as DNA or RNA, in a matrix of agarose. Electrophoresis uses an electrical field to separate DNA fragments in an agarose gel matrix. When an electrical field is applied, negatively charged DNA would move through the matrix towards a positive electrode. The Agarose gel matrix acts as a molecular sieve that interferes slightly with the motion of small molecules, but drastically slows down the movement of large molecules. Agarose gels are characterised by a mean pore size, which is closely related to Agarose concentration in the matrix. Molecules smaller than the mean pore size are almost unaffected, while the migration of those that are larger than the mean pore size is significantly influenced. Thus, the approximate length of a DNA fragment can be determined by running it on an agarose gel along with a DNA ladder, which is a set of DNA standards that are used to identify the approximate size of a sample molecule run on a gel during electrophoresis. When

DNA or RNA fragments are condensed to other materials such as proteins or polymers to form strongly bound complexes, the behaviour is determined by the overall parameter of the complex. For example, when DNA fragments are condensed to cationic lipids or polymers and form a positively charged particle, instead of moving towards the positive electrode, it would stay still or move towards the negative electrode, depending on the size of the complex. Thus, agarose gel electrophoresis can also be used to determine the formation of certain complexes.

2.8.2. Experimental Conditions and Sample Preparation

The low molecular weight (~185 bp) dsDNA molecules extracted from salmon sperm was purchased from Sigma Aldrich UK. Agarose gel was prepared with a Sub-Cell GT UV-Transparent Mini-Gel Tray and caster (with 8- and 12-well comb). Electrophoresis was performed with Mini-Sub® cell GT system (Bio-Rad UK) with PowerPac™ Basic Power Supply (Bio-Rad UK). Bands were visualised by using Gel Doc™ XR+ Gel Documentation System (trans-UV, 302nm) and figures captured and analysed with Image Lab™ software (Ver.5.2.1). Another alternative approach for visualising bands was using ChemiDoc-It®2 810 imager at trans-UV 302 nm (U.V.P, USA) and data collected and analysed using the software provided.

The TAE buffer (50X) was prepared by dissolving 24.2g of Trizma® Base (Tris-base, Sigma Aldrich UK), 5.71 mL acetic acid, 10 mL of 0.5M sodium EDTA in deionised water and topped up to 100 mL. The working TAE buffer(1X) is diluted from 50X TAE buffer by adding deionised water.

Two different fluorescent nucleic acid dyes were used in this study. Ethidium bromide, a classic, reliable but highly toxic intercalating agent was used at a concentration of 0.006% (0.6 µg/mL) for post-casting staining of the agarose gel. The working solution was prepared by adding 30 µL of EtBr stock solution (10 mg/mL in deionised water) in 500 mL of 1X TAE buffer. GelRed® (Biotium, USA), which is another sensitive, stable and environmentally safe dye, was used as purchased.

2.9. General Cell and Tissue Culture

2.9.1. 3T3 Mouse Fibroblast and Adult Horse Achilles Tenocyte Culture

All cell culture operations were performed under an aseptic environment in a class II microbiology safety cabinet (NUAIRE, Inc. USA). Adult horse Achilles tenocyte, kindly donated by Dr D. Guest (Animal Health Trust, UK), were collected at post-mortem from horses with the approval of the Animal Health Trust Ethical Review Committee (AHT_02_2012) and received frozen at passage 7. Mouse NIH3T3 fibroblast was obtained from the European Collection of Cell Cultures (ECACC, No. 93061524).

Cells were cultured as monolayers in Dulbecco's modified Eagle media supplemented with 10% heat-inactivated fetal calf serum (FCS), 1% L-glutamine (final concentration 2 mM, original stock concentration at 200 mM, Invitrogen) and 1% penicillin-streptomycin (final concentration 100U/mL, original stock concentration at 10,000 U/mL, GibcoTM, Thermo Fisher). This media is referred to as complete medium in the rest of the thesis.

Cells were cultured in Thermo ScientificTM NuncTM T175 (for Horse tenocyte) or T75 (for 3T3 Fibroblast) cell culture flasks with filter caps under 37°C with 5% CO₂ in a humidified incubator. A typical cell passage procedure was performed as follows: Cells were cultured until 80-90% confluence was reached, the media was removed, and the cells were washed once with fresh sterile 1X PBS. Two microlitres of Trypsin/EDTA (for T175 flask, 1mL for T75 flask) solution (0.025% trypsin and 0.01% EDTA in Phosphate Buffered Saline, Gibco) were added and incubated for five minutes before topping up to 10 mL with complete medium to neutralise trypsin. Cells were collected by centrifugation at 3000 rpm using a centrifuge (VWR) for five minutes. Cells were re-dispersed in fresh complete media and transferred to a new culture flask. Cells used in all experiments were between passages 9-14 (Horse Tenocyte) and passages 20-24 (3T3 Fibroblast).

2.9.2. Cell Count and Optical Microscopy

Cell counts were performed using Trypan blue exclusion assay and counted using haemocytometer. Ten microlitres of cell suspension and trypan blue solution were

mixed and placed in a Neubauer improved haemocytometer chamber (with a depth of 0.1 mm, Marienfeld) and sealed with a glass coverslip. The mixture was viewed under an optical microscope (EVOS Cell Imaging Systems, Thermo Fisher) with 10X or 20X objectives. Colourless cells were counted as live cells, while the dead cells would lose membrane integrity and thus stained by trypan blue.

The concentration of cells was calculated as the following equation:

$$\text{Concentration} = \frac{(\text{number of cells counted})(\text{dilution factor})}{(\text{volume of chambers counted})}$$

The volume of chambers counted represents the total volume of chambers counted which in all experiments are $4*1*1*0.1 \text{ mm}^3$ (0.4 μL).

2.10. CellTiter 96® AQ One Solution Cell Proliferation Assay

2.10.1. Introduction and the Basic Principle

The CellTiter 96® AQ One Solution Cell Proliferation Assay (MTS assay) is a colourimetric method for determining the number of viable cells in proliferation. The CellTiter96® AQ One Solution Cell Proliferation Assay contains a tetrazolium compound 5-[3-(carboxymethoxy)phenyl]-3-(4,5-dimethyl-2-thiazolyl)-2-(4-sulfophenyl)-2H-tetrazolium inner salt (also known as MTS) and an electron coupling reagent (phenazine ethosulfate; PES). PES was used as a stabiliser to be combined with MTS to form a stable solution.

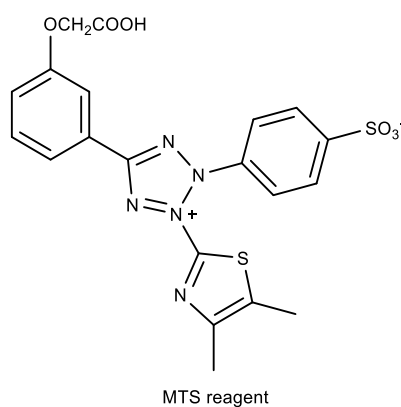


Figure 2.6 Chemical structure of MTS reagent.

The MTS assay is based on the bio-reduction of MTS tetrazolium compound into a formazan product, which is coloured and soluble in culture media, by viable cells

(figure 2.7). The reduction is caused by NADPH or NADH produced by dehydrogenase in viable cells. Generated formazan products could be detected by an absorbance at 490 nm, and the quantity is proportional to the metabolic activity of the living cells in culture.

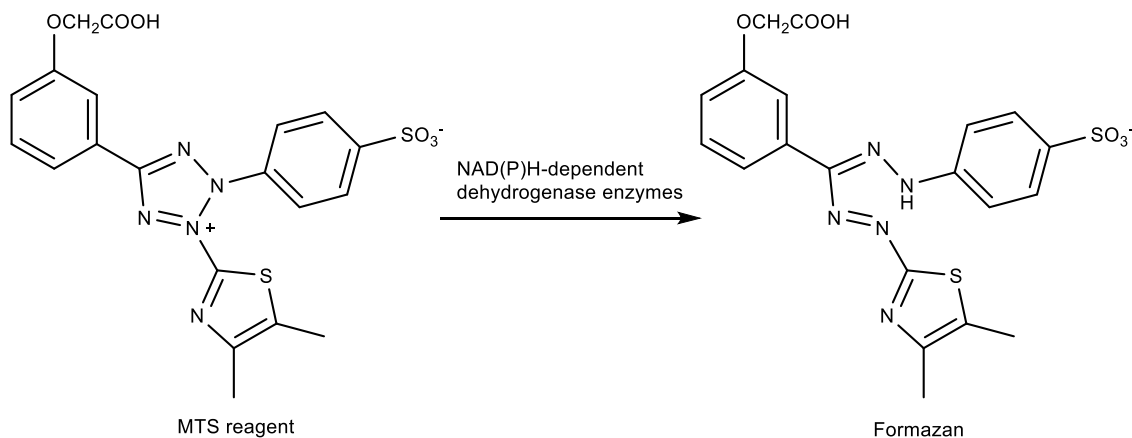


Figure 2.7 The bio-reduction of MTS tetrazolium compound into a formazan product.

2.10.2. Experimental Conditions and Sample Preparation

CellTiter 96® Aqueous One Solution Cell Proliferation Assay was used as purchased and will be referred to as MTS assay in the rest of the thesis. 10 μ L (per 100 μ L of media) of MTS reagent was added to the sample solution and incubated at 37°C for one hour. The sample plate was measured for absorbance at 490 nm in an Omega FLUOstar plate reader (BMG LABTECH).

2.11. Cell Proliferation Assay (CyQUANT® NF Kit)

2.11.1. Introduction and the Basic Principle

The CyQUANT® NF assay is based on cellular DNA staining and the measurement of fluorescent dye. Because cellular DNA content is highly proportional to cell number, the cell viability can be determined by the measure of cell proliferation extent of treated cells compared with the untreated cells ^{8,9}. This assay is designed to be easily manipulated in only a few steps: removal of culture media, the addition of DNA binding dye, incubation and measurement. This enabled quick and efficient measurement and determination of cell viability.

2.11.2. Experimental Conditions and Sample Preparation.

Cells were cultured in Corning® 96 well black polystyrene clear bottom microplate. CyQUANT® NF Cell proliferation assay was used as purchased. Upon usage, 1X dye binding solution was prepared by adding 22 µL of CyQUANT® NF dye reagent to 11 mL of 1X HBSS buffer. Growth medium was removed from samples cells and 100 µL of 1X dye binding solution was dispensed into each well. The plates were covered and incubated at 37°C for 45 minutes, and fluorescence intensities were measured by using CLARIOstar® microplate reader with excitation at 485 nm, and emission at 530 nm and the instrument was set to detect signal from the bottom of the well. Cells treated with saline were employed as -ve control; no +ve control was employed in this assay.

2.12. Quantitative real-time Polymerase Chain Reaction

2.12.1. Introduction and the Basic Principle

Quantitative polymerase chain reaction (qPCR), also referred to as real-time polymerase chain reaction (Real-Time PCR), is a technique based on the polymerase chain reaction (PCR) to analyse target DNA molecule amplification. Compared with traditional PCR, qPCR monitors the amplification of a targeted DNA in real time. Quantitative PCR has many applications in molecular biology, for example in diagnosis, detection of phytopathogens or quantification of gene expression. In this study, qPCR is mainly used to quantify the expression level of a certain target gene (Equine *COL3a1*) compared to the reference gene.

The basic principle of qPCR is described as follow:

The key feature of qPCR is to monitor the amplification as the PCR happens. Therefore, qPCR is carried out in a thermal cycler with fluorescence detector to detect the fluorescence signal emitted by the excited fluorophore. Also, it is essential for the thermal cycler to be equipped with an illuminator that can excite samples with a beam of light at a specific wavelength. The PCR process generally consists of the following three phases: the first phase is the denature phase where the sample is heated to 95°C to allow the separation of double-stranded nucleic acid into single strands. The second phase is the annealing, where the temperature is reduced to 50-60°C to allow the primers to bind with its DNA template. The third phase is the extension phase where the

temperature is increased to 70°C where the DNA polymerase would assist the extension of DNA chains in forming new double-stranded DNA. The three phases were repeated for 25-40 times to amplify enough DNA. The produced DNA would bind to a DNA-binding dye that only fluoresce after binding to DNA when excited. The sample would be excited, and the fluorescence intensity measured as the PCR proceeds.

One problem is that the template used in PCR must comprise DNA molecules, the extracted RNA molecules cannot be applied directly. Therefore, reverse transcription polymerase chain reaction is used to convert RNA into complementary DNA (cDNA). The complementary DNA is later used as a template in qPCR and amplified. With the combination of RNA extraction, reverse transcription PCR and quantitative PCR, it is made possible to quantify the expression of the target gene.

In quantitative real-time polymerase chain reaction, there are two strategies: absolute quantification and relative quantification. In absolute quantification, by using the standard curve method, the quantity of unknown samples is based on a known quantity. The advantages of the absolute quantification include high sensitivity, and also provides the absolute quantification of the original sample. However, using absolute quantification could be difficult due to drawbacks such as a high demand for sample purity and complicated manipulation procedurals ¹⁰. Therefore, relative quantification was selected. In relative quantification, changes in gene expression are analysed by comparison of a given sample to another reference sample, normally referred to as a reference gene. The expression of the reference gene should be consistent in different tissue, and the expression of the reference gene could be used as an internal reference. The role of a reference gene includes: 1) it is essential as it is used to compare with target gene 2) it is used to monitor whether the manipulation process has introduced errors that would cause changes in sample gene level. Commonly used reference genes include GAPDH and β 2-actin. In this thesis, the *18s* ribosomal RNA gene (*18s* gene) is selected as a reference gene, for it is reported to be widely employed in the analysis of equine samples ^{11,12}.

2.12.2. RNA Extraction

Growth medium was removed, and cells were lysed directly by using TRI ReagentTM Solution. The lysed solution was transferred to a clean centrifuge tube and stored at -80°C overnight. The lysed solution was defrosted, added with 100 μ L of 1-Bromo-3-

chloropropane (BCP) and mixed before incubating at room temperature for ten minutes. Then the mixture solution was centrifuged at 12000g for 30 minutes at 4°C using a HERAEUS FRESCO 17 centrifuge (Thermo Scientific). After centrifugation, phase separation was observed, and 400 µL of clear phase (upper phase) was transferred to a clean centrifuge tube and 500 µL of bioreagent grade isopropanol was added. The mixture was vortexed for ten seconds and incubated at room temperature for ten minutes before centrifuged at 12000g, 4°C for 20 minutes. A pellet was observed at the bottom of the centrifuge tube. The excess liquid was aspirated, and 750 µL of 70% ethanol solution (made in bioreagent grade water) was added. The pellet was quickly vortexed and then centrifuged at 12000g, 4°C for 15 minutes. The clear supernatant was removed, and RNA pellet was dissolved in 20 µL of bioreagent grade water.

2.12.3. Reverse Transcription

RNA concentration and purity were determined by using the NanoDrop® ND-1000 Spectrophotometer. An appropriate amount of RNA solution containing 1 µg of total RNA was transferred into a clear 0.2 mL centrifuge tube and topped up to 5 µL with bioreagent grade water. Five microlitres of High Capacity cDNA Reverse Transcription (Applied Biosystems™, Thermo Scientific) reagent master mix, which contains 1.0 µL of 10X RT buffer, 0.4 µL of 25X dNTP mix (100mM), 1.0 µL of 10X RT random primers, 0.5 µL of MultiScribe™ Reverse Transcriptase, 0.5 µL of RNase inhibitor and 1.6 µL of bioreagent grade water, was added to RNA solution. The centrifuge tube containing RNA-RT reagent mixture was loaded into a PTC-100 thermal cycler (MJ research, UK). The thermal cycler was programmed with the following conditions: 25°C for 10 minutes, 37°C for 120 minutes, 85°C for 5 minutes, terminates and remains at 4°C.

2.12.4. Quantitative Polymerase Chain Reaction (qPCR)

Working primer solution was prepared by mixing 5 µL of the forward primer and 5 µL of reverse primer stock solution (100 µM) and topped up to 100 µL with bioreagent grade water. 18 µL of the qPCR master mix was prepared by mixing 10 µL of SYBR® Green JumpStart™ Taq ReadyMix™, 1 µL of working primer solution and 7 µL of bioreagent grade water. Two microlitres of cDNA solution was mixed with 18 µL of qPCR master mix and loaded into Non-Skirted PCR Plate (Starlab) or Rotor Gene®

PCR strip tubes with caps (Qiagen). The qPCR was performed on Bio-Rad C1000 Touch thermal cycler (using PCR plates, Bio-Rad) and Rotor-Gene Q PCR cycler (using strip-tubes, Qiagen). The PCR cycler was programmed to execute the following cycle conditions: Initial denaturation at 94°C for two minutes, followed by cycles of denaturation at 94°C for 15 seconds, annealing, extension and fluorescence reading at 60°C for one minute. Data were collected and analysed with CFX Manager (Bio-Rad) or Rotor-gene Q software.

2.12.5. Relative Quantification using $2^{-\Delta\Delta C_t}$ Method

The basic principle of the $2^{-\Delta\Delta C_t}$ method is reported by Livak et al.¹³. To describe briefly, the $2^{-\Delta\Delta C_t}$ method is based on the following equation:

$$X = X_0 \times (1 + E_X)^n \quad (1)$$

Where X represents the quantity of target gene molecule; X_0 represents the initial quantity of target molecule; E_X represents the amplification efficiency of the target molecule; n is the cycle number.

Assume that X reached a threshold value, equation (1) could be expressed as:

$$X_t = X_0 \times (1 + E_X)^{C_{t,x}} \quad (2)$$

Where X_t represents the quantity of target gene molecule reached threshold value, $C_{t,x}$ represents the cycle number of the target gene when it has threshold value.

The same equation applies to the reference gene as well:

$$R_t = R_0 \times (1 + E_r)^{C_{t,r}} \quad (3)$$

Where R_t represents the quantity of target gene molecule that reached threshold value, $C_{t,r}$ represents the cycle number of the target gene when reached threshold value. R_0 represents the initial quantity of reference gene.

Dividing X_t by R_t , and assuming that the target gene and reference gene have the same amplification efficiency E, a new equation is generated as follows:

$$\frac{X_t}{R_t} = \frac{X_0 \times (1 + E)^{C_{t,x}}}{R_0 \times (1 + E)^{C_{t,r}}} = K \quad (4)$$

Where K is a constant, equation (4) simplifies as follows:

$$X_n = K \times (1 + E)^{-\Delta C_t} \quad (5)$$

Where X_n represents the number of gene molecules in a quantified sample where the ratio of X_0 and R_0 is fixed. ΔC_t represents the difference between $C_{t,x}$ and $C_{t,r}$.

Eventually, assuming that $X_{n,s}$ is the quantity of gene in the treated sample, $X_{n,cb}$ is the quantity of gene in the untreated sample, dividing $X_{n,s}$ by $X_{n,cb}$ results in:

$$\frac{X_{n,s}}{X_{n,cb}} = (1 + E)^{-\Delta\Delta C_t} \quad (6)$$

In the equation, $-\Delta\Delta C_t = -(\Delta C_{t,s} - \Delta C_{t,cb})$.

In optimised experimental conditions, the amplification efficiency is controlled at ~ 1 , where the fold change between the treated group and the untreated group is $2^{-\Delta\Delta C_t}$.

2.13. Fluorescent Cytochemistry

2.13.1. Introduction and the Basic Principle

Immunocytochemistry (ICC) is a commonly used technique to visualise the location of a specific protein or antigen in cells. The visualisation involves the use of a protein specific primary antibody and the use of a fluorescent secondary antibody that can specifically bind to the primary antibody. Immunocytochemistry is considered to be a powerful tool for researchers to evaluate the protein expression visibly.

2.13.2. Experimental Conditions

All cell culture related manipulation is performed as described in section 2.9. Glass coverslips (VWR, 14mm) were sterilised by 70% ethanol or by UV light for one hour. The coverslips were placed in Nunc 24 well plates and coated with 2% gelatine for 20 min at room temperature to enhance cell attachment. After cell seeding and treatment, cells were fixed using a 3% paraformaldehyde solution. The 3% paraformaldehyde solution was prepared by adding 3.6g paraformaldehyde to 120mL and heating up to 50°C in a fume hood, adding a few drops of NaOH as it is necessary to promote dissolution. The solution was cooled down to room temperature, and the pH was adjusted to 7.0 - 7.4 by adding 1M HCl. The solution was then supplemented with 10µL 1M CaCl₂ and 10 µl 1 M MgCl₂, and then sterilised by filtering through a 0.22 µm filter.

Fixed cells were preserved in 1X PBS and stored at 4°C, ready for further permeabilisation, blocking and antibody staining. The details for cell seeding, treatment, permeabilisation and staining is further described and discussed in Chapter six.

The primary antibody, anti-collagen III produced from rabbit, was purchased from Abcam and received at a concentration of 1 mg/mL. A working solution was diluted at 1:100 from the original stock. The secondary antibodies, an anti-rabbit IgG-FITC antibody produced in goats was purchased from Sigma Aldrich UK and diluted in 1:100 as a working solution. The stained samples were mounted with Vectashield® hardest mounting media containing DAPI (cat. no. H-1500 vector laboratories) before visualising under fluorescent microscope.

Imaging was performed using a Zeiss Axioplan 2ie microscope with Axiovision software equipped with an FITC or DAPI filter. Pictures were taken with a 20x magnification PlanApochromat (0.6 NA) objective and a Zeiss AxioCam HRm CCD camera.

2.14. References

- 1 Jacobsen, N. E. *NMR spectroscopy explained : simplified theory, applications and examples for organic chemistry and structural biology.* (Wiley-Interscience, 2007).
- 2 Thomson, R. C., Yaszemski, M. J., Powers, J. M. & Mikos, A. G. Fabrication of Biodegradable Polymer Scaffolds to Engineer Trabecular Bone. *J Biomat Sci-Polym E* **7**, 23-38 (1995).
- 3 Cho, S. M. & Choi, W. Y. Solid-phase photocatalytic degradation of PVC-TiO₂ polymer composites. *J Photoch Photobio A* **143**, 221-228, doi:Doi 10.1016/S1010-6030(01)00499-3 (2001).
- 4 Liu, J. Q. *et al.* In situ formation of protein-polymer conjugates through reversible addition fragmentation chain transfer polymerization. *Angew Chem Int Edit* **46**, 3099-3103, doi:10.1002/anie.200604922 (2007).
- 5 Berne, B. J. & Pecora, R. *Dynamic light scattering : with applications to chemistry, biology, and physics.* Dover edn, (Dover Publications, 2000).
- 6 Aragon, S. R. & Pecora, R. General-Theory of Dynamic Light-Scattering from Cylindrically Symmetric Particles with Translational-Rotational Coupling. *J Chem Phys* **82**, 5346-5353, doi:Doi 10.1063/1.448617 (1985).
- 7 Banerjee, S. & Tyagi, A. K. *Functional materials : preparation, processing and applications.* 1st edn, (Elsevier, 2012).
- 8 Blaheta, R. A., Franz, M., Auth, M. K., Wenisch, H. J. & Markus, B. H. A rapid non-radioactive fluorescence assay for the measurement of both cell number and proliferation. *J Immunol Methods* **142**, 199-206 (1991).
- 9 Myers, M. A. Direct measurement of cell numbers in microtitre plate cultures using the fluorescent dye SYBR green I. *J Immunol Methods* **212**, 99-103 (1998).
- 10 Walker, N. J. Real-time and quantitative PCR: Applications to mechanism-based

toxicology. *J Biochem Mol Toxic* **15**, 121-127, doi:DOI 10.1002/jbt.8 (2001).

11 Barsby, T., Bavin, E. P. & Guest, D. J. Three-dimensional culture and transforming growth factor beta3 synergistically promote tenogenic differentiation of equine embryo-derived stem cells. *Tissue Eng Part A* **20**, 2604-2613, doi:10.1089/ten.TEA.2013.0457 (2014).

12 Paterson, Y. Z., Rash, N., Garvican, E. R., Paillot, R. & Guest, D. J. Equine mesenchymal stromal cells and embryo-derived stem cells are immune privileged in vitro. *Stem Cell Res Ther* **5**, 90, doi:10.1186/scrt479 (2014).

13 Livak, K. J. & Schmittgen, T. D. Analysis of relative gene expression data using real-time quantitative PCR and the 2(T)(-Delta Delta C) method. *Methods* **25**, 402-408, doi:10.1006/meth.2001.1262 (2001).

Chapter 3

The Synthesis and Characterisation of a Library of PDMAEA Polymers

3. Chapter 3 The Synthesis and Characterisation of a Library of PDMAEA Polymers

3.1. Introduction

Research in the drug delivery presently evaluated the potential and benefits of chemically synthesised gene delivery vectors, such as cationic lipids and polymers, for gene therapy. With regards to polymers, significant attention is paid to cationic polymers which possess positive charge and able to condense with nucleic acids to form nanocarriers called polyplexes. Cationic polymers usually refer to polymers with abundant primary, secondary, tertiary or quaternary amine group or other positively charged functional groups. Typical example includes polyethylenimine (PEI), chitosan, polyamidoamine (PAMAM), poly (2-dimethylaminoethyl methacrylate) (PDMAEMA) and poly (dimethylaminoethyl acrylate) (PDMAEA)^{1,2}.

PEI contains a wide range of primary, secondary and tertiary amines groups in its structure which can protonate to efficiently bind to DNA to form into condensing toroidal and globular nanostructures³, and can be internalised by cells via clathrin-mediated endocytosis⁴. However, PEI is also associated with severe toxicity, and some studies suggested that the mechanism by which PEI induces toxicity is related to its ability to disrupt the cell membrane and its integrity, followed by activation of mitochondrial-mediated apoptosis program^{5,6}. These unwanted adverse effects have spurred the design and engineering of new polycation-based gene delivery systems with different structures and compositions.

Poly (dimethylaminoethyl methacrylate) (PDMAEMA) has emerged as a potential substitute for PEI. This cationic polymer demonstrates relatively lower cytotoxicity in cultured cell lines and capability of protonation at natural pH and below⁷. A variety of PDMAEMA polymers with different structures have been reported in literatures, including linear, branched and dendritic, as transfecting agents⁷. For example, Georgiou et al. have discussed the role of star polymers in gene delivery and their structure-activity relationship, in which the effect of molecular mass on transfection efficiency and cell viability was investigated⁸. More recently, studies have suggested that branched PDMAEMAs perform better than their linear counterparts as transfecting agents, which is attributed to the ability of branched PDMAEMA to densely compact DNA, maintain buffering capacity and exhibit lower cytotoxicity⁹. Among the branched

PDMAEMA polymers, star-shaped polymers are most attractive due to their simple structure and ease of synthesis and scale-up. In another study, Yu et al., have reported that transfection efficiency of branched PDMAEMA polymers increases with increasing degree of branching¹⁰.

However, the acrylate version and homopolymer of PDMAEMA, Poly(dimethylaminoethyl acrylate) (PDMAEA), received little attention, despite its excellent loading capacity, low immunogenicity and capability of biodegradation¹¹. Nevertheless, a significant number of studies have been conducted exploring the potential development of PDMAEA into a delivery system. The success of developing new pH-sensitive miktoarm star terpolymer system, which refers to asymmetric branched macromolecules with tailored polymer side chains varying from each other, using PDMAEA as the pH-responsive blocks has been reported by Liu et al.¹². Another study by Dinari et al. reported crosslinking between gold nanorods and PDMAEA. The gold nanorods functionalized with PDMAEA have an increased transfection effect on HEK-293T cell line with reduced cytotoxicity¹³. A more recent study completed by Whitfield et al. accomplished the successful synthesis of star-shaped PDMAEA polymer via Cu(0)-mediated reversible-deactivation radical polymerization, though this study did not further explore other parameters such as binding ability, toxicity or the transfection efficacy of such polymer¹⁴. Despite these reports, a systematic study that can determine the effect of PDMAEA architecture and molecular weight on binding to polyanionic DNA and attempt to ascertain their cytotoxicity in cultured cell lines, in a directly comparable condition, is lacking and therefore requires further investigation.

The aim of the chapter:

To synthesise and characterise a series of new star-shaped and linear PDMAEA based polymers using the RAFT polymerisation technique. Two different molecular weights for each polymer structure are designed: 10kDa and 20kDa, representing a lower molecular weight level and a higher molecular weight level respectively. The RAFT polymerisation technique is employed for the synthesis of each polymer with pentaerythritol tetrakis [2-(dodecylthiocarbonothioylthio)-2-methylpropionate] (4-arm DDMAT) and 2-(dodecylthiocarbonothioylthio)-2-methyl propionate selected as the RAFT agent for the synthesis of star-shaped and linear polymer, respectively. The logic for using DDMAT and 4-arm DDMAT, which are chemically similar, was to maintain directly comparable synthesis routes and conditions, as well as to control the molecular

weight of each structure. Furthermore, the synthesis 10kDa and 20kDa polymers for each structure also enabled the possible comparison of DNA-binding efficiency to DNA and cytotoxicity between polymers of the same molecular weight but different structure, and vice versa. The structure and molecular weights of the synthesized polymers were characterised by ^1H NMR, GPC and potentiometric titration to provide an insight into the PDMAEA polymer parameters.

The main objectives:

This chapter described the synthesis and characterisation of a library of PDMAEA polymers. The following objectives will be achieved:

- Synthesise and purify linear and star-shaped PMDAEA polymers of 10kDa and 20kDa molecular weight.
- Confirm the polymerisation and determine the polymer structure and molecular weight by using ^1H NMR and GPC characterisation.
- Test the PDMAEA polymers by potentiometric titration to confirm the pKa values.

3.2. Material and Methods

3.2.1. Materials

The details of the materials used in this chapter can be found in Chapter Two section 2.2.

3.2.2. Synthesis and Characterisation of 10 kDa Linear PDMAEA (PL10)

The synthesis process is demonstrated schematically in figure 3.1. AIBN was recrystallized before use, and DMAEA monomer was de-inhibited with an aluminium oxide column (same for the synthesis other PDMAEA polymers). DDMAT (51.0 mg, 0.140 mmol), AIBN (4.6 mg, 0.028 mmol) and DMAEA (2.0 g, 0.014 mol) were dissolved in 8 mL of 2-butanone in a round-bottom flask. The mixture was degassed by purging with nitrogen for 25 minutes in the round-bottom flask with a rubber stopper. The mixture was then heated up to 70°C and allowed to react for four hours. The reaction was stopped by exposure to air. A sample was taken for NMR analysis to confirm the conversion rate.

Synthesis of 10kDa linear PDMAEA polymer (PL10)

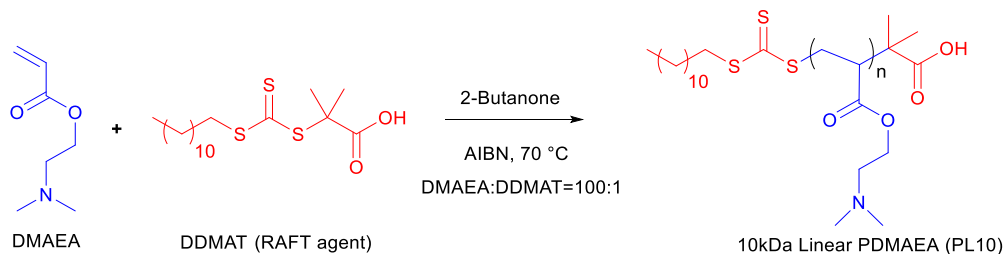


Figure 3.1 Synthesis of 10 kDa linear PDMAEA polymer (PL10).

The polymer was purified by precipitating into 100 mL cold hexane three times. Typically, the reaction mixture was added into cold hexane at the rate of 1~2 drops/second through a dropping funnel. Precipitation of yellow gel was observed during the procedure. The hexane-polymer solution was centrifuged at 4000 rpm for five minutes, and the yellow polymer precipitant was collected. The precipitant was re-dissolved in butanone and precipitated two more times before the final product was dissolved in acetone. The acetone was evaporated using a rotavapor under vacuum and samples were collected. The product thus obtained was a yellow viscous gel weighing 735 mg (yield 52.5%), which was then stored at 4°C for future use. The purified sample was analysed by GPC and NMR to confirm its molecular weight, purity and structure. To simplify future referencing, the 10 kDa linear PDMAEA polymer was abbreviated to PL10.

3.2.3. Synthesis and Characterisation of 20 kDa Linear PDMAEA(PL20)

The synthesis process is shown schematically in figure 3.2. DDMAT (260.0 mg, 0.070 mmol), AIBN (2.3 mg, 0.014 mmol) and DMAEA (2.0 g, 0.014 mol) were dissolved in 8 mL of 2-butanone in a round-bottom flask. The mixture was degassed by purging with nitrogen for 25 minutes in the round-bottom flask with a rubber stopper. The mixture was then heated and elevated at 70°C for 18 hours. The reaction was terminated by exposure to the air. Samples were taken for NMR to confirm the conversion rate.

Synthesis of 20kDa linear PDMAEA polymer (PL20)

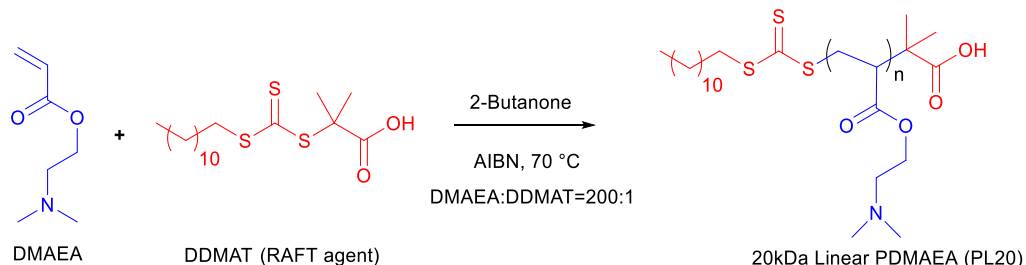


Figure 3.2 Synthesis of 20 kDa linear PDMAEA polymer (PL20).

The polymer was purified by precipitating into 100 mL cold hexane three times. The reaction mixture was added into cold hexane at the rate of 1~2 drops/second through a dropping funnel. Yellow precipitant was observed during the procedure. The hexane-polymer solution was centrifuged at 4000 rpm for five minutes, and the yellow precipitant was collected. The precipitant was re-dissolved in butanone and precipitated two more times before the final product was dissolved in acetone and evaporated a rotavapor. The product thus obtained was a yellow viscous gel weighing 808 mg (yield 49.3%), which was stored at 4°C for future use. The purified sample was analysed by GPC and NMR to confirm molecular weight, purity and structure. To simplify future referencing, the 20 kDa linear PDMAEA polymer was abbreviated to PL20.

3.2.4. Synthesis and Characterisation of 10 kDa Star-shaped PDMAEA(PS10)

The synthesis process is shown schematically in figure 3.3. AIBN (18.0 mg, 0.110 mmol), 4-arm-DDMAT (0.2g, 0.14 mmol) and DMAEA (2.0 g, 0.014 mol) were dissolved in 8 mL of 2-butanone in a round-bottom flask. The mixture was degassed by purging with nitrogen for 25 minutes in the round-bottom flask with a rubber stopper. The mixture was then heated up to 70 °C and allowed to react for eight hours. The reaction was terminated by exposure to air. A sample was taken for NMR analysis to confirm the conversion rate.

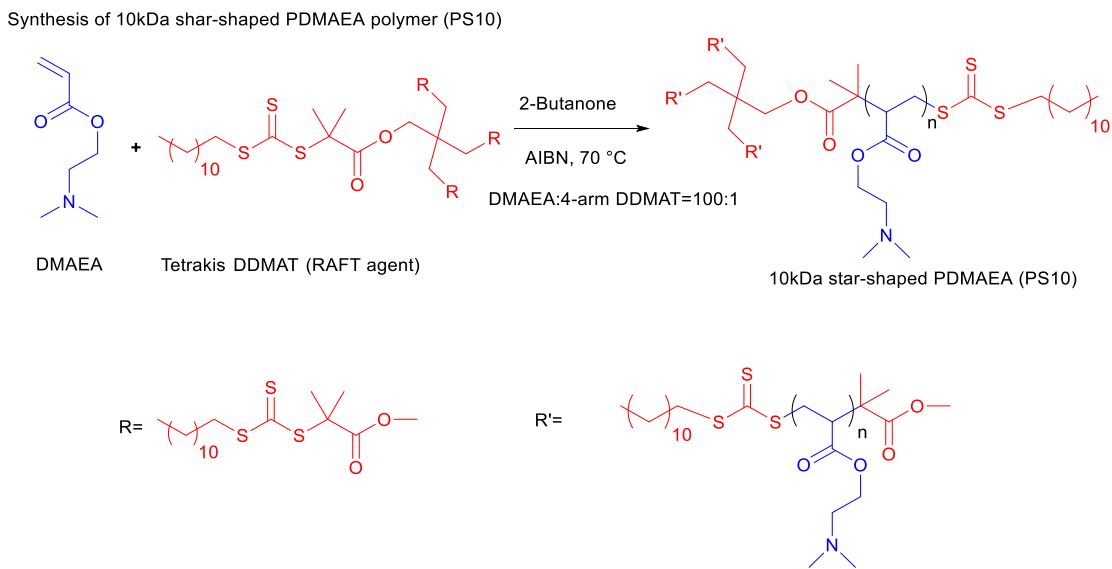


Figure 3.3 Synthesis of 10 kDa star-shaped PDMAEA polymer (PS10).

The polymer was purified by precipitating into 100mL cold hexane three times. The reaction mixture was added into cold hexane at the rate of 1~2drops/second through a dropping funnel. Formation of yellow precipitant was observed during the procedure. The hexane-polymer solution was centrifuged at 4000 rpm for five minutes, and the yellow polymer precipitant was collected. The precipitant was re-dissolved in butanone and precipitated two more times before the final product was dissolved in acetone and evaporated using a rotavapor. The product thus collected was a yellow viscous gel weighting 968mg (yield 64.5%), and the product was stored at 4°C for future use. The purified sample was analysed by GPC and NMR to confirm its molecular weight, purity and structure. To simplify future referencing, the 10kDa star-shaped PDMAEA polymer was abbreviated to PS10.

3.2.5. Synthesis and Characterisation of 20 kDa Star-shaped PDMAEA (PS20)

The synthesis process is shown schematically in figure 3.4. AIBN (9.0 mg, 0.055 mmol), 4-arm-DDMAT (0.11 g, 0.070 mmol) and DMAEA (2.0 g, 0.014 mol) were dissolved in 8 mL of 2-butanone in a round-bottom flask. The mixture was degassed by purging with nitrogen for 25 minutes in the round-bottom flask with a rubber stopper. The mixture was then heated up to 70 °C and allowed to react for 20 hours. The reaction was stopped by exposure to air. A sample was taken for NMR to confirm the conversion rate.

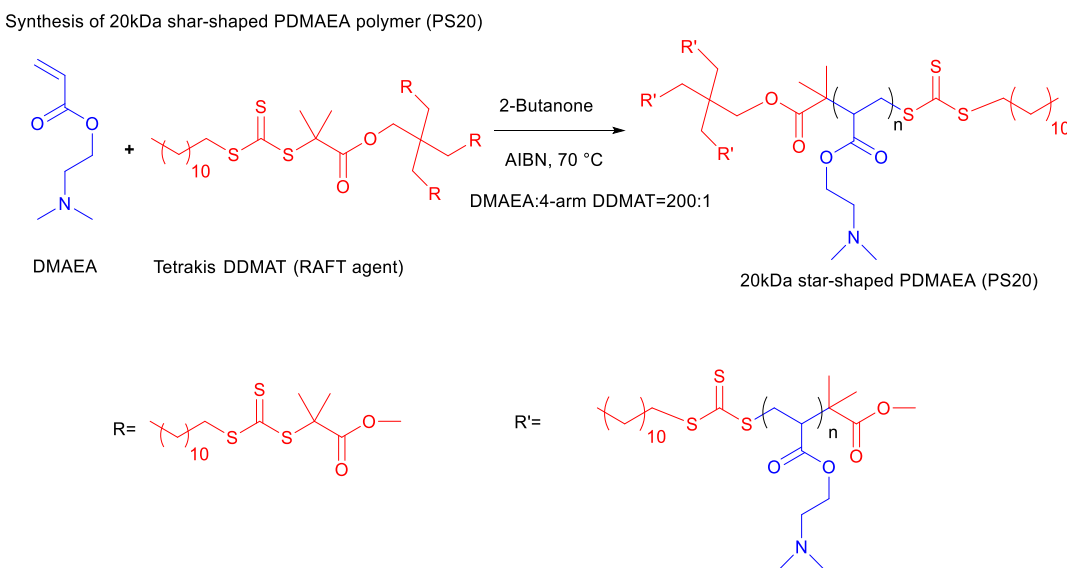


Figure 3.4 Synthesis of 20 kDa star-shaped PDMAEA polymer (PS20).

The polymer was purified by precipitating into 100 mL cold hexane three times. The reaction mixture was added into cold hexane at the rate of 1~2 drops/second through a dropping funnel. Yellow precipitant was observed during the procedure. The hexane-polymer solution was centrifuged at 4000 rpm for five minutes, and the yellow polymer precipitant was collected. The precipitant was re-dissolved in butanone and precipitated two more times before the final product was dissolved in acetone and evaporated using a rotavapor. The product thus collected was a yellow viscous gel weighing 686 mg (yield 40%), and the product was stored at 4°C for future use. The purified sample was analysed by GPC and NMR to confirm its molecular weight, purity and structure. To simplify future referencing, the 20 kDa star-shaped PDMAEA polymer was abbreviated to PS20.

3.2.6. Determination of Polymer pKa Values by Potentiometric Titration

Polymer solutions of PL10, PL20, PS10 and PS20 were prepared as described in Chapter Two section 2.6.2. All solutions were adjusted to pH 2 by using 0.1 M hydrochloride acid (HCl) measured by using a Mettler Toledo SevenEasy pH meter. Each solution was titrated stepwise by adding 0.1 M sodium hydroxide (NaOH), and the pH was monitored during the respective processes. The pKa values were calculated from the titration curve.

3.3. Results

3.3.1. Confirmation of Polymer Structure by $^1\text{H-NMR}$

The ^1H NMR spectrum of PL10, PL20, PS10 and PS20 was studied. The structure of the polymers was confirmed by comparison with data reported in other literature ^{13,15}. Through the analysis of the ^1H NMR spectrum of the polymers, the confirmation of polymerisation and calculates of the conversion rates could be achieved.

- The ^1H NMR spectrum of PS10

The ^1H NMR spectrum of PS10 is illustrated in figure 3.5. Peaks on the spectrum of PS10 were allocated based on previous studies and are shown in the figure ¹⁶. To briefly describe: ^1H NMR (400 MHz, CDCl_3 , δ in ppm): δ 4.05~4.25 (br s, 2H, CH_2), δ 2.53~2.66 (br s, 2H, CH_2), δ 2.31~2.45 (br s, H, CH), δ 2.25~2.30 (br s, 6H, $\text{N}(\text{CH}_3)_2$), 1.60~2.03(2br s, 2H, CH_2), δ 1.10~1.29 (2 br s, 6H, 2 CH_3), δ 1.05~1.10(t, 3H, CH_3).

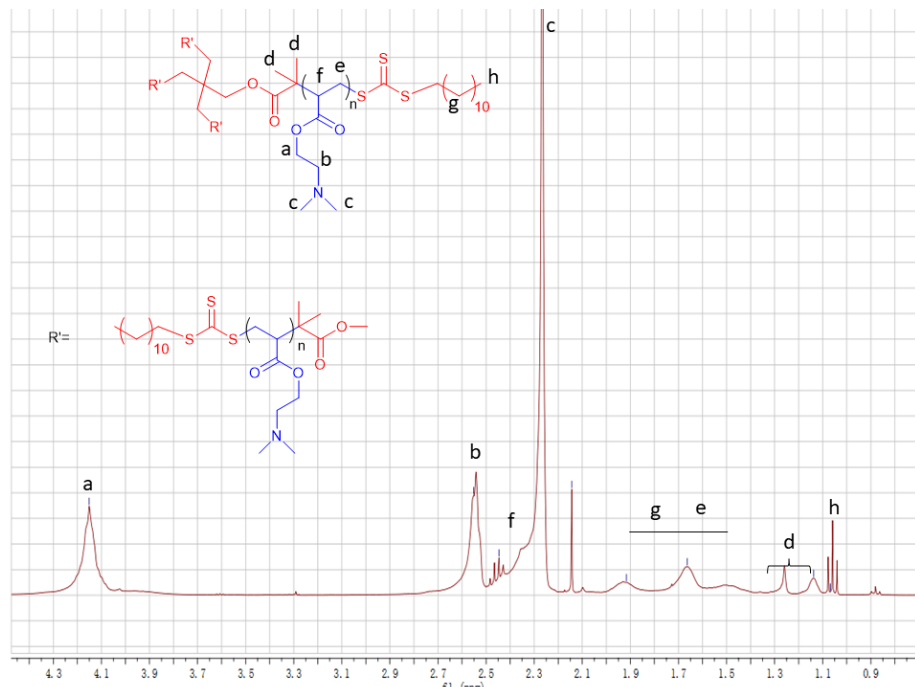


Figure 3.5 ^1H NMR spectrum of 10 kDa star-shaped PDMAEA polymers.

- The ^1H NMR spectrum of PL10

The ^1H NMR spectrum of PL10 is shown in figure 3.6. To briefly describe: ^1H NMR (400 MHz, CDCl_3 , δ in ppm): δ 4.00~4.32 (br s, 2H, CH_2), δ 2.53~2.61 (br s, 2H, CH_2), δ 2.29~2.41 (br s, H, CH), δ 2.18~2.29 (br s, 6H, $\text{N}(\text{CH}_3)_2$), 1.63~2.24(2br s, 2H, CH_2), δ 1.18~1.30 (2 br s, 6H, 2 CH_3), δ 1.05~1.10(t, 3H, CH_3).

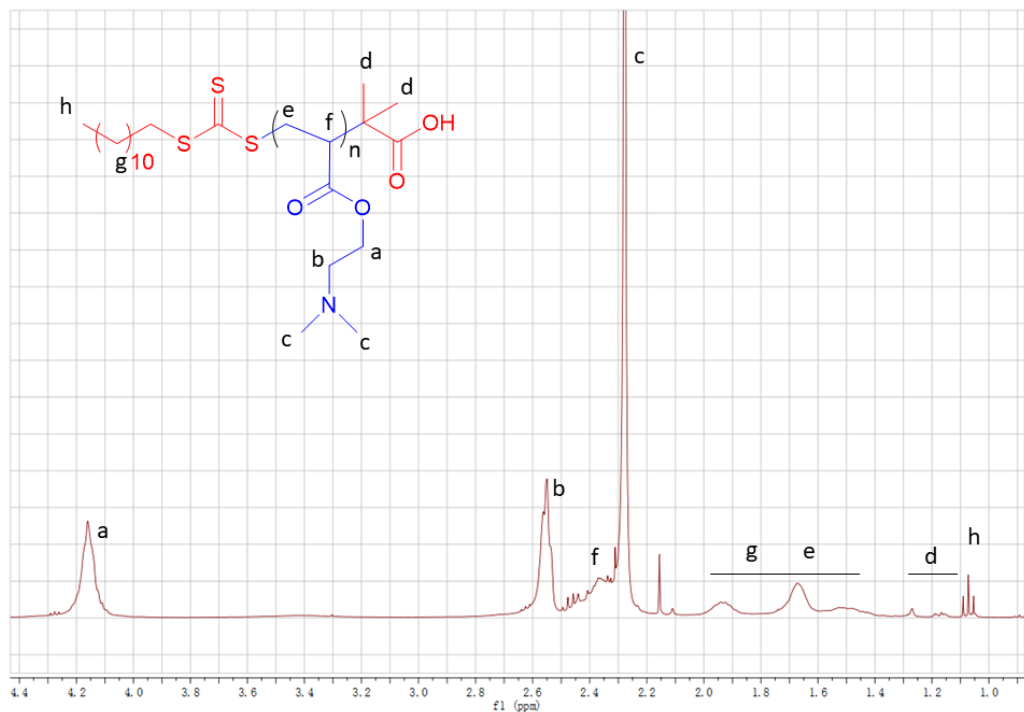


Figure 3.6 ^1H NMR spectrum of 10 kDa linear PDMAEA polymers.

- The ^1H NMR spectrum of PS20

The ^1H NMR spectrum of PS20 is demonstrated in figure 3.7. To briefly describe: ^1H NMR (400 MHz, CDCl_3 , δ in ppm): δ 4.09~4.26 (br s, 2H, CH_2), δ 2.51~2.64 (br s, 2H, CH_2), δ 2.30~2.45 (br s, H, CH), δ 2.38~2.34 (br s, 6H, $\text{N}(\text{CH}_3)_2$), 1.60~2.00(2br s, 2H, CH_2), δ 1.11~1.32 (2 br s, 6H, 2 CH_3), δ 1.06~1.10(t, 3H, CH_3).

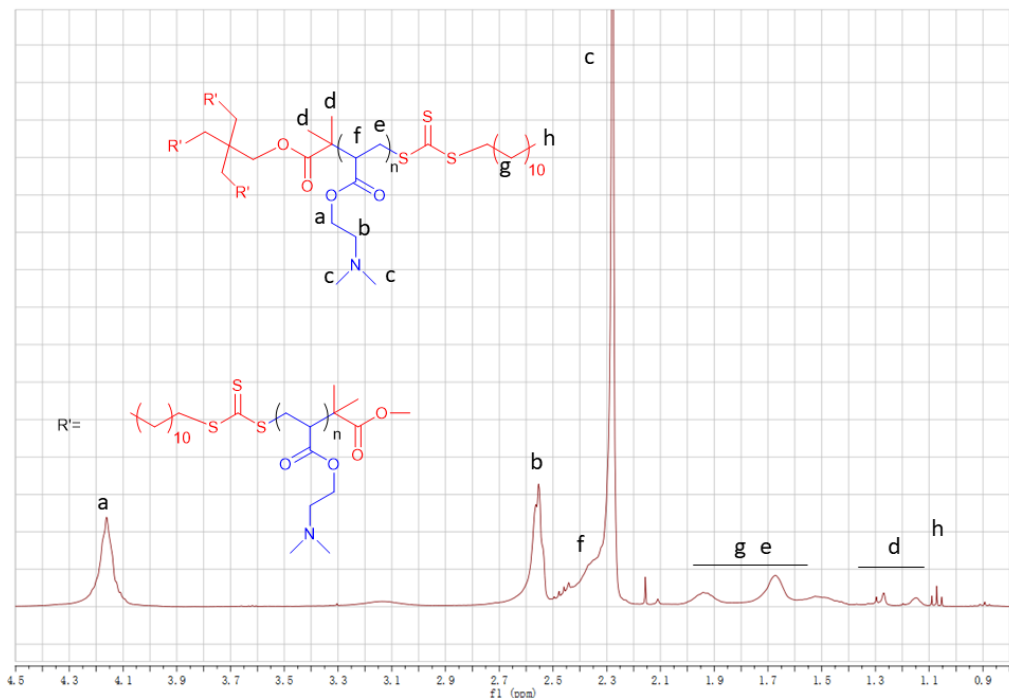


Figure 3.7 ^1H NMR spectrum of 20kDa star-shaped PDMAEA polymers.

- The ^1H NMR spectrum of PL20

The ^1H NMR spectrum of PL20 is shown in figure 3.8. Peaks were assigned as follows:

^1H NMR (400 MHz, CDCl_3 , δ in ppm): δ 4.09~4.26 (br s, 2H, CH_2), δ 2.51~2.64 (br s, 2H, CH_2), δ 2.30~2.45 (br s, H, CH), δ 2.38~2.34 (br s, 6H, $\text{N}(\text{CH}_3)_2$), 1.60~2.00(2br s, 2H, CH_2), δ 1.11~1.32 (2 br s, 6H, 2 CH_3), δ 1.06~1.10(t, 3H, CH_3).

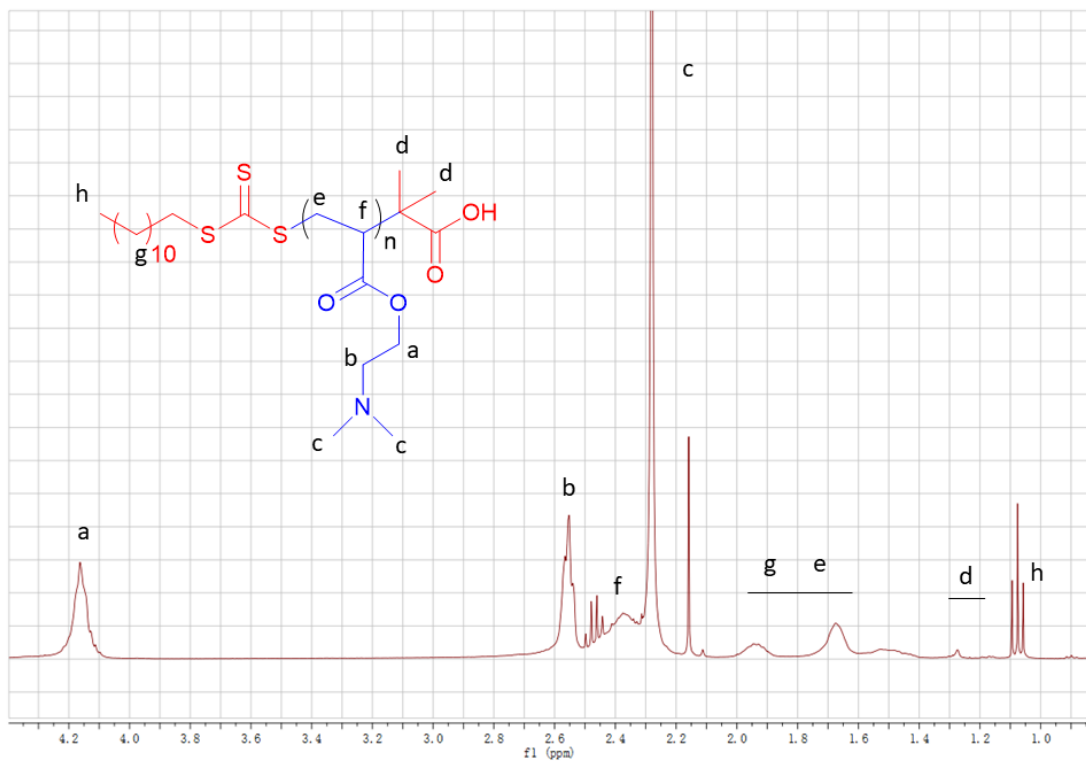


Figure 3.8 ^1H NMR spectrum of 20kDa linear PDMAEA polymers.

3.3.2. Confirmation of Molecular Weight by Gel Permeation Chromatography

Gel permeation chromatography was applied to confirm the molecular weight of the PDMAEA polymers. The molecular weight by number (M_n), molecular weight by weight (M_w), conversion rate, the degree of polymerisation (DP) and polydispersity (\mathcal{D}) are displayed in Table 3.1.

Table 3.1 Experimental conditions and molecular weight characterisation of linear and star-shaped polymers. ^a Abbreviation for linear and star-shaped PDMAEA polymers. ^b Monomer conversion was determined by ^1H NMR spectroscopy. ^c Degree of polymerisation ^d The number of average molecular weight and weight average molecular weight were determined by GPC using Agilent EasiVial PS standards in triethylamine-chloroform (5:95, v/v). ^e Dispersity

Polymer entry	Abbreviation ^a	Time(h)	Conv ^b (%)	DP ^c	M_n ^d (kDa)	M_w (kDa)	\mathcal{D} ^e
10k Linear	PL10	4	66%	65	9618	11063	1.15
20k Linear	PL20	18	82%	144	20996	24034	1.14
10k Star	PS10	8	75%	55	9354	12674	1.35
20k Star	PS20	20	85%	124	19283	24529	1.38

Additionally, the GPC spectrum of retention time versus signal intensity of PL10, PS10, PL20 and PS20 are shown in figure 3.9. The overlapped curves indicate the similarity in retention time.

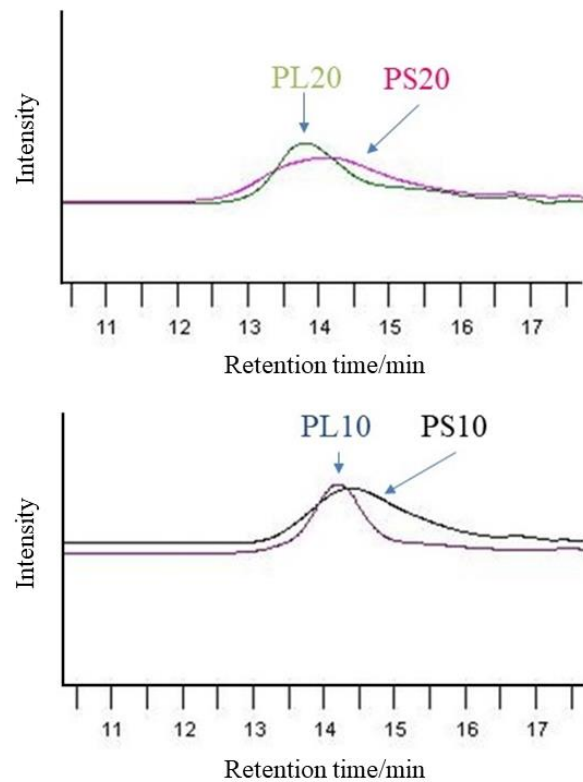


Figure 3.9 Gel permeation chromatography spectra of PS10, PS20, PL10 and PL20.

3.3.3. Calculated pKa Values of PDMAEA Polymers

The titration curves of PL10, PS10, PL20 and PS20 are demonstrated in figure 3.10.

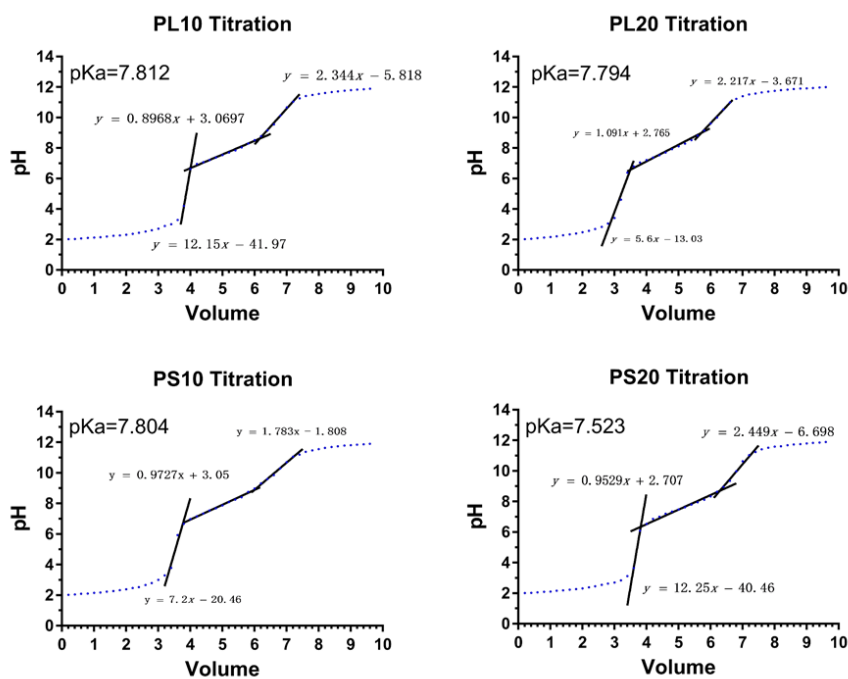


Figure 3.10 Potentiometric titration curves of PDMAEA polymers and calculated pKa values.

Based on the titration curves of PDMAEA polymers, it is considered that PDMAEA polymers are polyprotic with two “classes” of protons, though they have repeated units of tertiary amines. The apparent two-step titration behaviour has been suggested to be caused by the interactions between neighbouring pairs of charged sites in the polymer structure¹⁷, which will be further explained and discussed in detail in section 3.4.

In such cases, the pKa of PDMAEA amines is represented by pKa2 in the above figure. According to the Henderson–Hasselbalch equation, the pK_{a1} for the first dissociation could be expressed as:

$$pK_{a1} = pH - \log_{10} \frac{[HA^-]}{[H_2A]} \quad (1)$$

Likewise, for the amine dissociation process, according to Henderson–Hasselbalch equation, it could be described as:

$$pK_{a2} = pH - \log_{10} \frac{[HA^-]}{[A^{2-}]} \quad (2)$$

Therefore, the pKa values can be calculated based on the titration curve as shown in figure 3.10. The calculated pKa value for PL10, PL20, PS10 and PS20 were 7.8, 7.8, 7.8 and 7.5, respectively. These pKa values are highly consistent with other studies which have suggested that PDMAEA polymers usually have a pKa value of 7.1~8.5¹⁸⁻²⁰.

3.4. Discussion

A series of PDMAEA polymers have been successfully synthesized via RAFT polymerisation. Linear and star-shaped polymers with molecular weights of 10 kDa and 20 kDa were abbreviated as PL10, PL20, PS10 and PS20, representing linear 10 kDa, 20 kDa polymers and star-shaped 10 kDa, 20 kDa polymers respectively. The Linear PDMAEA polymers were synthesised with DDMAT employed as the RAFT agent. The selection of DDMAT as the RAFT agent is mainly based on its excellent reactivity compatibility with acrylate type monomers which in this case is DMAEA. On the other hand, the synthesis of star-shaped PDMAEA involves the use of pentaerythritol tetrakis [2-(dodecylthiocarbonothioylthio)-2-methylpropionate] (4-arm DDMAT) as the RAFT agent. The choice of 4-arm DDMAT is based on several reasons, the major one being its excellent reactivity with acrylate monomers such as DMAEA monomers as well. Another reason to select this RAFT agent is that such molecule has four trithiocarbonate

groups attached to a hydrophobic core structure enabling the propagation of four PDMAEA chains, thus creating a star-shaped polymer.

The rationale behind the use of control/living polymerisation for the synthesis of PDMAEA polymers was to provide control over the molecular weight, as well as the architecture of synthesized polymers with a relatively low polydispersity, compared to the conventional free radical polymerisation.

^1H NMR was applied in the characterisation of PDMAEA polymers, and the structure, conversion rate and purity could be determined from the ^1H NMR spectrum. By comparison with the literature, the structure could be associated with peaks from the ^1H NMR spectrum as shown in figure 3.5~3.8. The conversion rate could be determined by analysis of the reaction mixture of PDMAEA polymer and unreacted monomer. An example ^1H NMR spectrum of the polymer-monomer mixture is presented as below in figure 3.11.

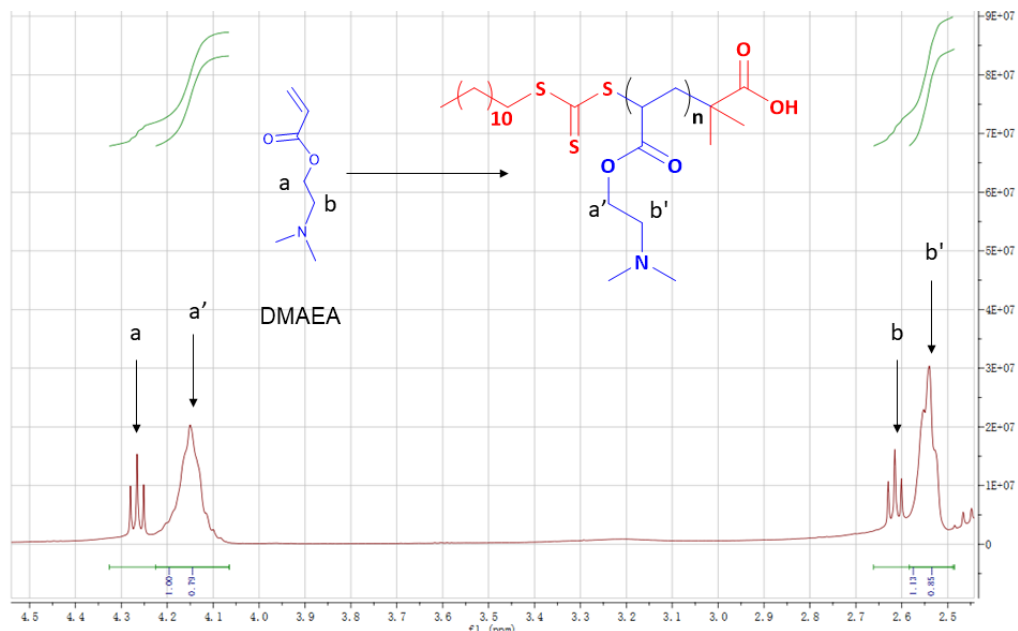


Figure 3.11 Chemical shift of methylene proton of unreacted DMAEA monomer and synthesized polymer.

As demonstrated in figure 3.11, the triplet peak with a chemical shift at δ 4.25(t, 2H, CH_2 , labelled as a) refers to the signal from the methylene group connected to the ester group in the unreacted DMAEA monomer. The generated polymers would have changed the chemical shift of these same protons at the same location resulting in a broad single peak chemical shift at around δ 4.12 (br s, 2H, CH_2 , labelled as a'), representing the signals of methylene group connected to the ester group in the

PDMAEA polymers. Through the integration of these peaks, the ratio between unreacted monomers and generated polymers could be calculated and then converted into conversion rates.

Furthermore, ^1H NMR is applied in the determination of the removal of unreacted monomers after the purification process. The DMAEA monomers possess a distinctive signal peak of a vinyl group with a chemical shift of around δ 5.5~6.5, as demonstrated in figure 3.12. Since no such peaks can be observed in figures 3.1~3.4, it is considered that no traces of DMAEA were present.

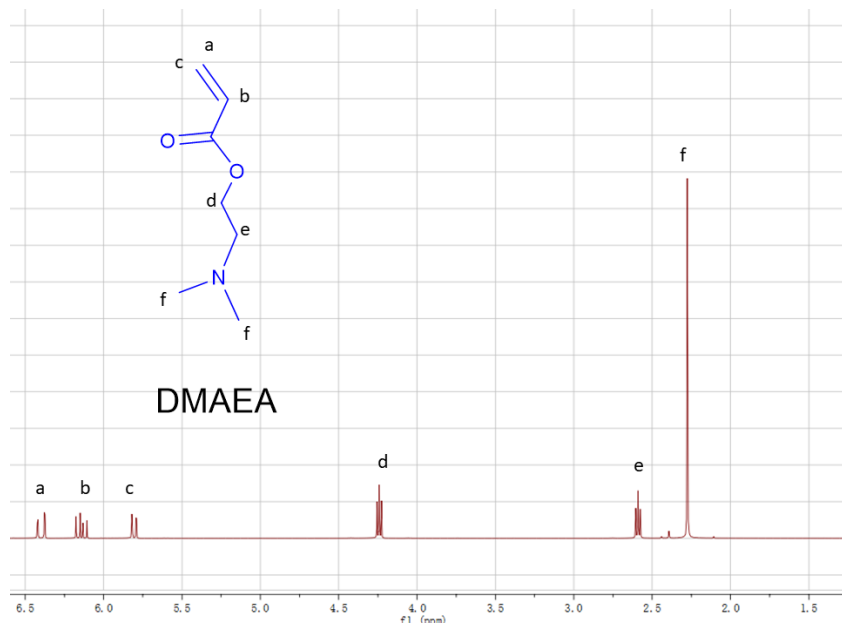


Figure 3.12 ^1H NMR spectrum of DMAEA monomers.

Polymers of two different molecular weight levels, the molecular weight of 10 kDa (representing low molecular weight) and 20 kDa (representing high molecular weight), were prepared and analysed. The molecular weight and polydispersity of all PL and PS PDMAEA polymers were analysed by gel permeation chromatography (GPC), using an available polystyrene standard calibration curve (note that the polystyrene standards give a relative molecular weight rather than the actual values). The results of M_n , M_w and \bar{D} , are presented in Table 3.1. Compared to the theoretical molecular weight 10 kDa and 20 kDa, the representative value of M_n for all the PL and PS polymers show a high degree of agreement between the theoretical and GPC (M_n value), indicating that good control over the molecular weight was possible using RAFT polymerisation^{21,22}. It must be noted that there is a subtle, yet apparent, difference in the molecular weight evolution as a function of time between the PL and PS polymers. The PS polymers take a slightly

longer time to achieve a similar molecular weight as the linear ones. This might be due to the steric hindrance imposed by branches of the star shape polymer during chain propagation²³. Similarly, the D (dispersity) value of the PL polymers shows a narrower distribution (D = 1.15 and 1.14) compared to the PS polymers (D = 1.35 and 1.38), the latter being a known characteristic of star – and branched-polymers. The broader D value of PS polymers agrees with published work²⁴. The degree of polymerisation (DP) determined by end group analysis based on ¹H NMR and the calculated DP for all the polymers are listed in table 3.1. The DP of PL10 and PL20 were 65 and 144 respectively, whereas the DP for the PS10 and PS20 polymers were 55 and 124 respectively. This end group analysis suggests a relatively higher DP was achieved for the linear polymers compared to their star counterparts.

The potentiometric titrations of PDMAEA polymers exhibited apparent two-step titration behaviour, and it has been suggested that the interaction between neighbouring pairs of charged sites are responsible²⁵. For polymers containing amine groups, such as LPEI and PDMAEA, the amine groups, whether primary, secondary, or tertiary amine groups, may protonate by taking a positively charged proton. Each amine group is considered as one charge site, which can be in two states, namely deprotonated state and protonated state. If a naive model, which assumes all sites the same affinity for protons and are arranged in a line and that only the nearest neighbouring site interact, is applied, the protonating behaviours can be demonstrated in figure 3.13²⁶. During the protonation process, to avoid the formation of energetically unfavourable site pairs in structures with multiple charged site lining up next to each other, the 50% protonation is first achieved, that is, when the intermediate plateau in a two-step titration was observed.

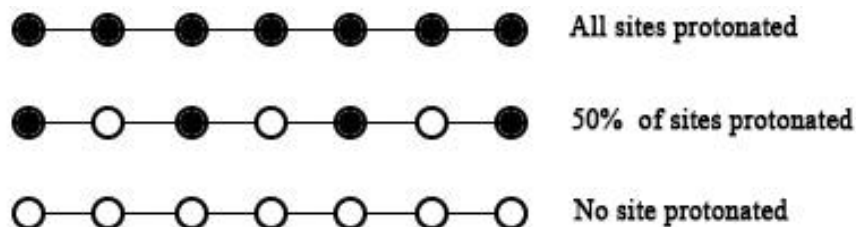


Figure 3.13 A schematic demonstration of the states of protonated sites in a polymer chain during potentiometric titrations. The black circle represents a protonated site in the structure, while the white circle represents unprotonated sites.

The 50% protonation state minimises the free energy by avoiding the nearest neighbouring site pair interactions. In the first stage of the titration, the number of the unprotonated isolated sites decreases as the pH increases. In the second step in the

titration, protons must bind to the unprotonated sites even if the neighbouring site is already protonated. Therefore, the titration curve of PDMAEA polymers appears to be a two-step titration curve with two “classes” of proton²⁷.

The pKa values of PDMAEA polymers were calculated based on the titration curve acquired from potentiometric titration. The pKa values for PL10, PL20, PS10 and PS20 were 7.8, 7.8, 7.8 and 7.5, respectively. However, as Grace et al. reported, DMAEA monomers have a pKa value of 8.4, it thus seems that the pKa values of PDMAEA have decreased compared to its monomer²⁸. The pKa values of monomers are readily measured through potentiometric titrations and are equivalent to the pH value when equal amounts of base and acid are present. However, unlike monomers, the protonation of polymers is closely related to the protonation of different sites in their structure, and can be affected by various factors, including the ionic strength of the solution, the distribution of ionisable units and the ionisation state of the neighbouring units²⁹⁻³¹. A study conducted by Borukhov et al. reported a difference between methacrylic acid (MAA) monomer and its copolymer with ethyl acrylate (P(MAA-EA))²⁹. Their work suggested that the difference might be caused by the formation of collapsed microdomains in the polymer chains due to the competition between the hydrophobic attraction and the Coulomb repulsion. Besides, it is also mentioned that the charges on the polymer chain may inhibit the dissociation of other charged groups²⁹. The electrostatic effects in solution may affect the measured pKa values as well. As Smits and his colleagues stated in their work, that the increase of salt concentration caused the pKa value of LPEI solution to shift to higher values³¹. This is explained by the increase of salt concentration which has screened the electrostatic potential of the polymer chains, resulting in a weaker repulsion of the protons in the solution from the positively charged polymer chains³¹. Their findings also supported the assumption that the distribution of ionisable units and electrostatic potential of the charged units might have an effect on the measured pKa values of polymers. Therefore, the pKa value of polymers should be reported with relevant information³². In addition, the literature has reported a wide range of pKa values between 7.1 and 8.5 for PDMAEA polymers in different studies, and the determined values in this study fit in the above range¹⁸⁻²⁰. Nevertheless, the determined pKa values of PDMAEA polymer are considered at the relatively high level, which indicates that PDMAEA polymers could be tightly bound to nucleic acids in a low pH environment. It is also reported by Sprouse et al. that the

methyl groups attached to the tertiary amine may also provide a hydrophobic character to the polymer, especially in the situation where the polymer is not protonated³³.

3.5. Conclusion

Hence, it has been demonstrated that a successful synthesis of a library of PDMAEA polymers with different molecular weight and chemical structure was achieved. ¹H NMR analyses have provided an insight into the polymers' structure, as well as the conversion rate of each polymerisation. The molecular weight and polydispersity were revealed by the application of GPC, and it has been demonstrated that the synthesized PDMAEA polymers are in the range of the desired range of molecular weight with low dispersity. Potentiometric titration has provided vital information regarding pKa values of PDMAEA polymers. The work presented in this chapter has also exhibited a simple and efficient way of synthesizing PDMAEA polymer via RAFT polymerisation.

The successful synthesis and characterisation of PDMAEA polymers is the first step in establishing a PDMAEA-based siRNA delivery system. In the next chapter, PDMAEA is condensed to dsDNA and siRNA to form stable polyplexes, followed by characterisation of these polyplexes via multiple means.

3.6. References

- 1 De Smedt, S. C., Demeester, J. & Hennink, W. E. Cationic polymer based gene delivery systems. *Pharmaceut Res* **17**, 113-126, doi:Doi 10.1023/A:1007548826495 (2000).
- 2 Pack, D. W., Hoffman, A. S., Pun, S. & Stayton, P. S. Design and development of polymers for gene delivery. *Nat Rev Drug Discov* **4**, 581-593, doi:10.1038/nrd1775 (2005).
- 3 Choosakoonkriang, S., Lobo, B. A., Koe, G. S., Koe, J. G. & Middaugh, C. R. Biophysical characterization of PEI/DNA complexes. *J Pharm Sci* **92**, 1710-1722, doi:10.1002/jps.10437 (2003).
- 4 Kichler, A. Gene transfer with modified polyethylenimines. *Journal of Gene Medicine* **6**, S3-S10, doi:10.1002/jgm.507 (2004).
- 5 Godbey, W. T., Wu, K. K. & Mikos, A. G. Poly(ethylenimine) and its role in gene delivery. *J Control Release* **60**, 149-160, doi:Doi 10.1016/S0168-3659(99)00090-5 (1999).
- 6 Boussif, O. *et al.* A Versatile Vector for Gene and Oligonucleotide Transfer into Cells in Culture and in-Vivo - Polyethylenimine. *P Natl Acad Sci USA* **92**, 7297-7301, doi:DOI 10.1073/pnas.92.16.7297 (1995).
- 7 Agarwal, S., Zhang, Y., Maji, S. & Greiner, A. PDMAEMA based gene delivery materials. *Mater Today* **15**, 388-393, doi:Doi 10.1016/S1369-7021(12)70165-7 (2012).
- 8 Georgiou, T. K. Star polymers for gene delivery. *Polym Int* **63**, 1130-1133, doi:10.1002/pi.4718 (2014).

9 Pafiti, K. S. *et al.* Cationic star polymer siRNA transfectants interconnected with a piperazine-based cationic cross-linker. *Eur Polym J* **48**, 1422-1430, doi:10.1016/j.eurpolymj.2012.05.008 (2012).

10 Yu, S. R. *et al.* Enhanced gene transfection efficiency of PDMAEMA by incorporating hydrophobic hyperbranched polymer cores: effect of degree of branching. *Polym Chem-Uk* **3**, 3324-3329, doi:10.1039/c2py20487h (2012).

11 Sun, F. X., Feng, C., Liu, H. Y. & Huang, X. Y. PHEA-g-PDMAEA well-defined graft copolymers: SET-LRP synthesis, self-catalyzed hydrolysis, and quaternization. *Polym Chem-Uk* **7**, 6973-6979, doi:10.1039/c6py01637e (2016).

12 Liu, C., Hillmyer, M. A. & Lodge, T. P. Multicompartment Micelles from pH-Responsive Miktoarm Star Block Terpolymers. *Langmuir* **25**, 13718-13725, doi:10.1021/la900845u (2009).

13 Dinari, A., Moghadam, T. T., Abdollahi, M. & Sadeghizadeh, M. Synthesis and Characterization of a Nano-Polyplex system of GNRs-PDMAEA-pDNA: An Inert Self-Catalyzed Degradable Carrier for Facile Gene Delivery. *Sci Rep-Uk* **8**, doi:ARTN 81110. 1038/s41598-018-26260-4 (2018).

14 Whitfield, R. *et al.* Well-defined PDMAEA stars via Cu(0)-mediated reversible deactivation radical polymerisation. *Abstr Pap Am Chem S* **253** (2017).

15 Truong, N. P., Jia, Z., Burges, M., McMillan, N. A. & Monteiro, M. J. Self-catalyzed degradation of linear cationic poly(2-dimethylaminoethyl acrylate) in water. *Biomacromolecules* **12**, 1876-1882, doi:10.1021/bm200219e (2011).

16 He, X. *et al.* A new strategy to prepare thermo-responsive multicompartment nanoparticles constructed with two diblock copolymers. *Polym Chem-Uk* **5**, 7090-7099, doi:10.1039/c4py01077a (2014).

17 Kitano, T., Kawaguchi, S., Ito, K. & Minakata, A. Dissociation Behavior of Poly(Fumaric Acid) and Poly(Maleic Acid) .1. Potentiometric Titration and Intrinsic-Viscosity. *Macromolecules* **20**, 1598-1606, doi:DOI 10.1021/ma00173a028 (1987).

18 Cotanda, P., Wright, D. B., Tyler, M. & O'Reilly, R. K. A comparative study of the stimuli-responsive properties of DMAEA and DMAEMA containing polymers. *J Polym Sci Pol Chem* **51**, 3333-3338, doi:10.1002/pola.26730 (2013).

19 Truong, N. P. *et al.* An influenza virus-inspired polymer system for the timed release of siRNA. *Nat Commun* **4**, doi:ARTN 1902 10.1038/ncomms2905 (2013).

20 Zhang, M. *Carbon nanomaterials for biomedical applications*. 1st edition. edn, (Springer Science+Business Media, 2015).

21 Saeed, A. O., Dey, S., Howdle, S. M., Thurecht, K. J. & Alexander, C. One-pot controlled synthesis of biodegradable and biocompatible co-polymer micelles. *J Mater Chem* **19**, 4529-4535, doi:10.1039/b821736j (2009).

22 Saeed, A. O. *et al.* Modular Construction of Multifunctional Bioresponsive Cell-Targeted Nanoparticles for Gene Delivery. *Bioconjugate Chem* **22**, 156-168, doi:10.1021/bc100149g (2011).

23 Ahmed, M. & Narain, R. Progress of RAFT based polymers in gene delivery. *Prog Polym Sci* **38**, 767-790, doi:10.1016/j.progpolymsci.2012.09.008 (2013).

24 Georgiou, T. K., Phylactou, L. A. & Patrickios, C. S. Synthesis, characterization, and evaluation as transfection reagents of ampholytic star copolymers: Effect of star architecture. *Biomacromolecules* **7**, 3505-3512, doi:10.1021/bm060657y (2006).

25 Marcus, R. A. Titration of Polyelectrolytes at Higher Ionic Strengths. *J Phys Chem-Us* **58**, 621-623, doi:DOI 10.1021/j150518a008 (1954).

26 Koper, G. J. M. & Borkovec, M. Proton binding by linear, branched, and hyperbranched polyelectrolytes. *Polymer* **51**, 5649-5662, doi:10.1016/j.polymer.2010.08.067 (2010).

27 de Groot, J., Koper, G. J. M., Borkovec, M. & de Bleijser, J. Dissociation behavior of poly(maleic acid): Potentiometric titrations, viscometry, pulsed field gradient NMR, and model calculations. *Macromolecules* **31**, 4182-4188, doi:DOI 10.1021/ma971768f (1998).

28 Grace, J. L. *et al.* Antibacterial low molecular weight cationic polymers: dissecting the contribution of hydrophobicity, chain length and charge to activity. *Rsc Adv* **6**, 15469-15477, doi:10.1039/c5ra24361k (2016).

29 Borukhov, I. *et al.* Polyelectrolyte titration: Theory and experiment. *Journal of Physical Chemistry B* **104**, 11027-11034, doi:DOI 10.1021/jp001892s (2000).

30 Lee, H. *et al.* Macroscopic lateral heterogeneity observed in a laterally mobile immiscible mixed polyelectrolyte-neutral polymer brush. *Soft Matter* **10**, 3771-3782, doi:10.1039/c4sm00022f (2014).

31 Smits, R. G., Koper, G. J. M. & Mandel, M. The Influence of Nearest-Neighbor and Next-Nearest-Neighbor Interactions on the Potentiometric Titration of Linear Poly(Ethylenimine). *J Phys Chem-US* **97**, 5745-5751, doi:DOI 10.1021/j100123a047 (1993).

32 Lee, H., Son, S. H., Sharma, R. & Won, Y. Y. A Discussion of the pH-Dependent Protonation Behaviors of Poly(2-(dimethylamino)ethyl methacrylate) (PDMAEMA) and Poly(ethylenimine-ran-2-ethyl-2-oxazoline) (P(EI-r-EOz)). *Journal of Physical Chemistry B* **115**, 844-860, doi:10.1021/jp109151s (2011).

33 Sprouse, D. & Reineke, T. M. Investigating the Effects of Block versus Statistical Glycopolycations Containing Primary and Tertiary Amines for Plasmid DNA Delivery. *Biomacromolecules* **15**, 2616-2628, doi:10.1021/bm5004527 (2014).

Chapter 4

Characterisation of PDMAEA Polymer
Solutions and PDMAEA-siRNA Polyplexes

4. Chapter 4 Characterisation of PDMAEA Polymer Solutions and PDMAEA-siRNA Polyplexes

4.1. Introduction

Polyplexes refer to a type of nanoparticle formed by electrostatic attraction between cationic polymers and anion molecules such as DNA or RNA. It is a type of nanoparticle that has been widely applied in the delivery of small molecules^{1,2}. Polyplexes showed great potential as a delivery vector for small molecules and have undergone clinical trials³⁻⁵. Synthetic polymers such as polyethylenimine (PEI), poly (dimethylaminoethyl methacrylate) (PDMAEMA) and poly (dimethylaminoethyl acrylate) (PDMAEA) have been applied in siRNA delivery. PDMAEA polymer has abundant amine groups in its structure and would be able to quickly protonate and become positively charged under a neutral and acid environment, which makes it able to condense to negatively charged ionic molecules such as siRNA. The PDMAEA can protect siRNA from nuclease degradation, and as PDMAEA polymer can be uptaken by cells via clathrin-mediated endocytosis, it also provides a route for the cellular internalisation of siRNA^{6,7}. The intracellular release of cationic polyplex was proposed to be achieved via “proton sponge” pathway⁸. Polyplexes uptaken by endosomal or lysosomes, would change the osmolarity of the organelle and eventual cause the rupture of the vesicle and release the polyplexes into the cytoplasm⁹, where siRNA are bound to RISC and trigger the degradation of target mRNA. In general, PDMAEA showed great potential as an siRNA delivery vector. To deliver siRNA, PDMAEA-siRNA polyplexes are typically prepared and administrated either systematically or locally to the patient. The extracellular interaction between cationic polyplexes and negatively charged serum proteins, and red blood cells could lead to the formation of precipitants and clusters and could provide hindrance for the systematic administration of the polyplexes. To avoid this, the PDMAEA-siRNA polyplexes prepared in this study are designed to be administrated into lesions (normally in tendon tissue or around tendon tissue) via local injection, which should reduce the probability of any undesired interaction between positively charged polyplexes with negatively charged serum proteins and red blood cells.

Some important parameters are critical to the evaluation of polyplexes. One of them is the N:P ratio, normally used to describe the molar ratio between amino groups from the polymer to the phosphate groups in siRNA, and has been reported to have an influence

on polyplex properties such as cellular uptake and endosomal activity⁹. It is reported that in polyplexes designed for the siRNA delivery, an excessive amount of polymer content is critical to the formation of stable polyplex, due to the low ionic charge centre provided by small RNA molecules^{10,11}. However, polyplexes with high N:P ratio or high overall net surface charge might induce extracellular and intracellular interaction with ionic large molecules such as serum protein or might cause cellular membrane disruption which is associated with cytotoxicity¹². Therefore, special attention should be paid to the monitoring of the overall surface charge and N:P ratio. The formation of PDMAEA-siRNA is based on the charge-mediated interactions between cationic polymer materials and nucleic acids, the successful formation could be determined by using agarose gel electrophoresis by comparing polyplex sample with free DNA, as Truong et al. reported¹³.

It is reported that the size and surface charge of nanoparticles would greatly affect their uptake rate by the target cell¹⁷, special attention should be paid to the hydrodynamic diameter of the polyplexes. Another important parameter that should be determined is the zeta potential. For charged particles dispersed in solutions, zeta potential is the electric potential in the interfacial double layer of dispersed particle versus a point in the continuous phase away from the interface (figure 4.1)¹⁴. It is the potential difference between the stern layer, which is the internal layer of the electric double layer formed at the surface of the particle, and the slipping plane, which is the boundary between the mobile fluid and fluid that remains attached to the surface¹⁴. Zeta potential is a measure of surface charge and reflects colloidal stability¹⁵.

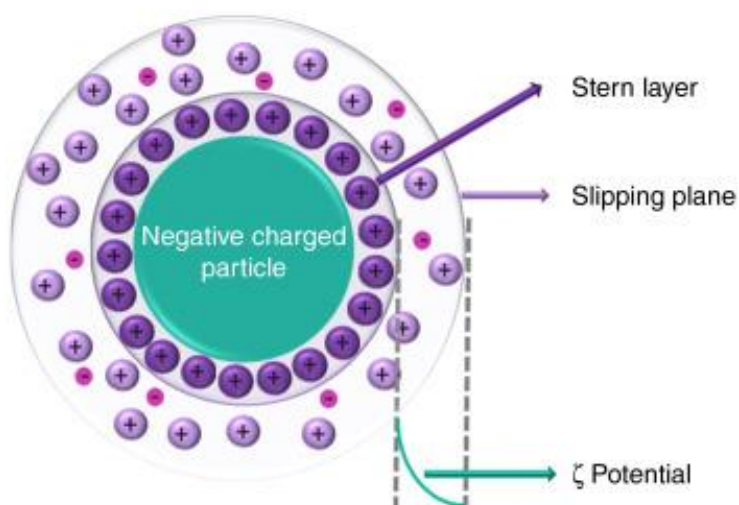


Figure 4.1 A schematic illustration of the electric double layer of a charged particle in solution. Figure adapted from Grumezescu¹⁴.

The stability of colloids in suspension can be explained by DLVO theory, which is developed by Derjaguin, Verwey, Landau, and Overbeek in the 1940s¹⁶. The DLVO theory suggests that the stability of a dispersion of colloids depends on the total interaction potential energy V_T :

$$V_T = V_A + V_R + V_S$$

Where V_A is the attractive energy from van der Waals force, V_R is the repulsive force from the electrical double layer of charged particles and V_S is the potential energy from the solvent. V_S contributes little compared to V_A and V_R for nanometer-scale separation of the particles and is negligible. Van der Waals force is a distance-dependent interaction between atoms or molecules, and V_A is affected only by the distance between particles and is insensitive to the ionic strength and pH of the solution. While Pan et al. suggested that V_R can be expressed as follows¹⁷:

$$V_R = 2\pi\epsilon a\zeta^2 e^{-\kappa D} \quad (4.1)$$

Where ϵ is the dielectric constant, π is the solvent permeability, a is the radius of the particle, D is the distance between the particles, κ is the ionic strength, and ζ is the zeta potential. As both V_A and V_R are related to the distance between particles, the interaction energy variation with the separation between the particles can be described as in figure 4.2. When the sum of the repulsion forces overcomes the attraction forces, the colloidal system is considered stable¹⁸.

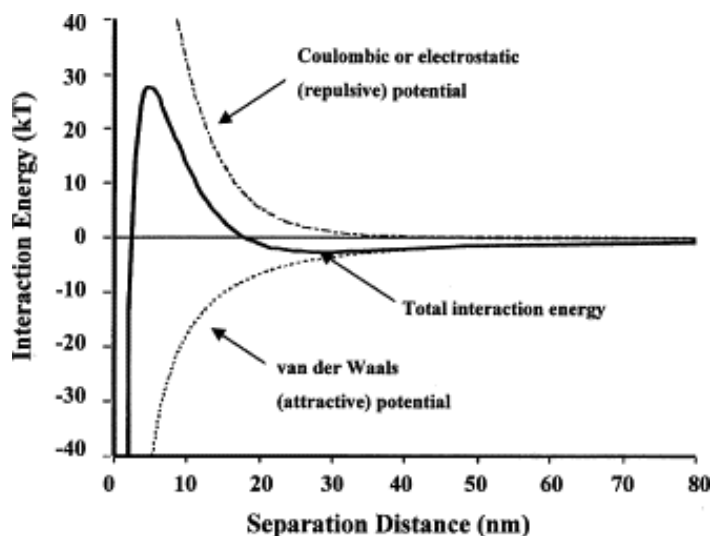


Figure 4.2 The interaction energy in relationship to particles separation distance. Figure adapted from Buschow et al.¹⁶.

Equation 4.1 indicates that the zeta potential contributes to the repulsion force between particles, and the larger the zeta potential is, the greater the repulsive force is. Particles with high zeta potential are electrically stable while particles with low zeta potentials tend to congregate or flocculate¹⁵.

Losso et al. reported that phosphatidylcholine-stabilized emulsions with zeta potential values of -41 to -50 mV had good stability¹⁹. Some other studies also suggested that various particles with zeta potential from 10 mV to 60 mV achieved good stability^{20,21}. It is suggested that a high positive or negative zeta potential greater than 30 mV may lead to good stability, and zeta potential of lower than 5 mV are likely to produce aggregation¹⁴. To conclude, it is necessary to determine the hydrodynamic diameter and surface charge at different pHs and different N:P ratio of PDMAEA polymers and their polyplexes.

The aim of the chapter:

In this chapter, the formation of PDMAEA polymers with dsDNA and siRNA into according polyplexes was described and discussed. Firstly, the dsDNA was used as a model molecule to study the formulation of PDMAEA polyplexes. PDMAEA-dsDNA polyplexes were prepared at different N:P ratio, and the successful formation of PDMAEA polyplexes was confirmed by using agarose gel electrophoresis comparing to free dsDNA. The critical polyplex formation N:P ratios were also determined by electrophoresis for each PDMAEA polymers. The hydrodynamic diameter and zeta potential of all PDMAEA polymer solutions and its polyplexes with dsDNA were obtained by using dynamic light scattering. PS10 is selected as to condense with *COL3a1* specific siRNA to form PS10-siRNA polyplex at N:P ratio of 10:1. The formation was confirmed by agarose gel electrophoresis, and the hydrodynamic diameter and zeta potential were determined by DLS. Eventually, the influence of molar mass and structure on polymer binding capability is discussed.

The main objectives:

The aim of this chapter is to study the formation of PDMAEA polyplexes and prepare PS10-siRNA polyplexes for the transfection of equine tenocyte and silencing the *COL3a1* gene. To achieve this goal, the following objectives were accomplished:

- Determine the hydrodynamic diameter and zeta potential of PDMAEA polymer solutions.
- Study the formulation of PDMAEA (PL10, PS10, PL20, PS20) polyplexes using dsDNA as a model cargo molecule and confirm polyplexes formation by agarose gel electrophoresis.
- Test the PDMAEA polyplexes for their hydrodynamic diameter and zeta potential.
- Prepare and characterise PS10-siRNA polyplex for the transfection of equine tenocyte and silencing the *COL3α1* gene.

4.2. Materials and Methods

4.2.1. Materials

The details of the materials used in this chapter can be found in chapter two section 2.2.

4.2.2. Characterisation of PDMAEA Polymers by DLS

Thirty milligrams of polymers (PS10, PS20, PL10 and PL20) were dissolved in 30 mL of HEPES Buffer (10 mM, pH 7.4) to a final concentration of 1 mg/mL respectively. Each polymer solution was divided into six aliquots in vials with a volume of 4 mL. The pH of six aliquots of polymers solution was adjusted to 6.0, 6.5, 7.0, 7.5, 8.0, and 8.5 using 1M HCl and NaOH, respectively. All the samples were left at 4°C overnight. The supernatant of all samples was taken for DLS and zeta potential measurement. The samples were analysed with a Malvern Nanosizer with Folded Capillary Cells DTS1060 (Malvern Instruments), and the data were recorded. All measurements were carried out in triplicate.

The hydrodynamic diameter of the PDMAEA polymers was measured in disposable plastic cuvette as a function of pH, and 15 sub runs were performed for each sample. The data was analysed using the Malvern analysis software. All the samples were made and measured in triplicates.

4.2.3. The Preparation of PDMAEA Polyplexes

The dsDNA stock solution was prepared in 1X Tris-acetate-EDTA (TAE) buffer. Briefly, a stock solution of 1 mg/mL solution was prepared by adding 10 mg of dsDNA in 10 mL of 1X TAE buffer (40 mM Tris-base, 2 mM acetic acid and 1 mM EDTA) and pH adjusted to 7.4. PDMAEA stock solutions were prepared by dissolving 10 mg of PDMAEA polymers (PS10, PS20, PL10 and PL20) in 10 mL of HEPES buffer (10 mM, pH at 7.4) to make a stock solution of polymers at the concentration of 1 mg/mL.

The calculation of N:P ratios was adapted and modified based on literature ⁹. Typically, for 25 μ L of the stock DNA solution (total DNA mass would be 25 μ g), the required volume and concentration of the polymer solution is shown in table 4.1.

Table 4.1 Preparation of PDMAEA polyplexes.

Charge ratio (N:P)	1	3	5	7	9	10	15
Polymer stock(μ L)	10.74	32.22	53.69	75.17	96.65	107.39	161.08
HEPES solution (10 mM)	239.26	217.78	196.31	174.83	153.35	142.62	88.92
concentration(μ g/mL)	42.95	128.86	214.77	300.67	386.58	429.54	644.31

For the preparation of polyplexes, 25 μ L of dsDNA solution was added into 250 μ L of polymer solution with different concentration based on N:P ratios. The polyplex mixture was vortexed for ten seconds before being incubated at room temperature for 30 minutes.

PS10 PDMAEA polyplexes were selected as the final candidate to condense with *COL3a1* gene-specific siRNA considering its good binding ability and low cytotoxicity. The formulation of PS10-siRNA polyplexes is described as follows: The siRNA (10 nmol) were resuspended in 100 μ L of 30 mM HEPES buffer to prepare a stock solution of 100 pmol/ μ L. Solution of 1 nmol of siRNA (13.2 μ g in 10 μ L) was diluted to 100 μ L in 30 mM HEPES buffer. The siRNA solution was added to 100 μ L of calculated PS10 PDMAEA polymer solution (N:P ratio at 10, concentration 6mg/ml) and topped up to 1 mL, resulting in a final siRNA concentration of 13.2 μ g/mL and a final polymer concentration of 0.6 mg/mL. The mixture was vortexed for ten seconds in a 1.5 mL microcentrifuge tube and incubated at room temperature for 30 minutes.

4.2.4. Agarose gel electrophoresis of PDMAEA (PL10, PL20, PS10, PS20)-dsDNA polyplexes

Agarose (0.6 g) was suspended in 60 ml of 1X TEA buffer to reach 1% final concentration. The agarose was heated in a microwave oven till molten. Afterwards, 5 μ L of GELRED DNA stain was added and mixed into the molten gel, and then the gel was cooled down to 50~60°C before casting. Ten microlitres of the polyplexes were loaded into each well, and the electrophoresis was performed at 80 V for 40 minutes. The gel was then visualized in GELDOC (BIO-RAD) and the data collected and analysed using the software provided.

4.2.5. Characterisation of PDMEA (PL10, PL20, PS10, PS20)-dsDNA polyplex by dynamic light scattering

Polyplex solution was adjusted to pH 7.4 using 1 M NaOH or 1 M HCl. All the samples were left at 4°C overnight. The supernatant of all samples was taken for DLS and zeta potential measurement. The sample zeta potential was measured by using a Malvern Zetasizer ZS in a DT1070 zeta cell. Data were recorded and analysed using Zetasizer Software. The hydrodynamic diameter of the polyplexes was measured in cuvettes with 15 sub runs for each sample and the data averaged using the Malvern analysis software. All the samples were made and measured in triplicate.

4.2.6. Characterisation of PS10-siRNA polyplex by DLS and electrophoresis

PS10-siRNA polyplex was adjusted to pH 5.4, 6.4 and 7.4 using 1 M NaOH or 1 M HCl. Samples were left at 4°C overnight before the supernatant was taken for DLS and zeta potential measurement. The sample zeta potential was measured by using a Malvern Zetasizer ZS in a DT1070 zeta cell. Data were recorded and analysed using Zetasizer Software. The hydrodynamic diameter of the polyplexes was measured in cuvettes with 15 sub runs for each sample and the data were analysed using the Malvern analysis software. All the samples were made and measured in triplicate.

1.5 g of agarose was suspended in 100ml of 1X TEA buffer to reach a final concentration of 1.5% and then heated in a microwave oven till molten. The molten gel was cooled down to 50~60°C before casting with the comb placed at the edge of the tray and left at room temperature in the dark. Ten microlitres of the polyplexes were

loaded into the well, and the electrophoresis was performed at 80 V for 40 minutes. To stain the siRNA, the gel was then immersed in 400 mL of 0.006% ethidium bromide for one hour before visualizing. The gel was then visualized in a ChemiDoc-It®2 810 imager (U.V.P, USA) and the data were collected and analysed using the software provided.

4.3. Results

4.3.1. The Hydrodynamic Diameter of PDMAEA Polymers

Typically, two different size analysis techniques, namely, cumulants analysis and distribution analysis, were used to analyse the correlation function. The cumulants analysis normally gives a mean particle size (z-average) and an estimate of the width of the distribution (polydispersity index, or PDI) and is ideal only when a single size population is present in sample solutions. One disadvantage of cumulants analysis is that it only describes the average size value, along with the PDI of a single population, and it becomes less descriptive as the sample type moves further away from monomodal. In an unknown sample with possible multiple size populations the cumulants analysis may become less accurate. The second approach, distribution analysis, is a mathematical analysis of the correlation function which can describe the size distribution in a sample solution. The distribution analysis becomes useful when the number of populations, the relative composition of these populations and the presence of a large/small population needs to be determined. The distribution analysis typically generates three types of size distribution, that is the size distribution by intensity, volume and number. The size distribution by intensity is the primary result generated based upon the intensity of light scattered by particles, and it is sensitive to the presence of large particles, aggregates, or contaminants (such as dust). The size distribution by volume and number are derived from the intensity distribution using Mie theory and are used for estimating the relative amounts of material in separate peaks.

The hydrodynamic diameter of PDMAEA polymers in solution was measured at different pHs (from 6.0 to 8.5), and the size distribution (intensity and volume) and the correlation curves are shown in figure 4.3 – 4.6. The data collected in this study indicate that there are multiple size populations present in the sample solutions, though only one size population is predominant. Data also suggest that cumulant analysis is not the most

suitable method for the analysis of the obtained data due to the high cumulant fit error. Therefore, a combination of intensity size distribution and number distribution is used to analyse the collected data.

Figure 4.3 demonstrates the intensity and volume size distribution of PL10 in solutions with a pH from 6.0 to 8.5. The intensity distribution data indicate that there are three size populations (≤ 10 nm, ~ 100 nm and ≥ 500 nm) in sample solutions at pH 6.0 - 8.0, though only the smallest size population (≤ 10 nm) is the major one. The intensity and volume size distribution data of PL10 in solution at pH 8.5 showed only two size groups, one is ~ 40 nm and the other is ~ 500 nm, and volume distribution suggests that the size group of ~ 40 nm is predominant. Combining these results, it is indicated that the majority of PL10 polymers possibly exist in the form of small particles with sizes of below 10 nm in solutions with pH from 6.0 - 8.0, while in a solution with pH 8.5 the polymers exist in the form of small particles with sizes of ~ 40 nm. The mean size based on intensity and volume distribution data of PL10 polymers in solutions from pH 6.0 - 8.5 are summarised in table 4.2. The possible structure of PL10 polymers is explained and discussed in section 4.4.

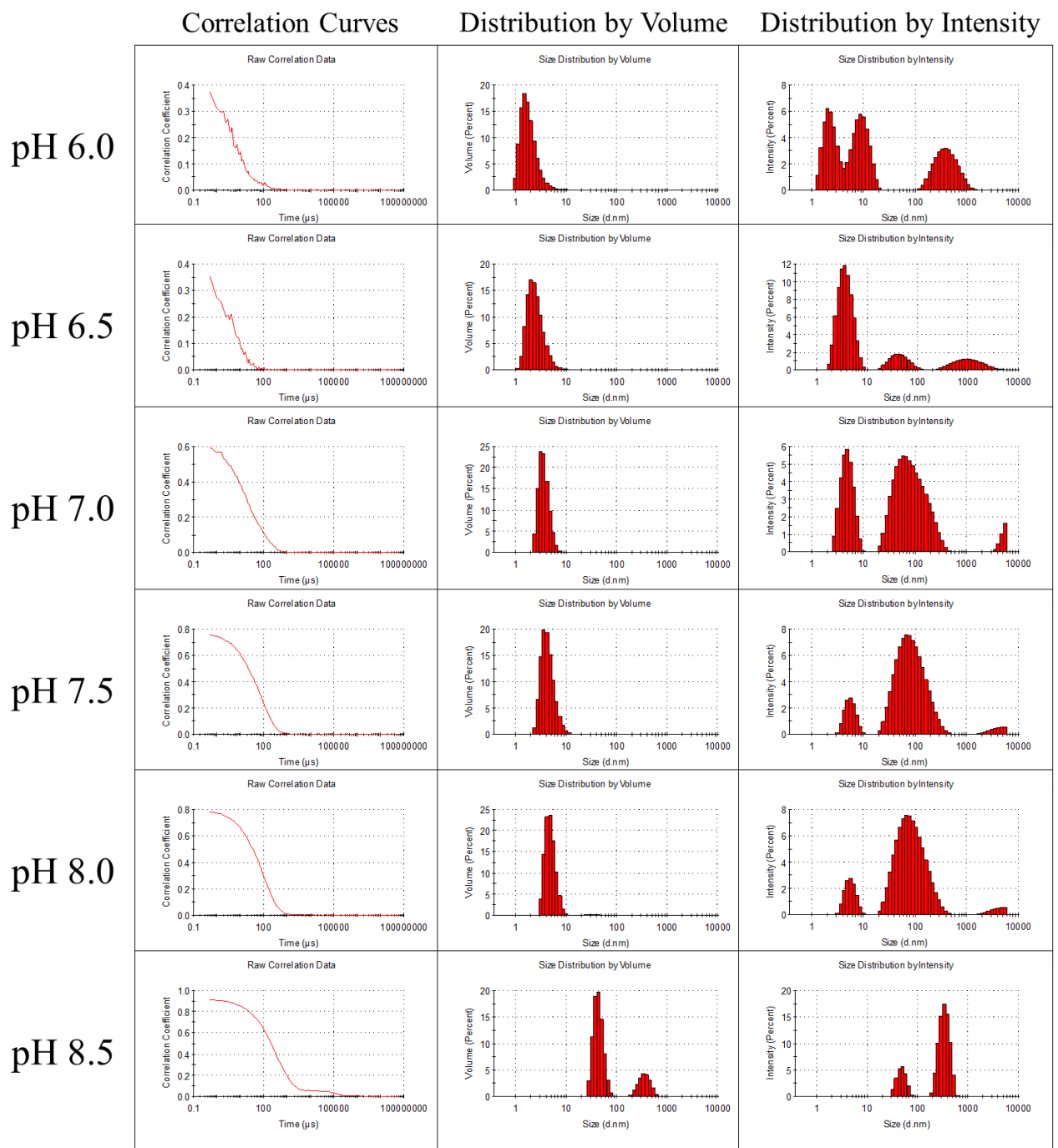


Figure 4.3 The correlation curves, intensity distribution and volume distribution of PL10 polymer in solutions with pHs from 6.0 to 8.5.

Table 4.2 Size distribution of PL10 polymers in solutions with pHs from 6.0 to 8.5. Size reported as mean value \pm SD(N=3).

pH	PL10	
	Intensity	Volume
6	4 \pm 1	2 \pm 1
6.5	4 \pm 1	3 \pm 1
7	5 \pm 1.	4 \pm 1
7.5	5 \pm 1	4 \pm 1
8	7 \pm 2	4 \pm 1
8.5	48 \pm 4	42 \pm 5

The correlation curves and size distribution of PS10 in pH 6.0 – 8.5 solutions are shown in figure 4.4. The intensity size distribution data indicate that at pH 6.0, 7.0, 8.0 and 8.5, three size populations were recorded in PS10 solutions, while only two size groups were observed at pH 6.5 and 7.5. The volume size distribution data suggest that through multiple size groups were recorded, only one size group at each pH is predominant, and it is the size group \leq 10 nm for pH 6.0 - 8.0 and \sim 40 nm size group for pH 8.5. These data suggest that PS10 showed a similar behaviour to PL10, possibly existing in the form of small particles with sizes of below 10 nm in solutions with pH from 6.0 - 8.0, while in a pH 8.5 solution the polymers exist in the form of particles with sizes of \sim 40 nm.

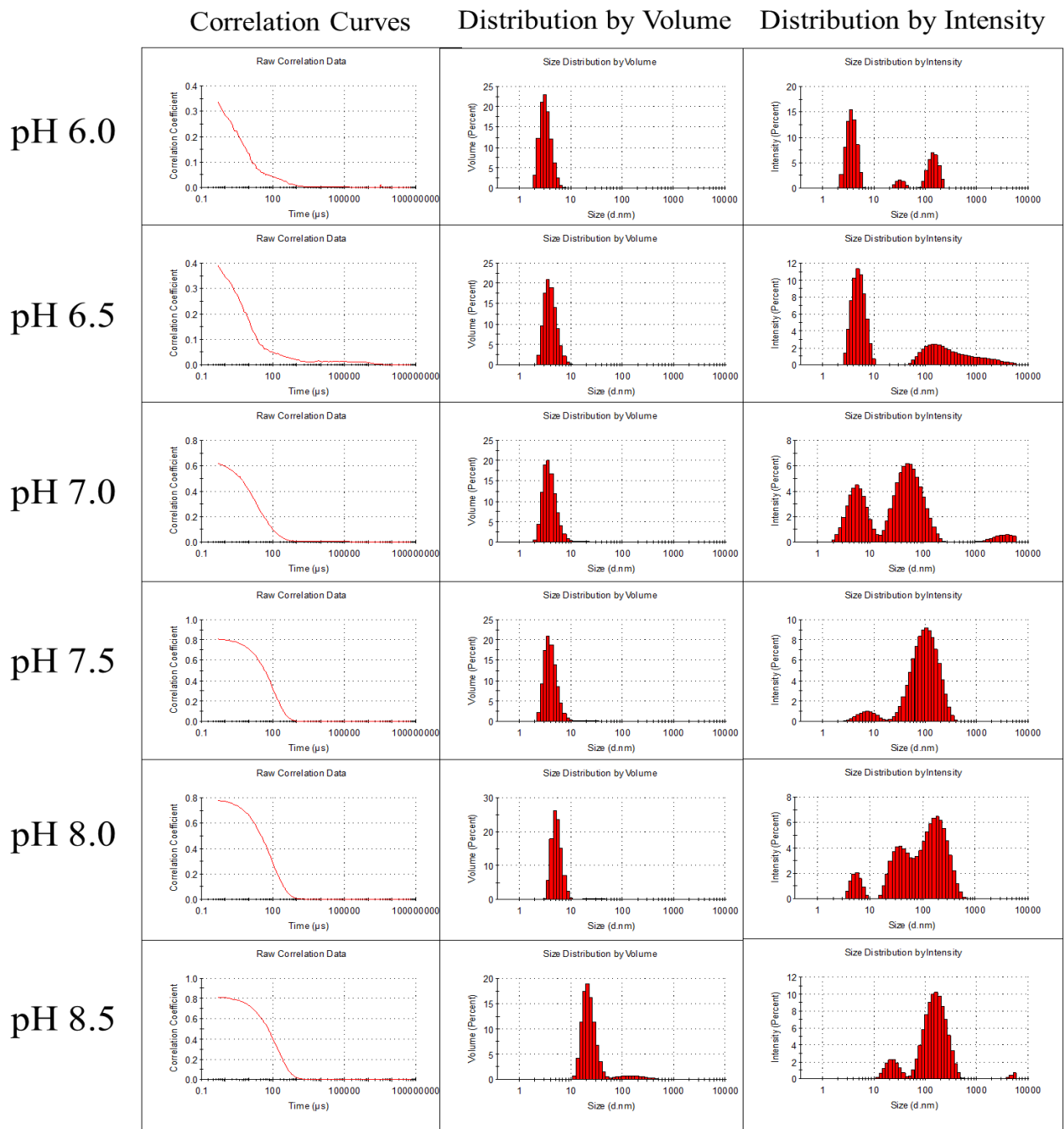


Figure 4.4 The correlation curves, intensity size distribution and volume distribution of PS10 polymer in pH 6.0 – 8.5 solutions.

The mean size base PS10 polymers in solutions from pH 6.0 - 8.5 are summarised in table 4.3.

Table 4.3 Size distribution of PL10 polymers in solutions from pH 6.0-8.5. Size reported as mean value \pm SD(N=3).

pH	PS10	
	Intensity	Volume
6	4 \pm 1	3 \pm 1
6.5	5 \pm 1	4 \pm 0
7	5 \pm 1	4 \pm 1
7.5	5 \pm 2	4 \pm 1
8	7 \pm 1	5 \pm 0
8.5	20 \pm 9	24 \pm 6

The size distribution and correlation curves of PL20 and PS20 in pH 6.0 - 8.5 solutions are presented in figure 4.5 and 4.6, respectively. The intensity distribution data suggest that in both PL20 and PS20 solutions, multiple size populations were observed in all pHs, though volume distribution data confirmed only one size group is predominant. For both PL20 and PS20, the majority of the polymers may exist in forms of particles with sizes below 10 nm at pH 6.0 – 7.5. However, the size increased dramatically to \sim 100 nm at pH 8.0 and 8.5 for both PL20 and PS20. The mean size values are reported in table 4.4.

Table 4.4 Size distribution of PL20 and PS20 polymers in solutions from pH 6.0-8.5. Size reported as mean value \pm SD(N=3).

pH	PL20		PS20	
	Intensity	Volume	Intensity	Volume
6	5 \pm 1	4 \pm 1	6 \pm 1	4 \pm 1
6.5	5 \pm 1	4 \pm 1	5 \pm 1	5 \pm 1
7	7 \pm 1	4 \pm 1	6 \pm 1	4 \pm 1
7.5	8 \pm 0	5 \pm 1	8 \pm 1	4 \pm 1
8	23 \pm 4	83 \pm 13	25 \pm 7	28 \pm 3
8.5	91 \pm 3	78 \pm 8	79 \pm 22	87 \pm 9

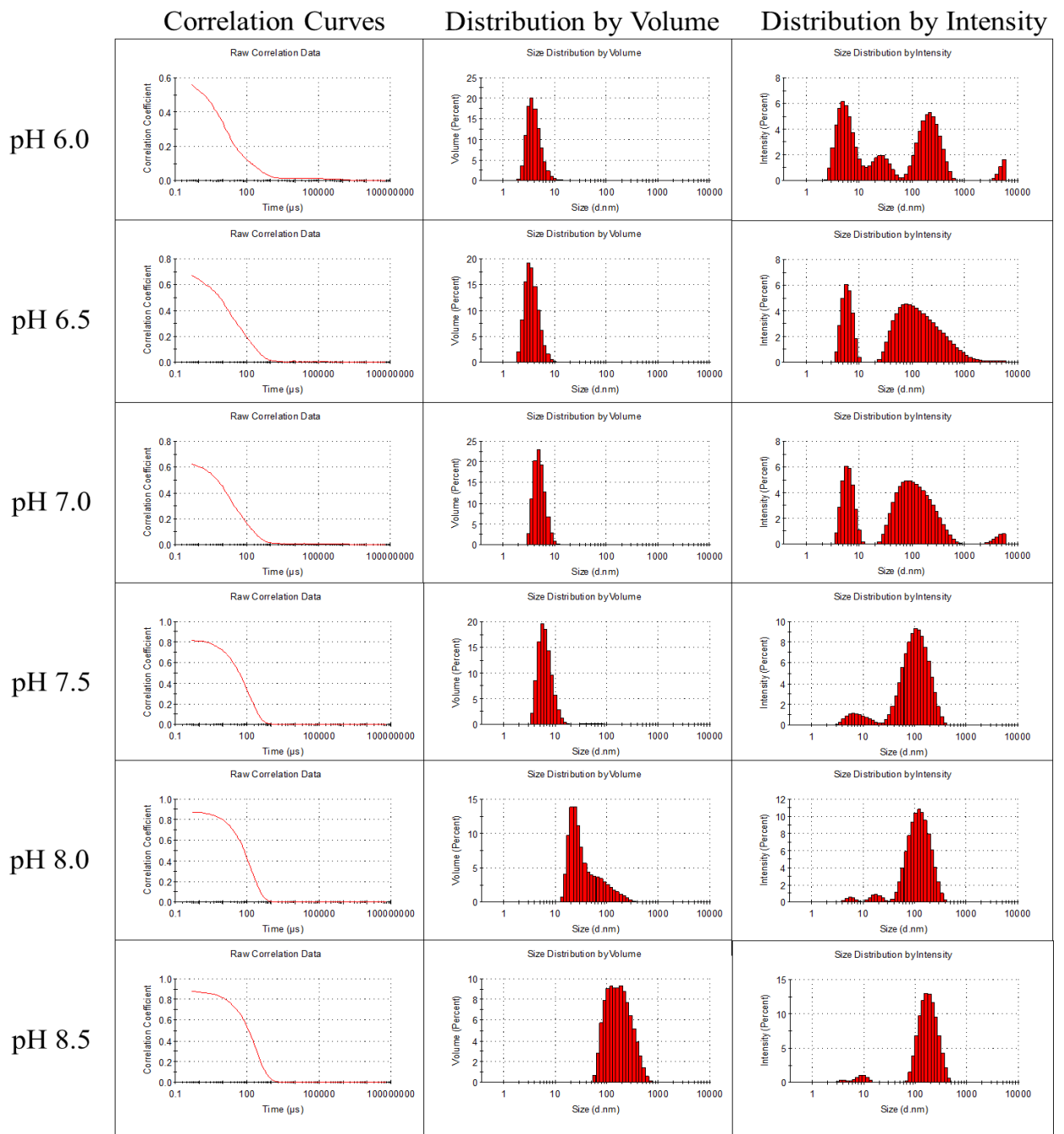


Figure 4.5 The correlation curves, intensity size distribution and volume distribution of PL20 polymer in pH 6.0 – 8.5 solutions.

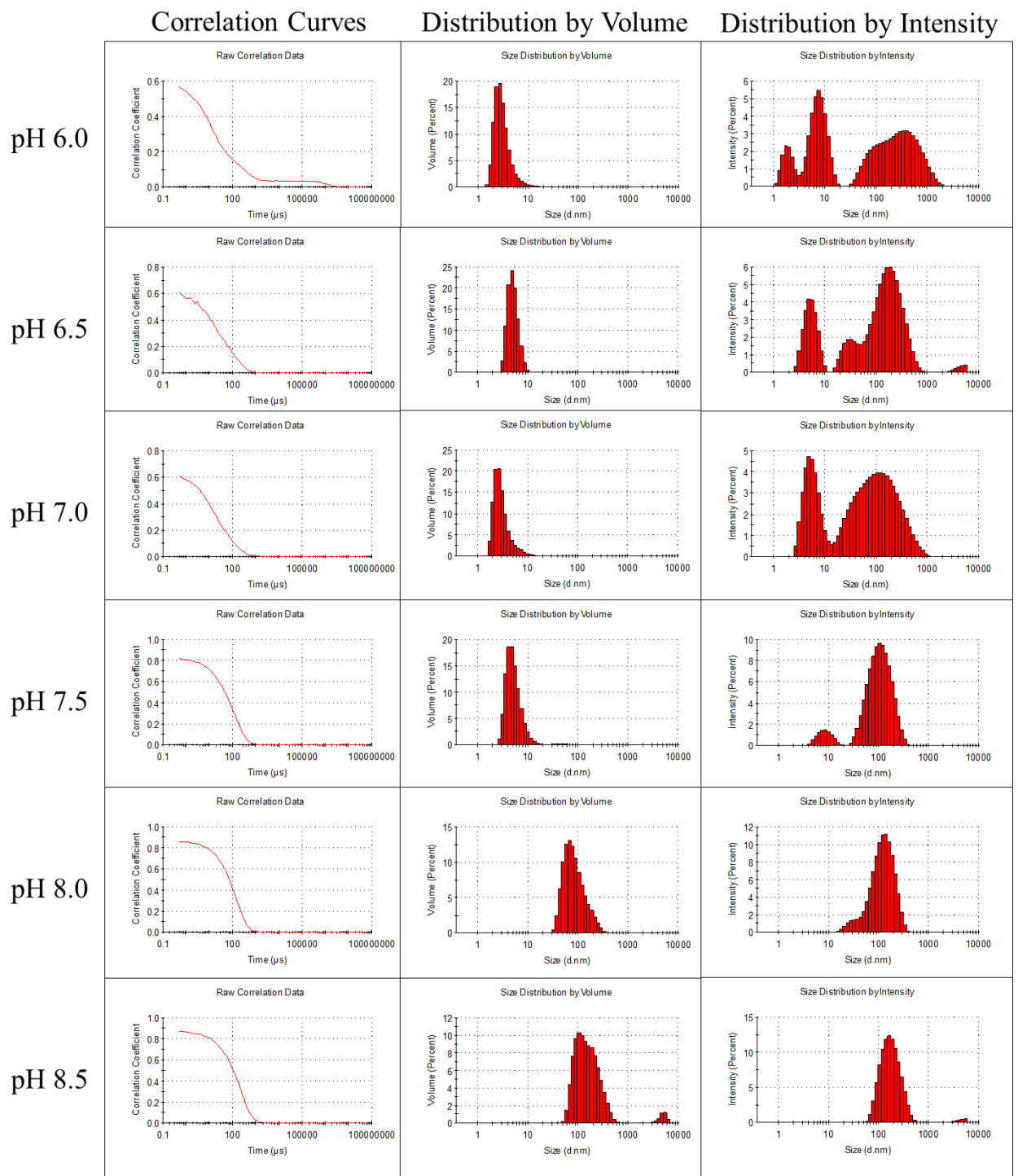


Figure 4.6 The correlation curves, intensity size distribution and volume distribution of PS20 polymer in pH 6.0 – 8.5 solutions.

To compare the difference of hydrodynamic diameter of PDMAEA polymer in solutions at different pHs, the mean size by volume distribution of all four polymers are plotted against pH and are presented in figure 4.7. Statistical analysis (t-test) has been performed between sizes at each pH to determine whether the difference between pHs in each polymer sample groups was significant.

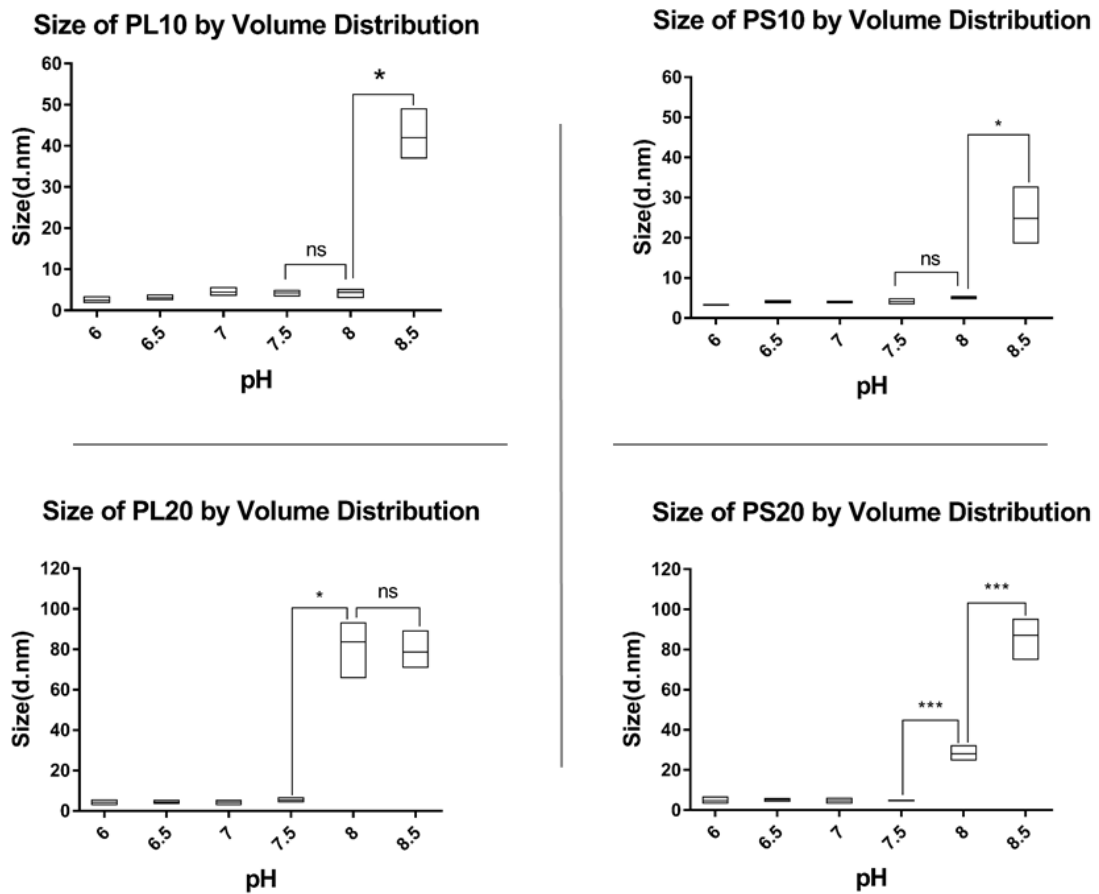


Figure 4.7 Statistical analysis within the group to determine the variation between sizes at each pH (ns: $p>0.05$, *: $0.05>p>0.01$, **: $0.01>p>0.005$, *: $0.005>p>0.001$, ****: $0.001>p$). The data represent the mean values \pm SD ($N=3$).**

The results suggest, for PL10 solutions, sizes at pH 8.0 are much smaller than those at pH 8.5. Similar results were observed in the PS10 sample solution where sizes at pH 8.5 are significantly larger than those at pH 8.0. For PL20 solutions, a significant difference in size was observed between pH 7.5 and 8.0, while PS20 solutions at pH 7.5, 8.0 and 8.5 showed significant differences between one another and the size increases as the pH goes up.

To determine whether the effect of pH on particle hydrodynamic diameter is influenced by polymer types, paired two-way ANOVA was used to analyse the data and the results are presented in figure 4.8. The two-way ANOVA compares the mean differences between groups that have been split on two independent variables (pH and polymer type). Statistical analysis indicates that there are no significant differences between each group. The results indicate that there are no significant variations among four types of PDMAEA polymer sample groups at different pHs.

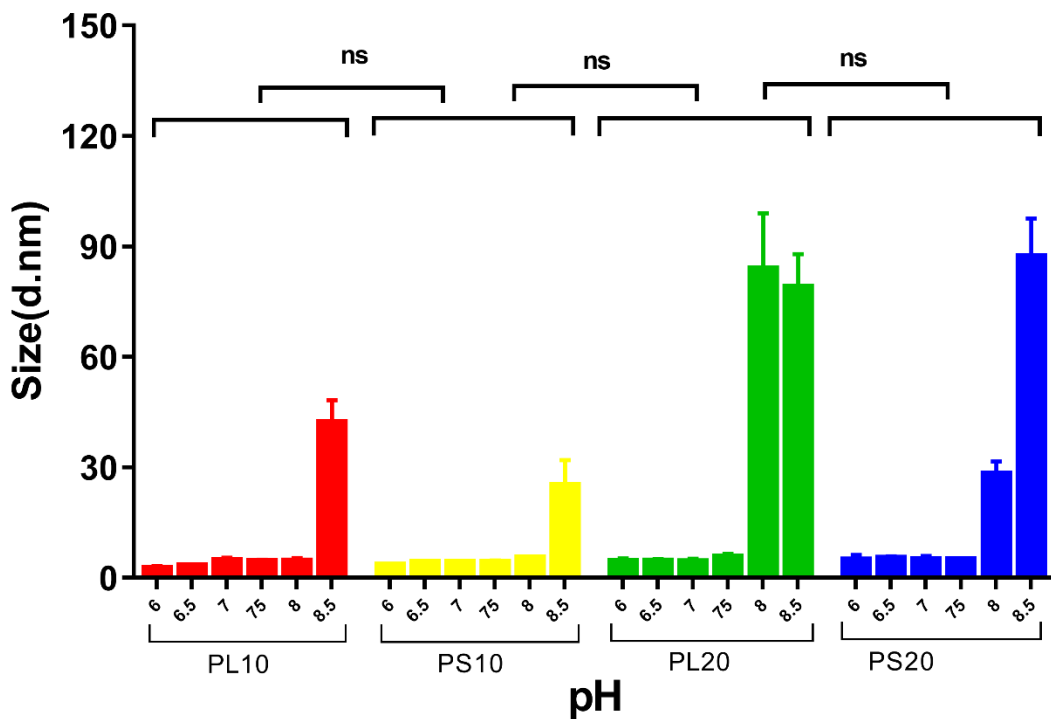


Figure 4.8 Statistical analysis between PS10, PS20, PL10 and PL20 polymers(ns:p>0.05, *:0.05>p>0.01, **:0.01>p>0.005, *: 0.005>p>0.001, ****: 0.001>p). The data represent mean values \pm SD (N=3).**

To conclude, all four PDMAEA polymers may exist in the form of particles with sizes below 10 nm at pH 7.5 and below. However, the analysis indicated that the particles sizes increased dramatically at pH 8.5 (for PL10 and PS10) and at pH 8.0 (for PL20 and PS20). The results also showed that there are no significant differences between the particle sizes of PL10, PS10, PL20 and PS20 polymer solutions at different pHs. The possible structure of PDMAEA particles in solution and the cause of the increase in their sizes at high pHs will be discussed in detail in section 4.4.

4.3.2. The Zeta Potential of PDMAEA Polymers

The zeta potential of PL10, PS10, PL20 and PS20 in solutions with pHs ranging from 6.0 – 8.5 are reported in figure 4.9. Analysis reveals the relationship between pH and zeta potential of polymer samples as follows: as the pH increases from 6.0 to 8.5, the zeta potential of all PDMAEA polymer solution decreases from above 40 mV to below 0 mV. This is possibly due to the reduction in the percentage of protonated amine groups as the pH increases, and the further triggering of polymers aggregation.

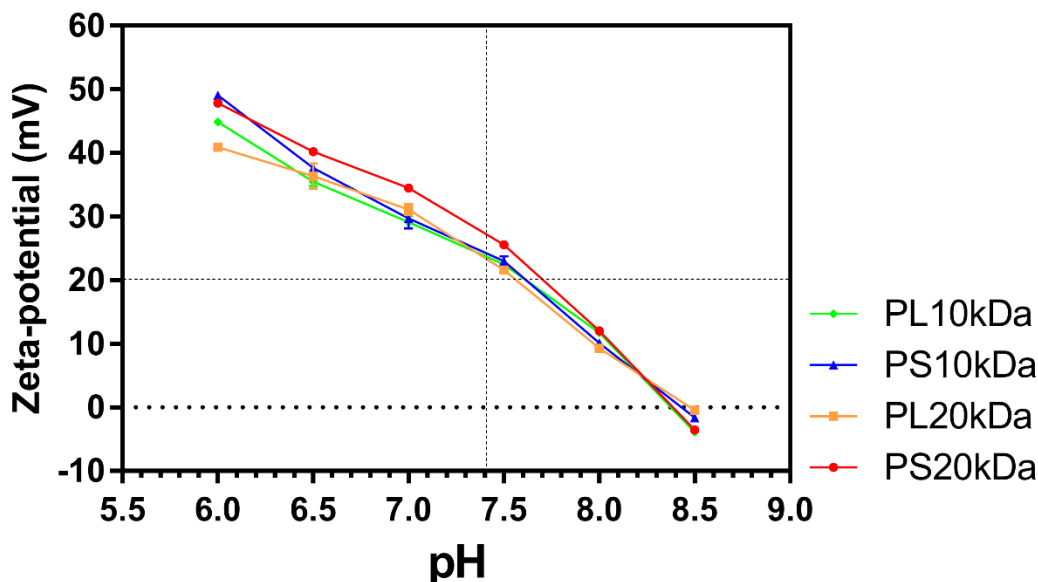


Figure 4.9 Zeta potential of four PDMAEA polymer solutions under different pH conditions. The data represent the mean values \pm SD (N=3).

Another fact observed was that at pH 7.4, all polymer samples retained a positive charge of above 20 mV, which suggests that the polymer solutions are colloidal stable at pH 7.4 and below.

4.3.3. Confirmation of PDMAEA (PL10, PL20, PS10, PS20)-dsDNA Polyplexes Formation by Electrophoresis.

Four different PDMAEA-dsDNA polyplexes were prepared with N:P ratios from 1 to 15 and were characterised with agarose gel electrophoresis and dynamic light scattering, and free DNA was used as -ve control to indicate whether the DNA was completely condensed to polymers. The dsDNA used in this experiment is low molecular weight DNA from salmon sperm (\sim 185 bp). The aim of this experiment is to determine the minimal N:P ratio required to completely condense to dsDNA for different PDMAEA polymers, and the molecular weight of the dsDNA used in this study is known to be \sim 185 bp; therefore no DNA ladder was employed in this experiment. The polyplexes were first characterised by electrophoresis to confirm successful polyplex formation. Data from agarose gel electrophoresis are presented in figure 4.10. The results indicated that for different polymers, the required N:P ratio to form polyplexes are variable. The PS10 formed polyplexes at an N:P ratio of 5:1 while PL10 polymer formed polyplexes at an N:P ratio of 7:1. A polymer with a larger molecular weight such as PS20 formed polyplexes at an N:P ratio of 3:1, while PL20 formed polyplexes at an N:P ratio of 5:1.

The missing DNA band at the bottom of the gel was a clear indicator for polyplex formation, compared to the bright band from free dsDNA control lane.

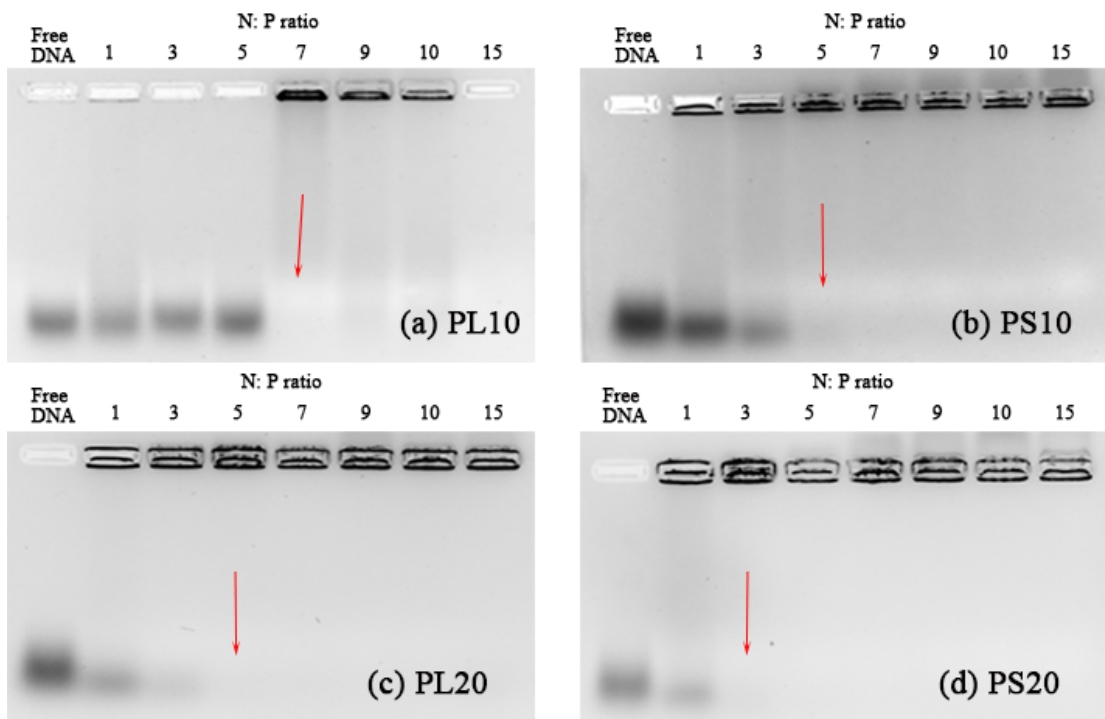


Figure 4.10 Agarose gel (1%) electrophoresis analysis of PDMAEA-dsDNA polyplexes. Low molecular weight dsDNA (~185 bp) from salmon sperm was used to form polyplexes with PDMAEA polymers. Red arrows indicate no DNA band was observed at corresponding N:P ratio. a) PS10kDa (star-shaped) b) PL10kDa, c) PS20kDa (star-shaped), and d) PL20kDa. The figure colour was reversed to better demonstrate the result.

Another underlying concept demonstrated by this result is that for PDMAEAs of different structures and molecular weights, the minimum required N:P ratio to form polyplex is different. While comparing linear and star-shaped PDMAEA, it is evident that star-shaped polymers require a lower N:P ratio to form polyplexes. For polymers of the same structure, the ones with larger molar masses require a low N:P ratio for the formation of polyplexes.

4.3.4. Hydrodynamic Diameter and Zeta Potential of PDMAEA (PL10, PL20, PS10, PS20)-dsDNA Polyplexes

The hydrodynamic diameter and zeta potential of PDMAEA-dsDNA polyplexes at pH 7.4 were determined by DLS. The correlation curves and size distribution were demonstrated in figure 4.11.

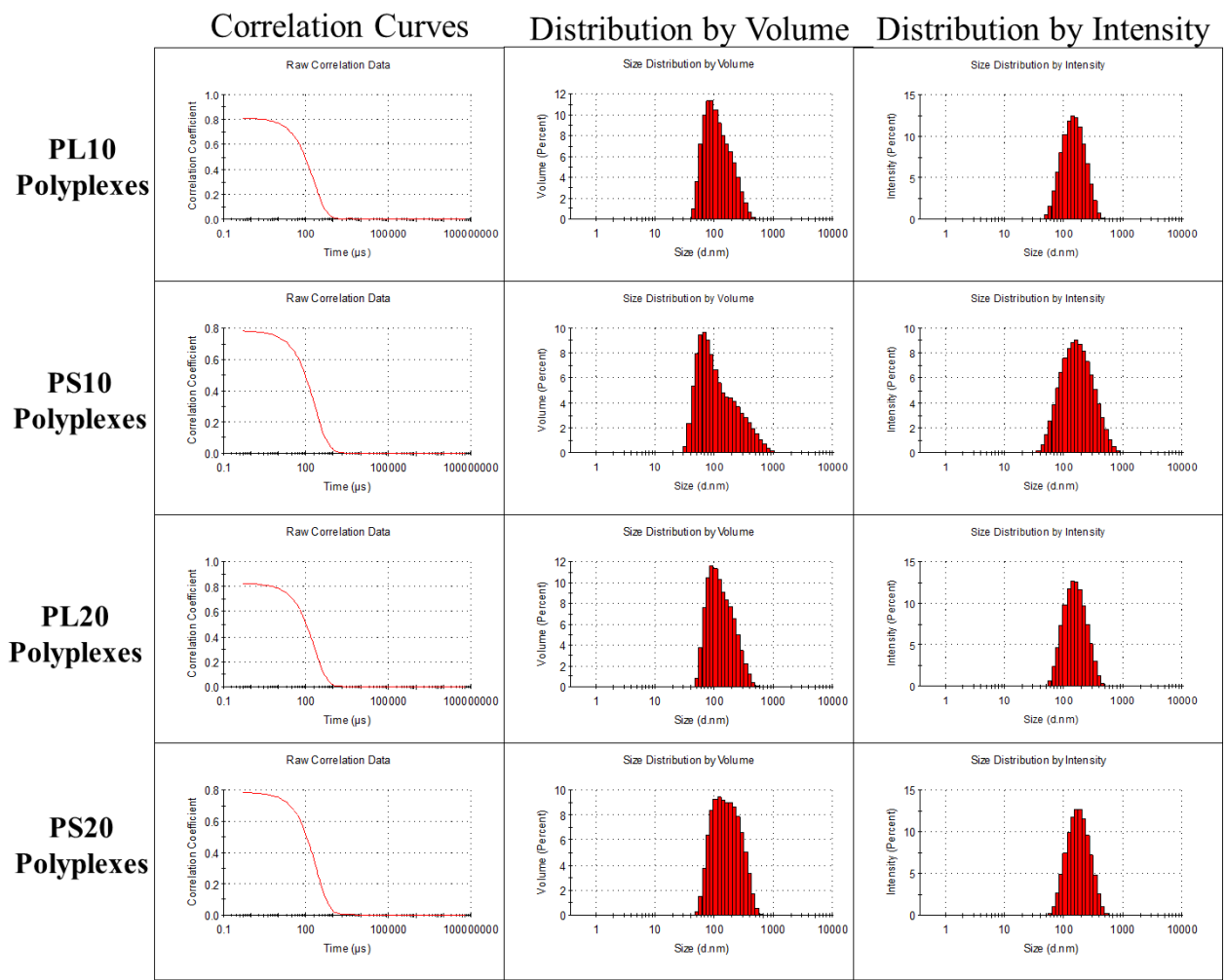


Figure 4.11 The correlation curves, intensity size distribution and volume distribution of PL10, PS10, PL20, PS20 polyplexes with dsDNA pH 7.4.

Intensity distribution data indicate that at pH 7.4, one particle size class was present in each sample solution. Combining the volume and intensity distribution data, it is suggested that PDMAEA (PL10, PS10, PL20, PS20)-dsDNA polyplexes possibly exist in the form of particles with a hydrodynamic diameter of ~150 nm. The mean size value \pm SD of four different PDMAEA-dsDNA polyplexes at pH 7.4 are summarised in table 4.5.

Table 4.5 Mean size values \pm SD (N=3) by intensity and volume distribution analysis of four PDMAEA-dsDNA polyplexes at pH 7.4.

Polyplex	N/P	D_H (Intensity mean \pm SD)/nm	D_H (Volume mean \pm SD)/nm
dsDNA-PL10	10:1	158 ± 1	122 ± 5
dsDNA-PS10	10:1	181 ± 13	145 ± 3
dsDNA-PL20	10:1	172 ± 3	145 ± 1
dsDNA-PS20	10:1	184 ± 8	145 ± 8

The zeta potential of four PDMAEA-dsDNA polyplexes at pH 7.4 was obtained via DLS and are reported in table 4.6.

Table 4.6 Zeta potential of four PDMAEA-dsDNA polyplexes. The data represent the mean values \pm SD (N=3) recorded at pH 7.4.

Polyplex	N/P	Zeta potential (mV)	Conductivity (mS cm ⁻¹)
dsDNA-PL10	10:1	36.9 \pm 0.5	0.15
dsDNA-PS10	10:1	37.3 \pm 1.3	0.11
dsDNA-PL20	10:1	40.8 \pm 0.7	0.11
dsDNA-PS20	10:1	45.1 \pm 0.4	0.41

The hydrodynamic diameter and zeta potential of four PDMAEA-dsDNA polyplexes are shown in figure 4.12. Results revealed that all polyplexes have a hydrodynamic diameter of below 200 nm, with a positive charge of above 35 mV at pH 7.4. Research done by Shang et al. has suggested that polyplexes with a hydrodynamic diameter of below 200 nm are the key to improve the stability and cellular uptake rate of nanoparticles²².

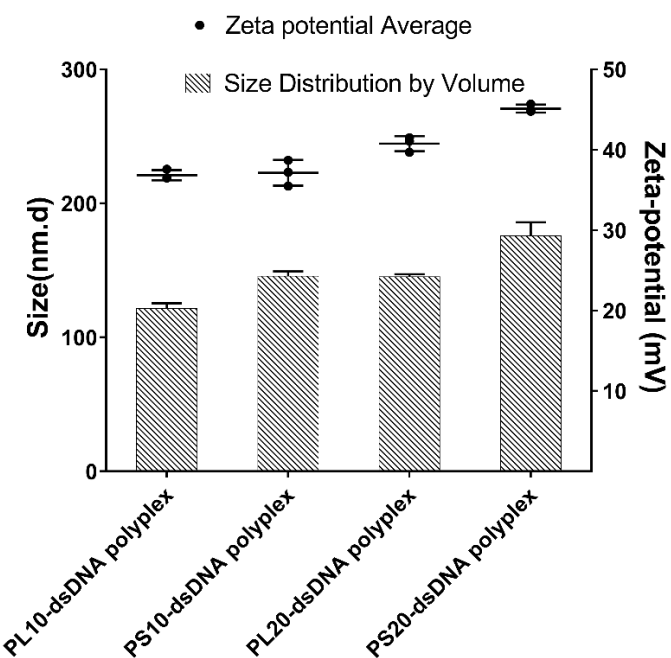


Figure 4.12 Mean size distribution by volume percentage and zeta potential of four PDMAEA-dsDNA polyplexes at pH 7.4. The data represent mean values \pm SD (N=3).

Furthermore, Valleau et al. suggested that polyplexes with a high positive charge have proven to be more colloidally stable based on the DLVO theory²³. While comparing the PDMAEA polyplexes, it is noticeable that the polyplexes with 20kDa molar mass have

a higher zeta potential than the 10kDa ones and the polyplexes of the star-shaped polymers showed a high zeta potential than linear ones.

4.3.5. Formation and Characterisation of PS10-siRNA Polyplexes.

PS10 PDMAEA polymer was selected due to its good binding capability and low toxicity to condense with *COL3a1* specific siRNA forming PS10-siRNA polyplex for the transfection of equine tenocyte. Characterisation on PS10-siRNA polyplex is performed by using electrophoresis and dynamic light scattering. The aim is to confirm the successful formation of polyplex and confirm its hydrodynamic diameter and zeta potential. Another objective was to confirm if there is any variance between the PS10-siRNA polyplex to PS10-dsDNA polyplex. The electrophoresis result is shown in figure 4.13; free siRNA was used as a negative control, which is not mixed with any polymer but with TAE buffer. PS10-siRNA polyplex samples were prepared at an N:P ration of 10:1. As shown in the figure, the free siRNA lane showed an obvious light band after staining and UV visualization while no bands were observed in PS10-siRNA lane. These data suggested that successful formation of PS10-siRNA polyplex was achieved and the siRNA had been completely condensed to PS10 polymers under the experimental conditions.

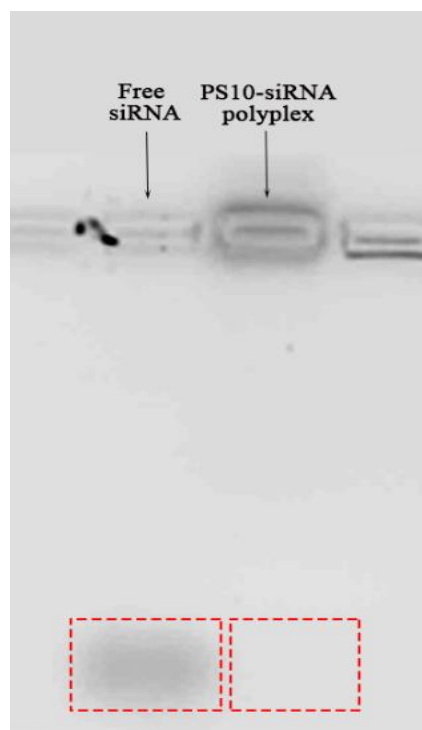


Figure 4.13 Agarose gel (1.5%) electrophoresis analysis of PS10-siRNA polyplexes. The figure colour was reversed to better demonstrate results. The figure is cropped from the original figure.

The hydrodynamic diameter and zeta potential of PS10-siRNA polyplex at pH 5.4, 6.4 and 7.4 were determined by dynamic light scattering. The correlation curves, volume and intensity distributions are shown in figure 4.14. The intensity and volume distributions confirmed that a single size population of ~150 nm was present in PS10-siRNA polyplexes solution from pH 5.4 to pH 7.4.

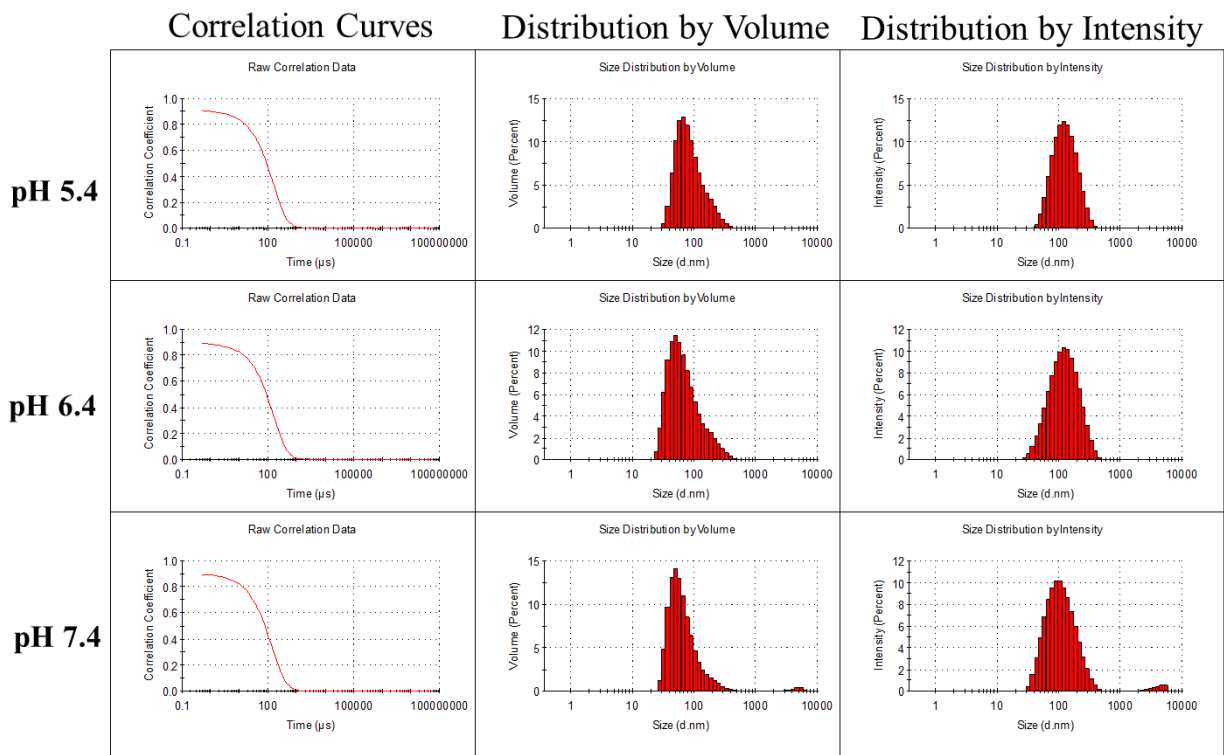


Figure 4.14 The correlation curves, intensity distribution and volume distribution of PS10-siRNA polyplexes at pH 5.4-7.4.

The mean size value \pm SD and the zeta potential of PS10-siRNA polyplexes at pH 5.4-7.4 are summarised in table 4.7 and table 4.8, respectively.

Table 4.7 Hydrodynamic diameter of PS10-siRNA polyplexes. The data represent mean values \pm SD (N=3) recorded at the corresponding pH.

Polyplex	pH	N/P	D_H (Intensity distribution \pm SD)/nm	D_H (Volume distribution \pm SD)/nm
siRNA-PS10	5.4	10:1	147 \pm 4	94 \pm 6
siRNA-PS10	6.4	10:1	134 \pm 18	79 \pm 21
siRNA-PS10	7.4	10:1	158 \pm 44	74 \pm 25

Table 4.8 Zeta potential of PS10-siRNA polyplexes. The data represent mean values \pm SD (N=3) recorded at the corresponding pH.

Polyplex	pH	N/P	Zeta potential (mV)	Conductivity (mS cm $^{-1}$)
siRNA-PS10	5.4	10:1	41.6 \pm 2.2	3.62
siRNA-PS10	6.4	10:1	38.9 \pm 1.6	0.44
siRNA-PS10	7.4	10:1	29.7 \pm 1.1	1.33

The size and zeta potential of PS10-siRNA polyplexes are summarised and plotted as a function of pH in figure 4.15. The results suggested that PS10-siRNA polyplex has a hydrodynamic diameter of \sim 150 nm by intensity distribution and zeta potential of above 25mV at pH 5.4, 6.4 and 7.4.

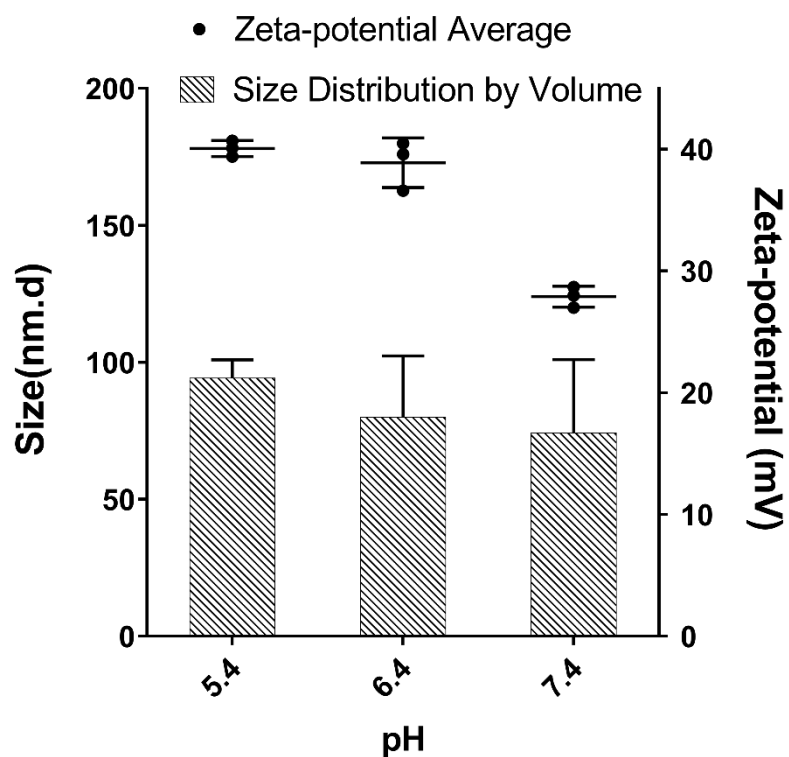


Figure 4.15 Size and zeta potential of PS10-siRNA polyplexes at pH 5.4, 6.4 and 7.4. The data represent mean values \pm SD (N=3).

It is evident that the standard deviation and D_H would increase as the pH of the solution increases, which is an indication of aggregation trends. Another fact is that the zeta potential drops as the pH increases, from 41.6 mV to 29.7 mV, possibly due to the deprotonation of amine functional groups in PDMAEA polymers.

4.4. Discussion

4.4.1. Hydrodynamic Diameter and Zeta Potential of PDMAEA Polymers and its Polyplexes

In this chapter, the hydrodynamic diameter (D_H) and zeta potential of PDMAEA polymers and its polyplexes, including PDMAEA-dsDNA polyplexes and PS10-siRNA polyplexes, is presented. Firstly, the PDMAEA polymers were dissolved in aqueous HEPES buffer solution without the addition of any DNA or RNA. The dissolved polymer molecules do not remain fully extended in a stationary state; instead they adopt various conformations due to the internal rotations that can occur through simple C-C bonds and Brownian motion²⁴. Numerous possible conformations can be formed, and although these confirmations do not have the same energy, the differences are negligible so that the polymers in solution can change from one conformation to another. Due to this, polymers dissolved in solution rarely adopt a linear form, rather they form an irregular structure known as the random coil (figure 4.16)²⁴.

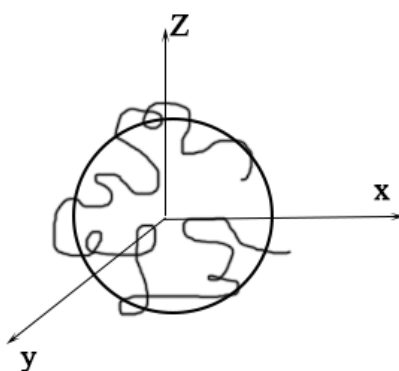


Figure 4.16 A schematic demonstration of a possible random coil structure of polymers in solution.

The average shape of the polymers with a random coil structure is typically found to be spherical, and the size of the spherical shape is affected by many factors such as the solvent, temperature and molecular weight of the polymer. For instance, the selection of solvent would affect the polymer-solvent interaction. The greater the interaction

between solvent and polymer is, the larger will be the hydrodynamic diameter²⁴. In this study, the intensity distribution and volume distribution data collected via DLS suggest that the PDMAEA polymers dissolved in HEPES solution have a hydrodynamic diameter smaller than 10 nm at pH 7.5 and below. One possible explanation is that the PDMAEA polymers dissolved in HEPES solution may have adopted the random coil structure and formed spherical particles.

It is evident that the D_H and zeta potential of PDMAEA polymers were affected by pH, and zeta potential decreases as the pH changes from low to high. As shown in figure 4.7, as the pH of the solution is adjusted to 8.0, the zeta potential of PDMAEA polymers dropped below 20 mV and reached 0 mV at pH 8.5. Correspondingly, the D_H of PDMAEA polymers remained at ~10 nm while the pH is below 7.5 but increase as the pH was adjusted to 8.0 and higher. One possible explanation is that at low pHs, the protonated polymers bearing a positive charge provided a repulsive force to prevent the formation of large aggregates (figure 4.17).

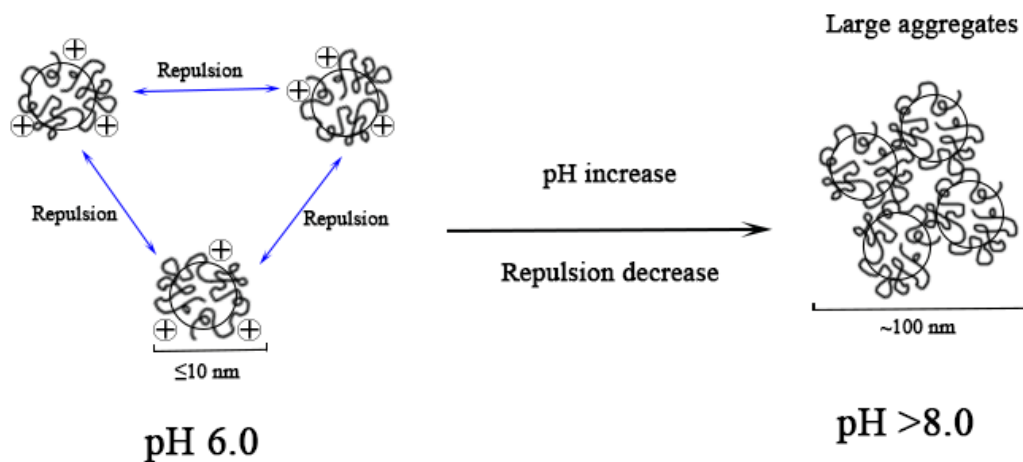


Figure 4.17 A schematic demonstration of PDMAEA polymers forming large aggregates at pH 8.0 and above.

At neutral pH and below, PDMAEA polymers, which have abundant amine groups, would quickly protonate and become positively charged. Explained by DLVO theory, in ionic dispersions, the colloidal stability is affected by two major forces: The Van der Waal forces and the electrostatic repulsive forces²⁵. The balance between the Van der Waal forces is an attractive force that would pull particles in solution together, and the electrostatic repulsive forces would keep nanoparticles in solution from aggregating. As the Van der Waals force is a distance-dependent force, the repulsive forces play an important role for charged particles and molecules such as PDMAEA polymers. At low

pH, due to the protonation of the polymer molecule, the repulsive force is strong enough to keep the balance, and the solution would remain colloidally stable. Once the pH is increased above 7.5, the deprotonation would result in a weakened repulsive force between molecules and be further overwhelmed by the Van der Waals forces, eventually leading to aggregation. This explanation could also be applied to the polyplexes, in the study of PS10-siRNA polyplex D_H and zeta potential, as pH increases from 5.4 to 7.4, it was noticed that the increase of the D_H of polyplexes and samples SD corresponds to the decrease of the zeta potential of polyplexes. However, the zeta potential was kept at above 25 mV at pH 7.4 and below. Therefore no aggregation was observed.

4.4.2. Formation of PDMAEA-dsDNA Polyplexes and PS10-siRNA Polyplexes.

A range of N:P ratio from 1:1 to 15:1 was tested for the formation of polyplexes. The purpose of designing multiple ratios is to determine the critical polyplex formation N:P ratio and compare different PDMAEA polyplexes. In this experiment, for all samples, a fixed amount of dsDNA was used to provide a quantified amount of phosphate in the preparation of all polyplexes. By changing the N:P ration, it is essentially changing the quantity amount of polymers used in the polyplex formation. In such a case, the N:P ratio could represent the amount of polymers needed to completely condense with a certain amount of dsDNA and siRNA. The lower N:P ratio needed for forming polyplexes, the stronger will be the binding ability of the polymer. As presented above, the critical polyplex formation ratio for PL10, PS10, PL20 and PS20 is 7:1, 5:1, 5:1 and 3:1 respectively. The underlying concept of this result is that there is a pattern for the formation of PDMAEA polyplexes. Firstly, comparing polymers with the sample structure (PL10-PL20, PS10-PS20), it is revealed that polymers with larger molar mass tend to require lower N:P ratio to form polyplexes with nucleic acids. Secondly, comparing polymers with the same molar mass, it is noticed that star-shaped polymers require a lower charge ratio to form polyplex. One possible explanation for the stronger binding ability is proposed by Stiriba et al. that an unusually compact (“collapsed”) structure, possibly related to branched amphiphiles structure, is responsible for the formation of an internal hydrophilic compartment that is capable of condensing with guest molecules (figure 4.18)²⁶.

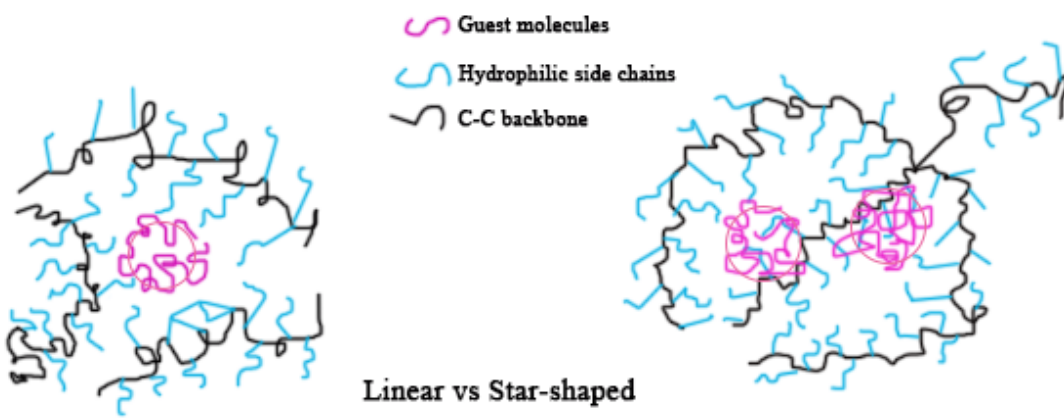


Figure 4.18 Schematic figure of the formation of a possible internal hydrophilic compartment in star-shaped polymers compared to linear polymers.

In general, it is concluded that PS10-siRNA polyplex has a D_H of $\sim 150\text{nm}$ and zeta potential of above 25mV at neutral pH and below, which is consistent with data gathered from PDMAEA-dsDNA and studies completed by other researchers^{27,28}.

4.4.3. Selection of PS10 as a Delivery Vector for the Delivery of siRNA.

PS10 was selected to condense with siRNA at an N:P ratio of 10:1. The selection of PS10 as the vector for the formation of siRNA polyplex was based on the polymer's binding ability and toxicity (discussed in detail in chapter 5). As discussed, star-shaped polymers have a better binding ability than linear ones, and as it is presented in chapter 5, polymers with larger molar mass have higher toxicities compared to the ones with lower molar mass. Considering all above, it was decided to select PS10 as the delivery vector to form PS10-siRNA polyplex at an N:P ratio of 10 :1 for the silencing of *COL3α1* gene. The selection of an N:P ratio at 10:1 is based on the facts reported by Ketola et al., that complexes formed at high N:P ratio may provide adequate stability in the extracellular space²⁹.

4.5. Conclusion

The work presented in this chapter described the solution behaviour, including hydrodynamic diameter and zeta potential, of PDMAEA polymers and its polyplex. It is demonstrated that PDMAEA polymers have a hydrodynamic diameter of $\sim 10\text{ nm}$ and with an average zeta potential of above 20 mV at neutral pH and below. Successful formation of PDMAEA-dsDNA polyplexes was confirmed by agarose gel electrophoresis. The hydrodynamic diameter and zeta potential of PDMAEA-dsDNA polyplexes were characterised by dynamic light scattering. The result indicated that the

PDMAEA-dsDNA polyplexes had a hydrodynamic diameter between 150 - 180 nm and showed zeta potential of above 25 mV. Moreover, it was established that PDMAEA polymers with larger molecular weight showed stronger DNA binding capabilities. Meanwhile, data also suggested that star-shaped PDMAEA polymers showed stronger binding capability compared to the linear ones. Furthermore, PS10 was selected as a delivery vector to condense with siRNA, resulting in successful formation of PS10-siRNA polyplex and confirmed by electrophoresis. The hydrodynamic diameter and zeta potential of PS10-siRNA were determined at different pH conditions from 5.4 to 7.4 by dynamic light scattering. The results suggested that the PS10-siRNA polyplex has a hydrodynamic diameter of ~150 nm or smaller diameter and a positive charge of 29 mV and higher at neutral pH and below. With the successful preparation and characterisation of PDMAEA polyplexes, the cytotoxicity profile of PDMAEA and PDMAEA polyplexes will be investigated in the next chapter.

4.6. References

- 1 Howard, K. A. Delivering the goods: realizing the clinical potential of RNAi. *Nanomedicine* **4**, 595-598 (2009).
- 2 Howard, K. A. & Kjems, J. Polycation-based nanoparticle delivery for improved RNA interference therapeutics. *Expert Opin Biol Th* **7**, 1811-1822 (2007).
- 3 Davis, M. E. The First Targeted Delivery of siRNA in Humans via a Self-Assembling, Cyclodextrin Polymer-Based Nanoparticle: From Concept to Clinic. *Mol Pharmaceut* **6**, 659-668 (2009).
- 4 Davis, M. E. *et al.* Evidence of RNAi in humans from systemically administered siRNA via targeted nanoparticles. *Nature* **464**, 1067-U1140 (2010).
- 5 Elbashir, S. M. *et al.* Duplexes of 21-nucleotide RNAs mediate RNA interference in cultured mammalian cells. *Nature* **411**, 494-498 (2001).
- 6 He, C., Hu, Y., Yin, L., Tang, C. & Yin, C. Effects of particle size and surface charge on cellular uptake and biodistribution of polymeric nanoparticles. *Biomaterials* **31**, 3657-3666, doi:10.1016/j.biomaterials.2010.01.065 (2010).
- 7 Gillard, M. *et al.* Intracellular trafficking pathways for nuclear delivery of plasmid DNA complexed with highly efficient endosome escape polymers. *Biomacromolecules* **15**, 3569-3576, doi:10.1021/bm5008376 (2014).
- 8 El-Sayed, A., Futaki, S. & Harashima, H. Delivery of Macromolecules Using Arginine-Rich Cell-Penetrating Peptides: Ways to Overcome Endosomal Entrapment. *Aaps J* **11**, 13-22 (2009).
- 9 Boussif, O. *et al.* A Versatile Vector for Gene and Oligonucleotide Transfer into Cells in Culture and in-Vivo - Polyethylenimine. *P Natl Acad Sci USA* **92**, 7297-7301, doi:DOI 10.1073/pnas.92.16.7297 (1995).
- 10 Howard, K. A. *et al.* RNA interference in vitro and in vivo using a novel chitosan/siRNA nanoparticle system. *Mol Ther* **14**, 476-484, doi:10.1016/j.ymthe.2006.04.010 (2006).
- 11 Liu, X. *et al.* The influence of polymeric properties on chitosan/siRNA nanoparticle formulation and gene silencing. *Biomaterials* **28**, 1280-1288, doi:10.1016/j.biomaterials.2006.11.004 (2007).

12 Fusco, G. *et al.* Structural basis of membrane disruption and cellular toxicity by alpha-synuclein oligomers. *Science* **358**, 1440-+ (2017).

13 Truong, N. P. *et al.* Self-Catalyzed Degradable Cationic Polymer for Release of DNA. *Biomacromolecules* **12**, 3540-3548, doi:10.1021/bm2007423 (2011).

14 Grumezescu, A. M. *Multifunctional systems for combined delivery, biosensing and diagnostics*. (Elsevier, 2017).

15 Lu, G. W. & Gao, P. in *Handbook of Non-Invasive Drug Delivery Systems* (ed Vitthal S. Kulkarni) 59-94 (William Andrew Publishing, 2010).

16 Buschow, K. H. J. *Encyclopedia of materials : science and technology*. (Elsevier, 2001).

17 Pan, H. *et al.* in *Methods in Enzymology* Vol. 508 (ed Nejat Düzgüneş) 17-39 (Academic Press, 2012).

18 Grzadka, E., Wisniewska, M., Gun'ko, V. M. & Zarko, V. I. Adsorption, Electrokinetic and Stabilizing Properties of the Guar Gum/Surfactant/Alumina System. *J Surfactants Deterg* **18**, 445-453, doi:10.1007/s11743-015-1673-y (2015).

19 Losso, J. N., Khachatryan, A., Ogawa, M., Godber, J. S. & Shih, F. Random centroid optimization of phosphatidylglycerol stabilized lutein-enriched oil-in-water emulsions at acidic pH. *Food Chem* **92**, 737-744, doi:10.1016/j.foodchem.2004.12.029 (2005).

20 Frankel, E. N., Huang, S. W., Kanner, J. & German, J. B. Interfacial Phenomena in the Evaluation of Antioxidants - Bulk Oils Vs Emulsions. *J Agr Food Chem* **42**, 1054-1059, doi:DOI 10.1021/jf00041a001 (1994).

21 Zhao, E. Y. *et al.* Surface engineering of gold nanoparticles for in vitro siRNA delivery. *Nanoscale* **4**, 5102-5109, doi:10.1039/c2nr31290e (2012).

22 Shang, L., Nienhaus, K. & Nienhaus, G. U. Engineered nanoparticles interacting with cells: size matters. *J Nanobiotechnol* **12**, doi:Artn 510.1186/1477-3155-12-5 (2014).

23 Valleau, J. P., Ivkov, R. & Torrie, G. M. Colloid Stability - the Forces between Charged Surfaces in an Electrolyte. *J Chem Phys* **95**, 520-532, doi:Doi 10.1063/1.461452 (1991).

24 Su, W.-F. in *Principles of Polymer Design and Synthesis* (ed Wei-Fang Su) 9-26 (Springer Berlin Heidelberg, 2013).

25 Gooch, J. W. *Encyclopedic Dictionary of Polymers*. 2 edn, 318 (2007).

26 Stiriba, S. E., Kautz, H. & Frey, H. Hyperbranched molecular nanocapsules: comparison of the hyperbranched architecture with the perfect linear analogue. *J Am Chem Soc* **124**, 9698-9699 (2002).

27 Troiber, C. *et al.* Comparison of four different particle sizing methods for siRNA polyplex characterization. *Eur J Pharm Biopharm* **84**, 255-264 (2013).

28 Dey, D., Kumar, S., Banerjee, R., Maiti, S. & Dhara, D. Polyplex Formation between PEGylated Linear Cationic Block Copolymers and DNA: Equilibrium and Kinetic Studies. *Journal of Physical Chemistry B* **118**, 7012-7025 (2014).

29 Ketola, T. M. *et al.* Role of polyplex intermediate species on gene transfer efficiency: polyethylenimine-DNA complexes and time-resolved fluorescence spectroscopy. *J Phys Chem B* **115**, 1895-1902, doi:10.1021/jp109984c (2011).

Chapter 5

Cytotoxicity of PDMAEA Polymers and PDMAEA Polyplexes

5. Chapter 5 Cytotoxicity of PDMAEA Polymers and PDMAEA Polyplexes

5.1. Introduction

RNA interference provides an efficient pathway to silence the expression of a specific gene by using small RNA molecules such as siRNA and miRNA, which makes it an attractive tool for gene therapy and genetic research. In mammalian cells, the use of siRNA is typically accompanied with delivery vectors to overcome biological barriers that provide hindrance for siRNA silencing. Although the delivery of siRNA shared many of the same intracellular steps as the delivery of DNA, siRNA activity is confined within the P-body in the cytoplasm, which does not require the entry into the nucleus. However, the delivery of siRNA has proven to be highly challenging, especially *in vivo*¹. Thus, it is important to better understand siRNA delivery and develop better delivery systems. It is suggested that an effective siRNA delivery system should have properties including efficient binding to the cell surface, the capability of being taken up via endocytosis, an endosomal escape mechanism, and the ability to release the siRNA cargo into the cytoplasm². Also, it is fundamental that the delivery vector should be able to condense efficiently with siRNA molecules and should be non-toxic.

The applications of cationic polymers as drug-delivery agents has been widely studied. The use of cationic polymer-DNA/RNA polyplexes in gene therapy are based on the hypothesis that the complexes adsorb more effectively to the anionic plasma membrane of mammalian cells through electrostatic interactions³. Studies have also demonstrated that cationic delivery systems can be internalised via clathrin-mediated endocytosis and can escape from the endosomes via a “proton sponge” pathway^{4,5}. For gene delivery vectors, especially *in vivo* delivery vectors, toxicity is a critical factor to consider when evaluating the potential of a polymer delivery system. As these polyplexes are intentionally designed to interact with cells, it is necessary to ensure that these polymer vectors are not causing any adverse effects. If a delivery system produces unacceptable cytotoxicity, the delivery system will be rendered useless regardless of how efficient the system is^{6,7,8}. Traditional cationic polymer-based systems such as PEI are highly valued owing to their high efficiency^{9,10}. Other advantages such as being simple, inexpensive and chemically manipulatable are also favoured in a gene delivery system¹¹. Many studies have been done using PEI as a delivery vector. Jiang et al. reported the use of DNA-PEI polyplexes encoding green fluorescent protein (GFP) to deliver into tumour

cells in six-week-old female C57/BL6 mice and achieved higher levels of GFP expression¹². Another study by Peng et al. reported plasmid DNA encoding *VEGF165* gene delivered to epidermal stem cells using PEI-pDNA polyplexes for the treatment of wound healing¹³. Many more studies on the use of PEI as a gene delivery vector for a variety of diseases have been summarised by Di Gioia et al. and others^{14,15}. With the development in the field of chemistry and polymer synthesis, several novel cationic polymer-based delivery systems have been synthesised and applied in siRNA delivery.

In recent years, many novel cationic polymer-based delivery systems with lower toxicity levels have been widely studied. Some have focused on the modification of PEI into blocker polymers, Merkel et al. reporting that PEG-PEI polyplexes with low toxicity were used in siRNA Delivery to the lung *in vivo*¹⁶. Other studies reported the use of novel cationic polymers, such as PDMAEA, in the delivery of siRNA. Convertine et al. suggested that PDMAEMA-PAA-BMA di-block copolymer is an effective and low cytotoxicity nanocarrier in the siRNA knockdown in HeLa cell¹⁷. Another study by Benoit showed a PDMAEMA-butyl methacrylate (pDbB) copolymer with low toxicity was applied in the siRNA knockdown of polo-like kinase 1 (*plk1*) gene¹⁸.

PDMAEA polymers have received significant attention for their potential in gene delivery in recent years. The success of developing new pH-sensitive star-shaped polymer systems using PDMAEA as the pH-responsive blocks has been reported by Liu et al.¹⁹. Furthermore, the cytotoxicity profile of a series of PDMAEA polyplexes with N:P ratio ranging from 10 to 200 was determined on HeLa cells by Truong et al. It is reported that at low N:P ratio such as 10:1, PDMAEA polyplexes showed no toxicity²⁰. However, there is a lack of detailed reports regarding the cytotoxicity of PDMAEA and its polyplexes in equine tenocytes.

In addition, the influence of structure and molecular weight on polymer chemical and physical behaviour has been reported^{21,22}. Research by Fischer et al. and Monnery et al. suggested that the molecular weights of polymers have a direct influence on the cytotoxicity level of polymers^{23,24}. On the other hand, another research study by Fischer et al. indicated that polymer structure has a vital role in the determination of polymer cytotoxicity²⁵. However, there is a lack of detailed reports on the influence that molecular weight and structure might have on PDMAEA toxicity. Therefore, the

cytotoxicity of PDMAEA polymers with different structures and the molecular weights was determined and compared in this Chapter.

In this study, the cytotoxicity profile of PDMAEA polymers and their polyplexes were determined. The 3T3 mouse fibroblast was selected as a model cell line for its easy manipulation and stable growth rate and 3T3 mouse fibroblast has been widely applied in the studies of polymer cytotoxicity as a model cell line²⁶⁻²⁸. The cytotoxicity of PDAMEA polymers was first tested on 3T3 mouse fibroblasts to provide a preliminary report of PDMAEA behaviour. Also, the 3T3 mouse fibroblast contributed to the establishment and optimization of experimental conditions. Based on the results gathered from cytotoxicity experiments on 3T3 mouse fibroblast, the cytotoxicity of PDMAEA polymers was evaluated on equine tenocyte by using an MTS assay.

Due to the limited availability of *COL3α1* gene-specific siRNA, a dsDNA with a short base pair similar to siRNA was employed as a model molecule for the study and optimization of PDMAEA polyplex formulation. PDMAEA-dsDNA polyplexes were first tested for their cytotoxicity to provide a preliminary view of polyplex cytotoxicity. Considering the balance of binding capability and cytotoxicity, as well as the limited availability of *COL3α1* gene-specific siRNA, PS10 was selected as the candidate vector polymer to condense with siRNA and was further used in the transfection of equine tenocyte. Considering that MTS assay is a metabolic assay based on the metabolizing of MTS to formazan compounds, it directly measures the metabolic activity of sample cells, rather than cell apoptosis. The same argument was raised by Moghimi et al., who suggested that the use of metabolic assay such as MTS are not indicative of apoptosis²⁹. This leads to a possibility that the reduction in viability might not be a result of the toxicity of PDMAEA polymers, but a result of suppressed in cell metabolic activity. Therefore, the Cyquant Cell Proliferation assay, which is based on live cell nucleus staining fluorescence, was introduced to address this issue.

PEI was selected as a reference for its reputation as an efficient delivery vector, and it's been widely used as a delivery system in other studies. However, literature reported that although PEI showed excellent transfection efficiency, its severe toxicity has created barriers in its application^{9,15,30-32}. By using PEI as a reference treatment group, the aim was to compare the toxicity of PDMAEA and PEI directly.

Aim of the chapter:

The aim of this chapter is to determine the cytotoxicity of PDMAEA and its polyplexes on equine tenocytes. The cytotoxicity of PDMAEA polymers and its polyplexes were determined by the use of MTS assay and Cyquant Cell Proliferation Assay. The influence of polymer concentration and incubation time on cell viability after treatment was also determined, as well as the influence of polymer molecular weight and structure on polymer cytotoxicity.

The main objectives:

- Study the cytotoxicity profile of PDMAEA polymers under a series of concentrations and incubation times using 3T3 mouse fibroblast as model cell line and MTS assay.
- Study the cytotoxicity profile of PDMAEA polymers on equine tenocytes over different polymer concentrations and incubation time using MTS assay.
- Determine the cytotoxicity of PDMAEA (PL10, PL20, PS10, PS20)-dsDNA polyplexes and PS10-siRNA polyplexes on equine tenocytes using MTS assay and cell proliferation assay.
- Analyse how the polymer structure, polymer molecular weight, polymer concentration and incubation time affect the cell viability post-treatment.

5.2. Materials and Methods

5.2.1. Materials

The details of the materials used in this chapter are reported in chapter two section 2.2.

5.2.2. Cytotoxicity of PDMAEA Polymers on Mouse Fibroblast and Equine Tenocytes by MTS Assay

The cytotoxicity of PDMAEA polymer on mouse 3T3 fibroblasts (passage 14) and equine tenocytes (Passage 7) were determined by using the MTS assay. The basic principle and experimental conditions of general tissue culture and the use of MTS assay are reported in detail in chapter two. In each well of a 96-well plate, 10,000 cells (for both mouse fibroblast and equine tenocytes) were seeded in 100 μ L of medium and

incubated for three hours before treatment for cell attachment. The treatment solution was made of PDMAEA polymers at different concentrations (2.5, 5, 10, 15, 20, 25, 30 and 50 μ M). Three time-points were designed at 24, 48 and 72 hours to determine the effect over time. At every time-point, 10 μ L of MTS was added into each well and incubated for one hour before reading at a wavelength of 490 nm with an Omega Plate reader. All the data were normalised to cells treated only with medium and analysed with BMG data software.

5.2.3. Cytotoxicity of PDMAEA Polyplexes on Equine Tenocytes Determined by MTS Assay

The cytotoxicity of PDMAEA polyplexes on equine tenocytes was determined by using the MTS assay. PDMAEA-dsDNA polyplexes and PS10-siRNA polyplexes were prepared at an N:P ratio of 10:1 as described in chapter four. Considering the balance between binding capability and cytotoxicity, PS10 was selected to condense with *COL3 α 1* gene-specific siRNA to form PS10-siRNA polyplex. The principle of MTS assay and experimental conditions are described in detail in chapter two. In each well of a 96-well plate, 10,000 cells (for both mouse fibroblast and equine tenocytes) were seeded in 100 μ L of medium and incubated for three hours before treatment for cell attachment. The treatment solution was PDMAEA-dsDNA polyplex or PS10-siRNA polyplex solution at different concentration (2.5, 5, 10, 15, 20, 25, 30 and 50 μ M calculated based on polymer content). Three time-points were designed at 24, 48 and 72 hours to determine the effect over time. At every time-point, 10 μ L of MTS was added into each well and incubated for one hour before reading at a wavelength of 490nm with an Omega Plate reader. All the data were normalised to cells treated with medium and analysed with BMG data software provided before being presented.

5.2.4. Cytotoxicity of PS10-siRNA Polyplexes on Equine Tenocytes Determined using Cyquant NF Cell Proliferation Assay

PS10-siRNA polyplexes were prepared as described in chapter four at an N:P ratio of 10:1. The basic principle of Cyquant NF cell proliferation assay and experimental conditions were described in detail in chapter two. A calibration curve was first made to obtain the optimal seeding density. In each well of a Corning® 96 Well Black polystyrene microplate, 2,500 cells were seeded in 100 μ L of medium and incubated for

three hours to allow cell attachment. The treatment solution was PS10-siRNA polyplexes solution at different concentrations (2.5, 5, 10, 15, 20, 25, 30 and 50 μ M calculated based on polymer content). Three time-points were designed at 24, 48 and 72 hours to determine the effect over time. At every time-point, growth medium was removed, and 100 μ L of 1X dye binding solution was dispensed into each microplate well. The plate was then incubated in the dark for 45 minutes before measuring the fluorescence intensity of each sample using a fluorescence microplate reader. All the data were normalised to cells treated with medium only and analysed with BMG data software provided before being presented.

5.3. Results

5.3.1. Cytotoxicity of PDMAEA Polymers on 3T3 Mouse Fibroblast Cells Determined by MTS assay

The cytotoxicity of PDMAEA polymer was evaluated on 3T3 mouse fibroblasts by using MTS assay. The metabolic activity at 24-hour post-treatment are demonstrated in figure 5.1. The metabolic activity of all samples were normalised to cells treated with medium. As shown in figure 5.1 (A), polymers of 10kDa molecular weight (PL10 and PS10) showed high metabolic activity (of above 95%) across different concentrations, whereas polymers of 20kDa molecular weight (PL20 and PS20) showed decreased metabolic activity, especially PS20. For cells treated with PL20, with concentrations of 15 μ M and above, samples started to show consecutive decreases in metabolic activity over increased concentration at 24 hours post-treatment. The same trend was observed in PS20 as well but with a much more significant decrease in metabolic activity. Cells treated with PEI showed a much more severe reduction in viability, with an average of 43.5% across all concentrations. Variation between PEI and PDMAEA polymers were analysed with two-way ANOVA and are shown in figure 5.1 (B). It is demonstrated that all PDMAEA treated sample groups showed significantly higher viability compared to PEI treated samples. As shown in figure 5.1 (C), it is also demonstrated by the comparison of viability between each polymer at 24 hours post-treatment. The data indicate that there is no significant difference between PS10-PL10 (when comparing the structural effect) and PL10-PL20 (when comparing the molecular weight's effect). However, when comparing the PS20 group to PL20 (structural effect) and PS10 (molecular weight's effect), the results showed significant differences. The results from

24 hours post-treatment can be considered as an indicator of PDMAEA polymer's acute cytotoxicity. However, it is reported that for certain polymers, delayed cytotoxicity following treatment is commonly observed^{23,33}. Also, in some cases, the transfection process may be followed by a long period of incubation. Thus, the cytotoxicity effect of PDMAEA polymer was further monitored at 48- and 72-hours post-treatment.

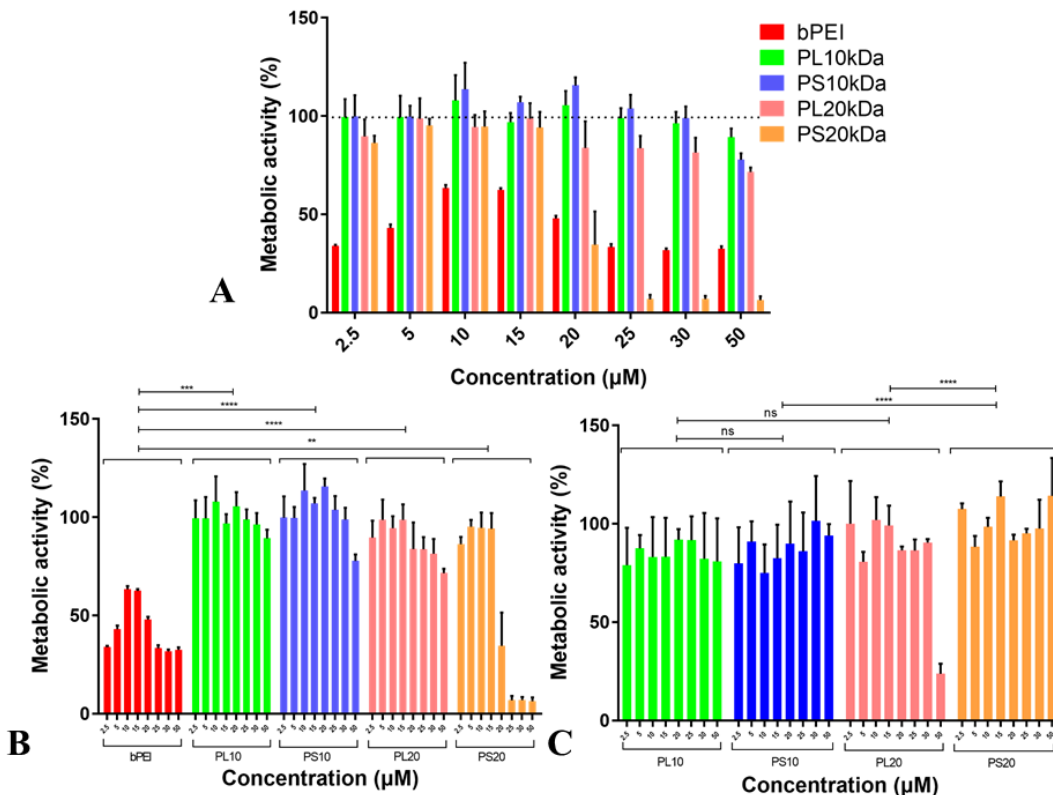


Figure 5.1 Mouse 3T3 fibroblast metabolic activities at 24 hours post-treatment. Samples were treated with PDMAEA polymer solutions at different concentrations, and metabolic activities were determined using MTS assay. All the results were normalised against cells treated with complete medium. The data represent mean values \pm SD, N=3 (technical replicates). A) Metabolic activity-concentration relationship of sample cells treated with PDMAEA polymers solutions at the 24-hour time point. B) Statistical analysis between PDMAEA polymers and PEI. C) Statistical analysis among four PDMAEA polymers groups (two-way ANOVA, ns: $p>0.05$, *: $0.05>p>0.01$, **: $0.01>p>0.005$, ***: $0.005>p>0.001$, ****: $0.001>p$).

Figure 5.2 demonstrated the metabolic activity at 48 hours post-treatment. The results indicated that cells treated with PL10 and PS10 showed high viability, which is consistent with data collected at 24 hours post-treatment. Interestingly, cells treated with PL20 and PS20 showed a significant decrease in metabolic activity at 48 hours compared with the results from the 24 hours group. For PS20 and PL20 treated samples, metabolic activity dropped to 70% and below, even at 2.5 μM (being the lowest designed concentration). While comparing all polymers groups to PEI treated group, all samples showed significantly higher metabolic activity than PEI treated group. Comparison

between the metabolic activity of samples treated with PL10 and PS10 indicated that between PL10 and PS10 there is no significant difference. While comparing samples treated with PS10 and PS20, or PL10 and PL20, it was found that groups with high molar mass tend to have lower metabolic activity. Besides, the variance between PL20 and PS20 had decreased in the 48-hour group, probably due to the reduction of viability in PL20 treated samples.

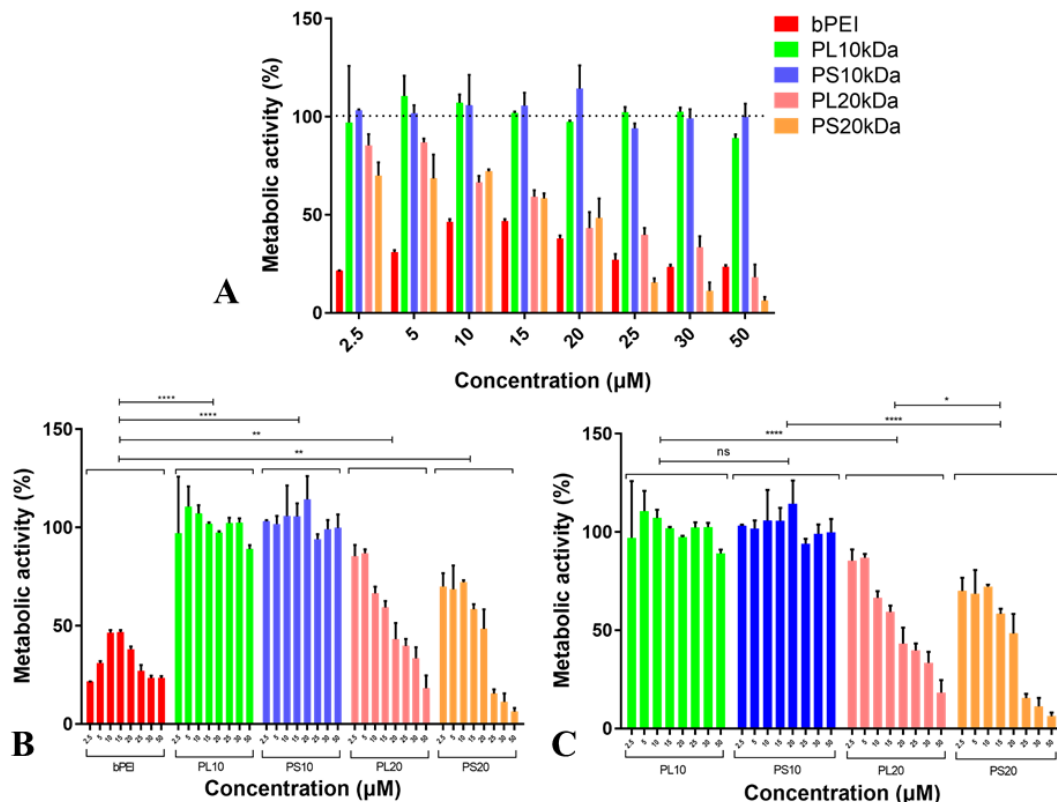


Figure 5.2 Mouse 3T3 fibroblast metabolic activities at 48 hours post-treatment. Samples were treated with PDMAEA polymer solutions at different concentrations, and metabolic activities were determined using MTS assay. All the results were normalised against cells treated with complete medium. The data represent mean values \pm SD, N=3 (technical replicates). A) Metabolic activity-concentration relationship of sample cells treated with PDMAEA polymers solutions at the 48-hour time point. B) Statistical analysis between PDMAEA polymers and PEI. C) Statistical analysis among four PDMAEA polymers groups (two-way ANOVA, ns: $p>0.05$, *: $0.05>p>0.01$, **: $0.01>p>0.005$, ***: $0.005>p>0.001$, ****: $0.001>p$).

Data collected from samples at 72 hours post-treatment group are shown in figure 5.3. Results suggested that the major trend is consistent with results from 24- and 48-hour timeframes. Cells treated with PL10 and PS10 remained at high metabolic activity while cells treated with PS20 and PL20 showed comparatively lower viability. Comparing all polymer groups to the PEI-treated group, all PDMAEA-treated groups showed higher metabolic activity. Comparing between PDMAEA polymer treated groups, the PS20 treated group showed much lower viability compared to other groups.

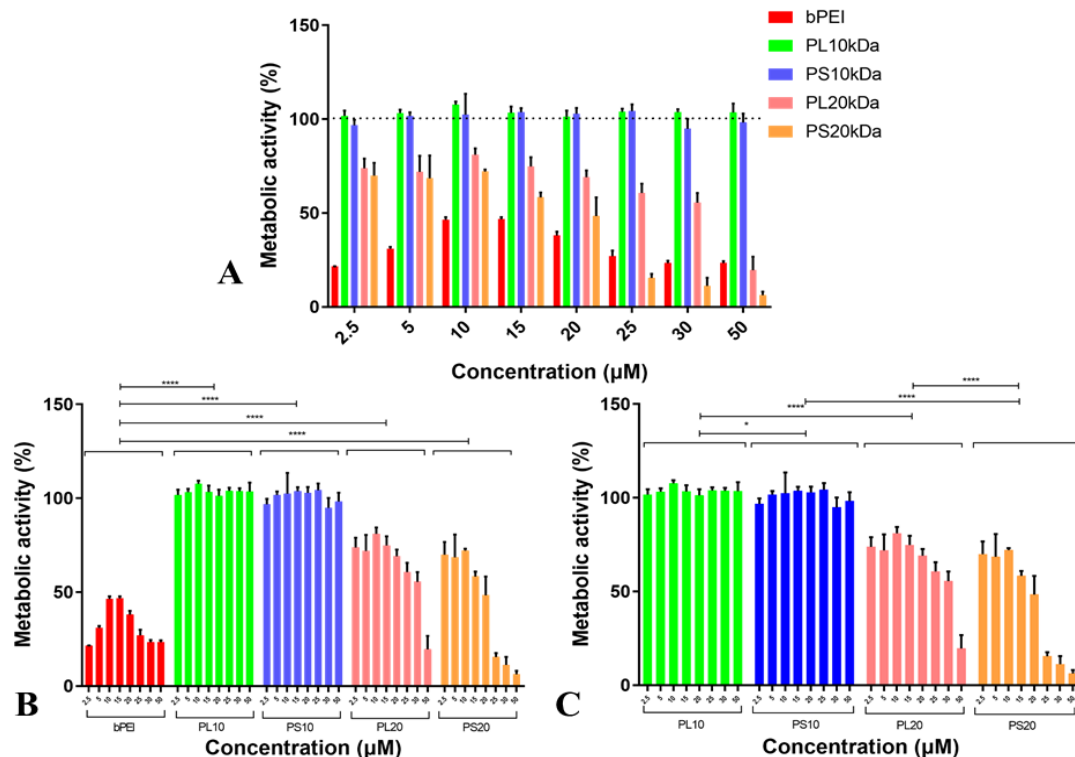


Figure 5.3 Mouse 3T3 fibroblast metabolic activities at 72 hours post-treatment. Samples were treated with PDMAEA polymer solutions at different concentrations, and metabolic activities were determined using MTS assay. All the results were normalised against cells treated with complete medium. The data represent mean values \pm SD, N=3 (technical replicates). A) Metabolic activity-concentration relationship of sample cells treated with PDMAEA polymers solutions at the 72-hour time point. B) Statistical analysis between PDMAEA polymers and PEI. C) Statistical analysis among four PDMAEA polymers groups (two-way ANOVA, ns: $p > 0.05$, *: $0.05 > p > 0.01$, **: $0.01 > p > 0.005$, ***: $0.005 > p > 0.001$, ****: $0.001 > p$).

The morphology of most cells treated with PDMAEA solutions showed typical healthy morphologies, with except those cells treated with PEI across all concentrations and cells treated with high concentration solutions of PS20 and PL20. In these groups, most of the cells changed their morphologies, cells becoming rounded, and lysed cells being visible, along with squibs and cell debris.

5.3.2. Cytotoxicity of PDMAEA Polymers on Equine Tenocytes by using MTS Assay

The cytotoxicity of PDMAEA polymers on equine tenocytes was determined by using the MTS assay. Cultured equine tenocytes were treated with PDMAEA polymer solution of different concentrations over 24, 48 and 72 hours. PEI solution was employed as positive control. Results at 24 hours post-treatment are illustrated in figure 5.4. It is shown that all PDMAEA polymer treated sample showed high metabolic

activity except for PL20 at a concentration of 50 μ M, while PEI treated samples showed comparatively lower viability as demonstrated in figure 5.4 (A). Statistical analysis on the metabolic activity further suggested that all PDMAEA treated samples showed a higher level of viability compared to PEI treated the group as presented in figure 5.4 (B). Figure 5.4 (C) exhibited the comparison between PS10 and PL10, or PL10 and PL20, and the results suggested that there are no significant differences between polymers of the same molecular weight with a different structure. However, the comparison between PS20 and PS10, or PS20 and PL20, indicated a variance of different degree, possibly due to the high viability of PS20 group. The morphology of all equine tenocyte cells treated with PDMAEA solutions showed typical healthy morphologies at 24 hours, with except those cells treated with PEI solutions.

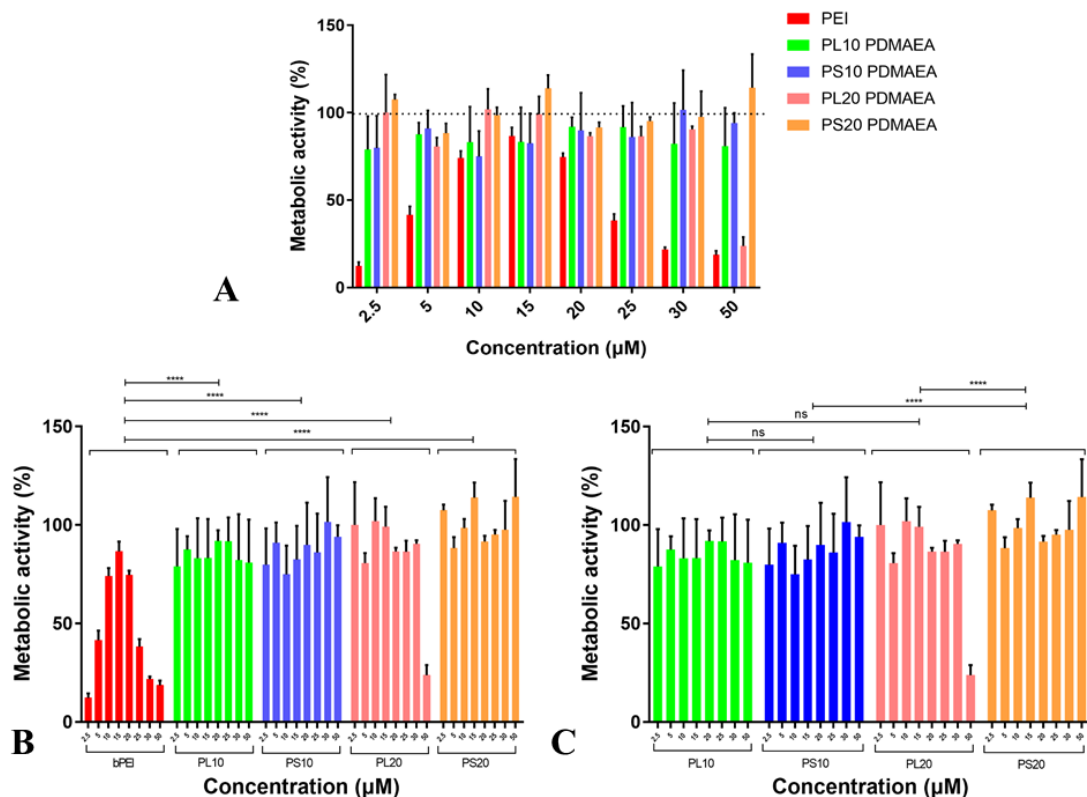


Figure 5.4 Equine tenocyte metabolic activities at 24 hours post-treatment. Samples were treated with PDMAEA polymer solutions at different concentrations, and metabolic activities were determined using MTS assay. All the results were normalised against cells treated with complete medium. The data represent mean values \pm SD, N=3 (technical replicates). A) Metabolic activity-concentration relationship of sample cells treated with PDMAEA polymers solutions at the 24-hour time point. B) Statistical analysis between PDMAEA polymers and PEI. 3) Statistical analysis among four PDMAEA polymers groups (Two-way ANOVA, ns: $p>0.05$, *: $0.05>p>0.01$, **: $0.01>p>0.005$, ***: $0.005>p>0.001$, ****: $0.001>p$).

At 48 hours post-treatment, samples showed reduced levels of metabolic activities, especially at high concentrations (30-50 μ M). A similar reduction was observed on 3T3

fibroblast cells at 48 hours as well. As in the previous timeframe, all PDMAEA treated samples showed a significant difference in viability compared to PEI treated samples. In addition, statistical analysis of the data from PS10 treated group and PL10 treated group indicated that there is no significant difference between the viability. However, the comparison between PS10 - PS20, PL10 - PL20 and PS20 – PL20 showed differences by statistical analysis. The morphology of all equine tenocyte cells treated with PDMAEA solutions showed typical healthy morphologies.

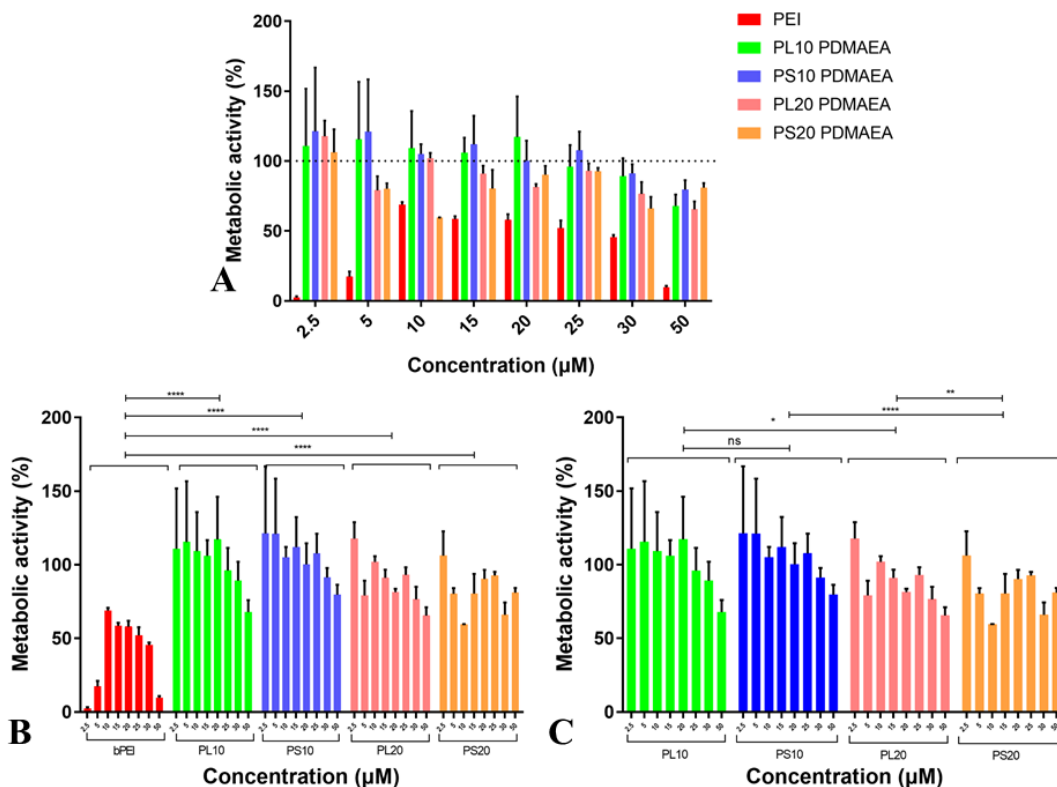


Figure 5.5 Equine tenocyte metabolic activities at 48 hours post-treatment. Samples were treated with PDMAEA polymer solutions at different concentrations, and metabolic activities were determined using MTS assay. All the results were normalised against cells treated with complete medium. The data represent mean values \pm SD, N=3 (technical replicates). A) Metabolic activity-concentration relationship of sample cells treated with PDMAEA polymers solutions at the 48-hour time point. B) Statistical analysis between PDMAEA polymers and PEI. C) Statistical analysis among four PDMAEA polymers groups (Two-way ANOVA, ns: $p>0.05$, *: $0.05>p>0.01$, **: $0.01>p>0.005$, ***: $0.005>p>0.001$, ****: $0.001>p$).

At 72 hours post-treatment, an uprise in metabolic activity levels across all PDMAEA samples at all concentrations were observed. In most of the concentrations, the metabolic activity is of the same level as cells treated with medium, while in some concentrations, such as 2.5, 5, and 10 μM in PS10 and PL10 treated groups, the sample viability was at ~130% or even higher (figure 5.6 (A)). Samples treated with PEI still showed the comparatively low level of viability, consistent with previous timeframes. A

significant difference in viability between PEI and PDMAEA treated samples was also observed (figure 5.6 (B)). Comparing PDMAEA samples, the difference in viability is significant between PS20 and PS10, and also between PL20 and PL10 (figure 5.6 C). The morphology of equine tenocyte cells treated with PEI solutions became rounded, and lysed cells being visible, along with squibs and cell debris.

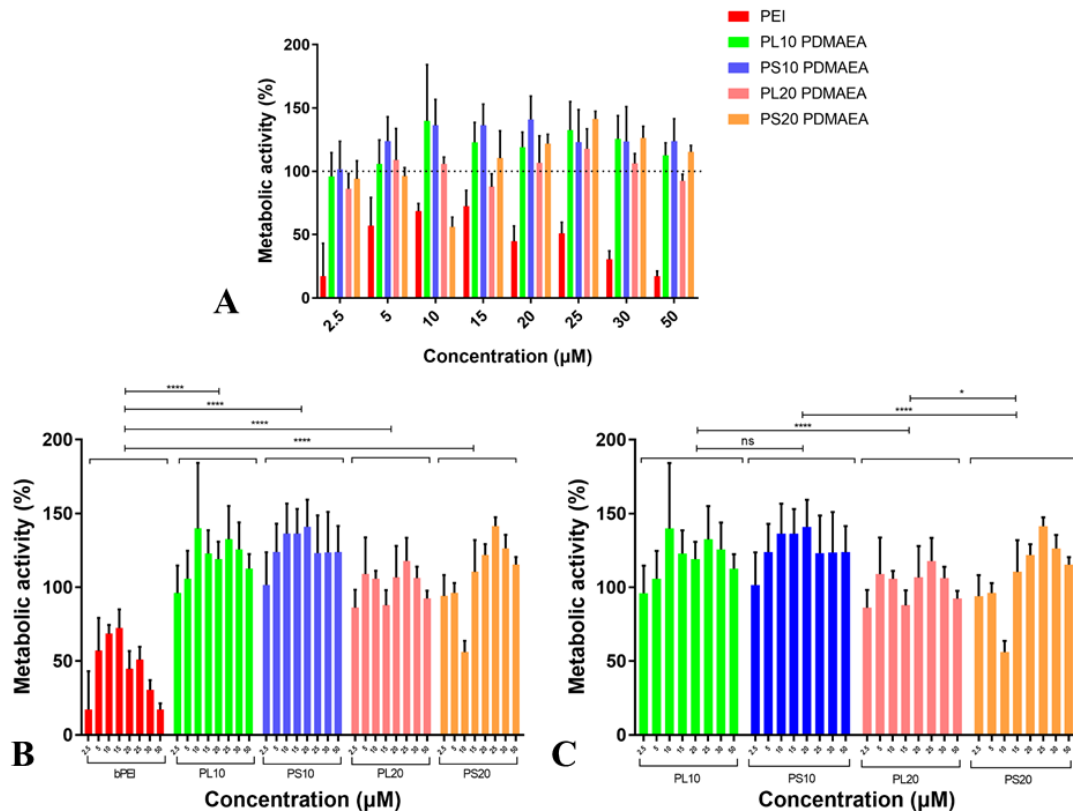


Figure 5.6 Equine tenocyte metabolic activities at 72 hours post-treatment. Samples were treated with PDMAEA polymer solutions at different concentrations, and metabolic activities were determined using MTS assay. All the results were normalised against cells treated with complete medium. The data represent mean values \pm SD, N=3 (technical replicates). A) Metabolic activity-concentration relationship of sample cells treated with PDMAEA polymers solutions at the 72-hour time point. B) Statistical analysis between PDMAEA polymers and PEI. C) Statistical analysis among four PDMAEA polymers groups (Two-way ANOVA, ns: $p>0.05$, *: $0.05>p>0.01$, **: $0.01>p>0.005$, ***: $0.005>p>0.001$, ****: $0.001>p$).

5.3.3. Cytotoxicity of PDMAEA-dsDNA Polyplexes on Equine Tenocyte using MTS Assay

Cytotoxicity of PDMAEA-dsDNA polyplexes on equine tenocytes was determined by using the MTS assay. Figure 5.7 demonstrates the viability of tenocytes treated with PDMAEA polymers at 24 hours post-treatment. The results indicate that cells treated with PS10 and PL10 PDMAEA-DNA polyplexes showed high metabolic activity in all

concentrations, while cells treated with PS20 and PL20 PDMAEA-dsDNA polyplexes showed high viability only in low concentrations (2.5-20 μ M). As the concentration increased to 50 μ M, viability dropped rapidly. Furthermore, polyplexes with high molecular weights showed higher toxicity at higher concentration. For instance, PS20-dsDNA polyplex treated group showed the viability of below 30% at 25, 30 and 50 μ M, while PL20 polymers treated groups showed the viability of below 30% at 50 μ M.

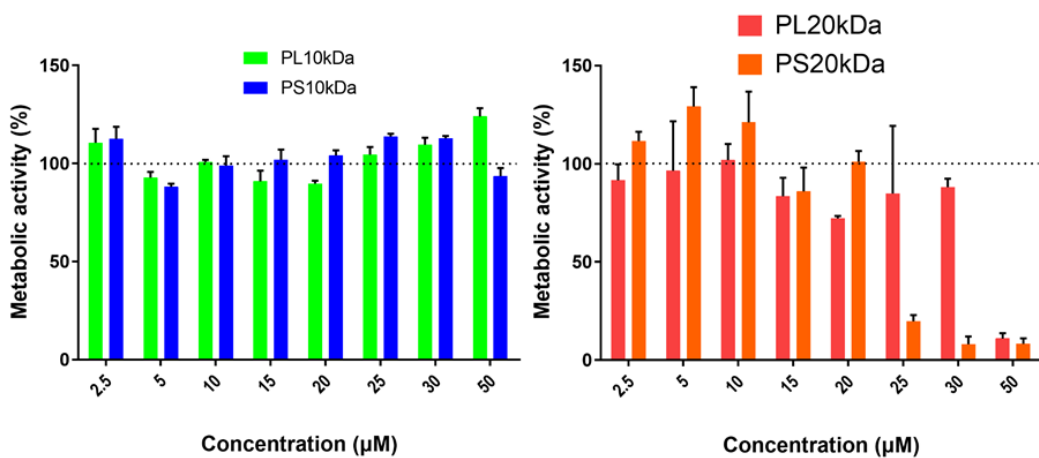


Figure 5.7 Equine tenocyte metabolic activities at 24 hours post-treatment. Samples were treated with PDMAEA-DNA polyplex solutions at different concentrations (based on polymer content), and metabolic activity was determined using MTS assay. All the results were normalised against cells treated with complete medium. The data represent mean values \pm SD, N=3 (technical replicates). Left: the metabolic activity of cells treated with PS10 and PL10 PDMAEA. Right: the metabolic activity of cells treated with PS20 and PL20 PDMAEA.

At 48 post-treatment, cells treated with PS10-DNA polyplexes and PL10-DNA polyplexes exhibited high levels of metabolic activity (figure 5.8 left). However, cells treated with PS20 and PL20 polyplexes showed relatively lower viability. Both PS20 and PL20 polyplexes treated group showed viability levels of below 50% at 50 μ M.

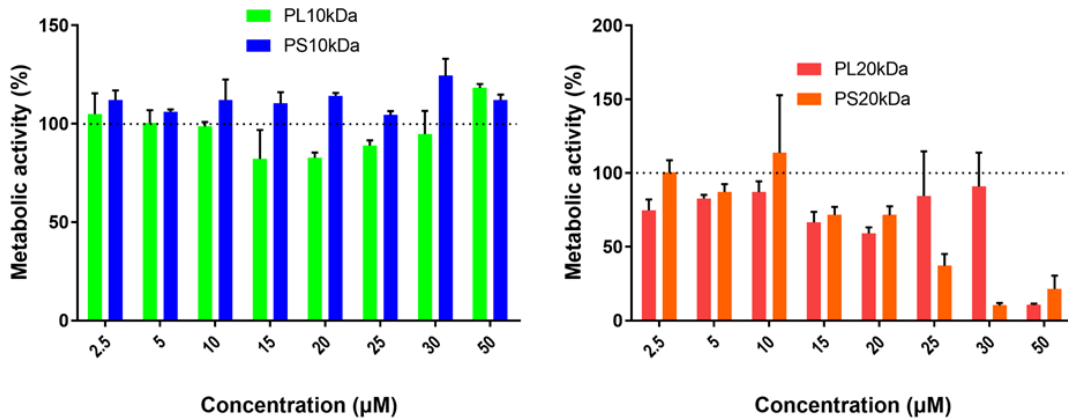


Figure 5.8 Equine tenocyte metabolic activities at 48 hours post-treatment. Samples were treated with PDMAEA-DNA polyplex solutions at different concentrations (based on polymer content), and metabolic activity was determined using MTS assay. All the results were normalised against cells treated with complete medium. The data represent mean values \pm SD, N=3 (technical replicates). Left: the metabolic activity of cells treated with PS10 and PL10 PDMAEA. Right: the metabolic activity of cells treated with PS20 and PL20 PDMAEA.

At 72 hours post-treatment, samples treated with PS10 and PL10 polyplexes showed a viability level similar to cells treated with medium for most of the concentrations, except for 20, 25 and 50 μ M, which had a slightly lower viability level.

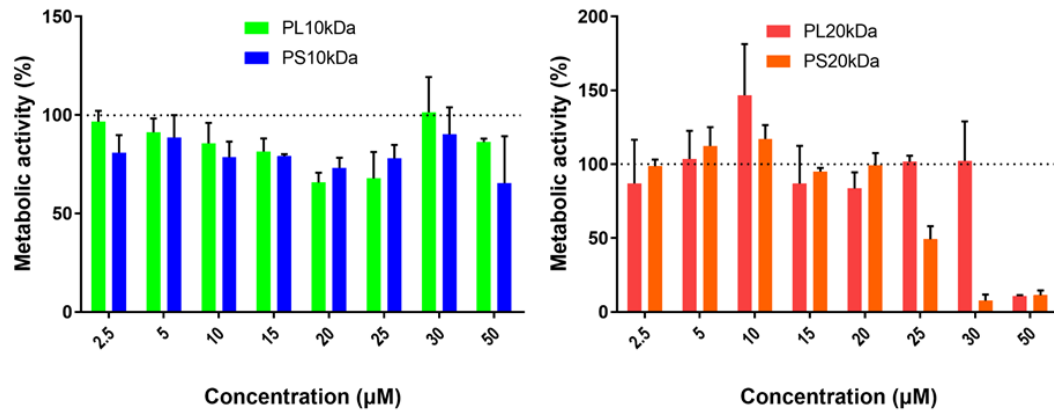


Figure 5.9 Equine tenocyte metabolic activity at 72 hours post-treatment. Samples were treated with PDMAEA-DNA polyplex solutions at different concentrations (based on polymer content), and metabolic activity was determined using MTS assay. All the results were normalised against cells treated with complete medium. The data represent mean values \pm SD, N=3 (technical replicates). Left: the metabolic activity of cells treated with PS10 and PL10 PDMAEA. Right: the metabolic activity of cells treated with PS20 and PL20 PDMAEA.

5.3.4. Cytotoxicity of PS10-siRNA Polyplexes on Equine Tenocyte Cells

PS10 was selected as a vector to condense with therapeutic siRNA to form polyplex used to transfect equine tenocyte, hence it is essential to determine the toxicity of PS10-

siRNA polyplexes. It is well established that the MTS assay measures the metabolic activity, and it is possible that the viability change is not caused by actual cell death but suppressed metabolic activity. To address this problem, the Cyquant Cell Proliferation assay, which is based on cell nucleus staining, was selected as a supplementary method. PS10-siRNA polyplex was prepared and characterised as described in chapter four. Cells were treated with PS10-siRNA polyplex solution of various concentration from 2.5-50 μ M and their metabolic activity was monitored and recorded at three different timeframes.

Firstly, the cytotoxicity of PS10-siRNA on equine tenocyte cells was determined using the MTS assay and results are shown in figure 5.10. At 24 hours post-treatment, all experimental samples showed high levels of metabolic activity (of above 90%) (figure 5.10 (A)). At 48 hours post-treatment, samples at specific concentrations, such as 2.5 and 10 μ M, showed a short-lived reduction in viability (figure 5.10 (B)). Nevertheless, at 72 hours post-treatment, viability in all samples increased to a normal level and were maintained at a metabolic activity of above 90% (figure 5.10 (C)).

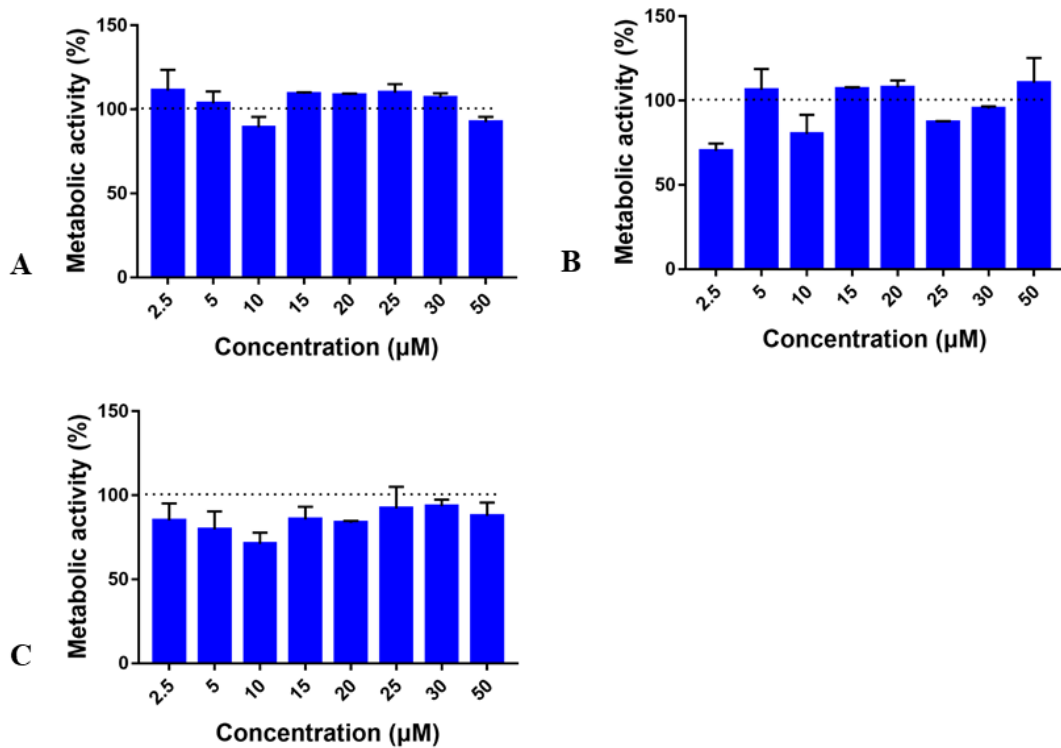


Figure 5.10 Equine tenocyte metabolic activities post-treatment. Samples were treated with PS10-siRNA polyplex solutions at different concentrations (based on polymer content), and metabolic activity was determined using MTS assay. All the results were normalised against cells treated with complete medium. The data represent mean values \pm SD, N=3 (technical replicates). A) viability at 24 hours post-treatment B) viability at 48 hours post-treatment C) viability at 72 hours post-treatment.

Secondly, the cytotoxicity of PS10-siRNA on equine tenocyte was determined using the Cyquant Cell Proliferation assay, and the results are shown in figure 5.11. The data suggest that at 24 hours post-treatment, all sample groups showed moderate viability of about 50% compared to cells treated with medium except for samples at 2.5 μ M which showed higher viability around 90%. Furthermore, it is observed that viability decreases as PS10-siRNA concentration increases. However, at 48 hours, an increase of viability across all concentrations was observed, with samples treated with 5 μ M PS10-siRNA polyplexes reaching 150%. Viability data at 72 hours post-treatment shared a similarity with data from 48 hours.

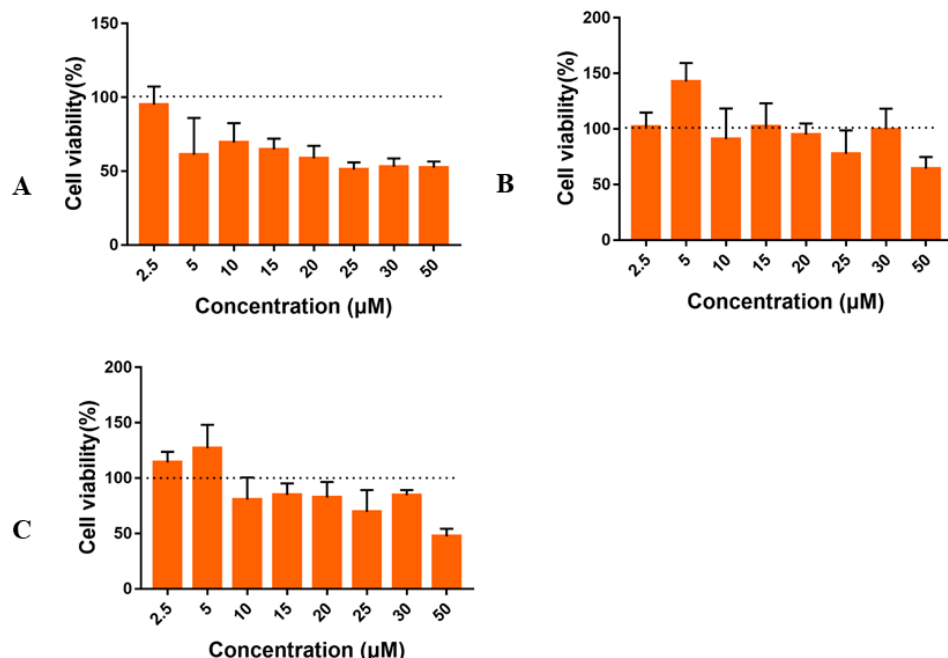


Figure 5.11 Equine tenocyte metabolic activity post-treatment. Samples were treated with PS10-siRNA polyplex solutions at different concentrations (based on polymer content), and metabolic activity was determined using Cyquant Cell Proliferation assay. All the results were normalised against cells treated with complete medium. The data represent mean values \pm SD, N=3 (technical replicates). A) viability at 24 hours post-treatment B) viability at 48 hours post-treatment C) viability at 72 hours post-treatment.

5.4. Discussion

5.4.1. PDMAEA Cytotoxicity on 3T3 Mouse Fibroblast and Equine Tenocyte

The results presented in figure 5.1 – 5.6 indicated that PL10 and PS10 showed extremely low cytotoxicity in both cultured 3T3 mouse fibroblast and equine tenocyte

samples. It is demonstrated that cells treated with PS10 and PL10 showed a similar level of viability compared to cells treated with medium across all timeframes and concentrations. However, for PL20 and PS20, the situation is more complicated. As shown in figure 5.1, 3T3 mouse fibroblast samples treated with PL20 showed similar or slightly lower metabolic activity levels compared with cells treated with medium, whereas the viability of PS20 treated group decreases dramatically as the concentration of PS20 solution exceeds 20 μ M. At 48- and 72-hour post-treatment, as shown in figure 5.2 and 5.3, all 3T3 mouse fibroblast samples treated with PL20 and PS20 solutions showed a reduction in viability compared with 24-hour group.

In addition, the cell morphology of most cells treated with PDMAEA solutions showed typical healthy morphologies, being long spindle-like shapes, with exceptions of those cells treated with PEI across all concentrations and timeframes and 3T3 mouse fibroblast cells treated with high concentration solutions of PL20 and PS20. In these groups, most of the cells changed their morphologies, cells becoming rounded, and lysed cells being visible, along with squibs and cell debris. This might suggest that in PEI treated groups and samples treated with high concentration PL20 and PS20 solutions, metabolic activity suppression and cell death might have occurred at the same time.

Summarising the finding, it is evident that PS10 and PL10 polymers showed extremely low or no cytotoxicity across all concentrations at different time points whereas the cytotoxicity of PL20 and PS20 is concentration and time-dependent.

5.4.2. The Influence of Molecular Weight and Structure on PDMAEA Cytotoxicity

One of the objectives in this study is to determine whether polymer structure and molecular weight can affect its cytotoxicity. Therefore, PDMAEA polymers of different structures and molecular weights were designed and synthesised. While comparing polymer with the same molecular weight but with different structures across different timeframes on various cell lines, it is demonstrated that for polymers with low molecular weight level (10kDa), there is no significant variation between linear and star-shaped PDMAEA, as statistics indicate in figure 5.1~5.6. However, star-shape PDMAEA polymers with a higher molecular weight (20kDa) showed slightly higher toxicity than linear ones in studies conducted with 3T3 mouse fibroblast. Though this

difference between linear and star-shaped at the high molecular weight was not observed in studies conducted in equine tenocyte samples at any timeframe. The underlying explanation of such difference could be related to the difference in biological properties between 3T3 mouse fibroblast and equine tenocyte cells, but the detailed mechanism remains unclear. One possible explanation is that the difference in metabolic activity level between mouse 3T3 fibroblast and equine tenocytes are responsible. Though no study on the direct comparison of the metabolic activity between mouse 3T3 fibroblasts and equine tenocytes has been conducted, it is reported by Zhang and his colleagues that fibroblasts have a higher activity level compared to tenocytes under the same culturing conditions ³⁴. The difference between the suppressive effect of PL20 and PS20 cells may be subtle in cell lines with a low metabolic activity, yet the difference could be amplified in cell lines with a higher metabolic activity. Therefore, the observed variance between tenocytes treated with PL20 and PS20 are less obvious compared to the results from mouse 3T3 fibroblasts.

The influence of molecular weight on the toxicity of PDMAEA could be determined by comparing the viability data of polymers with the same structure but different molecular weight. Combining all the information gathered from figure 5.1~5.6, it is shown that molecular weight has a more direct effect on PDMAEA polymers. Polymers with larger molecular weights are found to have a higher level of cytotoxicity. As demonstrated in figure 5.1~5.6, PS20 treated group have significantly lower viability compared to PS10 treated groups across all timeframes on two different cell lines. Similarly, although PL20 treated groups showed the same level of viability at 24 hours timeframes compared to PL10 treated groups, data collected at 48- and 72-hours timeframes indicated the difference in viability between PL20 and PL10. Therefore, it is concluded that for PDMAEA polymer, the cytotoxicity is proportional to its molecular weight. Similar results were reported by Cai et al., as they observed a cytotoxicity increase with the chain length in PDMAEMA polymers ³⁵. Another work conducted by Monnery and his co-workers reported the relationship of toxicity and molar mass in detail also mentioned molecular weights of a polymer could influence the cytotoxicity ^{23,24}. It is suggested that the cytotoxicity of cationic polymers is the result of a combination of the disruptive effect to the cellular membrane and damages to cellular organelles including mitochondria and endosomes^{35,21}. The relationship between increasing cytotoxicity and high molecular weight can be explained by the fact that polymers with longer chains can interact with negatively charged proteins and membranes more effectively in the

intracellular space than short ones, due to a relatively less entropic loss from the pure thermodynamic point of view³⁵. That is to say, the influence of molecular weight on the membrane-damaging potential and, subsequently, on the metabolic activity of cells are possibly the result of a more efficient interaction capability of cationic molecules with plasma membranes, and increases with increasing molecular weight, due to multiple attachments to cell surfaces³⁶.

To summarise, it is determined by data collected from this study for PDMAEA polymer, that the cytotoxicity is proportional to its molecular weight, whereas linear PDMAEA polymer showed lower cytotoxicity at higher molecular weight levels compared to star-shaped ones. However, only two different levels of molecular weight and two different structures were selected to contribute to this study, and such a small sample size would only support the phenomenon observed between linear and star-shaped PDMAEA. Further investigation with a much larger sample size including a broader range of different molecular weight, structure and cationic polymers types are required to fully determine the relationship of how molar mass and structure would affect polymer cytotoxicity.

5.4.3. Cytotoxicity of PDMAEA Polyplexes in Equine Tenocytes by MTS Assay

As described in chapter four, PDMAEA-DNA polyplexes were prepared using PDMAEA polymers and dsDNA. The PDMAEA-dsDNA polyplexes were reported to have a particle size of ~150nm and a surface charge of 40 mV. It is well established that the toxicity of polyplexes largely depends on the toxicity of polymer materials, yet some recent studies announced that properties of polyplexes such as charge ration, particle size and zeta-potential would affect the toxicity of polyplexes as well^{37,38}. Chapter four presented the formulation and properties of PDMAEA-dsDNA polyplexes. In this chapter, cytotoxicity of PDMAEA polyplexes on equine tenocyte cells was determined by MTS assay.

All PDMAEA-dsDNA polyplexes were prepared at N:P ratios of 10:1 with desired concentrations based on their polymer content. Comparing data from all three timeframes, it is concluded that at all timeframes, PS10 and PL10 polyplexes showed no or minimum level of cytotoxicity. It is noticeable that at high concentration (25-50 μ M), cells treated with PS20 and PL20 polyplexes showed reduced metabolic activity, especially PS20-dsDNA treated group (viability below 25%). It is suggested that the

particle size and zeta potential would influence polyplex toxicity, for they may affect polyplex stability. Low zeta potential may lead to aggregation of polyplexes due to the lack of repulsive forces against attraction forces and results in the formation of aggregated large particles and precipitant. The precipitant and large aggregates may interact and attach to the cell surface to form a blockage that prevents the effective delivery of nutrients and oxygen to cells, which thus leads to suppressed cellular activity and cell death³⁹. It is also reported that polyplexes bearing high positive charges can either directly or by the detachment of readily adsorbed polymers cause membrane damage⁴⁰. Furthermore, Shao et al. have shown in their publication that nanoparticles with high positive zeta potentials caused significantly higher cytotoxic effects than those with lower positive or negative zeta potentials ⁴¹. The underlying concept might be that though high positive zeta potential can provide a polyplex solution with good stability, it might also be responsible for high cytotoxicity due to the membrane disruption effect.

To summarise, results indicated that PDMAEA-dsDNA polyplexes showed low cytotoxicity at low concentration (below 20 μ M based on polymer content). This may provide vital information for the selection of optimal polyplex concentration for transfection studies. In fact, the siRNA concentration in transfection study is designed at 50 nM, and the working polyplex concentration in transfection is approximately 0.3 μ M (with PS10 polymers at a charge ratio of 10:1), which is lower than the lowest concentration (2.5 μ M) presented in this chapter and should not cause any toxicity effect.

5.4.4. Cytotoxicity of PS10-siRNA polyplex in Equine Tenocytes by using MTS and Cyquant Assays

Work presented in this chapter has employed MTS assay as the primary approach for the determination of cellular viability. MTS assay is a metabolic assay based on the metabolizing of MTS to formazan compounds. In other words, the MTS assay directly measures the metabolic activity of sample cells, rather than cell apoptosis. The same argument was raised by Moghimi et al., who suggested that the use of metabolic assay such as MTS are not indicative of apoptosis²⁹. This leads to a possibility that the reduction in viability might not be a result of toxicity of PDMAEA polymers, but a result of suppressed in cell metabolic activity. That could be one reason why in some

cases, the observed viability level is above 100% as indicated in figure 5.1~ 5.6. It is observed that in some polymer treated samples, metabolic activity would increase as the polymer concentration increases to a certain point. Beyond this point, viability would start to decrease as the concentration increases. For example, PEI treated samples showed a low level of viability at 2.5 μ M but increases as polymer concentration increased, peaking at 15 μ M. Beyond this concentration, sample viability reduced as concentration further increases. Furthermore, equine tenocytes treated with 10 μ M PL10 and PS10 solutions also showed higher metabolic activity compared to samples treated with 5 μ M PL10 and PS10 solutions, and in some cases, for example, equine tenocytes treated with PL20-dsDNA polyplexes at 24 hours post-treatment showed activity values in excess of 100% (normalised to cells treated with medium). This could possibly be explained by the higher exposure concentrations provoking greater mitochondrial activity, which has been suggested to be involved in the reduction of MTT and MTS compounds into formazan products⁴². However, increased polymer concentration provoking the mitochondrial activity cannot explain the low metabolic activity in samples treated with low concentrations of PEI, as shown in figure 5.1 – 5.6, for studies conducted by other researchers reported that at low concentrations PEI of different molecular weight and structure showed low toxicity in various cell lines^{33,43}. The low metabolic activity in samples treated with low concentration PEI solution might be due to a technical error in the preparation of PEI sample solutions that resulted in a higher final concentration than the designed value.

To address the issue that MTS assay measures the metabolic activity rather than cell death, the Cyquant Cell Proliferation assay, which is based on live cell nucleus staining fluorescence, was introduced. Due to the biological changes in apoptosis cell including blebbing and apoptotic DNA fragmentation, the DNA content in apoptosis cells was removed by washes before staining. Such an assay would reflect the number of living cells samples have at selected timeframe. Studies done by Jones et al. demonstrated that Cyquant Cell Proliferation assay is a sensitive method to determine cell number⁴⁴.

The viability of PS10-siRNA polyplex treated equine tenocytes were determined using MTS assay, and results are presented in figure 5.10 and 5.11, respectively. As exhibited in figure 5.10, PS10-siRNA polyplex treated cell showed similar viability compared to the cells treated with medium at all timeframes. However, the cell viability detected by using Cyquant Cell Proliferation assay suggests a much lower value compared to MTS

assay at 24 hours post-treatment, as illustrated in figure 5.11 (A). Data collected at 24 hours suggested that at polyplex concentration of 2.5 μ M, cells showed viability close to 100%. However, as the polyplex concentration increases, the viability gradually decreases. At the highest polyplex concentration, the viability level is around 50%. Nevertheless, with further incubation at 48 and 72 hours, an increase in cell viability was observed. The increase of viability level could be explained by the self-proliferation of tenocytes which survived the acute toxicity phase ^{45,46}. Though at high concentration, PS10-siRNA polyplex showed acute toxicity effect on the cells, this occurs only at a concentration above 10 μ M, which provided critical information in polyplex dosage selection.

5.5. Conclusion

To conclude, data from this study indicated that PDMAEA showed lower toxicity within the tested range than PEI. It is also found that in PDMAEA with a molar mass of 10kDa showed much lower toxicity than the 20kDa one. Though PS20 and PL20 PDMAEA polymers showed high toxicity at high dosage, their toxicity at low concentration was found to be acceptable. Another outcome was that within the test range of the experiment, it was found that star-shaped PDMAEA polymers showed higher toxicity level than linear ones at high molar mass in mouse 3T3 fibroblast cells. Although the data on how the structure of polymers would affect its toxicity was performed using a small sampling size, it has provided preliminary insight into the relationship between structure and PDMAEA polymer toxicity. The cytotoxicity studies of PS10-siRNA on equine tenocytes using two different assays suggested the use of PS10-siRNA polyplex at a concentration of below 5 μ M is an ideal dosage for the transfection and silencing in the future. In general, it is concluded that PDAMEA is considered as a vector with low toxicity and suitable for further testing of its transfection efficiency. In the next chapter, PS10-siRNA polyplexes were applied on TGF- β 1 stimulated equine tenocytes, and the transfection and silencing effect on *COL3 α 1* gene was evaluated by means of qPCR and immunocytochemistry.

5.6. Reference

- 1 de Fougerolles, A., Vornlocher, H. P., Maraganore, J. & Lieberman, J. Interfering with disease: a progress report on siRNA-based therapeutics. *Nat Rev Drug Discov* **6**, 443-453, doi:10.1038/nrd2310 (2007).
- 2 Kwok, A. & Hart, S. L. Comparative structural and functional studies of

nanoparticle formulations for DNA and siRNA delivery. *Nanomed-Nanotechnol* **7**, 210-219, doi:10.1016/j.nano.2010.07.005 (2011).

3 de Ilarduya, C. T., Sun, Y. & Duezguenes, N. Gene delivery by lipoplexes and polyplexes. *Eur J Pharm Sci* **40**, 159-170, doi:10.1016/j.ejps.2010.03.019 (2010).

4 Kaksonen, M. & Roux, A. Mechanisms of clathrin-mediated endocytosis. *Nat Rev Mol Cell Bio* **19**, 313-326, doi:10.1038/nrm.2017.132 (2018).

5 Gao, Y., Liu, X. L. & Li, X. R. Research progress on siRNA delivery with nonviral carriers. *Int J Nanomedicine* **6**, 1017-1025, doi:10.2147/IJN.S17040 (2011).

6 Xu, C. F. & Wang, J. Delivery systems for siRNA drug development in cancer therapy. *Asian J Pharm Sci* **10**, 1-12, doi:10.1016/j.ajps.2014.08.011 (2015).

7 vandeWetering, P., Cherng, J. Y., Talsma, H. & Hennink, W. E. Relation between transfection efficiency and cytotoxicity of poly(2-(dimethylamino)ethyl methacrylate)/plasmid complexes. *J Control Release* **49**, 59-69, doi:10.1016/S0168-3659(97)00059-X (1997).

8 Lewinski, N., Colvin, V. & Drezek, R. Cytotoxicity of nanoparticles. *Small* **4**, 26-49, doi:10.1002/smll.200700595 (2008).

9 Godbey, W. T., Wu, K. K. & Mikos, A. G. Poly(ethylenimine) and its role in gene delivery. *J Control Release* **60**, 149-160, doi:10.1016/S0168-3659(99)00090-5 (1999).

10 Sadekar, S. & Ghandehari, H. Transepithelial transport and toxicity of PAMAM dendrimers: Implications for oral drug delivery. *Adv Drug Deliver Rev* **64**, 571-588, doi:10.1016/j.addr.2011.09.010 (2012).

11 Baker, A. *et al.* Polyethylenimine (PEI) is a simple, inexpensive and effective reagent for condensing and linking plasmid DNA to adenovirus for gene delivery. *Gene Ther* **4**, 773-782, doi:DOI 10.1038/sj.gt.3300471 (1997).

12 Jiang, G., Min, S. H., Oh, E. J. & Hahn, S. K. DNA/PEI/Alginate polyplex as an efficient in vivo gene delivery system. *Biotechnol Bioproc E* **12**, 684-689, doi:10.1007/Bf02931086 (2007).

13 Peng, L. H. *et al.* Epidermal Stem Cells Manipulated by pDNA-VEGF165/CYD-PEI Nanoparticles Loaded Gelatin/beta-TCP Matrix as a Therapeutic Agent and Gene Delivery Vehicle for Wound Healing. *Mol Pharmaceut* **10**, 3090-3102, doi:10.1021/mp400162k (2013).

14 Di Gioia, S. & Conese, M. Polyethylenimine-mediated gene delivery to the lung and therapeutic applications. *Drug Des Devel Ther* **2**, 163-188 (2009).

15 Urban-Klein, B., Werth, S., Abuharbeid, S., Czubayko, F. & Aigner, A. RNAi-mediated gene-targeting through systemic application of polyethylenimine (PEI)-complexed siRNA in vivo. *Gene Ther* **12**, 461-466, doi:10.1038/sj.gt.3302425 (2005).

16 Merkel, O. M. *et al.* Nonviral siRNA Delivery to the Lung: Investigation of PEG-PEI Polyplexes and Their In Vivo Performance. *Mol Pharmaceut* **6**, 1246-1260, doi:10.1021/mp900107v (2009).

17 Convertine, A. J., Benoit, D. S. W., Duvall, C. L., Hoffman, A. S. & Stayton, P. S. Development of a novel endosomolytic diblock copolymer for siRNA delivery. *J Control Release* **133**, 221-229, doi:10.1016/j.jconrel.2008.10.004 (2009).

18 Benoit, D. S. W., Henry, S. M., Shubin, A. D., Hoffman, A. S. & Stayton, P. S. pH-Responsive Polymeric siRNA Carriers Sensitize Multidrug Resistant Ovarian Cancer Cells to Doxorubicin via Knockdown of Polo-like Kinase 1. *Mol Pharmaceut* **7**, 442-455, doi:10.1021/mp9002255 (2010).

19 Liu, C., Hillmyer, M. A. & Lodge, T. P. Multicompartment Micelles from pH-Responsive Miktoarm Star Block Terpolymers. *Langmuir* **25**, 13718-13725, doi:10.1021/la900845u (2009).

20 Truong, N. P. *et al.* Self-Catalyzed Degradable Cationic Polymer for Release of DNA. *Biomacromolecules* **12**, 3540-3548, doi:10.1021/bm2007423 (2011).

21 Monnery, B. D. *et al.* Cytotoxicity of polycations: Relationship of molecular weight and the hydrolytic theory of the mechanism of toxicity. *Int J Pharm* **521**, 249-258, doi:10.1016/j.ijpharm.2017.02.048 (2017).

22 Davaran, S. *et al.* Preparation and in vitro evaluation of linear and star-branched PLGA nanoparticles for insulin delivery. *J Bioact Compat Pol* **23**, 115-131, doi:10.1177/0883911507088276 (2008).

23 Fischer, D., Bieber, T., Li, Y. X., Elsasser, H. P. & Kissel, T. A novel non-viral vector for DNA delivery based on low molecular weight, branched polyethylenimine: Effect of molecular weight on transfection efficiency and cytotoxicity. *Pharmaceut Res* **16**, 1273-1279, doi:10.1023/A:1014861900478 (1999).

24 Monnery, B. D. *et al.* Cytotoxicity of polycations: Relationship of molecular weight and the hydrolytic theory of the mechanism of toxicity. *Int J Pharm* **521**, 249-258, doi:10.1016/j.ijpharm.2017.02.048 (2017).

25 Fischer, D., Li, Y., Ahlemeyer, B., Kriegstein, J. & Kissel, T. In vitro cytotoxicity testing of polycations: influence of polymer structure on cell viability and hemolysis. *Biomaterials* **24**, 1121-1131 (2003).

26 Safi, M. & Berret, J. F. The role of the coating and aggregation state in the interactions between iron oxide nanoparticles and 3T3 fibroblasts. *Physcs Proc* **9**, 266-269, doi:10.1016/j.phpro.2010.11.059 (2010).

27 Boussif, O. *et al.* A Versatile Vector for Gene and Oligonucleotide Transfer into Cells in Culture and in-Vivo - Polyethylenimine. *P Natl Acad Sci USA* **92**, 7297-7301, doi:DOI 10.1073/pnas.92.16.7297 (1995).

28 Agarwal, A. *et al.* Surfaces modified with nanometer-thick silver-impregnated polymeric films that kill bacteria but support growth of mammalian cells. *Biomaterials* **31**, 680-690, doi:10.1016/j.biomaterials.2009.09.092 (2010).

29 Moghimi, S. M. *et al.* A two-stage poly(ethylenimine)-mediated cytotoxicity: Implications for gene transfer/therapy. *Mol Ther* **11**, 990-995, doi:10.1016/j.moltherap.2005.02.010 (2005).

30 Choosakoonkriang, S., Lobo, B. A., Koe, G. S., Koe, J. G. & Middaugh, C. R. Biophysical characterization of PEI/DNA complexes. *J Pharm Sci* **92**, 1710-1722, doi:10.1002/jps.10437 (2003).

31 Yin, H. *et al.* Non-viral vectors for gene-based therapy. *Nature Reviews Genetics* **15**, 541-555, doi:10.1038/nrg3763 (2014).

32 Lv, H. T., Zhang, S. B., Wang, B., Cui, S. H. & Yan, J. Toxicity of cationic lipids and cationic polymers in gene delivery. *J Control Release* **114**, 100-109, doi:10.1016/j.jconrel.2006.04.014 (2006).

33 Florea, B. I., Meaney, C., Junginger, H. E. & Borchard, G. Transfection efficiency and toxicity of polyethylenimine in differentiated Calu-3 and nondifferentiated COS-1 cell cultures. *Aaps Pharmsci* **4**, doi:ARTN 12 DOI 10.1208/ps040312 (2002).

34 Zhang, Q., Yang, Z. & Peng, W. [Experimental study on biological characteristics of tenocyte and fibroblast in rabbit]. *Zhongguo Xiu Fu Chong Jian Wai Ke Za Zhi* **11**, 46-48 (1997).

35 Cai, J. G. *et al.* Effect of Chain Length on Cytotoxicity and Endocytosis of Cationic Polymers. *Macromolecules* **44**, 2050-2057, doi:10.1021/ma102498g

(2011).

36 Ryser, H. J. P. A Membrane Effect of Basic Polymers Dependent on Molecular Size. *Nature* **215**, 934-&, doi:DOI 10.1038/215934a0 (1967).

37 Oskuee, R. K. *et al.* Investigating the influence of polyplex size on toxicity properties of polyethylenimine mediated gene delivery. *Life Sci* **197**, 101-108, doi:10.1016/j.lfs.2018.02.008 (2018).

38 Gebhart, C. L. & Kabanov, A. V. Evaluation of polyplexes as gene transfer agents. *J Control Release* **73**, 401-416, doi:Doi 10.1016/S0168-3659(01)00357-1 (2001).

39 Mellati, A. *et al.* Influence of polymer molecular weight on the in vitro cytotoxicity of poly (N-isopropylacrylamide). *Mat Sci Eng C-Mater* **59**, 509-513, doi:10.1016/j.msec.2015.10.043 (2016).

40 Frohlich, E. The role of surface charge in cellular uptake and cytotoxicity of medical nanoparticles. *Int J Nanomed* **7**, 5577-5591, doi:10.2147/Ijn.S36111 (2012).

41 Shao, X. R. *et al.* Independent effect of polymeric nanoparticle zeta potential/surface charge, on their cytotoxicity and affinity to cells. *Cell Prolif* **48**, 465-474, doi:10.1111/cpr.12192 (2015).

42 Saravanan, B. C. *et al.* A rapid MTT colorimetric assay to assess the proliferative index of two Indian strains of Theileria annulata. *Vet Parasitol* **113**, 211-216 (2003).

43 Yan, X. B. *et al.* Amphiphilic polyethylenimine (PEI) as highly efficient non-viral gene carrier. *Org Biomol Chem* **12**, 1975-1982, doi:10.1039/c3ob42279h (2014).

44 Jones, L. J., Gray, M., Yue, S. T., Haugland, R. P. & Singer, V. L. Sensitive determination of cell number using the CyQUANT (R) cell proliferation assay. *J Immunol Methods* **254**, 85-98, doi:Doi 10.1016/S0022-1759(01)00404-5 (2001).

45 Bisht, S. *et al.* Polymeric nanoparticle-encapsulated curcumin ("nanocurcumin"): a novel strategy for human cancer therapy. *J Nanobiotechnology* **5**, 3, doi:10.1186/1477-3155-5-3 (2007).

46 Arote, R. *et al.* A biodegradable poly(ester amine) based on polycaprolactone and polyethylenimine as a gene carrier. *Biomaterials* **28**, 735-744, doi:10.1016/j.biomaterials.2006.09.028 (2007).

Chapter 6

Transfection Efficiency of PDMEAE- siRNA Polyplexes Based on qPCR and Immunocytochemistry

6. Chapter 6 Transfection Efficiency of PDMEAE-siRNA Polyplexes Based on qPCR and Immunocytochemistry

6.1. Introduction

Tendon injuries are one of the most common types of soft tissue injury affecting millions worldwide, and currently, there is a lack of effective treatment in a clinical situation¹. Nowadays, the most common applied clinical therapeutic approach is the use of Non-steroidal anti-inflammatory drugs (NSAIDs) for pain control and surgical operation, which requires a long recovery period and has a risk of re-injury^{2,3}. Therefore, there is an urgent need for novel effective therapeutic strategies for tendon injury.

In recent years, gene therapy has attracted enormous attention as a novel therapeutic strategy for tendon injury and numerous studies have been conducted. Earlier in 2001, Luo et al. reported the use of adenovirus to transfer the *BMP-12* gene into chicken tenocytes *in vitro* to increase collagen type I synthesis⁴. Another study by Suwalski et al. suggested that the delivery of pDNA encoding *PDGF* gene successfully improved the healing of injured tendons in a rat model and achieved a lasting expression of two weeks⁵. The use of the liposome-based system to transfet the fibromodulin gene was reported by Delalande et al. The delivery of fibromodulin gene has achieved fast wound closure speed and a pronounced migration of tenocytes *in vivo* and *in vitro*⁶. A more recent study by Abbah et al. showed the use of pDNAs encoding decorin and interleukin-10 to co-transfect human tenocytes via polyplexes to suppress the expression of TGF- β and demonstrated positive results *in vitro*⁷. The literature mentioned above and many more indicated that the gene therapy has a prominent potential in the future therapy of tendon injury.

However, one of the issues the researchers confront is that the repaired tendon has a weakened mechanical property compared with the native tendon. This is believed to be caused by the formation of scar tissue during the healing process^{1,8}. In native tendon tissue, collagen type I accounts for 95% of the extracellular matrix, which is highly organised, compact, aligned and responsible for the mechanical strength of tendon tissue⁹. In contrast, collagen type III has a relatively low abundance but has an important role in the healing process. The upregulation of collagen type III, during the healing process and in degenerative conditions, may cause weakening of the mechanical

strength of the tissue, since type III fibres are thinner, smaller, disorganised and more extensible than type I due to less crosslinking sites present in type III collagen ³. Moreover, upregulation of type III collagen could form adhesion sites and reduce lubrication between the tendon and surrounding tissues causing friction, pain or even scar tissue formation ¹⁰. It appears that collagen type III and its regulator gene could be a potential target for gene therapy in tendon injury.

In order to gain a deeper understanding of collagen type III upregulation, Eriksen et al, compared the amount of collagen type I and III at the rupture and two other sites of the same tendon tissue and showed collagen type content was significantly higher at the rupture site, whereas no changes were observed for the two healthier sites ¹¹. Attempts to diminish the adhesion by targeting related genes has been reported by Chen et al. It is reported that *RelA/p65* inhibition may be a promising therapeutic approach to prevent tendon adhesion ¹². A similar study by Freeberg et al. targeted *Serpine1* gene, which is related to the suppression of protease activity such as MMP, aiming to enhance the activity of MMPs and further reduce the formation of adhesion in tendon tissues¹³. Moreover, the studies by Chen et al. and Freeberg et al. both employed siRNA as a means to suppress the expression of their target gene.

Several studies have involved the application of small interfering RNA (siRNA) as a therapeutic molecule to alter collagen synthesis in tendon repair. siRNA has gained popularity from its ability to knock down a specific selected gene, thereby leading to down-regulation of target proteins. For instance, Ruan et al. reported targeting extracellular signal-regulated kinase (*ERK 2*), which is involved in the regulation of collagen expression and proliferation of fibroblast cells, as well as joint adhesion. In the study, an intra-articular administration of siRNA was achieved through the use of lentivirus and resulted in a reduction of joint adhesion ¹⁴. In addition, another study by Lu et al. showed the efficacy of siRNA in regulating the isoform of collagen type V. Collagen type V was reported to be significantly elevated in tendon healing and play an important role in fibrillogenesis. Lu et al. reported the selective silencing of the collagen V $\alpha 2$ chain in cultured tenocytes resulted in similar fibre morphology as normal tenocytes. On the other hand, treating the tenocytes with collagen V $\alpha 1$ chain siRNA resulted in smaller and abnormal fibre morphology, which indicated that the influence of $\alpha 1$ chain is more apparent than the $\alpha 2$ chain on the formation of fibrils ¹⁵. To summarise, these studies demonstrated great potential for siRNA application and local

delivery of siRNA to control collagen expression during the healing process. Nonetheless, there is a lack of research studies on the application of siRNA targeting collagen type III in the treatment of tendon injuries. However, one of the challenges in gene delivery, including siRNA, is the need for a safe and efficient delivery system.

The work presented in previous chapters has described the synthesis of a new synthetic polymer-based gene delivery system from four-armed Poly[2-(Dimethylamino) ethyl acrylate] (PDMAEA). It is also demonstrated that such cationic polymer-based delivery systems have good condensation ability with low toxicity. Considering the balance between nucleic acid binding ability and toxicity, PDMAEA polymer PS10 was selected to condense with siRNA, forming PS10-siRNA polyplex as described in chapter four.

Aim of the chapter:

The aim of this chapter is to provide an insight into the effects that PS10-siRNA has on the expression of *COL3α1* gene and related protein production. In this chapter, the transfection efficiency of PS10-siRNA polyplex was evaluated on TGF-β1 stimulated equine tenocytes. The stimulation effect of different dosages and times of TGF-β1 stimulation on *COL3α1* gene were determined by qPCR. The expression of *COL3α1* gene in equine tenocytes was first up-regulated by the addition of TGF-β1. Afterwards, the expression level of the *COL3α1* gene was knocked down by using PS10-siRNA polyplexes containing *COL3α1* gene-specific siRNA. The post-transfection expression level of *COL3α1* gene in all samples was analysed by qPCR, and the collagen type III protein expression in samples was investigated by immunocytochemistry.

The main objectives:

- Study the TGF-β1 stimulation on *COL3α1* gene at different concentrations and stimulus times.
- Determine the *COL3α1* gene expression level in TGF-β1 stimulated equine tenocytes transfected with PS10-siRNA by qPCR over different timeframes.
- Examine the collagen type III production level of TGF-β1 stimulated equine tenocytes transfected with PS10-siRNA by immunocytochemistry.

6.2. Material & Methods

6.2.1. Materials

The details of the materials used in this chapter can be found in chapter two section 2.2.

6.2.2. Effect of TGF- β 1 Stimulation on *COL3 α 1* Gene by qPCR and Determination of Optimal Dosage

Ten micrograms of Recombinant Human Transforming Growth Factor- β 1 (TGF- β 1) was reconstituted in 100 μ L of 10 mM citric acid (pH 3.0) and further diluted to 10 ng/ μ L by adding PBS buffer with 0.1% BSA as suggested in manufacturer's protocol. Adult equine tendon cells were cultured in six-well plates at a density of 600,000 cells/well in 2 mL of complete DMEM medium and incubated for 24 hours before treatment. To determine the desired stimulation dose of TGF- β 1, the culture medium was replaced with complete DMEM medium supplemented with TGF- β 1 at different final concentrations (0.5, 1, 10, 25 and 50 ng/mL). Cells were then incubated for 24 hours prior to harvest. To determine the effect of TGF- β 1 on the upregulation of the *COL3 α 1* gene, cells were cultured under the same conditions as described previously but replacing medium supplemented with TGF- β 1 at a concentration of 10 ng/mL. Cells were then harvested after 24, 48 and 72 hours. The harvested cells were lysed, RNA extracted, and reverse transcribed to cDNA and finally analysed by qPCR, as described in chapter two.

6.2.3. Transfection of Equine Tenocyte using PS10-siRNA Polyplex

PS10-siRNA polyplex was prepared as described in the previous chapter. The final siRNA concentration used for transfection was 50 nM. The siRNA buffer was prepared according to the manufacturer's protocol. To briefly describe, 0.303 g of Tris-base and 0.29 g of sodium chloride was dissolved in 50 mL of bio-reagent grade water before pressed through a 0.22 μ m pore size membrane filter to make 50 mL of the buffer with 100 mM NaCl and 50 mM Tris-base. The siRNA was received as a dried powder. Tubes were quickly spun down before reconstituting by adding siRNA buffer solution. Appropriate bio-reagent grade water was added to reach a concentration of 100 μ M. Then the siRNA solution was aliquoted into 10*10 μ L 100 μ M (1000 pmol/aliquot)

aliquots and kept at -80°C. Cultured adult equine tendon cells were seeded onto 6-well plates at a density of 600,000 cells/well. Cells were incubated for 24 hours to allow attachment, and then the media was supplemented with TGF- β 1 at 10 ng/mL.

Twenty-four hours after TGF- β 1 stimulation, the cells were treated with samples including siRNA solution, PS10 solution, PS10-random-siRNA polyplex, PS10-siRNA polyplex and PEI-siRNA polyplex. The cells were incubated for 24, 48 and 72 hours before harvesting, followed by RNA extraction and reverse transcription. *COL3 α 1* and endogenous control *18S* gene mRNA levels were analysed by qPCR. Unstimulated cells with no TGF- β 1 and cells treated with PS10-random-siRNA were used as negative control, whereas PEI-siRNA was used as positive control. The data are presented as relative expression (fold change) normalised using the *18s* reference gene. All the transfection experiments were performed in duplicates.

6.2.4. Immunocytochemistry on Equine Tenocyte Cells

Cells were seeded at a density of 15,000 cells/well in a total volume of 500 μ L of complete DMEM onto a 24-well plate and left at 37°C for 24 hours. Culture medium was replaced with 500 μ L of complete DMEM supplemented with TGF- β 1 at a concentration of 1 ng/mL (due to the change of cell density) and incubated for 24 hours. Cells were then treated with samples including siRNA solution, PS10 solution, PS10-random-siRNA polyplex, PS10-siRNA polyplex and PEI-siRNA polyplex at a final siRNA concentration of 50 nM (25pmol/ well). After treatment, cells were incubated for 72 hours before the medium was removed and washed three times with PBS. 500 μ L of 3%PFA was added to each well and incubated at room temperature for 20 minutes. Subsequently, PFA was removed, and the cells were washed three times with ice-cold PBS and kept in fresh PBS before permeabilization. PBS was removed before adding 0.5 mL/well 0.1% Triton-X-100 PBS solution and incubated for one hour at room temperature. Cells were washed three times with cold sterile PBS and then incubated with blocking buffer (2.5% horse serum in PBS) at room temperature for 20 minutes. Blocking buffer was removed and the cells were then incubated with the rabbit anti-collagen III primary antibody diluted to the appropriate concentration (1:100 dilution to 10 μ g/ml) in PBS in a humid box overnight at 4°C. After overnight incubation, samples were washed three times and incubated with goat anti-rabbit secondary antibody at an appropriate concentration (1:100 dilution) in PBS for three hours at room temperature.

Samples were then washed three times with PBS and rinsed with milliQ water, and then mounted with Vectashield® hard mounting media containing DAPI (cat. no. H-1500 vector laboratories). Imaging was performed using a Zeiss Axioplan 2ie microscope using Axiovision software with FITC or DAPI filter. Pictures were taken with a 20x magnification PlanApochromat (0.6 NA) objective and a Zeiss AxioCam HRm CCD camera.

6.3. Results

6.3.1. TGF- β 1 Stimulation on *COL3 α 1* Gene Expression

TGF- β 1 was used to increase the synthesis of type III collagen in cultured equine tenocytes. Cultured tenocytes were supplemented with different concentrations of TGF- β 1 (0.5, 1, 10, 25 and 50 ng/mL) and incubated for 24 hours. The results in figure 6.1 showed the relative expression of the *COL3 α 1* gene normalized to the *18s* reference gene, both measured by qPCR. Due to the lack of sufficient replicates, it wasn't able to perform any statistical analysis to determine the variation between groups. Nevertheless, some indications can be observed in these data. The data suggested that the relative gene expression of *COL3 α 1* (up-regulation fold change) increased in a dose-dependent manner after TGF- β 1 stimulation, and the expression reached three-fold when stimulated with TGF- β 1 at a concentration of 10 ng/mL. However, the relative expression gradually decreased to two-fold and one and a half fold as the TGF- β 1 concentration increased to 25 and 50 ng/mL. Based on the results, it is considered that 10 ng/mL is the optimal stimulus concentration and was applied in the forthcoming experiments.

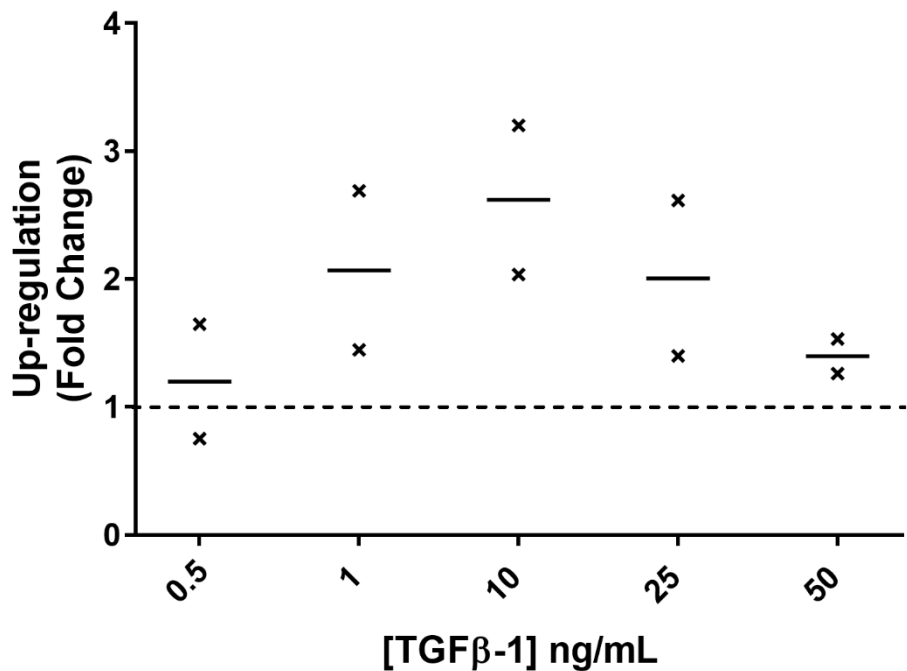


Figure 6.1 Effect of TGF- β 1 treatment on cultured equine tenocytes treated with different concentrations of TGF- β 1 for 24 hours. The *COL3 α 1* relative expression was normalised to *18s* reference gene. The relative expression at different concentrations were normalised to the untreated group. The data represent individual values and mean values, N=2 (technical replicated).

In addition, to study the stimulus effect of TGF- β 1 on *COL3 α 1* gene expression over time, cultured tenocytes were treated with TGF- β 1 at a concentration of 10ng/mL and incubated for 24, 48 and 72 hours. The results are presented in figure 6.2, showing that the fold change of *COL3 α 1* gene was higher in TGF- β 1 stimulated samples compared to unstimulated samples at all timeframes. Furthermore, the *COL3 α 1* gene expression level, in the presence of TGF- β 1, was slightly higher at 48 hours, with a mean up-regulation fold change of three compared to an ~ two-fold change at 24 and 72 hours. However, due to the lack of sufficient replicates, it wasn't able to perform any statistical analysis to determine the variation between the expression levels at different timeframes.

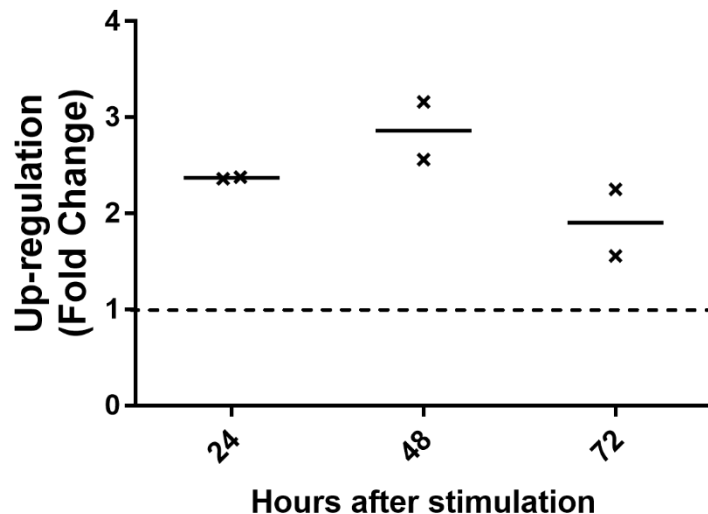


Figure 6.2 TGF- β 1 stimulation effect on the expression of *COL3α1* gene in equine tenocytes over time. Cultured equine tenocytes were treated with 10 ng/mL of TGF- β 1 and incubated for 24, 48 and 72 hours. The *COL3α1* gene relative expression was normalised to *18s* reference gene. The relative expression was normalised to the untreated group. The dotted line indicates the *COL3α1* gene expression level of untreated groups. The data represent individual values and mean values, N=2 (technical replicates).

6.3.2. Silencing Effect of siRNA Interference using PS10 as a Delivery Vector on TGF- β 1 Stimulated Cells

The silencing effect of PS10-siRNA polyplex on *COL3α1* gene in the TGF- β 1 stimulated equine tenocytes cultured cells was investigated. Tenocytes were treated with PS10-siRNA polyplexes, as well as other controls. The results are shown in figure 6.3, the mRNA levels being presented as a up-regulated fold change in all samples, determined by qPCR at three different timeframes.

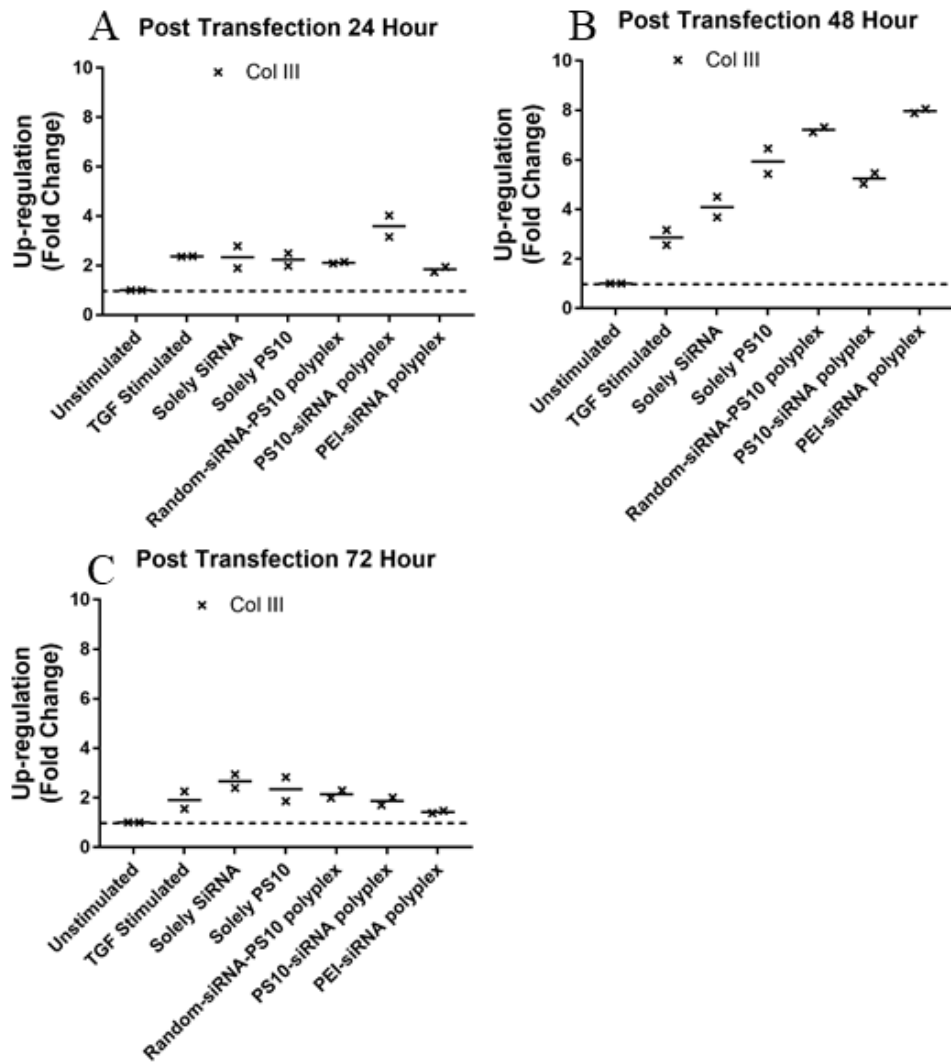


Figure 6.3 PS10-siRNA mediated silencing of *COL3α1* in cultured equine tenocytes. The relative expression of *COL3α1* was monitored and presented. Relative gene expression of cultured tenocytes stimulated with TGF- β 1 at 10 ng/ml concentration was calculated and presented at (A) 24 hours, (B) 48 hours and (C) 72 hours. The *COL3α1* relative expression was normalized to *18s* reference gene. The data represent individual values (scattered dots) and mean values, N=2(technical replicates).

To describe, at 24 hours post-treatment (figure 6.3 A), an up-regulated expression of *COL3α1* gene was observed in all treated samples (about 1.5-fold to 2-fold change), while PS10-siRNA polyplexes treated sample had a slightly higher fold change of about 3.5-fold, compared to untreated samples. Furthermore, the results at 48 hours post-treatment (figure 6.3 B) revealed that the expression level of the *COL3α1* gene increased dramatically. When normalized with unstimulated cells, the expression of TGF- β 1 solely treated group showed the same level as at 24 hours, while other treated samples showed significant increases. Samples treated solely with PS10, PS10-siRNA polyplex, PS10-random-siRNA polyplex and PEI-siRNA polyplex showed a fold

change of about 8-fold or higher when normalized with the unstimulated sample. At 72 hours post-treatment, the expression level of *COL3α1* reduced to the two-fold level in all samples. However, due to the lack of enough replicates, it wasn't able to perform statistical analysis to determine the variation between different groups. Nevertheless, some trend and indications can be observed in these data. Interestingly, the PS10-siRNA polyplex treated group displayed a lower expression level (about 20% lower) of *COL3α1* gene at 48 hours, compared to non-therapeutic PS10-random-siRNA treated group, indicating a possible PS-siRNA mediated-silencing (knockdown) effect. In contrast, the PEI-siRNA complex treated group showed no significant reduction compared to the non-therapeutic PS10- random -siRNA treated group. Statistical analysis indicated that the difference between PS10-random-siRNA polyplexes treated group and PS10-siRNA polyplexes treated samples are significant. Contrarily, and as shown in figure 6.3, at 72 hours post-transfection, the PS10-siRNA treated group showed no significant silencing effect compared to non-therapeutic PS10-random-siRNA treated ones, while PEI-siRNA polyplex showed a reduction of 0.5-fold compared to the non-therapeutic PS10-random-siRNA treated samples. Nonetheless, the overall fold change of *COL3α1* was lower at 72 hours post-treatment, compared to the 48 hours post-treatment.

6.3.3. Immunocytochemistry

Previously stimulated tenocytes with TGF-β1 were subsequently treated with PS10-siRNA polyplex and other controls and incubated for 72 hours before samples were fixed for immunocytochemical staining. As shown in figure 6.4, the nuclei in all samples were stained with DAPI (blue), and collagen type III was labelled with a fluorescent secondary antibody and coloured in green. Images captured indicated both production and distribution of collagen type III within the cellular cytoplasm and in the extracellular space of the cells. Note that due to the possible toxicity and manipulation during the immunocytochemistry process, the cell density is significantly lower than other samples.

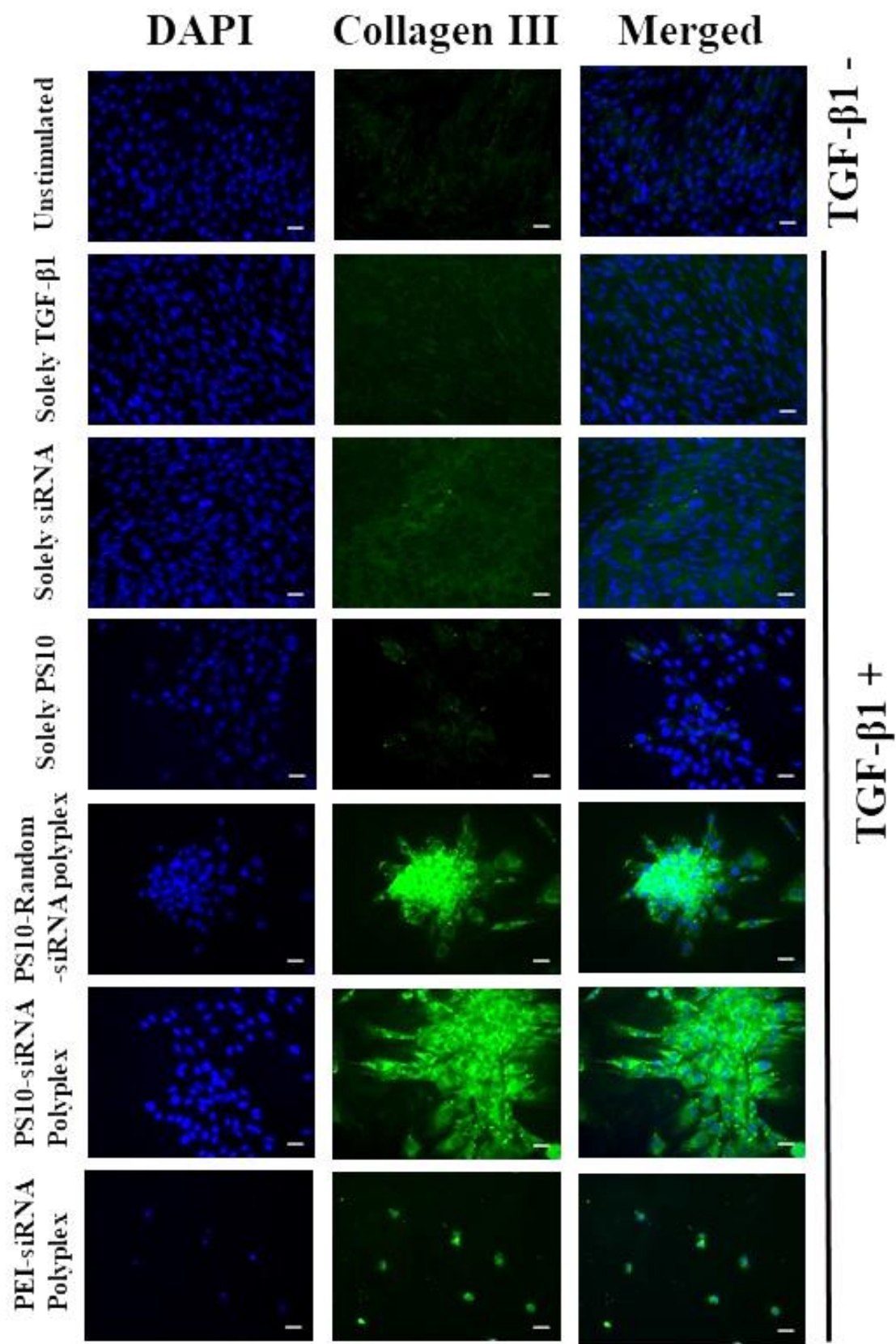


Figure 6.4 Immunocytochemistry of TGF- β 1 stimulated tenocytes treated with PS10-siRNA polyplex as well as other controls. The scale bar represents 30 μ m. Exposure time was fixed at 650 ms. Nuclei were stained with DAPI (blue) and Collagen III was coloured in green. Merged images were created with Image J software.

After fixation of the exposure time while capturing the images, fluorescent intensity analysis was carried in order to quantify the amount of collagen type III within the sample. Three random fields on the sample slip were selected, exposed and analysed. The overall fluorescent intensity of the selected field was determined and normalized by the total number of cells within the field. The data are presented in table 6.1.

Table 6.1 Normalised fluorescent intensity of TGF- β 1 stimulated tenocytes treated with PS10-siRNA polyplex as well as other controls. The data were presented as the mean value of three random fields with SD.

	Unstimulated	Solely TGF β 1	Solely siRNA	Solely PS10	PS10-random-siRNA polyplex	PS10-siRNA polyplex	PEI-siRNA polyplex
Mean intensity	0.067	0.084	0.073	0.150	0.373	0.385	N/A
SD	0.002	0.004	0.009	0.009	0.130	0.035	N/A

Based on the data, all TGF β 1 treated samples showed higher fluorescent intensity levels, compared to the unstimulated group. Moreover, both the PS10-siRNA polyplex treated group and the PS-10-random-siRNA treated group showed much higher fluorescent intensity, compared to the other groups. Specifically, it was about five times higher than the unstimulated group, solely TGF- β 1 treated and solely siRNA treated group. Note that the cell number in PEI-siRNA polyplexes sample groups are significantly lower than other groups, and the intensity signal is not enough for analysis. Therefore, the mean intensity of samples treated with PEI-siRNA polyplexes has not been reported.

6.4. Discussion

- TGF- β 1 stimulation on *COL3 α 1* gene in cultured tenocytes

TGF- β 1 was used to stimulate the *COL3 α 1* gene expression in cultured equine tenocytes in order to mimic the pathological process in injured tendon tissue. Though it would be ideal to use equine tenocytes isolated from injury sites of an adult horse, rather than cells isolated from healthy tendon tissue, due to the complexity of isolating the cells from freshly wounded horse tendon, lack of fresh biomaterials and considering that the up-regulation of *COL3 α 1* gene expression in an injured tendon is a result of multiple factors involving inflammatory cells and cytokines, an alternative approach of using TGF- β 1 to stimulate cells from a healthy tendon was adopted. A similar approach has also been reported by Freeberg et al.¹³. The effect of the concentration and incubation time of TGF- β 1 stimulation in cultured equine tenocytes was investigated by qPCR to determine the relative expression of *COL3 α 1* gene. The results revealed that

the optimal TGF- β 1 stimulation dosage for *COL3 α 1* gene is 10 ng/mL. Moreover, the stimulation effect is maximized at 48 hours post-stimulation.

- Silencing of *COL3 α 1* gene by PS10-siRNA polyplex delivery

The potential of the PS10-siRNA polyplex in specifically silencing the *COL3 α 1* gene expression in TGF- β 1 stimulated tenocytes was studied. Apart from the therapeutic PS10-siRNA polyplex, a variety of controls were also introduced to TGF- β 1 stimulated tenocytes. A randomly sequenced siRNA, considered to be non-*COL3 α 1* specific, was purchased and used to form PS-random-siRNA polyplex which was employed as the negative control. PEI-siRNA polyplex was prepared by using 10kDa branched PEI and *COL3 α 1* specific siRNA and employed as the positive control. The PEI-siRNA polyplex was designed to carry the same amount of siRNA as the PS10-siRNA polyplexes and was prepared with same N:P ratio. Other control groups including PS10 group (only PS10) and siRNA group (only siRNA) were also prepared to study the potential effect they might have on the expression level of *COL3 α 1* gene. TGF- β 1 treated group (only TGF- β 1), and unstimulated groups were designed to provide a base-line in both stimulated and non-stimulated situations, respectively. Three different timeframes of 24-, 48- and 72-hours post-treatment were designed to investigate the influence of incubation time on the *COL3 α 1* gene expression. The mRNA level of *COL3 α 1* gene was analysed in all samples and normalized with *18s* gene mRNA level. The choice of *18s* gene as a reference gene is based on previous studies conducted in equine cell lines^{16,17}.

At 24 hours post-transfection, all samples showed an increase of about 2-fold in the expression level of *COL3 α 1* gene. At 48 hours post-transfection, the up-regulation of *COL3 α 1* gene expression peaked in samples treated with PS10-siRNA polyplex, PS10-random-siRNAPolyplex and PEI-siRNA polyplex, with ~8-fold change in their expression level. This is most probably because the highest TGF- β 1 stimulation of *COL3 α 1* synthesis was achieved at 48 hours. At 72 hours post-transfection, the level of expression *COL3 α 1* gene reduced to about 2-fold compared to the unstimulated group. It seems that all polyplexes (PS10-siRNA polyplex, PS10-random-siRNA polyplex and PEI-siRNA polyplex) treated samples showed either similar (at 24- and 72-hours post-transfection) or higher (at 48 hours post-transfection) levels of *COL3 α 1* expression, compared to the unstimulated group and to the solely TGF- β 1 treated group. Though no studies have reported the stimulus effect of PDMAEA polymer on the up-regulation of *COL3 α 1* gene, it was suggested by De Rosa et al. that the cationic charges on polymer

surface increased the synthesis of collagen I and III ¹⁸. One explanation is that the polycations coupling to plasma membrane lipid bilayers can induce a redistribution of oppositely charged lipids into regions known as domains ¹⁹. The formation of domains can influence cellular membrane functioning, such as altering the local transmembrane permeability or act as sequester enzyme substrates and thereby controlling enzymatic activity and/or cell signalling processes ¹⁸.

Though it seems that polyplexes treated groups have triggered an unexpected up-regulation of *COL3α1* gene at 48 hours, by comparison between the polyplexes treated groups, the data suggested that the siRNA induced silencing effect might be successful. As demonstrated in figure 6.3, the PS10-siRNA polyplex treated group showed about 20% lower expression level compared to the PS10-random-siRNA treated group, which is the negative control, at 48 hours post-transfection. This is possibly due to the *COL3α1* gene-specific siRNA mediated RNAi under the delivery of PS10 polymer. However, due to the unexpected increase in *COL3α1* gene expression in the polyplexes treated samples, it might not accurately reflect the silencing effect, and further study is required.

- Immunocytochemistry on PS10-siRNA transfected tenocytes

The immunocytochemistry of TGF-β1 stimulated tenocytes transfected with PS10-siRNA polyplexes at 72 hours post-transfection was demonstrated in figure 6.4, as well as other control groups. The newly synthesised type III collagen are typically secreted into ECM, therefore most of the type III collagen is expected to be found outside of the cells. However, in this study, to examine the total type III collagen produced, cells were permeabilised to allow staining of collagen both inside and outside of the cells. Since the tenocytes were permeabilized before conjugation with primary antibody, the fluorescent signal indicated the localisation of intracellular collagen type III as well as on the cell surface. The exposure time during the imaging is fixed at 650 ms, and intensity analysis could be performed to quantify the amount of collagen type III protein. As shown in table 6.1, the samples treated with PS10-siRNA polyplex and PS10-random-siRNA show much higher intensities compared to other control groups, indicating that a larger amount of collagen type III protein was produced. The data properly correlate with qPCR data at 48 hours post-treatment, connecting the high mRNA level to the high protein production. Unfortunately, possibly due to the toxicity of PEI, the cell density in the PEI-siRNA polyplexes treated group is significantly lower

than other groups, and might not correctly reflect the collagen type III production, hence it was not possible to perform intensity analysis on those samples.

6.5. Conclusion

In this chapter, the transfection efficiency of PS-siRNA polyplex has been evaluated on TGF- β 1 stimulated equine tenocytes. Firstly, the *COL3 α 1* expression level in cultured tenocytes was successfully stimulated by adding exogenous TGF- β 1. Cells treated with an optimal dose of TGF- β 1 were incubated with PS-10 siRNA, over 24, 48 and 72 hours, as well as other controls. The results of qPCR analysis suggested that cells incubated with PS-siRNA polyplex showed about a 20% lower expression level in *COL3 α 1* gene compared with non-specific siRNA-PS10 polyplex treated cells at 48 hours timeframe, at which the expression of *COL3 α 1* gene is maximised. However, data analysis also indicated that all cells treated with TGF- β 1 and PS10 polyplexes showed a high expression level of *COL3 α 1* gene compared to cells treated solely with TGF- β 1. The mechanism behind this phenomenon remains unclear and possible explanation has been discussed, further studies might be required to provide a detail and more reliable explanation on this observation. The immunocytochemistry at 72 hours confirmed the production of collagen type III protein in all stimulated samples, while PS containing polyplex treated samples exhibited a higher fluorescent intensity, which is consistent with data acquired from qPCR. To summarise, results from this chapter might have suggested a successful transfection of tenocytes using PS10-siRNA polyplex, though the suppression effect of *COL3 α 1* gene is unsatisfactory due to an unexpected stimulation of *COL3 α 1* gene in all PS10 treated samples. Further study into the cause of the PS10 trigger *COL3 α 1* gene up-regulation is required.

6.6. References

- 1 Docheva, D., Muller, S. A., Majewski, M. & Evans, C. H. Biologics for tendon repair. *Adv Drug Deliver Rev* **84**, 222-239, doi:10.1016/j.addr.2014.11.015 (2015).
- 2 Thevendran, G., Sarraf, K. M., Patel, N. K., Sadri, A. & Rosenfeld, P. The ruptured Achilles tendon: a current overview from biology of rupture to treatment. *Musculoskelet Surg* **97**, 9-20, doi:10.1007/s12306-013-0251-6 (2013).
- 3 Riley, G. Tendinopathy--from basic science to treatment. *Nat Clin Pract Rheumatol* **4**, 82-89, doi:10.1038/ncprheum0700 (2008).
- 4 Lou, J. R., Tu, Y. Z., Burns, M., Silva, M. J. & Manske, P. BMP-12 gene transfer augmentation of lacerated tendon repair. *J Orthopaed Res* **19**, 1199-1202, doi:10.1016/S0736-0266(01)00042-0 (2001).
- 5 Suwalski, A. *et al.* Accelerated Achilles tendon healing by PDGF gene delivery

with mesoporous silica nanoparticles. *Biomaterials* **31**, 5237-5245, doi:10.1016/j.biomaterials.2010.02.077 (2010).

6 Delalande, A. *et al.* Enhanced Achilles tendon healing by fibromodulin gene transfer. *Nanomedicine* **11**, 1735-1744, doi:10.1016/j.nano.2015.05.004 (2015).

7 Abbah, S. A. *et al.* Co-transfection of decorin and interleukin-10 modulates pro-fibrotic extracellular matrix gene expression in human tenocyte culture. *Sci Rep* **6**, 20922, doi:10.1038/srep20922 (2016).

8 Lomas, A. J. *et al.* The past, present and future in scaffold-based tendon treatments. *Adv Drug Deliv Rev* **84**, 257-277, doi:10.1016/j.addr.2014.11.022 (2015).

9 Sabari, J. S. Joint structure and function: A comprehensive analysis, 3rd edition. *Am J Occup Ther* **55**, 358-358, doi:DOI 10.5014/ajot.55.3.358a (2001).

10 Williams, I. F., Heaton, A. & McCullagh, K. G. Cell Morphology and Collagen Types in Equine Tendon Scar. *Res Vet Sci* **28**, 302-310 (1980).

11 Eriksen, H. A., Pajala, A., Leppilahti, J. & Risteli, J. Increased content of type III collagen at the rupture site of human Achilles tendon. *J Orthopaed Res* **20**, 1352-1357, doi:Pii S0736-0266(02)00064-5 Doi 10.1016/S0736-0266(02)00064-5 (2002).

12 Chen, S. *et al.* RelA/p65 inhibition prevents tendon adhesion by modulating inflammation, cell proliferation, and apoptosis. *Cell Death Dis* **8**, doi:ARTN e2710 10.1038/cddis.2017.135 (2017).

13 Freeberg, M. A. T. *et al.* Serpine1 Knockdown Enhances MMP Activity after Flexor Tendon Injury in Mice: Implications for Adhesions Therapy. *Sci Rep-Uk* **8**, doi:ARTN 5810 10.1038/s41598-018-24144-1 (2018).

14 Ruan, H. J., Liu, S., Li, F. F., Li, X. J. & Fan, C. Y. Prevention of Tendon Adhesions by ERK2 Small Interfering RNAs. *International Journal of Molecular Sciences* **14**, 4361-4371, doi:10.3390/ijms14024361 (2013).

15 Lu, P. *et al.* Col V siRNA engineered tenocytes for tendon tissue engineering. *PLoS One* **6**, e21154, doi:10.1371/journal.pone.0021154 (2011).

16 Paterson, Y. Z., Rash, N., Garvican, E. R., Paillot, R. & Guest, D. J. Equine mesenchymal stromal cells and embryo-derived stem cells are immune privileged in vitro. *Stem Cell Res Ther* **5**, 90, doi:10.1186/scrt479 (2014).

17 Barsby, T., Bavin, E. P. & Guest, D. J. Three-dimensional culture and transforming growth factor beta3 synergistically promote tenogenic differentiation of equine embryo-derived stem cells. *Tissue Eng Part A* **20**, 2604-2613, doi:10.1089/ten.TEA.2013.0457 (2014).

18 De Rosa, M. *et al.* Cationic polyelectrolyte hydrogel fosters fibroblast spreading, proliferation, and extracellular matrix production: Implications for tissue engineering. *J Cell Physiol* **198**, 133-143, doi:10.1002/jcp.10397 (2004).

19 Macdonald, P. M., Crowell, K. J., Franzin, C. M., Mitrakos, P. & Semchyschyn, D. 2H NMR and polyelectrolyte-induced domains in lipid bilayers. *Solid State Nucl Magn Reson* **16**, 21-36 (2000).

Chapter 7

Conclusions and Future Work

7. Chapter 7 Conclusions and Future Work

7.1. General Conclusions and Discussions

The main aim of this study was to investigate the potential of PDMAEA polymers as a siRNA delivery vector. Firstly, four different PDMAEA polymers, including 10kDa linear PDMAEA (PL10), 10kDa star-shaped PDMAEA (PS10), 20kDa linear PDMAEA (PL20) and 20kDa star-shaped PDMAEA (PS20), have been successfully synthesised via RAFT polymerisation, as reported in chapter three. Analysis of polymer samples confirmed that the produced polymers have designed molecular weights, unique structures of linear and star-shaped and low polydispersity values. Though the use of RAFT polymerisation technique in the synthesis of linear PDMAEA polymers and copolymers has been widely reported, and Whitfield et al. have achieved successful production of star-PDMAEA polymers using Cu-mediated ATRP, the synthesis of star-shaped PDMAEA polymers via core-first RAFT polymerisation approach are rarely mentioned¹⁻⁴. The results from this work have provided a simple and efficient one-step synthesis of star-shaped PDMAEA polymers with controlled molecular weight and low dispersity via RAFT polymerisation. The PDMAEA polymers also have pKa values of ~7.8, which suggested that the amine groups could become protonated and the positive charges may maintain the solubility of the polymers in aqueous solution and may provide an advantage in condensation with nucleic acids. It has also been observed that there is a difference between the pKa values of the DMAEA monomers (pKa ~8.4)⁵ and PDMAEA polymers, possibly due to the protonation of polymers having been affected by various factors, including solution ionic strength, distribution of ionisable units and ionisation state of the neighbouring units⁶⁻⁸.

Secondly, as presented in chapter four, this study explored the zeta potential, hydrodynamic diameter in solution and DNA binding ability of the PDMAEA polymers, as well as the formation of polyplexes between PDMAEA polymers and dsDNA/siRNA molecules. The results suggested that PDMAEA polymers have small hydrodynamic diameters (of ≤ 10 nm) in solutions with pH value, and the measured hydrodynamic diameter increased as the pH increases. Furthermore, it was also observed that the zeta potential of PDMAEA polymers in solution decreased as the pH increases. It is possible that the PDMAEA polymers dissolved in aqueous solution, rather than remaining fully extended in a stationary state, they adopted irregular random coil structures which are typically found to be spherical⁹. In lower pH environments, the amines groups within

the PDMAEA polymers' structure would protonate and become positively charged, which may have provided repulsive forces between polymer particles sufficiently adequate to keep the system colloidal stable, and further enabled PDMAEA polymers to stay in forms of small particles. As the pH increases, amine groups in the polymer structure deprotonated and the polymer particles begin to aggregate to form large particles. These findings indicated that the PDMAEA polymers have high positive charges and relatively small hydrodynamic diameter in aqueous solution with low pH, which may be advantageous for the formation of polyplexes with negatively charged nucleic acid molecules. In addition, the DNA/RNA condensation ability of the PDMAEA polymers were determined by mixing polymers with a quantitative amount of dsDNA molecules based on different N:P ratios. The results showed that polymers with larger molecular weights would require a lower N:P ratio to completely condense to the dsDNA molecules, and star-shaped polymers require a lower N:P ratio to form polyplexes compared to their linear counterparts. This could be possibly explained by a "collapsed" structure formed by the star-shaped polymers, perhaps due to branched amphiphiles side chains, which can condense with guest molecules more efficiently. Taken together, it is concluded that polymers with larger molecular weights and a higher level of branching are provided with an advantage in the process of condensation. Moreover, polyplexes of four PDMAEA polymers with dsDNA and PS10 with siRNA were analysed. All the polyplexes have moderate hydrodynamic diameters of (less than 200 nm), which suggested that the polyplexes could be efficiently taken up by cells via clathrin-mediated endocytosis ^{10,11}. The determined hydrodynamic diameter of these PDMAEA-dsDNA/siRNA polyplexes are similar to the values reported in other studies¹²⁻¹⁴. When compared to other nanoparticles, including silver nanoparticles, poly(ethylene glycol)-containing liposomes and PEI-PEG polyplexes, the PDMAEA-DNA/RNA polyplexes have similar hydrodynamic diameters ¹⁵⁻¹⁷. The zeta potential of PDMAEA polyplexes were also measured under relevant pH values and results showed that the polyplexes have high positive charges, indicating moderate colloidal stabilities of these PDMAEA polyplex solutions ¹⁸.

Chapter five explored the cytotoxicity of the PDMAEA polymers on different cell lines. The synthesised PDMAEA polymers were tested on mouse 3T3 fibroblast and equine tenocyte samples and have provided several insights into the toxicity of PDMAEA polymers. PDMAEA polymers showed low cytotoxicity at low concentrations. When compared to PEI, PDMAEA polymers showed lower cytotoxicity at medium and high

concentrations at all timeframes on both mouse 3T3 fibroblasts and equine tenocytes. Besides, the data revealed that for polymers with molecular weights of 10kDa, both linear and star-shaped (PL10 and PS10) showed low toxicity across all concentrations and timeframes on both cell lines, while polymers with molecular weights of 20kDa (PL20 and PS20) showed significantly higher toxicity at high concentrations. Therefore, it is concluded that PDMAEA toxicity is proportional to molecular weight and sample concentration. It has been suggested that the cytotoxicity of cationic polymers is caused by the disruptive effect on the cellular membrane and resulting in damages to cellular organelles including mitochondria and endosomes ¹⁹. It has been reported that the membrane disruptive ability of the polymers may be related to the quantity of cationic functional groups in the structure, in the case of PDMAEA polymers, these are the amine groups ²⁰. The increase in amine content in polymer structure and in polymer solution may explain the increased toxicity in polymers with larger molecular weights and in polymer solutions at higher concentration. It is also suggested that polymers with larger molecular weight and longer chains can interact with negatively charged proteins and membranes more effectively in the intracellular space than short ones ¹⁹, which might also explain the increased toxicity in polymers with larger molecular weights.

However, the relationship between polymer architecture and cytotoxic remained unclear. Although in experiments conducted on mouse 3T3 fibroblasts, the toxicity of PS20 is slightly higher than PL20, this difference was not seen in cell samples treated with PL10 and PS10. Moreover, in experiments conducted on equine tenocytes there is no significant difference in cytotoxicity between linear polymers and star-shaped polymers. There is a lack of evidence to support any conclusion relating PDMAEA polymer architecture to its cytotoxicity in this study. Yet, cases of high branching results in high toxicity in PEI were observed and reported by Kafil et al. ²¹. This indicates that further enquiry into an architecture-toxicity relationship is required. To summarise, it is suggested that PDMAEA polymers showed lower cytotoxicity than PEI and are capable of protonation under neutral environment conditions, plus the ability to enhance condensation with nucleic acids. Among the four PDMAEA polymers, PL20 and PS20 have shown better binding ability at the cost of higher toxicity, while PL10 and PS10 have slightly compromised binding ability but displayed good biocompatibility. It is also evident that the toxicity of PDMAE polymers is time and concentration dependent. Thus, proper treatment concentration and incubation time should be considered. The cytotoxicity profile of PDMAEA polyplexes was determined by incubation with 3T3

fibroblast cells and horse tenocytes then analysed with MTS assay. The data indicated that the PDMAEA-dsDNA and PS10-siRNA polyplexes are well tolerated by the tenocyte and 3T3 fibroblast cells at low polyplex concentrations. In addition, when compared to other studies using unmodified PEI delivery systems (25kDa, linear), the PDMAEA polymers showed much lower cytotoxicity, while the PEI delivery systems showed stronger DNA binding capability, as PEI-dsDNA/siRNA polyplexes were prepared at lower N:P ratios of 2:1^{21,22}.

Concluding the findings in chapter four and five, the PDMAEA-dsDNA polyplexes and PS10-siRNA polyplex have appropriate hydrodynamic diameters with high zeta-potential, which indicated potential good cellular uptake and moderate colloidal stability. Toxicity studies of these polyplexes revealed good biocompatibility with different cell lines. The results suggested that PDMAEA polyplexes can be used as safe gene delivery vectors.

Finally, in chapter six, the transfection ability of PDMAEA polymer were explored. One PDMAEA polymer (PS10) was condensed to therapeutic siRNA to form *COL3α1* gene specific polyplexes and introduced into equine tenocytes. Cell samples were first stimulated with TGF-β1, with the intention of mimicking the behaviour of tenocytes in injured tissue, to up-regulate the expression of the *COL3α1* gene. Then, these stimulated samples were treated with therapeutic polyplexes. However, at 48 hours post-transfection, an unexpected increase in the expression of the *COL3α1* gene in samples treated with PS10 was observed compared with unstimulated ones. Immunocytochemistry at 72 hours post silencing confirmed the production of the increased amount of collagen type III. The reason for this dramatic increase remains unclear, however. Although no studies have reported the stimulus effect of PDMAEA polymer on the up-regulation of the *COL3α1* gene, it was suggested by De Rosa et al. that the presence of cationic charges on cell adhesion-resistant polymer surface increased the synthesis of collagen I and III, the release of their metabolites, and the expression of their mRNA in fibroblasts²³. This could be explained by polyelectrolyte coupling to plasma membrane lipid bilayers which can induce a redistribution of oppositely charged lipids into regions known as domains^{24,25}. The formation of domains can influence cellular membrane functioning, for example, by altering the local transmembrane permeability, or by acting as sequester enzyme substrates or activator/inhibitors, thereby signalling processes²³. Furthermore, though cells treated

with PS10-siRNA polyplexes showed lower levels of *COL3α1* expression when compared to PS10-random-siRNA treated group at 48 hours, but due to the stimulation effect of PDMAEA polymer on the expression of *COL3α1* gene, there isn't enough evidence and it is difficult to draw the conclusion that the specific silencing was successful. Further studies are required to determine the transfection efficiency of PDMAEA polymers.

To summarise, a PDMAEA cationic polymer siRNA delivery system has been successfully developed and proven to be biocompatible with good nucleic binding efficiency. Such a system may have good potential in the application siRNA delivery or improving tendon healing and the treatment of tendon injury. However, PDMAEA polymers would trigger an up-regulation of *COL3α1* gene expression and the transfection efficiency cannot be clearly demonstrated with current data. Further enquiries into the transfection efficiency of PDAMEA polymers and the cause of the increase are required.

7.2. Future Work

- Determination of PDMAEA polymer transfection efficiency

In this study, the original intention was to use PS10-siRNA polyplexes, which contains a *COL3α1* gene-specific siRNA sequence, to determine the transfection efficiency of PDMAEA polymers by the analysis of the *COL3α1* gene expression level before and after transgene. However, PDMAEA polymer triggered an unexpected up-regulation effect on the expression of the *COL3α1* gene, thus the transgene efficiency of PDMAEA polymers cannot be accurately determined. Future studies could focus on the use of other methods, for example, delivering plasmid DNA (pDNA) expressing either luciferase or green fluorescent protein in equine tenocytes. The PDMAEA polymers could be condensed to pDNA to form polyplexes and introduced to equine tenocytes. After transfection, the quantity of luciferase could be determined by using relative assays²⁶. This may provide a more efficient approach to determine the transgene ability of PDMAEA polymers without the influence of other factors such as TGF-β1 and siRNA specificity.

- PDMAEA modification

One advantage of the synthetic polymer-based delivery system is that various modifications are available. PDMAEA polymers synthesised in this thesis study have the potential to be developed into other copolymers with PDMAEA blocks. The combination of PDMAEA polymer with other polymer blocks would provide infinite possibilities to form multifunction polymers or stimulus responsive polymers. Another possible route is with PDMAEA synthesised via RAFT polymerisation, resulting in polymers with the thiol-containing functional group at one end of the polymer. In some cases, polymers containing thiocarbonylthio groups were prepared via RAFT polymerisation, which could react with nucleophiles and ionic reducing agents to generate thiols (figure 7.1)²⁷. The thiol group may provide potential applications in radical-mediated thiol-ene click reactions or a potential crosslinking site for thiol cross-linking^{28,29}.

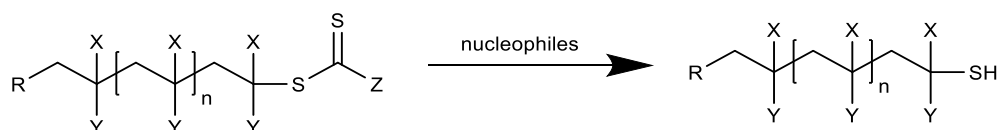


Figure 7.1 Processes for thiocarbonylthio removal to generate thiols.

- Would the suppression of collagen type III production reduce the formation of scar tissue?

The research work presented in this thesis describes the attempt to suppress the expression of collagen type III in an *in vitro* situation. Though the delivery system has been proven to be capable of transfection, due to the up-regulation effect of PDMAEA polymers, the suppression of the *COL3a1* gene was less satisfactory. Besides, this study is mainly conducted *in vitro*, thus how PDMAEA polymer or collagen type III could affect tendon tissue cannot be observed directly. Hopefully, in the future, the improved PDMAEA delivery system could be employed to suppress collagen type III on an injury animal model *in vivo*. It would be interesting to find out if suppression of collagen type III production could reduce the formation of scar tissue.

- Controlled release system

Compared to the viral delivery system or pDNA transfection, one trait of siRNA silencing is that the effective period is limited. Generally, siRNA mediated gene silencing can be observed as early as 24 hours post-transfection and the effect would last up to seven days, though the duration and level of knockdown are dependent on cell

type and concentration of siRNA. In some cases, prolonged siRNA interference is required; to achieve prolonged siRNA silencing with single dosage siRNA transfection could increase the cost and could be inconvenient. Therefore, a controlled release siRNA delivery system would be ideal for situations which needs a prolonged siRNA silencing. PDMAEA polymer has the potential of being modified and developed into a hydrogel-based controlled release system which could be interesting. Functional groups such as thiol groups could be generated with proper cleavage. Thiol groups could be applied in the bioconjugation with multiple crosslinking reagents. One interesting thought would be to use cleaved PDAMEA polymers with thiol end groups to crosslink with PEG-maleimide polymers to generate a hydrogel-network which potentially has the ability to entrap siRNA molecules and slowly release as the PEG-rich network degrades.

7.3. References

- 1 Sun, F. X., Feng, C., Liu, H. Y. & Huang, X. Y. PHEA-g-PDMAEA well-defined graft copolymers: SET-LRP synthesis, self-catalyzed hydrolysis, and quaternization. *Polym Chem-Uk* **7**, 6973-6979, doi:10.1039/c6py01637e (2016).
- 2 Suchao-in, N., Chirachanchai, S. & Perrier, S. pH- and thermo-multi-responsive fluorescent micelles from block copolymers via reversible addition fragmentation chain transfer (RAFT) polymerization. *Polymer* **50**, 4151-4158, doi:10.1016/j.polymer.2009.06.047 (2009).
- 3 Dinari, A., Moghadam, T. T., Abdollahi, M. & Sadeghizadeh, M. Synthesis and Characterization of a Nano-Polyplex system of GNRs-PDMAEA-pDNA: An Inert Self-Catalyzed Degradable Carrier for Facile Gene Delivery. *Sci Rep-Uk* **8**, doi:ARTN 8112 10.1038/s41598-018-26260-4 (2018).
- 4 Whitfield, R. *et al.* Well-defined PDMAEA stars via Cu(0)-mediated reversible deactivation radical polymerisation. *Abstr Pap Am Chem S* **253** (2017).
- 5 Grace, J. L. *et al.* Antibacterial low molecular weight cationic polymers: dissecting the contribution of hydrophobicity, chain length and charge to activity. *Rsc Adv* **6**, 15469-15477, doi:10.1039/c5ra24361k (2016).
- 6 Borukhov, I. *et al.* Polyelectrolyte titration: Theory and experiment. *Journal of Physical Chemistry B* **104**, 11027-11034, doi:DOI 10.1021/jp001892s (2000).
- 7 Lee, H. *et al.* Macroscopic lateral heterogeneity observed in a laterally mobile immiscible mixed polyelectrolyte-neutral polymer brush. *Soft Matter* **10**, 3771-3782, doi:10.1039/c4sm00022f (2014).
- 8 Smits, R. G., Koper, G. J. M. & Mandel, M. The Influence of Nearest-Neighbor and Next-Nearest-Neighbor Interactions on the Potentiometric Titration of Linear Poly(Ethylenimine). *J Phys Chem-US* **97**, 5745-5751, doi:DOI 10.1021/j100123a047 (1993).
- 9 Su, W.-F. in *Principles of Polymer Design and Synthesis* (ed Wei-Fang Su) 9-26 (Springer Berlin Heidelberg, 2013).
- 10 de la Fuente, J. M. & Grauz, V. *Nanobiotechnology: Inorganic Nanoparticles vs Organic Nanoparticles*. (Elsevier Science, 2012).
- 11 Shang, L., Nienhaus, K. & Nienhaus, G. U. Engineered nanoparticles interacting

with cells: size matters. *J Nanobiotechnol* **12**, doi:Artn 5 10.1186/1477-3155-12-5 (2014).

12 Pezzoli, D., Giupponi, E., Mantovani, D. & Candiani, G. Size matters for in vitro gene delivery: investigating the relationships among complexation protocol, transfection medium, size and sedimentation. *Sci Rep* **7**, 44134, doi:10.1038/srep44134 (2017).

13 Zhang, L., Chen, Z. & Li, Y. Dual-degradable disulfide-containing PEI-Pluronic/DNA polyplexes: transfection efficiency and balancing protection and DNA release. *Int J Nanomedicine* **8**, 3689-3701, doi:10.2147/IJN.S49595 (2013).

14 Zhang, J., Bae, S., Lee, J. S. & Webb, K. Efficacy and mechanism of poloxamine-assisted polyplex transfection. *J Gene Med* **15**, 271-281, doi:10.1002/jgm.2719 (2013).

15 Bastus, N. G., Merkoci, F., Piella, J. & Puntes, V. Synthesis of Highly Monodisperse Citrate-Stabilized Silver Nanoparticles of up to 200 nm: Kinetic Control and Catalytic Properties. *Chem Mater* **26**, 2836-2846, doi:10.1021/cm500316k (2014).

16 Litzinger, D. C., Buiting, A. M. J., Vanrooijen, N. & Huang, L. Effect of Liposome Size on the Circulation Time and Intraorgan Distribution of Amphiphatic Poly(Ethylene Glycol)-Containing Liposomes. *Bba-Biomembranes* **1190**, 99-107, doi:Doi 10.1016/0005-2736(94)90038-8 (1994).

17 Adolph, E. J. *et al.* Enhanced performance of plasmid DNA polyplexes stabilized by a combination of core hydrophobicity and surface PEGylation. *J Mater Chem B* **2**, 8154-8164, doi:10.1039/c4tb00352g (2014).

18 Byrn, S. R., Zografi, G. & Chen, X. *Solid-State Properties of Pharmaceutical Materials*. (Wiley, 2017).

19 Cai, J. G. *et al.* Effect of Chain Length on Cytotoxicity and Endocytosis of Cationic Polymers. *Macromolecules* **44**, 2050-2057, doi:10.1021/ma102498g (2011).

20 Zheng, Z. *et al.* Structure-Property Relationships of Amine-rich and Membrane-Disruptive Poly(oxonorbornene)-Coated Gold Nanoparticles. *Langmuir* **34**, 4614-4625, doi:10.1021/acs.langmuir.7b04285 (2018).

21 Kafil, V. & Omidi, Y. Cytotoxic impacts of linear and branched polyethylenimine nanostructures in a431 cells. *Bioimpacts* **1**, 23-30, doi:10.5681/bi.2011.004 (2011).

22 Sun, J., Zeng, F., Jian, H. & Wu, S. Conjugation with betaine: a facile and effective approach to significant improvement of gene delivery properties of PEI. *Biomacromolecules* **14**, 728-736, doi:10.1021/bm301826m (2013).

23 De Rosa, M. *et al.* Cationic polyelectrolyte hydrogel fosters fibroblast spreading, proliferation, and extracellular matrix production: Implications for tissue engineering. *J Cell Physiol* **198**, 133-143, doi:10.1002/jcp.10397 (2004).

24 Welti, R. & Glaser, M. Lipid domains in model and biological membranes. *Chem Phys Lipids* **73**, 121-137 (1994).

25 Macdonald, P. M., Crowell, K. J., Franzin, C. M., Mitrakos, P. & Semchyschyn, D. 2H NMR and polyelectrolyte-induced domains in lipid bilayers. *Solid State Nucl Magn Reson* **16**, 21-36 (2000).

26 Dai, F. & Liu, W. Enhanced gene transfection and serum stability of polyplexes by PDMAEMA-polysulfobetaine diblock copolymers. *Biomaterials* **32**, 628-638, doi:10.1016/j.biomaterials.2010.09.021 (2011).

27 Chong, Y. K., Moad, G., Rizzardo, E. & Thang, S. H. Thiocarbonylthio end group removal from RAFT-synthesized polymers by radical-induced reduction.

28 *Macromolecules* **40**, 4446-4455, doi:10.1021/ma062919u (2007).

28 Pfeifer, H. *et al.* Identification of a specific sperm nuclei selenoenzyme necessary for protamine thiol cross-linking during sperm maturation. *Faseb J* **15**, 1236-1238 (2001).

29 Hoyle, C. E. & Bowman, C. N. Thiol-ene click chemistry. *Angew Chem Int Ed Engl* **49**, 1540-1573, doi:10.1002/anie.200903924 (2010).